Standortspezifische Quantifizierung temperaturinduzierter hydrogeochemischer Effekte oberflächennaher Wärmespeicher

Dissertation
zur Erlangung des Doktorgrades
der Mathematisch-Naturwissenschaftlichen Fakultät
der Christian-Albrechts-Universität zu Kiel

vorgelegt von

Klas Lüders

Kiel, Juli 2023

Erster Gutachter: Prof. Dr. Andreas Dahmke

Zweiter Gutachter: Prof. Dr. Oliver Opel

Datum der Disputation: 20.12.2023

Zum Druck genehmigt: 20.12.2023

gez. Prof. Dr. Frank Kempken, Dekan:

Danksagung

Zuerst möchte ich mich ganz herzlich bei Dr. Ralf Köber für zahlreiche hilfreiche Diskussionen, ein stetig offenes Ohr, aufmunternde Worte wenn Sie mal nötig waren und die umfängliche Unterstützung bei der Planung und Auswertung der Laborversuche und den schriftlichen Ausarbeitungen in den vergangenen Jahren bedanken. Auch Dr. Götz Hornbruch gilt hinsichtlich dieser Punkte mein herzlicher Dank, wobei ich auch die unzähligen Diskussionen über unsere Feldversuche und die gemeinsamen Feldarbeiten in Wittstock nicht unerwähnt lassen möchte. Besonders bedanken möchte ich mich auch bei meinem Betreuer Prof. Dr. Andreas Dahmke: Durch die Möglichkeit einer Promotion in ihrer Arbeitsgruppe konnte ich über die gesamten Jahre an thematisch sowohl aktuellen als auch sehr spannenden Projekten mitarbeiten und mit ihren kritisch-konstruktiven Anregungen haben Sie häufig nochmal neue Aspekte in die Arbeit eingebracht. Auch PD Dr. Markus Ebert gilt mein Dank für die Hilfe bei vielen kleinen oder größeren Fragen zwischendurch, viele Diskussion auch mal abseits von Arbeitsthemen und die Bewältigung des oft sehr umfangreichen Analyseaufkommens.

Ebenso bedanken möchte ich mich bei Prof. Dr. Oliver Opel und Prof. Dr. Nicola Fohrer für die Bereitschaft das Zweitgutachten für meine Dissertation zu übernehmen. Auch den weiteren Mitgliedern der Prüfungskommission bei der Disputation gilt mein Dank.

Bedanken möchte ich mich auch bei allen weiteren, die mir auf die eine oder andere Weise während meiner Zeit als Doktorand geholfen haben: Frank Dethlefsen für seine Unterstützung bei Festphasenanalysen; Dirk Schäfer für seine hilfreichen Hinweise in den Seminaren; Linda Firmbach für das geoelektrische Monitoring unserer Säulenversuche; Michelle Fiedler für die Betreuung einer ganzen Batterie an Batchversuchen; Nilufar Zarrabi für ihren unermüdlichen Einsatz bei den Feldarbeiten; Stefan Heldt für die Auswertung der Temperaturdaten aus Wittstock; Nicolas Koproch, Kerstin Meier zu Beerentrup, Marco Mahnecke, Enno Borgeest und Nina-Sophie Keller für die immer nette Zusammenarbeit bei den Feldarbeiten; Klaus-Dieter Stüwe, Birgit Jacobsen und Bithja Indome für ihre Hilfe mit der Bürokratie; Alina Kabuth und Sönke Bohm für die Projektkoordination; dem Werkstattteam um Ralf Doose für die Bearbeitung allerlei kurzfristiger Anfragen; sowie Jutta Salamon, Joachim Lippke, Jens Wemhöner, Peggy Wefers, Vincent Sanmann, Ulrike Westernströer und Dieter Garbe-Schönberg für die Analyse über die Jahre nicht mehr zu zählender Proben.

Ein Dank geht auch an meine bisher nicht genannten Doktoranden-Kollegen Tessa Strutz, Svea Hausberg, Janine Struß, Alexander Schwardt, Louisa Lagmöller, Bo Wang und Johannes Nordbeck, die mir in den verschiedenen Phasen meiner Promotion mit Rat und Tat zur Seite standen. Im Büro hatte ich das Glück mit Márton Berta und Adrian Metzgen zwei Kollegen zu haben, die mich mit vielen Ideen unterstützt aber auch mit zahlreichen Gesprächen von A-Z wenn nötig mal auf andere Gedanken gebracht haben, Danke euch Beiden!

Die täglichen Labor- und Feldarbeiten wären ohne die Unterstützung durch HiWis (Laurenz Böttcher, Alica Broertjes, Eva Dieterich, Fabian Dietzel, Leon Kausch, Charlotte Schmidt, Alexander Utecht, Jan Voß), Bachelor- (Charlotte Decker, Lars Detjens, Jan Gustmann, Svenja Heimann, Lena-Sophie Kuhr, Daniel Posanski) und Masterstudenten (Malte Hoppe, Anna Kempermann, Bernd Willms) nicht möglich, auch euch allen gilt daher mein herzlicher Dank.

Zu guter Letzt möchte ich auch meiner Familie für die konstante und vielseitige Unterstützung danken, ihr habt mir über alle Herausforderungen des Alltags hinweg wenn immer nötig den Rücken freigehalten!

Kurzfassung

Mit knapp 50 % des Endenergieverbrauchs in Europa nimmt der Wärmesektor eine Schlüsselrolle beim Erreichen globaler Klimaschutzziele ein. An Wärmenetze gekoppelte saisonale Wärmespeicher können dabei helfen regenerative Wärmequellen, wie z. B. Solarthermie, Geothermie oder industrielle Abwärme, effizient in Wärmeversorgungssysteme zu integrieren. Aufgrund benötigter Speichervolumina in urbanen Gebieten, eignen sich dafür besonders Wärmespeicher im geologischen Untergrund. Speichertemperaturen von 50-100 °C werden jedoch mit potentiellen Beeinträchtigungen des Anlagenbetriebs oder der Grundwasserbeschaffenheit durch verschiedene hydrogeochemische Prozesse assoziiert. Im Fokus dieser Arbeit stehen daher

a) welches Ausmaß einer temperaturinduzierten Gasphasenbildung bei unterschiedlichen geochemischen Randbedingungen zu erwarten ist und wie dieses abgeschätzt werden kann,
b) das Freisetzungs- und Wiederfestlegungsverhalten von Spurenkomponenten und Schwermetallen in vier Aquifersedimenten unter variierenden Temperaturbedingungen, und
c) die Prognostizierbarkeit initialer hydrogeochemischer Effekte bei einem kurzzeitigen Eintrag ~75 ° heißen Wassers in einen glazigenen Aquifer durch Batchversuche mit Standortsediment.

Die in Durchflusssäulenversuchen bei 10, 25, 40 und 70 °C quantifizierte Gasphasenbildung lag innerhalb der thermodynamisch zu erwartenden Spannbreite. Darauf basierende Szenarienrechnungen für verschiedene geochemische Bedingungen zeigten, dass eine temperaturinduzierte Gasphasenbildung in Aquiferen mit gelösten Gaskonzentrationen im Gleichgewicht zur Bodenluft in den allermeisten Fällen vernachlässigbar sein wird. In Aquiferen mit zusätzlichen Gasquellen, wie bspw. der Umwandlung organischen Materials, könnte eine Gasphasenbildung hingegen den Grundwasserfluss und damit die Speichereffizienz beeinflussen.

Die Mobilisierung und Wiederfestlegung von 20 teils umweltrelevanten Spurenkomponenten und Schwermetallen wurde anhand der Temperierung von vier Aquifersedimenten auf 10, 25, 40 und 70 °C in Durchfluss- und Kreislaufsäulenversuchen untersucht. Erhöhte Temperaturen führten in allen Versuchen zu sedimentspezifisch ansteigenden Li, As, Mo, Sb und Ba und abnehmenden Ni Konzentrationen, wohingegen der Effekt bei V, Mn, Co, Tl und U sedimentspezifisch variierte. Die in einem Puls ablaufende Freisetzung bei der initialen Aufheizung deutet bei allen Komponenten außer Ba auf einen endlichen Freisetzungspool hin. Eine Rückkühlung auf 10 °C führte zu einer komponentenspezifischen Wiederfestlegung von 30-95 %, woraus sich eine räumlich und zeitlich begrenzte Ausdehnung temperaturinduzierter Konzentrationsänderungen ableiten lässt. Exemplarisch wurde dies mit einem vereinfachten analytischen 1D-Ansatz für As abgeschätzt.

Um deren Eignung für die Prognose initialer temperaturinduzierter hydrogeochemischer Effekte zu prüfen, wurden Batchversuche mit je 28 Sedimentproben bei 10, 40 und 70 °C mit einem Feldversuch kombiniert, bei dem über 4,5 d Wasser mit bis zu 78 °C in einen glazigenen Aquifer infiltriert wurde. Ein Vergleich der Feldmessungen mit auf den relativen Konzentrationsänderungen in den Batchversuchen basierenden prognostizierten Konzentrationsbereichen zeigte die beste Prognosefähigkeit dort, wo die Temperaturen noch am nächsten zu denen des infiltrierten Wassers waren. Die gemessenen und prognostizierten Konzentrationen stimmten dabei vor allem bei Komponenten überein, deren temperaturinduzierten Konzentrationsänderungen durch Ionenaustausch- bzw. (De)sorptionsprozesse kontrolliert werden. Der präsentierte Ansatz ermöglicht somit die Prognose maximal zu erwartender temperaturinduzierter Konzentrationsänderungen für die meisten umweltrelevanten Spurenkomponenten wie bspw. As.

Übergeordnet ist die Reversibilität temperaturinduzierter Konzentrationsänderungen hervorzuheben, wodurch diese räumlich und zeitlich begrenzt bleiben. Vorausblickend sollte der Fokus auf potentielle Speicherformation mit anderen geochemischen Randbedingungen erweitert werden. Offene Fragen hinsichtlich des hydrogeochemischen Verhaltens im saisonalen Langzeitbetrieb von Wärmespeichern werden sich in Anbetracht der notwendigen räumlichen und zeitlichen Dimensionen am besten betriebsbegleitend in Pilot-Wärmespeichern untersuchen lassen.

Abstract

With nearly 50 % of total energy consumption in Europe, the heating sector plays a key role in achieving global objectives of climate protection. Seasonal heat storages coupled to district heating systems can help to efficiently integrate renewable heating sources such as solar thermal energy, geothermal energy or industrial waste heat into heating supply systems. Based on the storage volume demand in urban areas, especially underground thermal energy storages are suitable for this task. However, storage temperature of 50-100 °C get associated with a potential impairment of the technical installations or the groundwater condition by various hydrogeochemical processes. Therefore, this work focusses on

a) which extent of temperature induced gas-phase formation is expectable at different geochemical boundary conditions and how this can be estimated,
b) the release and refixation behaviour of trace elements and heavy metals in four aquifer sediments at varying temperature conditions, as well as
c) the predictability of initial hydrogeochemical effects during a short-term infiltration of ~75 °C hot water into a glaciogenic aquifer by laboratory batch tests with sediment from the test site.

The quantified gas-phase formation in through-flow column tests at 10, 25, 40 and 70 °C was within the thermodynamically expectable range. Based on these results, scenario calculations for varying geochemical boundary conditions showed, that in most cases no relevant temperature induced gas-phase formation would occur in aquifers with dissolved gas concentrations in equilibrium with the soil vapour. In aquifers with additional sources for dissolved gases, as e.g. the metabolization of organic matter, a gas-phase formation could influence the groundwater flow and in doing so the storage efficiency.

The mobilisation and refixation of 20 partly environmentally relevant trace elements and heavy metals was investigated in through-flow- and circular-flow column tests at 10, 25, 40 and 70 °C for four aquifer sediments. Elevated temperatures caused increasing Li, As, Mo, Sb and Ba concentrations and decreasing Ni concentrations in all of the sediments with a sediment-specific extent, whereas effects on V, Mn, Co, Tl and U concentrations varied sediment-specifically. Apart from Ba, all these components were released as a pulse in the initial heating phase, indicating a temperature dependent, finite, elutable pool. Re-cooling of the previously heated circular-flow column tests to 10 °C caused reversals of concentration changes by 30 to 95 %, which indicates a spatially and temporally limited extent of temperature induced concentration changes. This was exemplarily estimated for As with a simplified analytical 1D-approach.

To test their suitability for prediction of initial temperature induced hydrogeochemical effects, batch tests at 10, 40 and 70 °C, with 28 sediment samples each, were combined with a field test, in which water was infiltrated into a glaciogenic aquifer for 4.5 d with up to 78 °C. A comparison of field measurements with concentration ranges predicted by using the relative temperature induced concentration changes in the batch tests showed the best predictive power, where temperatures were nearest to those of the infiltrated water. The measured and predicted concentrations primarily coincided for groundwater components which temperature induced concentration changes are controlled by ion exchange or (de)sorption processes. Thus, the presented approach enables the prediction of maximal expectable temperature induced concentration changes for most of the environmentally relevant trace elements and heavy metals as e.g. As.

The reversibility of temperature induced concentration changes needs to be emphasised, as this limits their spatial and temporal spreading. Prospectively, the focus should be extended to potential storage formations with different geochemical boundary conditions. Due to the necessary temporal and spatial dimensions, open questions regarding the hydrogeochemical behaviour in seasonal long-term operation of subsurface heat storages are probably addressed most suitably by conducting investigations accompanying the regular operation at pilot heat storage sites.

Inhaltsverzeichnis

Abbildungsverzeichnis

Tabellenverzeichnis

1. Einleitung

1.1. Wärmewende als Teil der Energiewende

Zum Erreichen der globalen Klimaschutzziele bedarf es der verstärkten Einbindung regenerativer Quellen in die Energiesysteme (IEA, 2015). Dabei zeigen sich sowohl in Deutschland als auch auf europäischer Ebene, insbesondere in den letzten zehn Jahren, höhere Wachstumsraten im Anteil erneuerbarer Energien (EE) am Bruttoendenergieverbrauch im Elektrizitätssektor, als in den Sektoren Wärme- und Kälteerzeugung sowie Verkehr (Abb. 1.1).

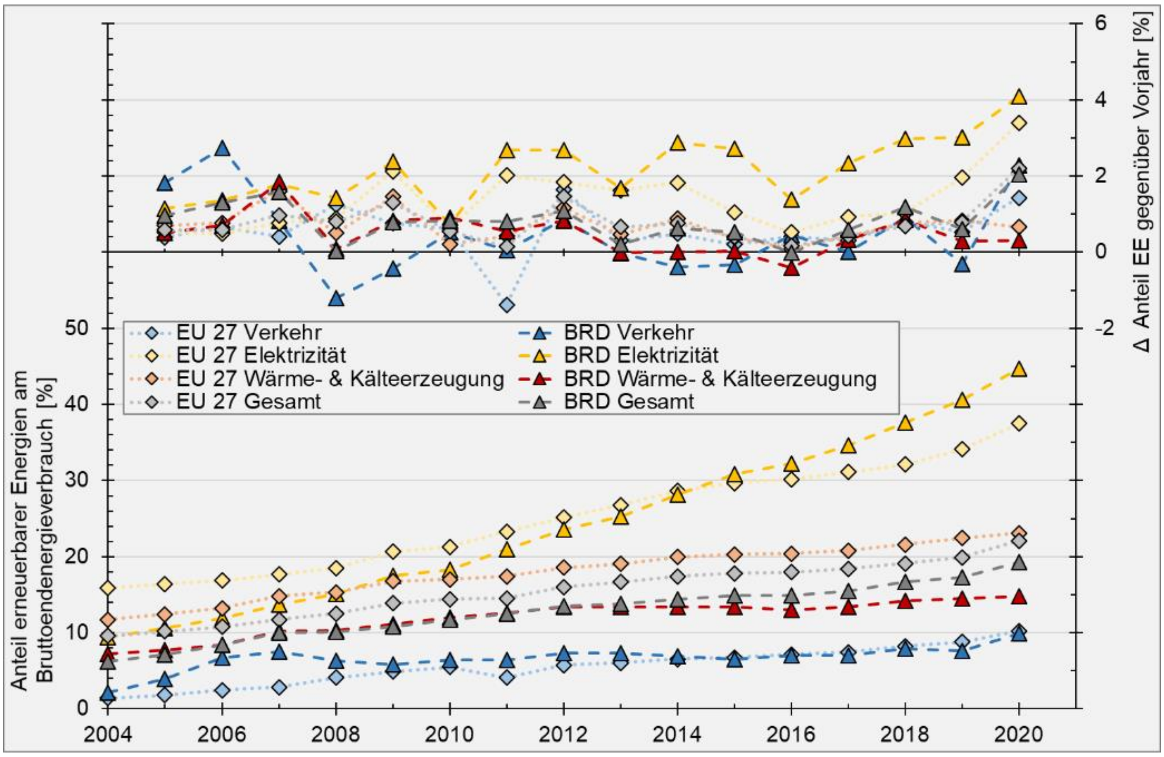

Abb. 1.1: Entwicklung des Anteils erneuerbarer Energien am Bruttoendenergieverbrauch in den Bereichen „Verkehr“, Elektrizität“ und „Wärme- & Kälteerzeugung“ für Deutschland (BRD) und die Europäische Union (EU 27) im Zeitraum der Jahre 2004 bis 2020 (Datenquelle: Eurostat, 2022).

Die Kombination von ~15 % EE-Anteil am Endenergieverbrauch bei der Wärme- und Kälteerzeugung (Abb. 1.1), mit deren Anteil von ~55 % am Gesamt-Endenergieverbrauch im Jahr 2020, verdeutlicht am Beispiel der Bundesrepublik Deutschland (Abb. 1.2a) das große Einsparpotential bei fossilen Energieträgern und die Schlüsselrolle, die dieser Bereich bei der Energiesystemtransformation einnehmen kann und muss. Während die Bereitstellung von Klima- und Prozesskälte bereits weitgehend strombasiert erfolgt, liegt der Anteil an Erdgas, Öl und Kohle bei der Bereitstellung von Raumwärme, Warmwasser und Prozesswärme in Summe zurzeit noch bei jeweils ~60-70 % des Endenergieverbrauchs (Abb. 1.2b), sodass insbesondere bei diesen Anwendungszwecken eine beschleunigte Dekarbonisierung erforderlich ist.

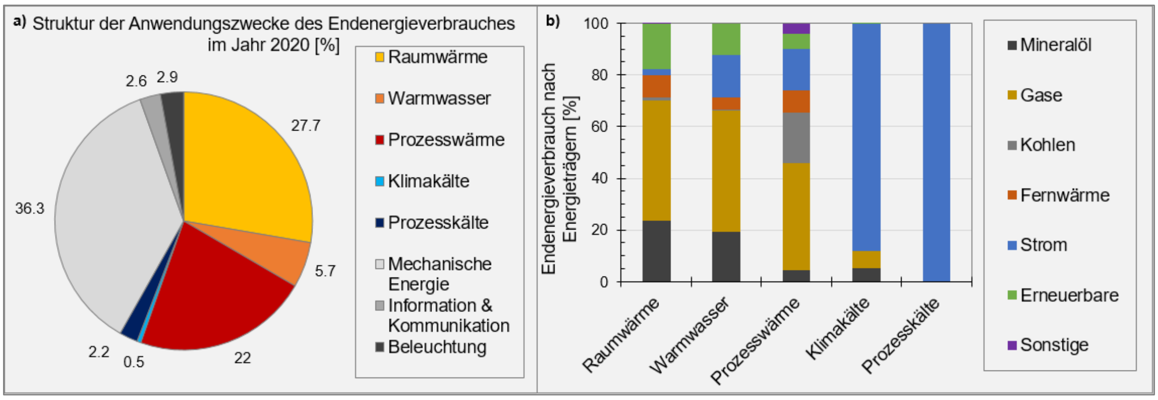

Abb. 1.2: Struktur der Anwendungszwecke des Endenergieverbrauchs in Deutschland im Jahr 2020 (a); sowie die Struktur des Endenergieverbrauchs nach Energieträgern für die Anwendungszwecke Raumwärme, Warmwasser, Prozesswärme, Klimakälte und Prozesskälte in Deutschland im Jahr 2020 (b); Datenquelle: AGEB (2021).

Um die bei der Prozesswärme häufig benötigten hohen Temperaturen zu erreichen, werden in diesem Bereich auch weiterhin oft dezentrale Systeme zum Einsatz kommen, sodass zur Erhöhung des EE-Anteils in diesem Bereich verstärkt auf Biomasse und strombasierte Brennstoffe (wie z. B. grünen Wasserstoff) gesetzt werden soll (BMWi, 2021). Bisher dominieren aber auch bei der Bereitstellung von Raumwärme und Warmwasser dezentrale Einheiten die Wärmebereitstellung, da mit ~8 % nur ein geringer Anteil der Bereitstellung des Wärmeendenergiebedarfs über Wärmenetze erfolgt (BMWi, 2021).

Insbesondere bei neueren oder sanierten Gebäuden, deren Dämmung niedrige Vorlauftemperaturen erlauben, kann eine Erhöhung des EE-Anteils bei der Wärmebereitstellung, bspw. durch die Nutzung von Wärmepumpen, auch weiterhin dezentral erfolgen (Bürger et al., 2017). Aber auch wenn in einem Gebiet nur geringe Vorlauftemperaturen benötigt werden, kann der Aufbau von dekarbonisierten Niedertemperatur-Wärmenetzen die gleichzeitige Umstellung vieler Haushalte auf eine EE-basierende Wärmeversorgung ermöglichen.

Bei teil- oder unsanierten Bestandsgebäuden kann die dezentrale Nutzung von Wärmepumpen jedoch entweder mit einem erheblichem Aufwand in der energetischen Sanierung und Erneuerung der Gebäudetechnik oder erhöhten Kosten für die strombasierte Anhebung des Temperaturniveaus über Wärmepumpen einhergehen (Gerhardt et al., 2019). Zudem ist auch bei erhöhten Sanierungsraten noch für die kommenden Jahrzehnte mit einem großen Anteil eines nur teil- oder unsanierten Gebäudebestandes zu rechnen (Gerhardt et al., 2019). Um gerade auch in dicht besiedelten Ballungsräumen, mit häufig geringem bzw. zumindestens stark heterogenen Sanierungsgrad, eine schnellere Umstellung auf eine wirtschaftliche Wärmeversorgung mit erneuerbaren Energien zu realisieren, bietet sich die zentrale Wärmeversorgung über ausgebaute und dekarbonisierte Fernwärmenetze mit dem Sanierungsgrad entsprechenden Vorlauftemperaturen an (BMWi, 2021; Gerhardt et al., 2021).

Welche Hebelwirkung für die Nutzung von EE im Wärmesektor durch die Umstellung der zentralen Wärmebereitstellung über Wärmenetze erreicht werden kann, sofern diese einen möglichst großen Anteil der Bevölkerung versorgen, zeigt sich bspw. dadurch, dass in allen europäischen Ländern in denen der EE-Anteil an der Wärme- und Kältebereitstellung über 50 % liegt (Dänemark, Estland, Finnland, Island, Lettland, Litauen und Schweden) jeweils auch mindestens 50 % der Bevölkerung mit Fernwärme versorgt werden (Abb. 1.3a). Auffällig ist dabei, dass in diesen Ländern nicht nur das Ausgangsniveau im EE-Anteil im Jahre 2004 bereits über dem in Deutschland lag, sondern, dass auch der weitere Anstieg des EE-Anteils zwischen 2004 und 2020 in allen 7 Ländern größer als in Deutschland war (Abb. 1.3b). Vor diesem Hintergrund weist auch der im Vergleich zu den skandinavischen und baltischen Ländern geringere EE-Anteil in der Wärme- und Kälteerzeugung in Polen, Tschechien und der Slowakei, trotz eines mit 35 bis 53 % ebenfalls vergleichsweise großen fernwärmeversorgten Anteils der Bevölkerung, in erster Linie darauf hin, dass gut ausgebaute Wärmenetze zwar bei einer schnelleren Umstellung zu mehr EE helfen können, dieses Potential auf Seiten der Energiebereitstellung für die Wärmenetze aber auch genutzt werden muss.

So konnte z. B. Dänemark durch den verstärkten Einsatz von Biomasse und Müll den Anteil alternativer Energiequellen in Kraftwerken mit Kraft-Wärme-Kopplung, die etwa die Hälfte der Wärme für dänische Fernwärmenetze zur Verfügung stellen, zwischen 1990 und 2019 von 20 auf 64 % steigern (Johansen und Werner, 2022). Dass über 70 % der Biomasse und 10 % des Mülls für den Energiesektor in Dänemark importiert werden (Johansen and Werner, 2022), erschwert allerdings die direkte Übertragung dieses Ansatzes auf andere Länder. Generell werden daher standortbezogen diverse regenerative Energiequellen für die Wärmebereitstellung über Wärmenetze in Betracht gezogen werden müssen (Abb. 1.4b).

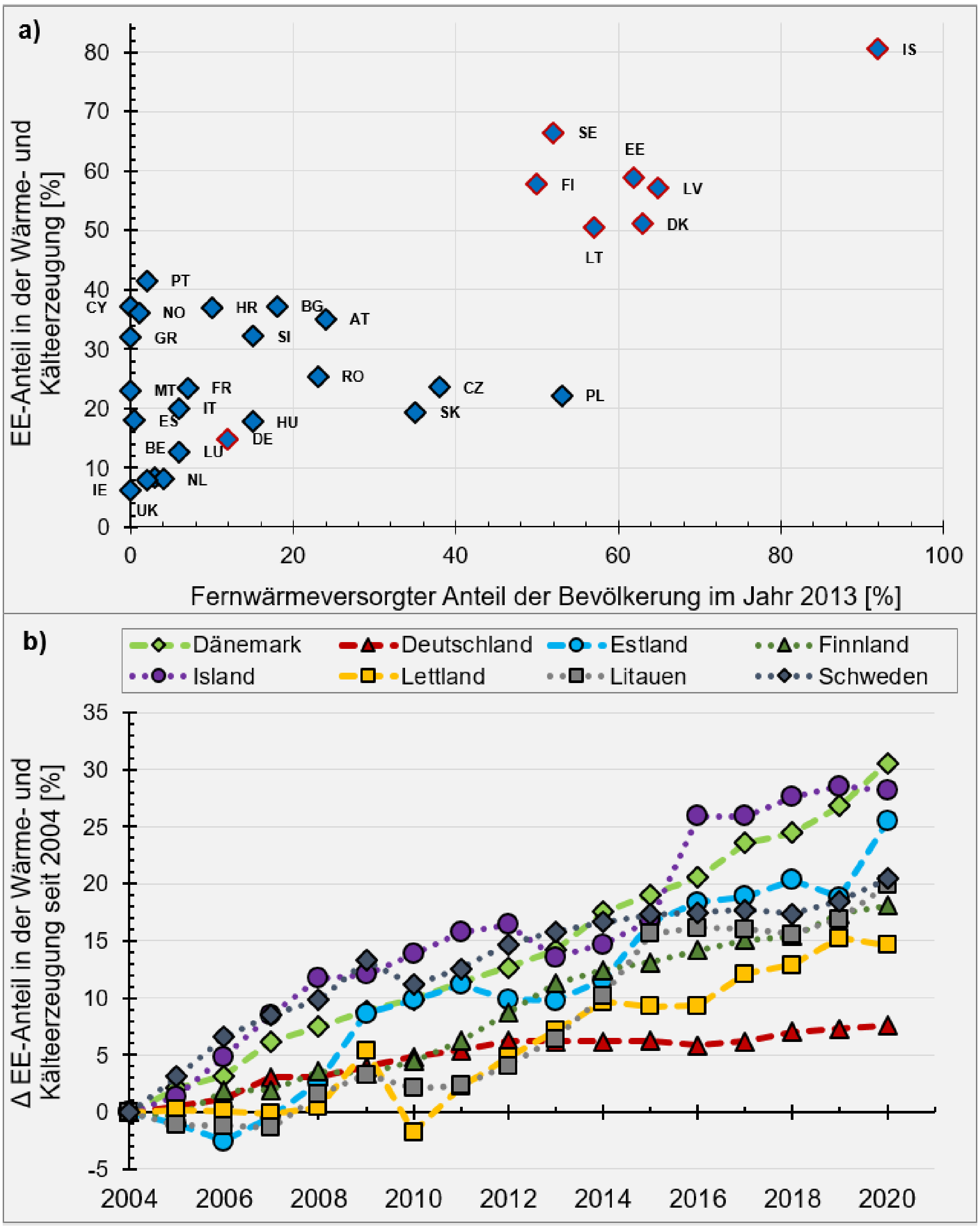

Abb. 1.3: Vergleich des Anteils der Bevölkerung welcher mit Fernwärme versorgt wird, mit dem EE-Anteil bei der Wärme- und Kälteerzeugung im Jahr 2020, sowie b) Entwicklung des EE-Anteils in der Wärme- und Kälteerzeugung zwischen 2004 und 2020 für ausgewählte Länder (umrandet in a; Datenquellen: Eurostat, 2022; Fleiter et al., 2016).

Die Grundlage für einen Ausbau der netzbasierten Wärmeversorgung ist in Form von bestehenden Fernwärmenetzen auch in Deutschland in vielen dichter besiedelten Gebieten gegeben (Abb. 1.4a). So sehen Klimaneutralitätsstudien, z. B. des Kopernikus-Projekt Ariadne (2021), in etwa eine Verdoppelung der über Wärmenetze bereitgestellten Energie bis 2045 vor. Dafür bedarf es dem Anschluss weiterer Haushalte durch Aus- bzw. Neubau und einer Nachverdichtung von Wärmenetzen, wobei eine Verdreifachung der Anzahl angeschlossener Gebäude angestrebt wird (BMWK, 2023). Neben dem reinen Ausbau der netzbasierten Wärmeversorgung, muss diese jedoch auch auf alternative Wärmequellen wie z. B. Solarthermie, industrielle Abwärme, Biomasse, tiefe- und oberflächennahe Geothermie sowie Power to Heat umgestellt werden (Abb. 1.4b; BMWK, 2023; Engelmann et al., 2021; Maaß and Sandrock, 2017). Während die Wärmebereitstellung aus diesen Quellen jedoch oft entweder in etwa gleichmäßig über das Jahr verteilt ist (z. B. Geothermie oder industrielle Abwärme) oder insbesondere in den Sommermonaten (Solarthermie) anfällt, liegt der Hauptbedarf für Raumwärme in den Wintermonaten, sodass Wärmenetzte für eine sowohl energetisch als auch wirtschaftlich effiziente Nutzung dieser Energiequellen auf großskalige saisonale Wärmespeicher angewiesen sind (BMWi, 2021; BMWK, 2023; Engelmann et al., 2021; Henning and Palzer, 2012; Maaß and Sandrock, 2017; Sanner et al., 2011).

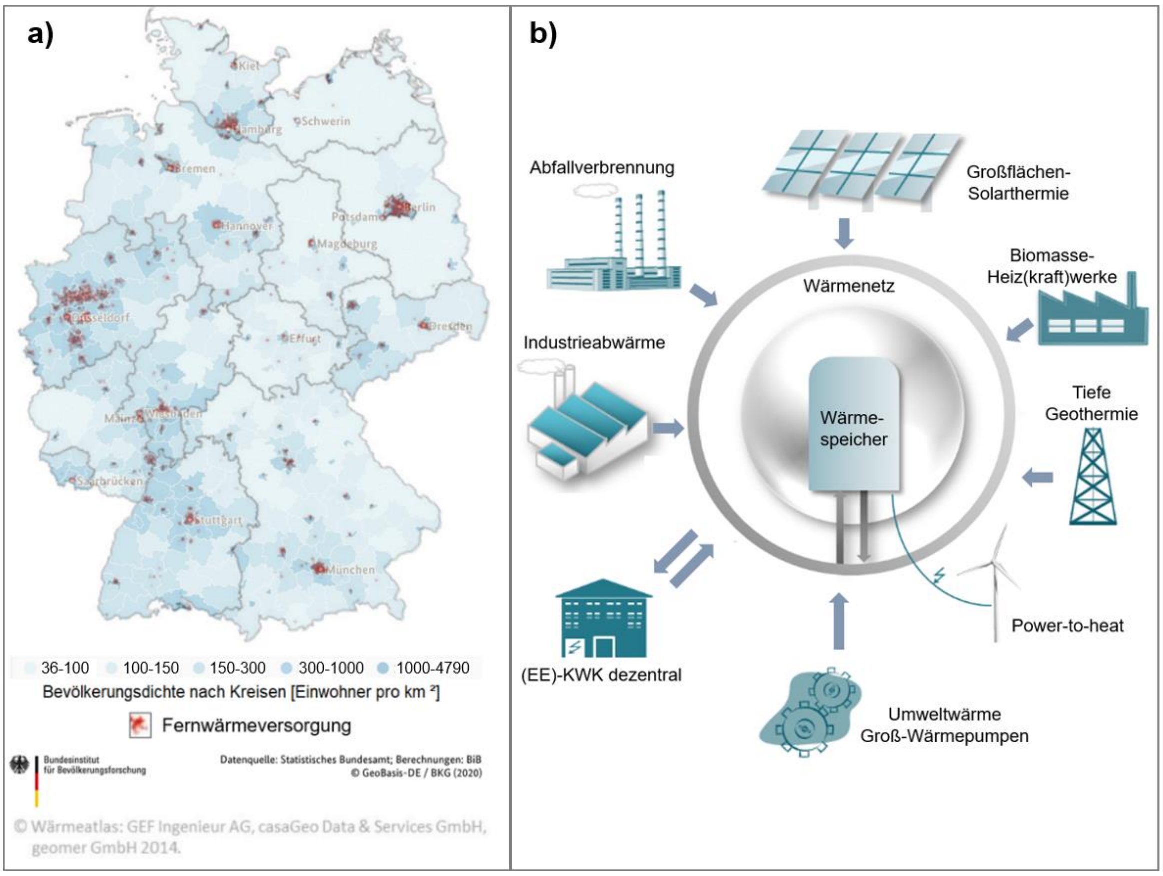

Abb. 1.4: a) Karte der Bevölkerungsdichte in Deutschland (BiB, 2020), überlagert mit der Verteilung bestehender Fernwärmenetze (Wärmeatlas, GEF Ingenieur AG et al., 2014), sowie b) Beispiele für die Einbindung alternativer Energiequellen in ein Fernwärmenetz mit Wärmespeicher (nach Maaß und Sandrock, 2017).

Im Bereich der Kälteversorgung zur Gebäudeklimatisierung dominiert Strom als Energieträger (Abb. 1.2b). Gerade in Geschäftsgebäuden hat die Zunahme technischer Installationen zu stetig steigendem Kühlbedarf geführt, was sich in verschiedenen Ländern bspw. in einer zunehmenden Verschiebung der Lastspitzen in den Stromnetzen von den Winter- in die Sommermonate wiederspiegelt (IEA, 2018; Sanner et al., 2011). Vor dem Hintergrund, dass selbst auf Basis eines relativ optimistischen Klimaszenarios (RCP 4.5; Thomson et al., 2011) Städte auf der nördlichen Hemisphäre, bezogen auf die heutigen klimatischen Bedingungen, jedes Jahr im Schnitt 20 km in südlicher Richtung verschoben werden (Bastin et al., 2019), ist auch weiterhin mit einem stetig steigenden Kühlbedarf zu rechnen (Obringer et al., 2022). Um hierbei den Energiebedarf aktiver Kühlsysteme möglichst niedrig zu halten, ist die verstärkte Nutzung natürlicher Kältequellen wie der Nachtluft oder dem geologischen Untergrund in Kombination mit ebenfalls zu errichtenden bzw. auszubauenden Kältenetzen und –speichern essentiell (Bürger et al., 2017; IEA, 2018; Sanner et al., 2011).

1.2. Energetische Nutzung des Untergrundes

Für die Speicherung von Wärme (oder auch Kälte) werden mit Heißwasser(Tank/Behälter)-Wärmespeichern, Kies/Wasser-Erdbecken-Wärmespeichern, geologischen Eis-Wärme-Speichern, Erdsonden-Wärmespeichern und Aquifer-Wärmespeichern in der Literatur verschiedene Optionen diskutiert (Dincer und Rosen, 2010; Engelmann et al., 2021; Fleuchaus et al., 2018; Meier zu Beerentrup et al., 2021; Schmidt et al., 2003; Abb. 1.5). Da bei Heißwasser(Tank/Behälter)- und Kies/Wasser-Erdbecken-Wärmespeichern jedoch das gesamte Speichervolumen umbaut werden muss, besteht ein ungünstiges Verhältnis zwischen dem verfügbaren Speichervolumen und dem Platzbedarf für die Errichtung der Speicher, welches insbesondere in dicht besiedelten Ballungsräumen mit entsprechend hohen Wärmebedarfsdichten zum Tragen kommt. Demgegenüber bieten geologische Eis-Wärme-Speicher, Erdsonden- und Aquifer-Wärmespeicher den Vorteil der direkten Nutzung des geologischen Untergrundes als Speichermedium (UTES; engl.: underground thermal energy storage).

Bei Erdsonden-Wärmespeichern (BTES; engl. borehole thermal energy storage; Abb. 1.5) wird die Wärme durch Sonden eingebracht bzw. extrahiert. Die Wärmeübertragung erfolgt entsprechend konduktiv ohne direkten Kontakt zwischen Wärmeträgerfluid und dem Untergrund. Dadurch eignen sich diese Speicher hauptsächlich für gering permeable Schichten im Untergrund (Dincer und Rosen, 2010; Fleuchaus et al., 2018). Bei Aquifer-Wärmespeichern (ATES; engl.: aquifer thermal energy storage; Abb. 1.5) werden Infiltrations- bzw. Extraktionsbrunnen zur Wasserzirkulation verwendet, wobei das Grundwasser direkt als Wärmeträgerfluid eingesetzt wird. Dies setzt entsprechend ausreichend permeable Sedimente im Speicherhorizont voraus. Die Nutzung des Untergrundes als Speichermedium bei BTES- und ATES-Anlagen erlaubt gegenüber Tank- und Kies/Wasser-Wärmespeichern entsprechend größere Speichervolumina und weniger Raumbedarf an der Oberfläche, wobei für die großskalige, saisonale Speicherung großer Wärmemengen für Fernwärmenetze insbesondere ATES-Anlagen als geeignet beschrieben werden (Dincer und Rosen, 2010; Engelmann et al., 2021; Fleuchaus et al., 2018).

Für ATES-Systeme gibt es in bestehender Literatur Kategorisierungen in die Temperaturbereiche LT- (engl.: low-temperature), MT- (engl.: mid-temperature) und HT-ATES-Systeme (engl.: high-temperature), wobei die Grenzen zwischen LT- und MT- bzw. zwischen MT- und HT-Systemen je nach Quelle bei maximalen Infiltrationstemperaturen von 25-30 °C bzw. 50-60 °C liegen (Fleuchaus et al., 2020). Trotz teils höheren Temperaturen in früheren Feldversuchen (Holm et al., 1987; Jenne et al., 1992) wird die obere Grenze für HT-ATES-Systeme in neueren Arbeiten bei 90-100 °C verortet (Bauer et al., 2013; Fleuchaus et al., 2020; Nielsen und Vangkilde-Pedersen, 2019).

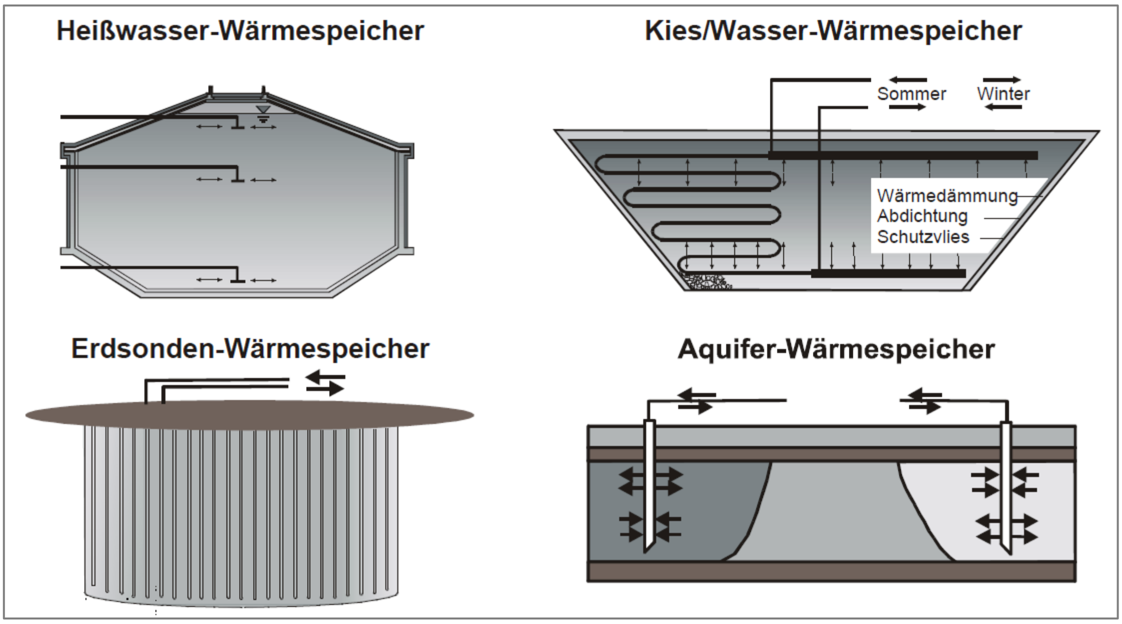

Abb. 1.5: In der Literatur diskutierte Optionen für Langzeit-Wärmespeicher (Schmidt et al., 2003).

Hauptsächlich in den Niederlanden, zunehmend aber auch in Schweden, Belgien und Dänemark, sind LT-ATES-Systeme bei der Wärme- und Kälteversorgung neuer Gebäude(komplexe) bereits als dezentrale Einheiten zur Wärme- (und teilweise Kälte-) Bereitstellung in der kommerziellen Anwendung (Fleuchaus et al., 2018). Werden ATES-Systeme zukünftig jedoch als zentrale (saisonale) Speicher für bereits bestehende und weiter ausgebaute Fernwärmenetze eingesetzt, werden die Temperaturen des ausgespeicherten warmen Wassers für einen möglichst geringen Strombedarf und damit effizienten Betrieb der Wärmepumpen möglichst nahe an den Vorlauftemperaturen der Fernwärmenetzte liegen müssen (Schout et al., 2014), welche derzeit in vielen Bestandsnetzen im Winter noch bei Temperaturen von über 100 °C liegen (Gerhardt et al., 2019). Um Leitungsverluste zu reduzieren und mehr alternative Wärmequellen über Wärmepumpen effizient in die Fernwärmenetze einbinden zu können, wird perspektivisch eine weitere Absenkung der Vorlauftemperaturen in den Wärmenetzen angestrebt, wobei Gerhardt et al. (2019) für das Jahr 2050 65-73 °C als Spannbreite möglicher Vorlauftemperaturen nennen. Solange der nur teil- oder unsanierte Anteil des Gebäudebestandes allerdings zu groß ist, um sinnvoll über dezentrale Nachheizung versorgt zu werden, nehmen Pehnt et al. (2017) 85 °C als weiterhin erforderliche Mindest-Vorlauftemperatur für betroffene Wärmenetze an.

Höhere Speichertemperaturen haben zudem eine höhere Energiedichte im Speicher zur Folge und führen somit zu einem geringeren Raumbedarf (Wang et al., 2021), sowie, bei gleicher Pumpleistung, höheren Wärmeaustauschraten. Um trotz hoher Speichertemperaturen von bis zu 90 °C eine für einen effizienten Betrieb ausreichende Wärmerückgewinnung erzielen zu können, bedarf es dabei möglichst großvolumiger Speicher mit einer möglichst kleinen Oberfläche. Um bspw. Rückgewinnungsraten von 70 % erreichen zu können, schätzen Nielsen und Vangkilde-Pedersen (2019) in einer Beispielrechnung für eine potentielle Niederländische Speicherformation benötigte Speichervolumina von 35000-180000 bzw. 250000-500000 m³ gepumpten Wassers pro Saison für HT-ATES Systeme mit 50 bzw. 90 °C ab. Als Randbedingungen nehmen die Autoren dabei eine hydraulische Durchlässigkeit von $1{,}2 \cdot 10^{-4}$ m/s, eine vertikale Anisotropie der hydr. Durchlässigkeit von 2 bis 5 und eine Filterlänge bzw. Speichermächtigkeit von 50 m an.

Gerade im urbanen Bereich treffen Pläne für unterirdische Wärme- oder auch Kältespeicher jedoch bereits heute auf anthropogen beeinflusste Temperaturfelder: als Ursachen zu nennen sind z. B. das Einbringen von Abwärme (García-Gil et al., 2016b), (unter)irdische Infrastruktur (Taniguchi et al., 2007), Kombinationen aus beidem (Epting et al., 2013) oder thermische Sanierungsmaßnahmen bei Grundwasserschadensfällen (Beyke und Fleming, 2005). Vor dem Hintergrund in verschiedenen Ländern stetig steigender Zahlen installierter geothermischer Anlagen (Bayer et al., 2012) und UTES-Systemen (wenn auch hauptsächlich im Temperaturbereich <25 °C; Bonte et al., 2011), treten vermehrt Befürchtungen bezüglich einer gegenseitigen thermischen Beeinflussung und potentieller langfristiger Umweltauswirkungen dieser und zukünftiger (höhertemperierter) Anlagen auf (Bonte et al., 2011; Hähnlein et al., 2013; Nielsen und Vangkilde-Pedersen, 2019).

Um verschiedene Nutzungen des Untergrundes, wie z. B. thermische Energiespeicher, oberflächennahe Geothermie oder Trinkwasserförderung, ohne negative gegenseitige Beeinflussung zu ermöglichen, empfehlen Bauer et al. (2013) und Bonte (2013) eine sektorübergreifende, unterirdische, dreidimensionale Raumplanung. Ein dafür notwendiger Aspekt ist die Charakterisierung des Raumbedarfes unterirdischer Energie- bzw. Wärmespeicher. Nach Kabuth et al. (2017) kann dabei zwischen a) dem direkt von den technischen Installationen und dem infiltrierten Wasser beanspruchtem „Nutzungsraum“, b) einem umgebenden „Auswirkungsraum“, in dem vom Speicherbetrieb induzierte Effekte wie erhöhte Temperaturen oder eine veränderte Grundwasserzusammensetzung auftreten und c) einem zur Überwachung möglicher Effekte des Speicherbetriebs genutztem „Monitoringraum“ unterschieden werden. Auch Hiester et al. (2022) greifen diese Ideen in einer neueren Studie wieder auf.

Hinsichtlich befürchteter langfristiger Umweltauswirkungen nennen bspw. Bonte et al. (2011) u. a. induzierte Vermischungseffekte, die Freisetzung von Schwermetallen, eine verstärkte Oxidation organischen Materials und von Eisensulfiden, die Mobilisierung ggf. bestehender Grundwasserkontaminanten, sowie Auswirkungen auf das Mikrobiom. Auch der jeweilige Stand von regulativen Bestimmungen und Implikationen für regulative Bestimmungen werden verschiedentlich diskutiert (Bonte et al., 2011; Hähnlein et al., 2013, 2011, 2010; Jesußek, 2012; Nielsen and Vangkilde-Pedersen, 2019; VDI, 2010), wobei Unsicherheiten unter welchen hydrogeologischen Randbedingungen und Speichertemperaturen potentielle Umweltauswirkungen von HT-ATES-Systemen ein relevantes Ausmaß annehmen jedoch entsprechend allgemein gehaltene Vorgaben bzw. Handlungsempfehlungen zur Folge haben: So sieht die VDI-Richtlinie 4640, Blatt 3 (VDI, 2010) bspw. die „Bestimmung einer aus geochemischer Sicht verträglichen Injektions- und Speichertemperatur“, sowie damit einhergehend die Prognose genehmigungsrechtlich relevanter thermischer, hydraulischer und chemischer Auswirkungen auf das Umfeld vor. Und Nielsen und Vangkilde-Pedersen (2019) empfehlen, dass hinsichtlich potentieller Umweltauswirkungen der Fokus u. a. darauf liegen sollte „unvorhergesehene hydro- und geochemische Herausforderungen im Speicherhorizont zu vermeiden“. Entsprechend wird auf die Notwendigkeit von standortbezogenen Einzelfallbetrachtungen und die zentrale Bedeutung eines vorsorgliches Monitoringprogramms für umweltrelevante Grundwasserparameter verwiesen (Nielsen und Vangkilde-Pedersen, 2019).

Insgesamt hemmen bisher sowohl technische, finanzielle, soziale und politische Risiken, als auch genehmigungsrechtliche Aspekte eine breitere Anwendung von ATES-Systemen im Temperaturbereich über 50 °C (Fleuchaus et al., 2020). Sowohl für potentiell genehmigungsrechtlich relevante Umweltauswirkungen, als auch für technische Herausforderungen spielen dabei die mit erhöhten Temperaturen von bis zu 90 °C einhergehenden hydro- bzw. biogeochemischen Prozesse eine wichtige Rolle und waren und sind deshalb Gegenstand der Forschung (Bauer et al., 2013; Fleuchaus et al., 2018; Jenne et al., 1992; Nielsen und Vangkilde-Pedersen, 2019). Die grundlegenden Zusammenhänge hinsichtlich der Temperaturabhängigkeiten in der Löslichkeit von Mineralen und Gasen, in Ionenaustausch- und Sorptionsgleichgewichten, sowie der Verfügbarkeit und Umwandlung von organischer Substanz und von kinetisch limitierten Reaktionen sind dabei bspw. in einer Literaturstudie von Jesußek (2012) zusammengestellt, während folgend der Fokus auf Labor- und Felduntersuchungen zu den hydro- und biogeochemischen Effekten vor dem Hintergrund einer thermischen Energiespeicherung im Untergrund liegt.

1.3. Feld- und Laborversuche zur thermischen Energiespeicherung im geologischen Untergrund

Während die ersten ATES-Systeme in den 1960er-80er Jahren in China im Wesentlichen als Kältespeicher genutzt wurden, begannen in den 1970er Jahren auch Überlegungen und Feldversuche ATES-Systeme als (saisonale) Wärmespeicher zu nutzen (Fleuchaus et al., 2018). Eine verminderte Wärmerückgewinnung durch dichtegetriebenen Aufstieg warmen Wassers, sowie Wärmeverluste an die Oberfläche in einigen dieser Feldversuche, führten zur Empfehlung tiefere, gespannte Aquifere mit ausreichender Permeabilität aber einer geringen natürlichen Grundwasserfließgeschwindigkeit als Speicher zu nutzen (Andersen et al., 1985; Tsang, 1979). Obwohl der Fokus vieler Feldversuche zunächst auf der Charakterisierung der Wärmeausbreitung und der erzielbaren Wärme-Rückgewinnung lag (Molz et al., 1981; Palmer et al., 1992), wurden temperaturinduzierte Sediment-Wasser-Wechselwirkungen, Scaling (Anlagerungen von Mineral-Präzipitaten in den oberirdischen Installationen), Clogging (reduzierte Permeabilität in Brunnen, Filterkies und Aquifer durch bspw. transportierte Feinstpartikel, Mineralausfällungen und Aufwachsen von Mikroorganismen) sowie Korrosionseffekte bereits als Bereiche mit weiterem Forschungsbedarf identifiziert (Tsang, 1979).

Entsprechend folgten in den 1980er und 1990er Jahren Labor- und Feldstudien zur Charakterisierung hydrogeochemischer Effekte beim Betrieb von ATES-Systemen, insbesondere auch im Temperaturbereich 50-115 °C und mit Fokus auf Prozesse, die potentiell die Anlageneffizienz oder den gesamten Anlagenbetrieb beeinträchtigenden können (Kap. 1.3.1). Potentielle Auswirkungen auf die Grundwasserqualität wurden dabei zunächst nur in einzelnen Studien adressiert (z. B. Brons et al., 1991) und kamen erst in den 2010er Jahren vermehrt in den Fokus (z. B. Bonte et al., 2013b, 2013a; Jesußek et al., 2013b, 2013a; Kap. 1.3.2).

1.3.1. Durch erhöhte Temperaturen (oder den Pumpbetrieb) induzierte hydrogeochemische Effekte mit Einfluss auf den Anlagenbetrieb

In verschiedenen Feldversuchen führten Fe- und Mn (Hydr)Oxid-Ausfällungen bei der Wasserextraktion zu Clogging in den Brunnen, was auf a) Vermischungseffekte von Wässern mit verschiedenen Redoxzuständen im Pumpbetrieb bspw. bei der Extraktion aus einem ungespannten Aquifer und einer Absenkung des Wasserspiegels im Extraktionsbereich, b) den Eintritt von Sauerstoff in den oberirdischen Installation oder c) eine durch Druckminderung im Förderbrunnen induzierte CO_2-Ausgasung zurückgeführt wurde (Andersson, 1990; Andersson und Sellberg, 1992; Jenne, 1990; Jenne et al., 1992; Willemsen, 1990). Allerdings existieren als Gegenmaßnahme einerseits Verfahren zur unterirdischen Enteisenung und Entmanganung (Kellner et al., 2016), welche zudem im zyklischen Speicherbetrieb in Abhängigkeit der Fe- und Mn-Reduktionkapazitäten im Speicherhorizont vermutlich nur bis zu deren Erschöpfung benötigt würden. Und andererseits geben aktuelle Leitfaden zur Errichtung von ATES-Systemen mit der Nutzung gespannter, anaerober Aquifere und einer Druckhaltung in den oberirdischen Installationen konzeptionelle Empfehlungen zur Verhinderung von Fe- und Mn (Hydr)Oxid-Ausfällungen (Nielsen und Vangkilde-Pedersen, 2019).

Bei nahezu allen bis dahin durchgeführten HT-ATES-Feldversuchen trat im Zuge der Wassererwärmung eine Übersättigung gegenüber Kalzit auf (Jenne, 1990; Willemsen, 1990). Bei der Erwärmung eisenhaltiger Wässer ist bei entsprechender Übersättigung zudem mit Ausfällungen von Ca-Fe-Mn- und Ca-Mg-Fe-Mn-Mischkarbonaten (Griffioen und Appelo, 1993) sowie von Siderit (Willemsen, 1990) zu rechnen. Zur Verhinderung von Scaling in Wärmetauschern und

Schläuchen bzw. Rohren und Clogging in Infiltrationsbrunnen wurde deshalb untersucht, unter welchen hydrochemischen Bedingungen es zu temperaturinduzierten Karbonatausfällungen kommt und welche Gegenmaßnahmen möglich sind:

Ein erprobter Ansatz Karbonatfällungen zu verhindern, ist die Zugabe von Säure in Form von HCl oder CO_2 (Jenne et al., 1992; Jollien et al., 1992; Koch und Ruck, 1992), wobei jedoch im Zuge der Abkühlung des Wassers eine Nachlösung von Karbonaten im Aquifer beobachtet wurde (Jenne et al., 1992). Dies würde mit jedem Speicherzyklus mehr Säureeinsatz zur Verhinderung einer Karbonatfällung bei erneuter Aufheizung des Wassers erfordern (Willemsen, 1990). Als alternative Technik zur Verhinderung von Karbonatausfällungen wurde der Einsatz von Ionentauschern getestet, um Ca^{2+}-Ionen im Wasser vor der Erwärmung durch je zwei Na^+-Ionen zu ersetzten (Jenne et al., 1992; Perlinger et al., 1987; van Loon und van der Heide, 1992), wobei es im Zuge der Abkühlung des Wassers im Aquifer ebenfalls zu einer Nachlösung von Karbonaten kam (Perlinger et al., 1987). Willemsen und Appelo (1985) und Willemsen (1990) schlugen alternativ vor, die Zugabe von HCl mit einer anschließenden Ausgasung von CO_2 zu kombinieren, um so effektiv das HCO_3^--Ion durch ein Cl^--Ion zu ersetzen und so sowohl die Karbonatfällung bei Erwärmung des Wassers, als auch die Nachlösung von Karbonaten im Aquifer zu unterbinden. Anstatt Karbonat-Ausfällungen zu verhindern, erfolgten auch Überlegungen und Versuche, diese durch die Zugabe von NaOH (Jenne et al., 1992) oder durch die Ausgasung von CO_2 (Jenne, 1990) zu forcieren, um die Präzipitate dann in Reaktionsbecken abzuscheiden, wobei jedoch teilweise auch weiterhin ein Clogging im Infiltrationsbrunnen beobachtet wurde (Jollien et al., 1992). Holm et al. (1987) testeten zudem die forcierte Karbonatfällung in einem Reaktionsbett mit zerkleinertem Kalkstein. Dabei musste die Füllung des Reaktionsbettes im Testbetrieb allerdings alle 1-2 Tage ausgewechselt werden. In der Folge konnten keine Clogging-Effekte im Brunnen beobachtet werden, jedoch führte auch diese Vorgehensweise zu einer Karbonat-Nachlösung bei Abkühlung des Wassers im Aquifer.

Bevor Maßnahmen ergriffen werden, um eine Karbonatfällung aktiv zu verhindern bzw. zu forcieren, sollte das Fällungspotential standortspezifisch anhand einer Erwärmung von Wasserproben vor Ort, im Labor und durch geochemische Modellrechnungen überprüft werden (Nielsen und Vangkilde-Pedersen, 2019; Sanner, 2004; Vail et al., 1992). So zeigten Laborversuche mit natürlichen Sedimenten und Wässern bei Temperaturen von 60-70 °C je nach Sediment bzw. Wasser eine Karbonatlösung, kaum Veränderungen oder eine Karbonatfällung (Bonte et al., 2013b; Jesußek et al., 2013a). Auch bei der Verwendung eines Feld-Teststandes war teilweise bis zu Temperaturen von 70 °C keine Karbonatfällung zu beobachten (Sanner, 2004). Zudem berichtet Snijders (1990), in einem Proceedings-Band ohne genauere Quellenangaben, von Kalzit-Sättigungsindizes von bis zu 1, bei denen in ATES-Feld- bzw. ATES-Pilotversuchen noch keine Karbonatfällung aufgetreten sei.

Allgemein angenommen wird, dass dafür eine Inhibierung der Fällungsreaktion durch im Wasser gelöstes organisches Material, Phosphat (Andersson und Sellberg, 1992; Brons et al., 1991; Griffioen und Appelo, 1993; Snijders, 1990) oder weitere inhibierend wirkende Komponenten (Jenne, 1990) verantwortlich ist. Dabei wird die notwendige Menge des Inhibitors zur Kontrolle einer Kalzitfällung als linear proportional zum Grad der Kalzit-Übersättigung (Ferguson, 1984) und der kombinierte Inhibierungseffekt von gelöstem organischem Kohlenstoff, Phosphat, Magnesium und Sulfat als linear-additiv beschrieben (Matty und Tomson, 1988). Griffioen und Appelo (1993) beobachteten jedoch, dass zwar eine Kalzitfällung effektiv von Phosphat und organischen Säuren inhibiert wurde, aber, bis gelöstes Fe^{2+} weitestgehend verbraucht war, Ca-Fe-Mn- und Ca-Mg-Fe-Mn-Mischkarbonate dennoch präzipitierten.

Sowohl in Feld- (Holm et al., 1987; Jollien et al., 1992; Perlinger et al., 1987; Saito et al., 2016) als auch in Laborstudien (Arning et al., 2006; Bonte et al., 2013b; Jesußek et al., 2013a; Willemsen and Appelo, 1985) wurden bei erhöhten Temperaturen zunehmende gelöste Silicium-Konzentrationen beobachtet, die auf die Lösung von amorphem SiO_2 oder Silikat-Mineralen zurückgeführt werden. Grundsätzlich besteht in der Folge bei der Wärmerückgewinnung aus dem ausgespeicherten Wasser daher die Möglichkeit einer Übersättigung des Wassers gegenüber amorphen SiO_2 oder Silikat-Mineralen und der Bildung entsprechender Präzipitate. Dies ist z. B. aus dem Bereich der tiefen Geothermie bekannt (Gunnarsson und Arnórsson, 2005) und trat auch in Laborversuchen bei der Abkühlung zuvor bei Sedimentkontakt auf 95 °C erwärmten Wassers zurück auf 25 °C auf (Willemsen und Appelo, 1985). Insgesamt werden Si-Ausfällungen in den oberirdischen Installationen aber nur in speziellen Fällen, wie bei sehr leicht löslichem biogenen Silicium im Speicherhorizont (Willemsen und Appelo, 1985) oder bei Speichertemperaturen über 100 °C als relevant eingeschätzt (Jenne, 1990).

Sofern Feinpartikel aus dem Extraktionsbrunnen oder nicht ablagerte Präzipitate durch die oberirdischen Installationen bis in den Infiltrationsbrunnen gespült werden, ist mit zunehmender Betriebsdauer mit einem Clogging im Infiltrationsbrunnen oder im Übergangsbereich zum Aquifer zu rechnen (Andersson, 1990; Molz et al., 1981; Palmer und Cherry, 1984). Um die Infiltrationsleistung wiederherzustellen kann der Wasserfluss kurzzeitig bei maximaler Pumpleistung umgekehrt werden (backflushing) und das zurückgeförderte Wasser dem System entnommen werden (Andersson, 1990; Molz et al., 1981).

Bei Wässern, welche bereits bei der vorliegenden Hintergrundtemperatur gelöste Gaskonzentrationen nahe der Gassättigung aufweisen, kann es sowohl durch Druckentlastung, als auch durch die Aufheizung im Wärmetauscher zur Bildung von Gasblasen kommen, die ebenfalls zu Clogging im Infiltrationsbrunnen führen können (Andersson, 1990; Jenne et al., 1992; van Loon und van der Heide, 1992). Um dies zu verhindern werden sowohl ein fortwährender Überdruck in den oberirdischen Installationen (Jenne et al., 1992; Nielsen und Vangkilde-Pedersen, 2019), als auch der Einsatz einer Entgasungseinheit als Gegenmaßnahmen vorgeschlagen (Andersson, 1990). Liegen gelöste Gase jedoch in Konzentrationen vor, die eine Gasphasenbildung, auch beim in der Speicherformation vorherrschenden Druck, auf Basis der Temperaturerhöhung im Wärmetauscher zur Folge hätten, würde ein Überdruck in den oberirdischen Installationen die Gasphasenbildung lediglich in den Nahbereich des Infiltrationsbrunnens verschieben. Obwohl Auswirkungen auf die Permeabilität im Aquifer als mögliche Folgen benannt werden (Jenne et al., 1992), sind das Ausmaß möglicher hydraulischer Effekte in Abhängigkeit geochemischer Randbedingungen bei der Bildung einer separaten Gasphase im Nahbereich von ATES-Brunnen, oder auch im Anstrom von BTES-Systemen, bisher weitestgehend ungeklärt.

In einzelnen Fällen können auch weitere Prozesse zu Clogging-Problem führen: So kann der Einsatz von Na^+/Ca^{2+}-Ionentauscher, und damit ein erhöhter Na^+-Anteil auf Austauscherplätzen, zu einem Aufschwellen von Tonmineralen (Levy, 1976) und damit zu Clogging im Nahbereich von Infiltrationsbrunnen führen (Jenne, 1990; Jenne et al., 1992; Vail et al., 1992). Für ein HT-ATES-Projekt der Universität Utrecht zeigten geochemische Berechnungen aber bspw. auch, dass sich dies mit einer Verringerung des Anteils den Ionentauscher durchströmenden Wassers auf 60 % verhindern ließe (van Loon and van der Heide, 1992; Willemsen, 1992). Clogging-Effekte durch das temperaturinduzierte Aufwachsen von Mikroorganismen in Infiltrationsbrunnen werden zwar bei ATES-Systemen mit Temperaturen <=40 °C als teilweise problematisch beschrieben, nicht aber bei HT-ATES-Systemen (Andersson, 1990; Lerm et al., 2011; Snijders, 1990).

Hinsichtlich möglicher verstärkender Einflüsse auf Korrosionsprozesse an Brunnenfiltern und Pumpen nennen Andersson (1990) und Jenne et al. (1992) die Zugabe von HCl oder CO_2 zur Verhinderung von Karbonatausfällungen, aber auch erhöhte O_2- und H_2S-Konzentrationen. Brons (1992) weist zudem auf eine verstärkte Metallkorrosion durch sulfatreduzierende Bakterien hin, was bspw. bei einem zwischen 45 und 85 °C betriebenen ATES als Ursache für die Beschädigung von Teilen der Anlage gesehen wird (Lerm et al., 2013).

Zusammengenommen traten insbesondere bei frühen ATES-Feldversuchen und ATES-Pilotversuchen in den 80er und 90er Jahren in Abhängigkeit u. a. hydrogeochemischer, standortspezifischer Rahmenbedingungen verschiedene technische Schwierigkeiten auf. Neuere Leitfäden zur Errichtung von ATES-Systemen adressieren diese jedoch (Nielsen und Vangkilde-Pedersen, 2019) und nennen einerseits sowohl konzeptionelle Vorschläge um deren Auftreten von vorne herein zu vermeiden bzw. die Effekte zu minimieren, schlagen falls benötigt andererseits aber auch konkrete technische Optionen zur Wasserbehandlung vor.

1.3.2. Temperaturinduzierte hydrogeochemische Effekte auf umweltrelevante Grundwasserkomponenten

Während die zuvor genannten hydrogeochemischen Effekte hauptsächlich innerhalb der technischen Installationen oder im Übergang zum Aquifer auftreten und somit hauptsächlich den Betrieb von ATES-Anlagen betreffen, können die durch die Einspeicherung von Wärme erhöhten Temperaturen im Untergrund auch Konzentrationsänderungen bei weiteren Grundwasserkomponenten zur Folge haben. Umwelt- und damit ggf. genehmigungsrelevante Komponenten oder Stoffgruppen sind dabei durch entsprechend vorliegende Geringfügigkeitsschwellenwerte (LAWA, 2017) oder Schwellenwerte (GrwV; BMJ, 2010) für das Grundwasser bzw. den diesen teilweise zugrundeliegenden Grenz- (TrinkwV; BMJ, 2001) oder Richtwerten (WHO, 2017) für das Trinkwasser gekennzeichnet (Table S.3.6).

Feld- (Saito et al., 2016; Willemsen und Appelo, 1985) und Laborstudien mit Aquifersedimenten (Bonte et al., 2013b, 2013a; Brons et al., 1991; Jesußek et al., 2013a) zeigten bei Temperaturerhöhungen einen Anstieg des gelösten organischen Kohlenstoffes (DOC). Zum Teil ist dies auf eine Desorption organischer Verbindungen als direkte Folge der Temperaturerhöhung zurückzuführen (Evanko and Dzombak, 1998; Ten Hulscher and Cornelissen, 1996; Xu and Saiers, 2010). Auch Durchflusssäulenversuche von Bonte et al. (2013b) und Durchflusssäulenversuche in Kombination mit Batchversuchen von Jesußek et al. (2013a) zeigten, gerade bei den höchsten untersuchten Temperaturen von 60 und 70 °C, mit einer je nach Sediment unterschiedlich stark ausgeprägten initialen Freisetzung und entsprechenden DOC-Konzentrationsmaxima, Hinweise auf eine sich mit der Zeit abschwächende Desorption von organischem Material. Ab welchen Temperaturen überhaupt erhöhte DOC-Konzentrationen auftraten, variierte dabei in Abhängigkeit der untersuchten Sedimente und betrachteten Temperaturen zwischen 25 und 60 °C. Bilden organische Säuren einen Anteil der desorbierten organischen Verbindungen (Filius et al., 2000), kann dies zu einer Absenkung des pH-Wertes führen (Jesußek et al., 2013a) und entsprechend Einfluss auf das Karbonatsystem nehmen (Brons et al., 1991).

Darüber hinaus führten die erhöhten Temperaturen auch zu einer verstärkten Umwandlung sedimentären organischen Materials (Andersson und Nilsson, 2001; Brons et al., 1991; Willemsen und Appelo, 1985), wobei der Einfluss dieses Prozesses auf die DOC-Konzentration auf dem Verhältnis der Raten der aufeinander folgenden Umwandlungsschritte basiert (Christ und David, 1996; Robador et al., 2010). Nach Robador et al. (2010) sammelt sich dabei insbesondere der nicht bioverfügbare Anteil des organischen Kohlenstoffs in der fluiden Phase an. Durch eine verstärkte mikrobiell katalysierte Umwandlung des bioverfügbaren Anteils des organischen Kohlenstoffes kann es zudem in der Folge, je nach Reduktionsreaktion, zu Konzentrationsanstiegen der entsprechenden Reaktionsprodukte (CO_2, NO_2^-, N_2, Mn^{2+}, Fe^{2+}, H_2S und CH_4; z. B. Appelo und Postma, 2005) kommen. Dabei ist bei einer Temperaturerhöhung durch die Einspeicherung von Wärme insgesamt mit der Ausbildung stärker reduzierender Bedingungen zu rechnen: So beobachten Jesußek et al. (2013a) in Durchflusssäulenversuchen mit einem tertiären Braunkohlesand und Sediment-Wasser-Kontaktzeiten von 36 Stunden bei allen untersuchten Temperaturen (10, 25, 40 und 70 °C) eine Nitratreduktion (wobei die Rate mit der Temperatur stetig zunahm), während eine Fe(III)-Reduktion erst bei 25 °C einsetzte und eine Sulfatreduktion nur bei 70 °C auftrat. In auf 5, 11, 25 und 60 °C temperierten Säulenversuchen mit zwei fluviatilen, pleistozänen Sanden und längeren Sediment-Wasser-Kontaktzeiten von bis zu 30 Tagen, setzte je nach Sediment hingegen bereits bei 5 oder 25 °C eine mit zunehmender Temperatur schneller ablaufende Sulfatreduktion ein (Bonte et al., 2013a). Eine Sulfatreduktion bei 5 und 11 °C, sowie zusätzlich eine Methanogenese bei 25 °C konnte dabei nur im Versuchsansatz mit der geringeren temperaturinduzierten DOC-Freisetzung beobachtet werden, was entsprechend darauf hindeutet, dass die DOC-Freisetzung als genereller Indikator für das zu erwartende Ausmaß von Verschiebungen im Redoxsystem ungeeignet ist. In einem weiteren Versuchsansatz mit schrittweiser Temperaturerhöhung von 5 bis 80 °C beobachten Bonte et al. (2013a) bei ~50 °C eine gegenüber geringeren und höheren Temperaturen stark verminderte Sulfatreduktion, sowie eine bei Temperaturen ≥50 °C abrupt stoppende Methanproduktion. Um die Temperaturabhängigkeit der Sulfatreduktion ohne variable Verfügbarkeit organischen Materials zu untersuchen, führten Jesußek et al. (2013b) weitere Durchflusssäulenversuche unter Zugabe von Acetat im Säulenzulauf durch. Dabei trat im Gegensatz zu den Versuchen mit natürlichem Sediment ohne Acetatzugabe (Jesußek et al., 2013a) sowohl bei 70, als auch bei 10, 25 und 40 °C eine Sulfatreduktion auf, welche bei 40 °C am schnellsten einsetzte und auch die höchsten Ratenkonstanten aufwies. Bei 25 °C kam auch in diesem Versuch eine Methanogenese hinzu. Eine mögliche Erklärung für die Beobachtungen von Bonte et al. (2013a) und Jesußek et al. (2013b) ist eine Limitierung im Wachstum der jeweiligen, die Redoxprozesse katalysierenden Mikroorganismengemeinschaften bei bestimmten Temperaturen im Zusammenspiel mit der bei ansteigenden Temperaturen erhöhten Verfügbarkeit organischen Materials. So fällt bspw. die verminderte Sulfatreduktion bei 45-50 °C mit dem Übergang von mesophilen zu thermophilen Mikroorganismengemeinschaften zusammen (Brielmann et al., 2011).

Neben temperaturinduzierten Verschiebungen im Redoxmilieu, kann eine Temperaturerhöhung die Grundwasserqualität auch durch Konzentrationsänderungen bei Spurenkomponenten und Schwermetallen beeinflussen: So beobachten Bonte et al. (2013b) in Säulenversuchen mit drei verschiedenen quartären Sanden bei 25 und 60 °C erhöhte As-Konzentrationen und bei 60 °C erhöhte Konzentrationen von P, Mo, V, B und F gegenüber den Versuchen bei 10 °C. Zudem traten in einem geothermisch genutzten Aquifer bei Temperaturen von bis zu 40 °C verringerte Konzentrationen von B, Cd und Ni auf, während Ba-Konzentrationen mit der Temperatur anstiegen (García-Gil et al., 2016b). Bei einem Feldversuch in einem holozänen Aquifer mit bis zu 25 °C stiegen B- und Li-Konzentrationen zunächst an, näherten sich bei einer nachfolgenden Abkühlung jedoch auch wieder den Ausgangswerten an (Saito et al., 2016). Eine Ursache für Konzentrationsänderungen bei Spurenkomponenten und Schwermetallen liegt in der Temperaturabhängigkeit von Ionenaustausch- bzw. Sorptionsgleichgewichten, wie z. B. von Jesußek (2012) für verschiedene Haupt- und Spurenkomponenten zusammengestellt. So vermuten Bonte et al. (2013b) auch Desorptionsprozesse als Hauptquelle für die As-Freisetzung in ihren Versuchen. Eine weitere Quelle kann auch die temperaturinduzierte reduktive Lösung von Eisen(III)-(Hydr)oxiden sein (Jesußek et al., 2013a), da so auch darin eingebaute oder daran sorbierte Spurenkomponenten bzw. Schwermetallen mobilisiert werden (Appelo und Postma, 2005; Smedley und Kinniburgh, 2002). Wird ein Teil des gelösten Fe(II) im Zuge einer ggf. ebenfalls temperaturinduziert auftretenden Sulfatreduktion (Bonte et al., 2013a; Jesußek et al., 2013a, 2013b) wieder in Eisensulfiden gebunden, können in diesen dann auch wieder Spurenkomponenten bzw. Schwermetalle eingebaut werden (Bonte et al., 2013b).

Insgesamt sind Untersuchungen hinsichtlich des Temperatureinflusses auf die Freisetzung von Spurenelementen und Schwermetallen aus natürlichen Aquifersedimenten im Temperaturbereich >40 °C bisher jedoch im Wesentlichen auf die Laborversuche von Bonte et al. (2013b) beschränkt, sodass die Datenbasis kaum ausreichend ist, um die Spannbreite möglicher Effekte für die Vielzahl zu betrachtender Spurenkomponenten und Schwermetalle zu erfassen. Darüber hinaus weisen Saito et al. (2016) und Van Breukelen und Bonte (2016) auf den bisher unbekannten Grad der Reversibilität temperaturinduzierter Konzentrationsänderung von Spurenkomponenten und

Schwermetallen hin, welcher bspw. die räumliche Ausbreitung von Konzentrationsänderungen im Abstrom erwärmter Aquiferbereiche entscheidend beeinflusst.

1.3.3. Weitere temperaturinduzierte hydrobiogeochemische Effekte

1.3.3.1. Temperatureinfluss auf das Grundwassermikrobiom

Neben potentiellen Auswirkungen auf die Grundwasserchemie werden auch temperaturinduzierte Veränderungen in der mikrobiellen Gemeinschaft und damit einhergehend ggf. Beeinträchtigungen in der Bereitstellung von Ökosystemfunktionen des Grundwassermikrobioms wie z. B. der Reinigung des Wassers, dem Schadstoffabbau und der Eliminierung pathogener Mikroorganismen (Brielmann et al., 2011; Griebler et al., 2016), sowie auch das potentielle Aufwachsen von pathogenen Mikroorganismen (Brielmann et al., 2009) als Risiken von unterirdischen Wärmespeichern genannt.

Ein durch erhöhte Temperaturen ausgelöstes vermehrtes Auftreten pathogener Mikroorganismen wurde bisher allerdings weder in Säulenversuchen (Brielmann et al., 2011), noch in einem nachgebauten Aquifer bei Temperaturen bis zu 55 °C (Adinolfi and Ruck, 1992) oder bei der Überwachung eines Feldversuches mit Temperaturen bis 80 °C (Jollien et al., 1992) beobachtet. García-Gil et al. (2018) stellten in einem geothermisch genutzten Aquifer zudem eine Verringerung pathogener Mikroorganismen bei erhöhten Temperaturen fest.
Wie es aufgrund jeweils spezifischer Temperaturoptima psychrophiler, psychrotoleranter, mesophiler oder thermophiler Arten zu erwarten ist (Brielmann et al., 2011), führten erhöhte Temperaturen jedoch zu einer verringerten mikrobiellen Diversität im Zusammenspiel mit größeren Abundanzen bestimmter Mikroorganismen (Brielmann et al., 2011; Jollien et al., 1992; Lerm et al., 2013, 2011; Lienen et al., 2017). Ob und inwieweit bei Temperaturerhöhungen dabei ggf. Ökosystemfunktionen beeinträchtigt werden und wie reversibel das Grundwassermikrobiom auf zyklische Temperaturänderungen reagiert, ist deshalb auch weiterhin Gegenstand aktueller Feldstudien (Projekt TestUM-II), wobei Ergebnisse von diesem Standort im Temperaturbereich bis 35 °C bisher keine signifikanten Veränderungen in der Zusammensetzung der mikrobiellen Gemeinschaft und den auftretenden Abundanzen zeigten (Keller et al., 2021).

1.3.3.2. Interaktion von Wärmespeichern mit Grundwasserkontaminationen

Wärmespeicher im geologischen Untergrund erfordern hydrogeologisch geeignete Speicherformationen. In den drei Stadtstaaten Berlin, Hamburg und Bremen, als Beispiele für urbane Gebiete in Deutschland, gibt es im Mittel allerdings ca. eine Altlast bzw. fünf altlastverdächtige Flächen pro km² (Datenbasis: UBA, 2022). Damit bei ansonsten vorhandener Eignung eines Standortes auch kontaminierte Bereiche potentiell als Wärmespeicher genutzt werden könnten, bedarf es jedoch entsprechender Kenntnisse über das Verhalten häufig vorkommender organischer Kontaminanten bei erhöhten Temperaturen. Kann eine Wärmespeicherung dann zu einer beschleunigten Sanierung oder auch nur zur Verhinderung einer weiteren Ausbreitung der Schadstoffe beitragen, könnten diese Bereiche so wieder einer sinnvollen Nutzung zugeführt werden (Brielmann et al., 2011; Picone et al., 2019; Slenders et al., 2010; Sommer et al., 2013).

Grundsätzlich können Veränderungen in der Temperatur dabei Auswirkungen auf die Löslichkeiten (Huang und Hong, 2002; Knauss et al., 2000; Koproch et al., 2019; Schwarz, 1977; Schwarz und Miller, 1980), Lösungsraten (Imhoff et al., 1997; Koproch et al., 2022), Gasphasenbildung bzw. Verflüchtigung (Arp und Schmidt, 2004; Gosset, 1987; Hegele und Mumford, 2014; Heron et al., 1998; Metzgen et al., 2021; Mumford et al., 2021; Schwardt et al., 2021), Sorptionsgleichgewichte (Bell und LeBoeuf, 2013) bzw. –Kinetiken (Cornelissen et al., 1997; ten Hulscher und Cornelissen, 1996) und den Abbau (Metzgen et al., 2022; Němeček et al., 2018; Zuurbier et al., 2013) von organischen Schadstoffen haben.

In Summe wird aber z. B. bei substratunterstütztem, mikrobiell katalysierten Schadstoffabbau mit einer Verbesserung der Abbau-Effektivität durch erhöhte Temperaturen und damit verkürzten Sanierungszeiten gerechnet (Wang et al., 2022), wobei für eine nachhaltige Umsetzung der thermischen Unterstützung auch auf mögliche Synergieeffekte mit ATES- und BTES-Systemen verwiesen wird. Weitere Studien betrachten vor dem Hintergrund einer Kombination aus Wärmespeicherung und Altlastensanierung auch das Zusammenspiel erhöhter Temperaturen mit bestehenden Sanierungstechnologien wie Fe(0)-Reaktionswänden (Metzgen et al., 2022) und dem Einsatz von Fe(0)-Nanopartikeln (Schwardt et al., in prep.), wobei erhöhte Temperaturen zu gesteigertem Abbauverhalten führten.

Insgesamt wird dabei für die Feldskala die Wahl eines geeigneten Temperaturniveaus für eine Optimierung der Abbauprozesse und der Sanierung als Herausforderung gesehen, da dies durch Prozess-Interaktionen von standort- und substanzspezifischen Parametern kontrolliert wird (Koproch et al., 2019; Wang et al., 2022).

1.4. Prognostizierbarkeit thermisch induzierter hydrogeochemischer Prozesse

Während sich dezentrale LT-UTES-Systeme zunehmend auch im kommerziellen Einsatz etablieren (Fleuchaus et al., 2018), ist dieser Durchbruch für saisonale betriebene HT-UTES-Systeme als potentielle Bausteine zukünftiger, regenerativ betriebener Wärmeversorgungssysteme bisher ausgeblieben. Trotz der verschiedenen Feld- und Laborstudien in den letzten Jahren und Jahrzehnten (Kap. 1.3), spielen dabei nach wie vor auch Unsicherheiten hinsichtlich temperaturinduzierter hydrogeochemischer Effekte eine Rolle (Fleuchaus et al., 2020).

So weisen die bestehenden Laboruntersuchungen im Temperaturbereich >50 °C trotz grundlegend immer wieder auftretender Prozesse (bspw. verstärkte Übersättigung und ggf. Ausfällung von Karbonatmineralen, Freisetzung und Umwandlung organischen Materials und dadurch tendenziell reduzierendere Bedingungen, sowie Mobilisierung bzw. Festlegung von Spurenkomponenten; s. Kap. 1.3.1 und 1.3.2) auf relevante Unterschiede in Ausmaß und Dauer der temperaturinduzierten Konzentrationsänderungen in Abhängigkeit der jeweiligen Sediment- bzw. Wasserzusammensetzung hin (vergl. z. B. Bonte et al., 2013b, 2013a; Jesußek et al., 2013a).

Daher könnten prognostische Voruntersuchungen sowohl bei der technischen Auslegung von ATES-Systemen helfen, als auch genehmigungsrechtliche Aspekte wie die räumlichen und zeitlichen Skalen bei der Reversibilität induzierter hydrogeochemischer Effekte adressieren. Die in bisherigen Laborstudien zur Untersuchung des Temperatureinflusses auf Sediment-Wasser-Wechselwirkungen häufig genutzten Batch- (Arning et al., 2006; Jesußek et al., 2013a; Kap. 4), Durchfluss- (Bonte et al., 2013b, 2013a; Griffioen und Appelo, 1993; Jesußek et al., 2013a, 2013b; Kap. 2) und Kreislaufsäulenversuche (Kap. 3) können je nach Auslegung jedoch maßgeblich bei Sediment-Wasser-Kontaktzeiten, Sediment-Wasser-Verhältnissen, der Betrachtung stofflich offener bzw. geschlossener Versuchssysteme und bei der Betrachtung eines statischen bzw. geschüttelten (Batchversuche) oder durchströmten Systems (Säulenversuche) variieren.

Demgegenüber stehen insbesondere im zyklischen Speicherbetrieb bei ATES-Systemen mit ihren zeitlich und räumlich variablen Temperatur- und Strömungsbedingungen verschiedene Systembereiche:

a) Brunnennahbereiche die während der Pumpphasen jeweils von Infiltration (bzw. Extraktion) und den entsprechenden Temperaturen dominiert werden;
b) Übergangsbereiche zum weiteren Umfeld des Speicherhorizontes, in welchen im Vergleich zum Nahbereich längere Kontaktzeiten, teilweise bereits wieder abnehmenden Temperaturen, sowie Vermischungseffekten zwischen infiltriertem und residualem Wasser zusammenkommen;
c) abstromige Bereiche, in denen zuvor erwärmtes Wasser bereits wieder abgekühlt und durch Vermischungseffekte verdünnt ist;
d) die oberirdischen Installationen (bspw. bei der Erwärmung bzw. Abkühlung des Wassers im Wärmetauscher).

Konzeptionell können initiale Temperatureffekte auf die Wasserzusammensetzung für die Bereiche a) und d) durch eine Temperierung von Wasser- (d), bzw. Wasser-Sediment-Gemischen (a) für verschiedene Temperaturen, sowie Temperierungs- bzw. Kontaktzeiten angenähert werden. Ungleich komplizierter gestaltet sich die Annäherung an eine Kombination aus variierenden Temperaturbedingungen mit Vermischungsprozessen und einer Verlagerung der Wassermassen im zyklischen Speicherbetrieb, sodass Laborversuche in dieser Hinsicht häufig lediglich Teilaspekte unter definierten Randbedingungen betrachten.

Da für verschiedene Wärmespeicher-Feldversuche (Andersson, 1990; Andersson und Sellberg, 1992; Holm et al., 1987; Jenne et al., 1992; Jollien et al., 1992; Molz et al., 1981; Němeček et al., 2018; Opel et al., 2014; Perlinger et al., 1987; Saito et al., 2016; Ueckert und Baumann, 2019; van Loon und van der Heide, 1992) allerdings keine systematischen Vergleiche mit begleitenden Laborversuchen mit Standortsediment und -wasser vorliegen, ist bisher weitestgehend ungeklärt, inwieweit sich die verschiedenen Laborversuchsansätze bzw. Kombinationen aus verschiedenen Laborversuchsansätzen als Prognoseinstrumente für temperaturinduzierte hydrogeochemische Effekte für die unterschiedlichen Systembereiche eines ATES-Systems eignen.

1.5. Zielsetzung der Arbeit

Obwohl das bessere Verständnis temperaturinduzierter hydrogeochemischer Effekte selbst nur eine von mehreren Säulen für die Unterstützung des zukünftigen Einsatzes von unterirdischen Wärmespeichern darstellen kann, stecken hinter diesem Oberbegriff bereits eine Vielzahl verschiedener Einzelaspekte, die bisher in unterschiedlicher Tiefe in vorrausgegangenen Studien untersucht wurden:

So lag der Fokus bisheriger Studien im Bereich möglicher hydrogeochemischer Einflüsse auf den Anlagenbetrieb im Wesentlichen auf den hydrochemischen Randbedingungen und dem Ausmaß und möglichen Gegenmaßnahmen von Korrosions- und Mineralfällungsprozessen mit besonderem Augenmerk auf der Karbonatfällung (Kap. 1.3.1). Die Möglichkeit einer thermisch induzierten Gasphasenbildung und daraus potentiell folgende negative Auswirkungen auf den Speicherbetrieb wurde zwar bereits verschiedentlich genannt, in welchem Ausmaß und mit welchen Auswirkungen eine Gasphasenbildung in Abhängigkeit hydrochemischer Randbedingungen zu erwarten ist, jedoch bisher nicht untersucht. Hier setzt, anhand von Laborversuchen und Modellrechnungen, Kapitel 2 dieser Dissertation mit dem Titel

„Gas-phase formation during thermal energy storage in near-surface aquifers: experimental and modelling results“

an, in dem folgenden Fragen adressiert werden:

i. Können thermodynamische Berechnungen die experimentell bestimmte Gasphasenbildung reproduzieren und eignen sich daher als Werkzeug zur Abschätzung einer möglichen thermisch induzierten Gasphasenbildung im Aquifer?
ii. Welches Ausmaß einer Gasphasenbildung kann bei unterschiedlichen geochemischen Randbedingungen bei der oberflächennahen Wärmespeicherung erwartet werden?
iii. Welche hydraulischen und thermischen Effekte mit Einfluss auf die Effizienz eines Wärmespeichers kann eine Gasphasenbildung zur Folge haben?

*[Kapitel 2 basiert auf einem im Jahr **2016** von Lüders, K., Firmbach, L., Ebert, M., Dahmke, A., Dietrich, P. & Köber, R. in Environmental Earth Sciences 75:1404 publiziertem Paper.]*

Bezüglich möglicher Effekte auf die Grundwasserqualität untersuchten bereits einige Studien die temperaturabhängige Freisetzung und mikrobiell katalysierte Umwandlung von organischem Kohlenstoff, sowie die damit einhergehenden Verschiebungen in der Redox-Zonierung (Kap. 1.3.2.). Auch die Freisetzung von Spurenkomponenten und Schwermetallen stand bereits im Fokus einzelner Arbeiten. Ohne jedoch dabei experimentell auch die Wiederfestlegung bei Abkühlung zu betrachten, blieb ein wesentlicher Aspekt für die Abschätzung der räumlichen Ausdehnung temperaturinduziert erhöhter Konzentrationen dieser Komponenten offen. Mit vier verschiedenen Aquifersedimenten als Untersuchungsgrundlage liegt der Fokus in Kapitel 3 dieser Dissertation mit dem Titel

“Temperature influence on mobilisation and (re)fixation of trace elements and heavy metals in column tests with aquifer sediments from 10 to 70 °C”

daher insbesondere auf den folgenden Fragen:

i. Welche komponentenspezifischen und zeitlichen Zusammenhänge zwischen den Temperaturbedingungen und den Spurenkomponenten- und Schwermetallkonzentrationen bestehen für die untersuchten Sedimente? Und wie reversibel sind die Konzentrationsänderungen unter variierenden Temperaturbedingungen?
ii. Wie Verhalten sich die temperaturinduzierten Konzentrationsänderungen von Spurenkomponenten und Schwermetallen im Verhältnis zu den Konzentrationsunterschieden in den Grundwässern im Kontakt zu den verschiedenen Aquifersedimenten bei natürlichen Grundwassertemperaturen?
iii. Für welche Elemente kann eine hohe Priorität bei zukünftigen hydrogeochemischen Vorabuntersuchungen an UTES-Standorten festgestellt werden?

[Kapitel 3 basiert auf einem im Jahr ***2020*** *von Lüders, K., Dahmke, A., Fiedler, M. & Köber, R. in Water Research 169 – 115266 publiziertem Paper.]*

Zudem stellt sich in Anbetracht verschiedener möglicher Monitoringpunkte auf der Feldskala und verschiedener Optionen an Laborversuchen grundsätzlich die Frage, inwieweit prognostische Voruntersuchungen bei der Abschätzung räumlich und zeitlich variabler temperaturinduzierter hydrogeochemischer Effekte auf der Feldskala helfen können. Allerdings legen bisherige Studien in diesem Themenfeld den Fokus entweder auf die Feldskala oder auf Laborversuche, jedoch nicht auf die beiden Skalen kombinierende Untersuchungsansätze (Kap. 1.4). Vor diesem Hintergrund wird in Kapitel 4 dieser Dissertation mit dem Titel

“Predictability of initial hydrogeochemical effects induced by short-term infiltration of ~75 °C hot water into a shallow glaciogenic aquifer”

durch die Kombination eines hydrochemisch zeitlich und räumlich eng überwachten Feldversuches, bei dem über 4,5 Tage Wasser mit bis zu 78 °C infiltriert wurde, und begleitenden Batchversuchen mit 28 Sedimentproben von der Testfeldlokation untersucht,

i. welche im Rahmen des Feldversuches beobachteten initialen, komponentenspezifischen, temperaturabhängigen geochemischen Effekte, in welchem Umfang mit den Laborversuchen prognostiziert werden können und
ii. wie die geochemische Heterogenität der untersuchten Sedimente die Varianz im geochemischen Verhalten auf der Labor- und Feldskala beeinflusst.

[Kapitel 4 basiert auf einem im Jahr ***2021*** *von Lüders, K., Hornbruch, G., Zarrabi, N., Heldt, S., Dahmke, A. & Köber, R. in Water Research X 13 – 100121 publiziertem Paper.]*

Abschließend werden die Ergebnisse aus diesen drei Kapiteln mit den weiteren im Kap. 1.3 angesprochenen temperaturinduzierten hydrogeochemischen Effekten in einem übergeordneten Kapitel Zusammenfassung und Ausblick (Kap. 5) eingeordnet, um daraus noch offene Fragen, weiteren Forschungsbedarf und mögliche Wege in eine beschleunigte Anwendung unterirdischer Wärmespeicher zu diskutieren.

2. Gas-phase formation during thermal energy storage in near-surface aquifers: experimental and modelling results

This chapter is based on a paper published 2016 by Lüders, K., Firmbach, L., Ebert, M., Dahmke, A., Dietrich, P. & Köber, R. in Environmental Earth Sciences 75:1404. https://doi.org/10.1007/s12665-016-6181-5

2.1. Abstract

Heating of groundwater by thermal energy storage (TES) poses a potential for the formation of a separate gas phase. Necessary boundary conditions, potential effects and monitoring feasibility of this process were not focused within previous studies. Since the formation of a gas phase could change groundwater flow conditions, hydrochemistry, porous media properties and thus efficiency of TES applications, improved understanding of the process is needed.

The temperature of percolated sediment column tests was adjusted to 10, 25, 40 and 70 °C to quantify temperature induced physical gas-phase formation and its effect on electrical resistance. Gas-phase formation, its accumulation and effects on hydraulic conductivity, heat conductivity and -capacity were investigated using scenario calculations based on a closed loop borehole thermal energy storage system at 60 °C for different geochemical conditions.

Experimentally quantified degassing ratios were within the expected range of thermodynamic calculations. The laboratory time-lapse electrical resistivity measurements proofed as a suitable tool to identify the onset and location of the gas-phase formation. Depending on the geochemical conditions, hydraulic conductivity in the area of the simulated heat storage site decreased between 60 % and up to one order of magnitude in consequence of degassing within the scenario calculations. Heat conductivity and -capacity decreased by maximally 3 and 16 %, respectively. The results indicate that gas-phase formation as a result of aquifer heating can have pronounced effects especially on groundwater flow conditions and therefore should be considered particularly for nearly or fully gas saturated groundwater and aquifers containing gas sources.

2.2. Introduction

Changes in global energy supply towards more renewables are necessary to achieve worldwide objectives of climate protection (IEA, 2015). Renewable energies reached 27.8 % of the gross electricity consumption in Germany by 2014 and took over the role as most important power source from the brown coal (BMWi, 2015). Beside the achievements in electricity generation, the share of renewable energies on heat production remained at around 10 % since 2010 (BMWi, 2015), although especially heating and acclimatisation hold capacious potentials to reduce CO_2 emissions (IEA, 2015). Improvements in efficiency as e.g. storing surplus heat from solar thermal applications or industrial processes in shallow aquifers is a feasible possibility to enhance the share of renewable energies on heat supply (Schmidt and Müller-Steinhagen, 2005). In addition, Bauer et al. (2015) suggest not only to use surplus heat but to convert surplus energy from other renewable power generation technologies as e.g. wind energy into heat for seasonal heat storage in the subsurface. For underground thermal energy storage (UTES) applications Schmidt and Müller-Steinhagen (2005) reported maximum temperatures of ~90 °C. Near surface aquifers can also be used for cyclic storage of heat and cold for heating and climatisation of houses or commercial buildings in winter- and summer times (Bridger and Allen, 2005).

Besides these potential economic advantages, the installation and operation of geothermal plants using near surface aquifers for heat storage may affect hydrological and hydro-geochemical properties of the underground. Since there is no monitoring obligatory, only some single point measurements at greater plants have been carried out but are rarely published. For example, Possemiers et al. (2014) analysed the temperature changes induced by seven aquifer thermal energy storages (ATES). Their results indicate no immediate risk for groundwater quality. On the other hand, Bockelmann et al. (2012) found at a geothermal system with 36 borehole heat exchangers (BHS) an inefficient operation indicated by more heat injection in summer time than extraction in winter. This results in a warming of the underground to such a high level that the plants cooling mode is impaired. Given the lack of time and cost efficient spatial high-resolution monitoring methods and the “unfinished business” in national and international regulations (Bonte et al., 2011; Ferguson, 2009; Hähnlein et al., 2010) concerns arise about possible negative long-term impacts for groundwater and soil.

Temperature changes in the shallow subsurface induced by underground thermal energy storage (UTES) may alter groundwater geochemistry through reactions triggered by the temperature dependence in the solubility of minerals and gases, sorption and ion exchange equilibria or kinetic rate constants. Previous studies mainly focused on sediment-water-interactions (Arning et al., 2006; Bonte et al., 2013b, 2013a; Brons et al., 1991; Griffioen and Appelo, 1993; Holm et al., 1987; Jesußek et al., 2013a; Possemiers et al., 2014; Saito et al., 2016; Willemsen and Appelo, 1985) while the formation of a separate gas phase which gets favoured by the decreasing gas solubilities with induced temperatures increases was addressed only marginally. Jenne et al. (1992) suggested to keep up an overpressure in aquifers with high dissolved gas concentrations to avoid the formation of a separated gas phase. Bonte (2013) proposed the observation of partial gas pressures within aquifers in running heat storage applications to monitor the possibility of a gas-phase formation. None of the studies investigated the specific physical and geochemical aquifer preconditions favouring or preventing the formation of a separate gas phase. The initial dissolved gas concentrations with respect to the corresponding solubility are key factors to assess the probability of a gas-phase formation. Unfortunately, except oxygen and carbon dioxide, dissolved gas concentrations are not measured as a matter of routine. O_2 concentrations tend to be lower in near surface aquifers than in equilibrium with the atmosphere as O_2 concentrations decrease by oxygen consumption in the vadose zone and the aquifer in case organic material and/or reduced substances as e.g. metal sulphides are available (e.g. Appelo and Postma, 2005). In contrast N_2 concentrations will rather increase due to nitrate reduction (e.g. Appelo and Postma, 2005) leading to higher dissolved concentrations of N_2 compared to equilibrium with the atmosphere as indicated by the dissolved gas pressures observed in several studies addressing groundwater dating or effects of land use on groundwater chemistry (see Table 2.1; Alikhani et al., 2016; Andrews et al., 2005; Feast et al., 1998; Puckett and Cowdery, 2002; Tesoriero et al., 2000; Visser et al., 2014, 2007; Vogel et al., 1981; Wilson et al., 1990).

Table 2.1: Statistical distribution of occurring dissolved gas pressures. The studies the raw data was taken from (Alikhani et al., 2016; Andrews et al., 2005; Feast et al., 1998; Puckett and Cowdery, 2002; Tesoriero et al., 2000; Visser et al., 2014, 2007; Vogel et al., 1981; Wilson et al., 1990) mainly focus on effects of land use on groundwater chemistry (as input of nitrate) and groundwater dating.

percentile	N_2 (n=82) [atm]	O_2 (n=40) [atm]	CO_2 (n=10) [atm]	**Ar** (n=82) [atm]	∑ (n=82) [atm]
0th (minimum)	0.54	0.000	0.0046	0.00014	0.55
5th	0.65	0.000	0.0046	0.00017	0.65
25th	0.77	0.000	0.0097	0.00857	0.85
50th (median)	0.98	0.010	0.0108	0.00932	1.02
75th	1.14	0.105	0.0117	0.01017	1.17
95th	1.40	0.131	0.0146	0.01124	1.41
100th (maximum)	1.58	0.190	0.0193	0.01622	1.59

Dissolved gas concentrations of CO_2, H_2S and CH_4 can also be increased by organic matter or organic pollutant degradation (e.g. Appelo and Postma, 2005). The contribution to dissolved gas concentrations by organic carbon degradation is controlled by the availability of degradable organic carbon, the degradation rate and -pathway. An induced temperature increase can have an impact on all three of these aspects: Enhanced dissolved organic carbon mobilisation due to increased temperatures has been measured in column experiments at 60 °C (Bonte et al., 2013b), in batch experiments with a peaty clay and a quartz rich sand at temperatures above 45 °C (Brons et al., 1991) and in batch experiments with a lignite sand at 70 °C (Jesußek et al., 2013a). Bonte et al. (2013a) and Jesußek et al. (2013a) observed a temperature induced shift in organic carbon degradation towards more reducing pathways. While the reduction rate of nitrate increased steadily with temperature (Jesußek et al., 2013a), the sulphate reduction rate increased up to 45 °C, showed a distinct minima at the mesophilic-thermophilic transition around 50 °C and increased again from 50 up to 70 °C (Bonte et al., 2013a).

At ambient groundwater temperatures the formation of a separate gas phase can be caused by denitrification processes as observed in a riparian wetland (Blicher-Mathiesen et al., 1998) or by methanogenic degradation of petroleum hydrocarbons (Amos et al., 2005). Another possible source for high dissolved gas concentrations in shallow aquifers is the natural upward migration of gas from deeper layers as it has been observed for CO_2 (Battani et al., 2010) and CH_4 (Coldewey and Melchers, 2011; McIntosh et al., 2014). Beside a natural upward migration, also leaky production wells have been reported to act as migration pathways for methane (e.g. van Stempvoort et al., 2005). Temperature and pressure conditions in an aquifer control the solubility, and thus also the saturation of any dissolved gases. The formation of a separate gas phase is thereby dependent on the site-specific interplay between initial dissolved gas concentrations, planned temperature increase and depth of the target aquifer.

Under field conditions, the spatially continuous observation of temperature variations with possible gas-phase formation as consequence caused by thermal energy storages poses a challenge. Electrical resistivity (ER) monitoring can provide images of bulk electrical resistivity variations which potentially could serve as proxy for assessing temperature variations and gas-phase formation. However, the imaged resistivity ground variability must be interpreted with regard to the requested target parameters, since the electrical resistivity of the ground depends on various soil parameters, e.g. porosity, water content, temperature, grain size and shape, the particle orientation and cementation, mineral composition and ionic strength (Archie, 1942; Brunet et al., 2010; Corwin and Lesch, 2005; Dachnov, 1962; Friedman, 2005; Friedman and Seaton, 1998; Knödel et al., 2005; Llera et al., 1990; McCleskey et al., 2011; Mualem and Friedman, 1991; Rhoades et al., 1999; Robinson and Friedman, 2003). Interpretation of a measured electrical resistivity value with regard to changes in a distinct underlying parameter, e.g. temperature or water content, is usually not possible. However, using time-lapse measurements allows for monitoring the change of electrical resistivity, which agrees for better inference of target parameter changes from initial conditions. For example, Daily et al. (1992), and Hoffmann and Dietrich (2004) successfully employed time-lapse ER measurements for monitoring water flow in the ground, whereas Dietrich (1999) analysed ER to monitor salt tracer experiments. Gunn et al. (2014) monitored soil moisture in clay embankments using ER supporting preventative geotechnical asset maintenance and Grellier et al. (2005) used time-lapse ER measurements for monitoring moisture changes in a bioreactor. ER measurements have been previously used in geothermal reservoir characterisation and monitoring of heat plumes. At laboratory scale, Giordano et al. (2013) evaluated surface ER measurements for monitoring groundwater and soil changes under induced temperature variations whereas Hermans et al. (2012) used surface time-lapse ER measurements for monitoring the induced heat diffusion in a shallow geothermal field experiment. In a further step, Giordano et al. (2015) tested surface time-lapse ER measurements in their integrated approach from laboratory to field scale for an economic and ecological design and monitoring of ground thermal energy storage. In another heat tracer experiment, Hermans et al. (2015) used cross-borehole time-lapse ER monitoring for quantifying induced temperature changes in the aquifer. However, the potential of ER measurements goes beyond monitoring heat flow in geothermal reservoirs, since the electrical resistivity of porous sediments increases with growing fractions of gas phase in the pore fluid. This effect has already been used for different studies. Yang et al. (2015) used 3D crosshole electrical resistivity tomography monitoring a CO_2 migration in a shallow aquifer while Bergmann et al. (2012) used surface-downhole electrical resistivity tomography monitoring CO_2 storage in a sandstone 650m below surface and Carrigan et al. (2013) used this method already for the monitoring of CO_2 in a deep geologic reservoir exceeding 3000m below surface. Consequently, time-lapse ER should also be considered as potential monitoring method of possible gas-phase formation induced by geothermal energy storage.

The formation of a separate gas phase reduces hydraulic conductivity by lowering pore space water saturation in the zone of gas-phase formation. Insertion of oxygen in formerly water saturated sand columns caused gas-phase saturations of 14 to 55 % and a corresponding decrease in hydraulic conductivity of 38 to 95 % (Fry et al., 1997). Degradation of ethanol by denitrification led to a gas-phase saturation of 23 % in laboratory flow cell experiments conducted with an upward water flow whereupon the gas phase was assumed to mainly consist of N_2 (Istok et al., 2007). Formation of a CH_4 (20-85 %), N_2 and CO_2 (15-80 %) gas phase by methanogenic degradation of methanol lowered the hydraulic conductivity in sand columns by 75 to 97 % under upward flow conditions (Sanchez de Lozada et al., 1994). Methanogenic degradation of methanol caused formation of an unspecified gas phase which led to gas-phase saturations of 40 to 50 % in the bioactive zone of gas-phase formation and up to 80 % below the sealing in a sand-filled cell under lateral flow conditions (Ye et al., 2009). Correspondingly Ye et al. (2009) calculated a decrease in hydraulic conductivity by 80 to 90 % in the bioactive zone of gas-phase formation and by over 99 % below the sealing. In contrast to such water saturation decreases due to gas-phase formation, the net effects of carbonate precipitation and silica dissolution at temperatures between 2 and 50 °C, with a maximum decrease in pore space of 0.2 % calculated by Arning et al. (2006), appear to be of minor relevance. Instead, Palmer and Cherry (1984) expect the threat of clogging caused by temperature induced carbonate precipitation in aquifer thermal energy storage (ATES) systems primarily either within the pipe system or, in case precipitates forming within the pipes of the heating system remain in suspension, at the interface between well and aquifer. Beside changes in hydraulic conductivity, replacement of water by a gas phase affects further important parameters regarding efficiency of heat storage applications as e.g. heat conductivity and -capacity.

Approaches to model a gas-phase formation by methanogenesis in a petroleum hydrocarbon contaminated aquifer have been undertaken by Amos and Mayer (2006) who included gas bubble formation and collapse depending on dissolved gas pressures into the reactive transport code MIN3P. Feedback on groundwater flow was considered, but the implementation did not allow any migration of gas bubbles. With these boundary conditions methanogenic degradation of petroleum hydrocarbons on the field scale lead to induced residual source zone gas-phase saturations of more than 30 % which resulted in a decrease in hydraulic conductivity to less than 25 % (Amos and Mayer, 2006). Krol et al. (2011) modelled gas bubble formation and mobilisation during subsurface heating of contaminated zones to 70, 80 and 90 °C. Gas-phase saturations increased up to a maximum of 30 % in the source zone. In contrast to the Amos and Mayers (2006) approach, gas migration was included into the combined ETM-MIP model approach by Krol et al. (2011), but no feedback on groundwater flow was implemented.

None of the studies investigated gas-phase saturations with solely temperature induced physical gas-phase formation under natural groundwater condition. Nevertheless, it was shown that a significant effect on aquifer hydraulics can be expected if a separate gas phase forms and accumulates over time. And since now, no gas-phase formation monitoring in geothermal reservoirs by means of time lapse ER measurements has been carried out striving to monitor alteration of the natural conditions in the ground caused by geothermal installations. Therefore in this study we focus on the following objectives:

- Do thermodynamic calculations on a gas-phase formation coincide with experimental results and are therefore a suitable tool to estimate a gas-phase formation in aquifers?
- Is it possible to monitor gas-phase formation and farther distribution of a gas phase in column tests using time-lapse ER measurements?
- Which extent of gas-phase formation with regard to different gases and different geochemical boundary conditions can be expected due to heat storage in near surface aquifers?
- What hydraulic and thermic effects relating to efficiency of a heat storage site are caused by a gas-phase formation?

To assess these objectives a combined approach using geochemical and geoelectrical measurements in laboratory column tests and proceeding hydrochemical scenario calculations is applied as described in detail in the following section.

2.3. Materials and Methods

2.3.1. Column Experiments

The column experiments within this study were predominantly designed to investigate temperature induced changes in geochemical sediment-water interactions (in a similar setup as it was used by Jesußek et al. (2013)). The corresponding results will be published elsewhere. For the present study, the columns were additionally equipped with a gas trapping system to quantify the gas-phase formation. This quantification was done by building the ratio of forming gas phase in litre or millilitre of gas per litre of flowed through water to enable the transfer to further boundary conditions regarding groundwater flow speed. In addition, measurements of the gas-phase accumulation within the columns were performed. For the column experiments which were conducted at 10, 25, 40 and 70 °C, two Pleistocene sands differing mainly in grain size and organic carbon content from aquifers in Bönebüttel (sediment sample BS – Bönebüttel shallow) and Odderade (sediment sample OR, Table 2.2), Schleswig-Holstein, northern Germany, were used.

Table 2.2: Characteristics of the sediments used ([1]Dethlefsen (2015); personal communication of unpublished data).

	BS	***OR***
sediment	Pleistocene sand	Pleistocene sand
grain size	slightly gravelly sand	muddy sand
depth	4-12 *[m under ground level]*	66-68, 69-72 *[m under ground level]*
Σ(Na, K, Ca, Mg, Fe, Mn)	1070 *[mmol/kg]*	1168 *[mmol/kg]*
$C_{org.}$[1]	142 *[mg/kg]*	1830 *[mg/kg]*
$C_{carb.}$[1]	5711 *[mg/kg]*	2322 *[mg/kg]*
pyrite[1]	221 *[mg/kg]*	1208 *[mg/kg]*
water in use	BS site water	tap water

The utilised HDPE columns were 110 cm long (internal diameter: 10 cm) and had nine sampling ports along the flow path with the distance in between increasing from the bottom to the top of the columns (Fig. 2.1). In order to avoid effects of variations in sediment composition with depth, eight (BS) and five (OR) meters of drilling cores were homogenised before filling the columns (Table 2.2).

The columns filled with sediment BS were operated using water from the same aquifer, whereas the ones containing OR sediment were percolated with tap water which had a composition comparable to the water in the corresponding aquifer. Four BS and four OR columns were filled alternately with water and sediment. To reach a homogeneous one-dimensional flow through the columns, the lower most 10 cm were filled with coarse-grained commercial quartz (1.0-2.5 mm) instead of sediment. The sediment was repeatedly consolidated while filling the columns to prevent gas-phase entrapment. The experimental setup is shown in Fig. 2.1.

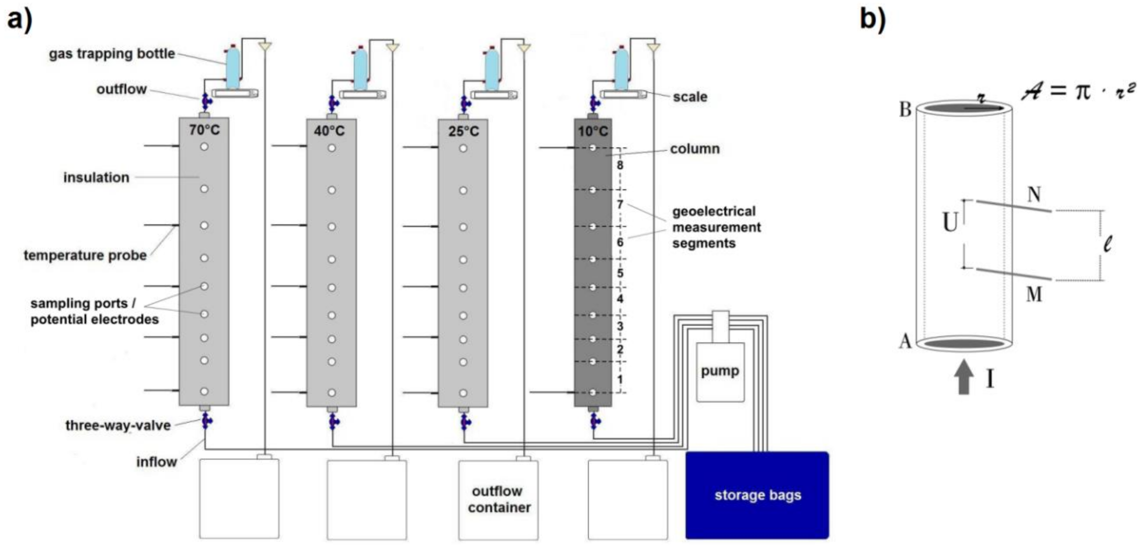

Fig. 2.1: Experimental column setup to measure the trapped gas volume, ratio of degassing and electrical resistivities (a) whereupon an induced current I flows between the two current electrodes A and B while the potential difference U is measured between the adjacent potential electrodes M and N (b). Using the cross section A and the distance l between the potential electrodes the measured voltages can then be converted into the bulk resistivities of the respective volumes (b).

The groundwater serving as inflow solution (Table 2.3) was stored at 10 °C in gas tight bags (PETP/AL/PE, tecotainer-inset; Tesseraux). A peristaltic pump (Ismatec Ecoline VC-MS/CA 8-6; Idex) pumped the inflow solution with 1 ml/min into the columns generating a flow from the bottom upwards through the columns. The (pumping-) tubes (internal diameter 1 mm, wall thickness 1 mm) connecting the water storage bags with the columns were coated with aluminium foil to minimise gas diffusion into the solution. The outflow of the columns was connected to a water filled gas trapping bottle on a scale which was heated to the same temperature as the corresponding column. Gas-phase formation ratios were measured by the decreasing weight of these gas trapping bottles as the water inside was replaced by gas bubbles flushed out of the columns from time to time.

All columns were equilibrated by percolation with the corresponding inflow solutions at 10 °C (±1 °C) for two (BS) and four (OR) months in a fridge before heating was started. One column per sediment remained in the fridge at 10 °C as reference while the other three columns were heated to 25 (±1), 40 (±2) and 70 °C (±2 °C) using heating tapes. Additionally the heated columns were covered with a 1.9 cm thick insulating mat (AF-19MM/E; Armacell).

Table 2.3: Composition of inflow solutions for the OR and BS column experiments.

		OR	***BS***
pH	*[-]*	7.69±0.26	7.21±0.15
TIC	*[mmol/L]*	5.91±0.17	5.51±0.11
NPOC	*[mmol/L]*	0.23±0.08	0.40±0.03
K^+	*[mmol/L]*	0.08±0.01	0.05±0.03
Na^+	*[mmol/L]*	0.64±0.02	0.71±0.03
Ca^{2+}	*[mmol/L]*	3.16±0.05	3.41±0.07
Mg^{2+}	*[mmol/L]*	0.36±0.01	0.23±0.01
Fe_{diss}	*[mmol/L]*	0.0001±0.0002	0.0011±0.0023
Mn_{diss}	*[mmol/L]*	0.0002±0.0003	0.0031±0.0007
Si_{diss}	*[mmol/L]*	0.50±0.01	0.46±0.01
Al_{diss}	*[mmol/L]*	0.0001±0.00007	0.00012±0.00005
Cl^-	*[mmol/L]*	0.87±0.02	0.80±0.04
NO_3^-	*[mmol/L]*	0.01±0.01	0.001±0.002
SO_4^{2-}	*[mmol/L]*	0.51±0.02	0.92±0.02
N_2	*[mmol/L] ([atm])*	0.51±0.02 (0.60)	0.9±0.04 (1.1)
O_2	*[mmol/L] ([atm])*	0.16±0.05 (0.093)	0.01±0.007 (0.0058)
CO_2	*[mmol/L] ([atm])*	0.29±0.01 (0.0054)	0.75±0.01 (0.014)
Σ dissolved gases	*[mmol/L] ([atm])*	0.96±0.08 (0.70)	1.66±0.05 (1.1)

Temperature monitoring by Pt100 probes (for positions see Fig. 2.1) showed that heating up of the inflowing water to the aimed temperature was restricted to the gravel layer at the bottom of the columns. The volume of gas phase trapped within the sediment was additionally calculated for the BS column experiments using pressure changes induced by water injections (using the inflow solution) into closed columns following the law of Boyle-Mariotte (Eq. 2.1). Thereby the pressure before water injection (p_1) divided by the pressure after water injection (p_2) was equalised to the volume after water injection (V_2) divided by the volume before water injection (V_1).

$$\frac{p_1}{p_2} = \frac{V_2}{V_1} \qquad (Eq. 2.1)$$

Water samples were retrieved from three-way-valves at the in- and outflow of the columns as well as from the sampling ports along the flow path (Fig. 2.1) and geochemically analysed using standard methods. The results are not included in this study but will be presented elsewhere. Dissolved CH_4- and N_2 concentrations were measured using gas chromatographs (GC 6890plus, HS7694 (for CH4) and GC 7890B, HS 7697A (for N_2); Agilent). Liquid N_2 samples were taken directly from the gas tight bags which contained the inflow solution and injected into closed, Argon flushed GC vials by using a gas tight syringe to avoid contamination by air. Though, the lowest measured value of tenfold measurements was considered to be most accurate as all contamination by air would have increased the N_2 concentration. Oxygen was measured with a phase fluorimeter (Neofox-GT; Ocean Optics) and an oxygen sensor (FOSPOR-R-Series Sensor Probe; Ocean Optics) within a tube attached to the three-way-valves were water diverged from the inflow, outflow or the sampling ports was flowing through.

2.3.2. Geoelectrical monitoring of gas phase accumulation and distribution within the experimental columns

The measured electrical bulk resistivity is an integral value of the resistivity of the sediment matrix and the fluid in the pore space. The electrical resistivity of sand grains significantly exceeds those of water filling the pore space. The electrical conductivity in the column is thus dominated by the electrolytic conductivity of the pore fluid and hence the measured bulk resistivity is governed by the resistivity of the pore water. Generally, the resistivity decreases with increasing temperature.

Corwin and Lesch (2005) report a resistivity change of 1.9 % per K, whereas Hem (1985) give 2 % and Keller and Frischknecht (1966) report 2.5 % per K.

Many authors describe the temperature dependence of the electrical resistivity by referencing it to a known resistivity $\rho(T_{ref})$, at a special temperature

$$\rho(T) = f_T \cdot \rho(T_{ref}) \qquad (Eq. 2.2)$$

with f_T being a temperature dependent conversion factor given differently by different authors (for a comprehensive review see Ma et al. (2011). Typical conversion values are given in Richards (1954). Dachnov (1962) formulated the relation for the reference value set to 18 °C with

$$\rho(T) = \frac{\rho(18°C)}{1 + \alpha_T(T - 18°C)} \qquad (Eq. 2.3)$$

Here, α_T is a temperature coefficient that decreases with increasing temperature. Around 18 °C it is set to approximately 0.025. Using this equation an expression not referring to a specific reference value can be derived:

$$\rho(T_2) = \rho(T_1)\frac{1 + \alpha_T(T_1 - 18)}{1 + \alpha_T(T_2 - 18)} \qquad (Eq. 2.4)$$

Thus, the reference conditions can be set arbitrary and the possibility of the comparison to another measured value can be done.

For sediments with negligible conductivity proportion of the matrix Archie (1942) empirically found the following link between fluid resistivity ρ_f and bulk resistivity ρ_{sat} of fully water saturated sediments

$$\rho_{sat} = F \cdot \rho_f \qquad (Eq. 2.5)$$

F is the formation factor describing the geometry of the pore space. If the pore space is partially filled by a non-conductive gaseous phase this affects the bulk resistivity similarly like a reduced porosity and equation 2.5 becomes

$$\rho_s = \frac{1}{S_w^n} \cdot \rho_{sat} \qquad (Eq. 2.6)$$

with ρ_s as the resistivity of sediments with water and gas phase in the pore space. S_w describes the degree of water saturation (S_w=1 for full saturation) and *n* is the saturation exponent, a constant depending on soil properties, that is set to n=2 for clean, consolidated or unconsolidated, water-wet sandstones (Archie, 1942). Many authors have investigated the effect of water saturation in the pore space on the electrical bulk resistivity of sediments. Keller and Frischknecht (1966) found a log-linear relation of saturation and resistivity for S_w >0.2.

The geophysical measurements were done only for the second set of columns experiment (sediment BS). In electrical resistivity applications, generally, four electrodes are used to measure the ground bulk resistivity. Two electrodes (A, B) are galvanically coupled to the ground material to inject a direct or very low frequency alternating current signal of strength *I* (Fig. 2.1). The potential difference *U* (voltage) between another pair of electrodes (M, N) is recorded. The recorded voltage is a function of electrode arrangement and current strength (Knödel et al., 2005). In the column experiments the two current electrodes (A, B) were placed inside the column and fixed directly on the upper and lower HDPE cover of the cylindrical column (Fig. 2.1). Both electrodes with the shape of circular discs of 10 cm diameter consisted of stainless steel and were installed prior to filling the column. The nine cannulas used for the groundwater sampling along the flow path served as potential electrodes (example in Fig. 2.1). Potential differences were recorded between adjacent cannulas (M, N) resulting in 8 voltage measurements distributed along the vertical axes of the column as shown in Fig. 2.1. Measured voltages were converted into electrical resistance R by

$$R = \frac{U}{I} \qquad (Eq. 2.7)$$

and can be related to bulk resistivity ρ of the filled material by

$$\rho = R \cdot \frac{A}{l} \qquad (Eq. 2.8)$$

where l is the distance between the pair of voltage electrodes (M, N) and A is the inner circular area of the column (comparable to Fig. 2.1). However, based on the arrangement of the nine cannulas, the most upper and lowest segments of the columns could not be observed by the electrical resistivity measurements (Fig. 2.1).

Measurements were carried out using a Resecs (RES6P, GeoServe) electrical resistivity measurement device. Voltage measurements were repeated every 6 hours over a period of 8 months. One measurement cycle resulted in 8 voltage readings (Fig. 2.1), which is one for every pair of electrodes and took approximately two minutes. During the first two months of recording, no heating took place to ensure a full adaptation of the columns to the constant surrounding temperature of 10 °C and to generate base measurements. Recorded data was stored automatically and regularly controlled by a human supervisor. Based on the quality of the checked data, the electrode coupling and system functionality was visually inspected and maintained if necessary.

2.3.3. Geochemical equilibrium modelling

Geochemical equilibrium modelling was done using the program PhreeqC v3.15 (Parkhurst and Appelo, 2013) with the database PhreeqC.dat (Argon data was obtained from the database llnl.dat also provided with PhreeqC v.3.15). In a first step, the measured ratio of gas phase formation per litre water for the different temperatures was compared to the calculated ratio of gas-phase formation per litre water. For this purpose the compositions of the inflow solutions and the experimentally investigated temperatures were set as input parameters (Table 2.4). The total pressure was set to 1.1 atm representing the bottom of the columns where heating up of the inflowing water was located by temperature monitoring. After that, the ratio of gas-phase formation per litre water was computed under equilibrium conditions. This comparison was then used to discuss plausibility of the experimental results and the predictability by using geochemical equilibrium modelling.

The inflow solution BS was equilibrated at 10 °C with a) the atmospheric partial pressures of N_2, O_2, Ar and CO_2 to simulate no changes in dissolved gas concentrations during infiltration of recharge water through the vadose zone of an aquifer and b) the atmospheric partial pressures of N_2 and Ar while, according to Matthes (1990), the partial pressure of CO_2 was increased to 0.05 atm and the partial pressure of O_2 was decreased correspondingly to simulate an use up of O_2 and production of CO_2 by aerobic respiration during infiltration. The temperature of these initial solutions (Table 2.4) was then increased to 25, 40, 55, 70 and 85 °C in a total pressure range from 1 to 2.6 atm to investigate if a gas-phase formation takes place under these physical and geochemical conditions.

For a first set of initial solutions pure water was set to equilibrium with a pure atmosphere of each of the gases H_2, N_2, O_2, CH_4, CO_2 and H_2S at 10 °C for total pressures varying from 1 to 10 atm to investigate the effect of an increasing pressure on the formation of a gas phase. Saturated conditions were used to simulate a source for the dissolved gases as e.g. microbial degradation processes or upward gas migration from deeper layers. Either solely the gas corresponding to the dissolved one or alternatively, additionally also water vapour were allowed to partition into the gas phase to determine if water vapour needs to be considered for calculating the gas-phase formation in the subsequent scenario calculations. In a second set of initial solutions the dissolved concentrations of H_2, N_2, O_2, CH_4, CO_2 and H_2S were adjusted in 30 steps from 1/30 up to saturation at constant 2 atm total pressure in pure water to compare the saturations of dissolved gases and thereby dissolved gas concentrations causing the onset of a gas-phase formation under specific temperature and pressure conditions. For CO_2 additionally calcite buffered water was used to demonstrate the dependency of CO_2 solubility and potential gas-phase formation on the buffering capacity and thus pH of an aquifer. For both sets of initial solutions (Table 2.4) it was then again calculated for temperatures between 25 and 85 °C if a separated gas phase is forming and which volume such gas phases would have.

2.3.4. Scenario calculations

The effects of a temperature induced gas-phase formation on water- and gas-phase saturation and subsequently hydraulic conductivity were investigated by scenario calculations representing future heat storage sites under different physical and geochemical boundary conditions. For a first scenario A the groundwater composition in the BS aquifer including 23.8 mg/L of N_2 (which corresponds to an equilibrium with a pure N_2 gas phase at 10 °C and 1 atm) was used to imply an aquifer fed by water that has been in equilibrium to the atmosphere first, but from which oxygen has been consumed- and nitrogen has been enriched by degradation of organic carbon via nitrate reduction during infiltration (Table 2.4). In a second scenario B the groundwater of scenario A was used as background and methane was chosen as an additional dissolved gas as it might be present in the subsurface due to methanogenic degradation processes (Amos et al., 2005; McIntosh et al., 2014) or gas leakages out of leaky production (or storage) wells (van Stempvoort et al., 2005) in considerable amounts. The methane concentrations increased by depth as due to the assumption of a source, saturated dissolved gas conditions were presumed (Table 2.4). Methane concentrations corresponding to 30-100 % in situ dissolved gas saturation in bedrock wells but also in surficial aquifers overlying organic-rich shale-bearing formations were e.g. measured by McIntosh et al. (2014). The third scenario C again used the groundwater composition from scenario A as background. For this scenario CO_2 (which has a solubility more than a magnitude higher than e.g. N_2 or CH_4) was chosen as a dissolved gas in addition to N_2. The dissolved gas concentrations were again set to match saturation (Table 2.4), as comparable to scenario B, an existing CO_2 source was assumed. Such a source might be natural upward migration of gaseous CO_2 from deeper layers along fault zones into shallower regions. The CO_2 can dissolve into the groundwater on its migration pathway and causes soil gas compositions with over 90 % CO_2 as it has been observed by Battani et al. (2010), Beaubien et al. (2003), Chiodini and Frondini (2001) and Shipton et al. (2005). For the interpretation of the results of these three scenarios it should be taken into account that only scenario A covers a common situation. For scenarios B and C additional processes which increase dissolved gas concentrations up to saturation are assumed which only represents the upper end of possible dissolved gas concentrations at ambient groundwater temperatures.

Table 2.4: List of initial 10 °C solutions used for the geochemical equilibrium- and scenario calculations.

initial solution for	*background*	*pH [-]*	*N_2 [mmol/L]*	*H_2 [mmol/L]*	*O_2 [mmol/L]*	*CH_4 [mmol/L]*	*CO_2 [mmol/L]*	*H_2S [mmol/L]*	*Ar [mmol/L]*	*results shown in*
OR columns calculated	OR inflow (Table 2.3)	7.69	0.5	-	0.156	-	0.29	-	-	Fig. 2.4a/Fig. 2.5
BS columns calculated	BS inflow (Table 2.3)	7.21	0.857	-	-	-	0.75	-	-	Fig. 2.4b/Fig. 2.5
equil. atmosphere	BS inflow (Table 2.3)	8.71	0.663	-	0.358	-	0.02	-	0.017	Fig. 2.9a
equil. to atm. w. incr. CO_2	BS inflow (Table 2.3)	6.65	0.663	-	0.273	-	2.70	-	0.017	Fig. 2.9b
1-10 atm C(sat) N_2	pure water	7	0.851-8.47	-	-	-	-	-	-	Fig. 2.10a
1-10 atm C(sat) H_2	pure water	7	-	0.881-8.83	-	-	-	-	-	Fig. 2.10a
1-10 atm C(sat) O_2	pure water	7	-	-	1.71-17	-	-	-	-	Fig. 2.10a
1-10 atm C(sat) CH_4	pure water	6.99	-	-	-	1.96-19.2	-	-	-	Fig. 2.10a
1-10 atm C(sat) CO_2	pure water	3.38-3.87	-	-	-	-	53.7-506	-	-	Fig. 2.10a
1-10 atm C(sat) H_2S	pure water	3.54-4.02	-	-	-	-	-	135-1237	-	Fig. 2.10a
C(sat) N_2 in 30 steps	pure water	7	0.0567-1.69	-	-	-	-	-	-	Fig. 2.10b
C(sat) H_2 in 30 steps	pure water	7	-	0.0588-1.75	-	-	-	-	-	Fig. 2.10b
C(sat) O_2 in 30 steps	pure water	7	-	-	0.114-3.4	-	-	-	-	Fig. 2.10b
C(sat) CH_4 in 30 steps	pure water	6.99-7	-	-	-	0.131-3.89	-	-	-	Fig. 2.10b
C(sat) CO_2 in 30 steps	pure water	3.72-4.46	-	-	-	-	3.53-106	-	-	Fig. 2.10b
C(sat) CO_2 buff. in 30 steps	calcite buffered water	5.84-6.78	-	-	-	-	12.1-137	-	-	Fig. 2.10b
C(sat) H_2S in 30 steps	pure water	3.87-4.61	-	-	-	-	-	8.9-265	-	Fig. 2.10b
scenario A 0-10m	BS inflow (Table 2.3)	7.21	0.849	-	0.005	-	0.74	-	-	Fig. 2.11/Fig. 2.12/Fig. 2.16
scenario B 10-11m	BS inflow (Table 2.3)	7.21	0.849	-	-	2.06	0.74	-	-	Fig. 2.13/Fig. 2.14/Fig. 2.16
scenario B 11-12m	BS inflow (Table 2.3)	7.21	0.849	-	-	2.25	0.74	-	-	Fig. 2.13/Fig. 2.14/Fig. 2.16
scenario B 12-13m	BS inflow (Table 2.3)	7.21	0.849	-	-	2.45	0.74	-	-	Fig. 2.13/Fig. 2.14/Fig. 2.16
scenario B 13-14m	BS inflow (Table 2.3)	7.21	0.849	-	-	2.64	0.74	-	-	Fig. 2.13/Fig. 2.14/Fig. 2.16
scenario B 14-15m	BS inflow (Table 2.3)	7.21	0.849	-	-	2.84	0.74	-	-	Fig. 2.13/Fig. 2.14/Fig. 2.16
scenario B 15-16m	BS inflow (Table 2.3)	7.21	0.849	-	-	3.03	0.74	-	-	Fig. 2.13/Fig. 2.14/Fig. 2.16
scenario B 16-17m	BS inflow (Table 2.3)	7.21	0.849	-	-	3.23	0.74	-	-	Fig. 2.13/Fig. 2.14/Fig. 2.16
scenario B 17-18m	BS inflow (Table 2.3)	7.21	0.849	-	-	3.42	0.74	-	-	Fig. 2.13/Fig. 2.14/Fig. 2.16
scenario B 18-19m	BS inflow (Table 2.3)	7.21	0.849	-	-	3.62	0.74	-	-	Fig. 2.13/Fig. 2.14/Fig. 2.16
scenario B 19-20m	BS inflow (Table 2.3)	7.21	0.849	-	-	3.81	0.74	-	-	Fig. 2.13/Fig. 2.14/Fig. 2.16
scenario C 20-21m	BS inflow (Table 2.3)	5.05	0.849	-	-	-	109	-	-	Fig. 2.15/Fig. 2.16
scenario C 21-22m	BS inflow (Table 2.3)	5.03	0.849	-	-	-	114	-	-	Fig. 2.15/Fig. 2.16
scenario C 22-23m	BS inflow (Table 2.3)	5.01	0.849	-	-	-	120	-	-	Fig. 2.15/Fig. 2.16
scenario C 23-24m	BS inflow (Table 2.3)	4.99	0.849	-	-	-	125	-	-	Fig. 2.15/Fig. 2.16
scenario C 24-25m	BS inflow (Table 2.3)	4.97	0.849	-	-	-	130	-	-	Fig. 2.15/Fig. 2.16
scenario C 25-26m	BS inflow (Table 2.3)	4.95	0.849	-	-	-	135	-	-	Fig. 2.15/Fig. 2.16
scenario C 26-27m	BS inflow (Table 2.3)	4.94	0.849	-	-	-	140	-	-	Fig. 2.15/Fig. 2.16
scenario C 27-28m	BS inflow (Table 2.3)	4.92	0.849	-	-	-	146	-	-	Fig. 2.15/Fig. 2.16
scenario C 28-29m	BS inflow (Table 2.3)	4.91	0.849	-	-	-	151	-	-	Fig. 2.15/Fig. 2.16
scenario C 29-30m	BS inflow (Table 2.3)	4.89	0.849	-	-	-	156	-	-	Fig. 2.15/Fig. 2.16

To predict the potential development of a case application based on the three postulated scenarios we used the numerical heat storage model of Popp et al. (2015) that simulates seasonal heat storage with a field of 72 borehole heat exchangers (BHE´s) heated to a maximum temperature of 60 °C in a near surface aquifer. Further the authors assumed a background groundwater temperature of 10 °C and a flow velocity of 0.02 m/d. Correspondingly to Popp et al. (2015), the horizontal extension of the field of BHE´s perpendicular to the groundwater flow was assumed to be 18 meters. Total pressures were set to 1-2, 2-3 and 3-4 atm simulating heat storage sites in water saturated depths of 0-10 m for scenario A, 10-20 m for scenario B and 20-30 m for scenario C. The particular depths were chosen in a way that each scenario is located within a sensitive depth range (e.g. scenario A would not cause any gas-phase formation in depths >10 meters) and that the calculations do not cause any errors in computation (as e.g. scenario C did in shallower depths). Maximum residual gas-phase saturation (S_{grm}) in the zone of gas-phase formation is reported to remain between 20 % (Istok et al., 2007) and 50 % (Ye et al., 2009), so the onset for an upward migration of further generated gas phase was set to a) 30 % and b) 50 % gas-phase saturation in the further calculations. The scenario area was divided into five sections (marked as S_1, S_2, S_3, S_4 and S_5 in Fig. 2.2) in the upstream flow of the heat storage site (which is marked by BHE´s for borehole heat exchangers in Fig. 2.2) where the temperature is elevated above the background aquifer temperature of 10 °C due to conductive heat transport to account for the lateral differences in gas-phase formation.

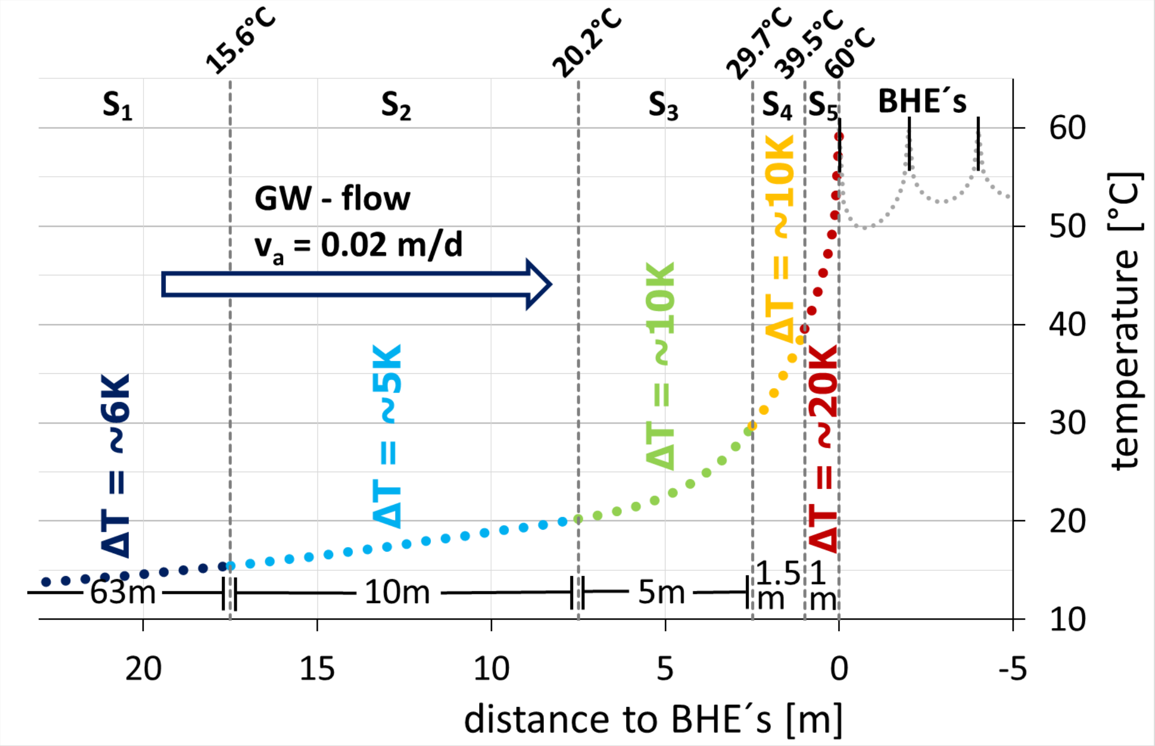

Fig. 2.2: Temperature profile of a numerical heat storage model developed to simulate seasonal heat storage in a near surface aquifer divided up into five sections (S1-S5) to calculate gas-phase formation in the three scenarios stepwise for the corresponding increase in temperature (after Popp et al., 2015).

Formation of a gas phase was subsequently calculated in each of the five sections (S_1-S_5) over time given in exchanged pore volumes for each of the three scenarios´ solutions (Table 2.4). The model of Popp et al. (2015) yielded a stepwise increase in temperature from 10 °C to 15.6, 20.2, 29.66, 39.52 and 59.86 °C for the selected extent of the five sections (see Fig. 2.2). For each meter in depth the corresponding total pressure was used. A gas phase formed and the dissolved gas concentrations decreased correspondingly in case partial pressures of the dissolved gases exceeded the total pressure in a temperature step at any depth, before the solution was used in the next temperature step. The amount of gas phase formed in moles(gas)/L(water) was converted to volume(gas)/L(water) by using ideal gas assumptions. In the appropriate cell (defined by temperature step and depth) the water saturation was then reduced by this factor. After gas phase saturation reached a S_{grm} of 30 or 50 %, further gas-phase formation was not effecting water saturation as an upward migration of this gas phase was assumed. This excess gas phase was then summed up for the whole volume of a section (11340m³, 1800m³, 900m³, 270m³ and 180m³ for the five sections (S_1-S_5, respectively) over time. Under confined conditions, as suggested for ATES sites (e.g. Schmidt and Müller-Steinhagen, 2005), gas phase exceeding S_{grm} will migrate upwards and accumulate in morphological traps at the top of the aquifer. Subsequent effects in the field of borehole heat exchangers on heat conductivity (Eq. 2.9) and heat capacity (Eq. 2.10) due to changes in the water saturation were calculated for a case scenario assuming all excess gas phase produced upstream of the BHE is being laterally transported into the heat storage field by the groundwater flow.

$$\lambda_{bulk} = \lambda_{sediment} \cdot (1-n) + \lambda_{water} \cdot \left(n - n_{eff} + n_{eff} \cdot S_w\right) + \lambda_{gas} \cdot n_{eff} \cdot S_g \quad (Eq. 2.9)$$

$$c_{V_{bulk}} = c_{V_{sediment}} \cdot (1-n) + c_{V_{water}} \cdot \left(n - n_{eff} + n_{eff} \cdot S_w\right) + c_{V_{gas}} \cdot n \cdot S_g \quad (Eq. 2.10)$$

For these calculations, volumetric heat capacity (c_V) and heat conductivity (λ) data from Pannike et al. (2006) for a fine grained sand (c_V=2.5 [MJ/(m³·K)], λ=2.2 [W/(m·K)])and from Lide (2005) for water at 60 °C (c_V=4.1 [MJ/(m³·K)], λ=0.65 [W/(m·K)]) and gases at 27 °C (c_V=0.0013 [MJ/(m³·K)], λ=0.026 [W/(m·K)]; averaged over water vapour, nitrogen and methane) were used. The porosity (n) for a fined grained (n=0.4) sand was taken from Pannike et al. (2006) while for effective porosity (n_{eff}) the value (n_{eff}=0.1) given in Popp et al. (2015) was used. Data for water- (S_w) and gas-phase saturation (S_g) resulted from the scenario calculations.

Frequency of pore water replacement is a crucial factor for estimations on the temporally evolution of the gas-phase saturation in the pore space. The frequency of pore water replacement can be calculated and converted into years of operational runtime by using the groundwater flow velocity of 0.02 m/d (as used by Popp et al., 2015) and the given lateral extent of the five sections stated above. By doing so, the number of computations is increasing with a decreasing lateral extent of the sections what results in the varying number of datapoints in the scenario calculations 30 years runtime (Fig. 2.9, Fig. 2.11, Fig. 2.13). Gas-phase formation was only considered for half the year as a seasonal heat storage site is assumed. Back dissolution in the other half of the year was not included in the calculations. The cumulative changes in water saturation were calculated for an operational runtime of 30 years. According to Amos and Mayer (2006) an approach for the unsaturated zone (Eq. 2.11; van Genuchten, 1980) was used to calculate the resulting change in hydraulic conductivity.

$$K_r(S) = S^{1/2} \cdot \left[1 - \left(1 - S^{1/m}\right)^m\right]^2 \qquad \left(m = 1 - 1/n\right) \qquad (Eq. 2.11)$$

Here K_r is the relative hydraulic conductivity, S the water saturation, m a fitting parameter calculated from n and n a grain size dependent, dimensionless fitting parameter of water retention which was taken from Schroth et al. (1996) for a medium grained sand. This approach was shown to be also suitable for gas entrapment into former water saturated zones by Fry et al. (1997). In addition, the temperature influence on the changes in hydraulic conductivity by viscosity and density changes of the water were included into the calculations. Feedback of changes in the hydraulic conductivity on the groundwater flow was only considered in terms of the reduced water saturation while the flow velocity was maintained. Focused- or deflected flow into areas with elevated- or reduced hydraulic conductivity on the vertical axis was neglected.

2.4. Results

2.4.1. Gas-phase formation and accumulation in the column experiments

Averaged over the heating period, ~100 ml (10 °C), ~280 mL (25 °C), ~530 mL (40 °C) and ~450 mL (70 °C) of residual gas phase remained inside the BS columns which corresponds to a gas-phase saturation of 5, 13, 25 and 21 %, respectively (Fig. 2.3a). For the column operated at 10 °C no separate gas phase was expected to develop, but gas-phase entrapment at the start of the experiments (Ch. 2.4.2) led to the detection of a gas phase which volume was decreasing by experimental runtime (Fig. 2.3a). The inflowing water with a total gas pressure of 1.1 atm (Table 2.3) is heated up within the first 10 cm of the columns, consequently also the geoelectrical resistance measurements first showed the build-up of a residual gas phase in the lowest measurement segment covering this zone of gas-phase formation (Ch. 2.4.2). Accumulation of a gas phase within the zone of gas-phase formation was also observed in column and tank experiments (Istok et al., 2007; Ye et al., 2009). These studies also report a subsequent channel build-up for upward gas migration in case S_{grm} is exceeded locally. The volume of entrapped gas phase at 25, 40 and 70 °C in the experiments done within this study was slightly varying over time which can be explained by build-up of channels for upward gas migration, partial degassing and possibly collapse of some existing channels at times, followed again by the build-up of new channels, when further gas phase was generated. Part of the gas phase that migrated upwards accumulated at the top of the columns as resistivities were increased in the highest monitored part of the column heated to 40 °C (Ch. 2.4.2). No electrodes covered the uppermost part of the columns (Fig. 2.1), so also at 25 and 70 °C accumulation of a gas phase at top of the columns might have occurred. Enhanced upward migration of gas bubbles compared to natural lateral flow conditions cannot be excluded as these column experiments were conducted with an upward water flow. Thus the residual gas phase that remained inside this sediment was possibly lower than it could be expected under natural lateral flow conditions. In the BS column experiments an averaged gas-phase formation ratio of ~1, ~4 and 12 mL(gas)/L(water) was measured for 25, 40 and 70 °C over the experimental runtime (Fig. 2.3b). The higher ratio of gas-phase formation at 70 °C compared to 40 °C might have caused an enhanced build-up of channels for upward gas-phase migration at 70 °C and thus resulted in a smaller gas volume trapped within the sediment. A limited channel build up at lower temperatures was also observed by Krol et al. (2011).

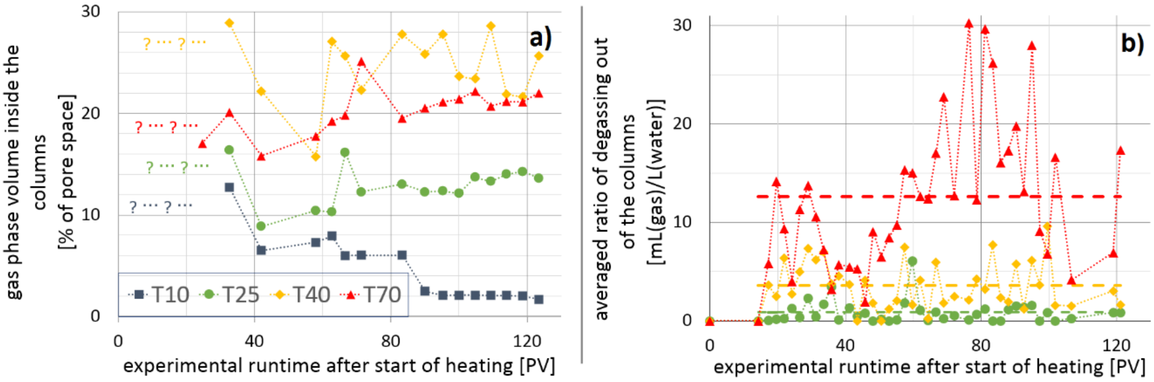

Fig. 2.3: Accumulated gas phase inside the sediment (a) and averaged ratio of gas phase flushed out as bubbles (b) for the BS columns displayed over the experimental runtime in exchanged pore volumes after heating of the columns was started.

The amount of gas phase trapped inside the BS columns showed less variation from 90 exchanged PV onwards (Fig. 2.3a), so the gas phase flushed out of the columns for comparison with the calculated gas-phase formation was measured from there on (Fig. 2.4b). For the OR columns, the gas phase flushed out of the columns was measured for a period of 12 exchanged PV (18 days) without interruption by measurements from 125 exchanged PV onwards when the ratio of degassing had reached a stable value (Fig. 2.4a).

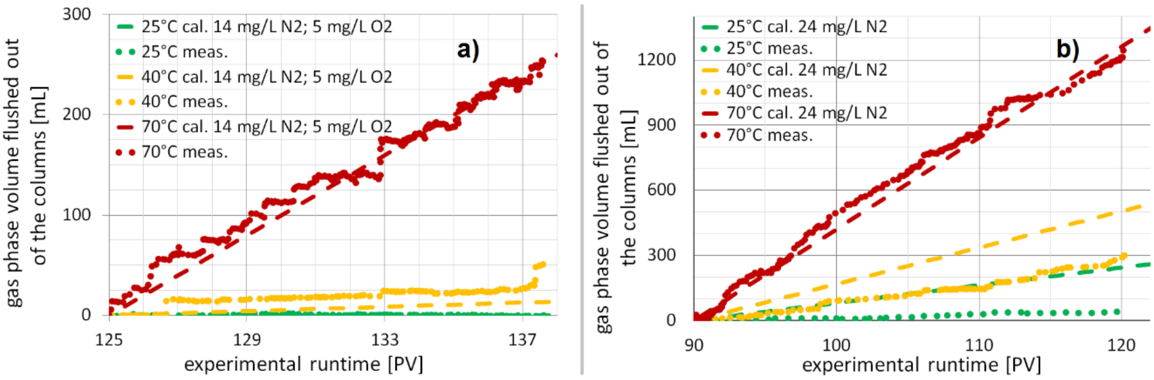

Fig. 2.4: Comparison between measured and calculated degassing for the OR (a) and BS (b) column experiments by using measured degassing from 125 and 90 PV onwards and the composition of the corresponding inflow solution as input parameters for the calculations.

By using the inflow solutions compositions the gas-phase formation in five out of six column experiments is assessable with an uncertainty factor of less than 2 (OR 25, 40, 70 °C and BS 40, 70 °C). The deviation between calculated and measured gas-phase formation ratio is less than 2.5 % at 70 °C where the highest gas-phase formation ratios within this study occur (Fig. 2.4). Calculated gas-phase formation in the column experiment OR 40 reproduces the slope of measured gas-phase formation between 127 and 137 PV while the overall deviation is due to two abrupt increases in gas-phase release. The overall deviation in the BS 25 and 40 °C column experiments is too large to be fully explained by retention of gas phase within the grain structure, as this would be clearly visible in Fig. 2.3a, though it might explain a part of the observed deviations. In addition, work needed to be brought up for formation of a gas phase embryo is possibly reducing the gas-phase formation at lower temperatures as the chance of successful nucleation increases with supersaturation which corresponds to temperature in this case (Debenedetti, 1996).

The calculated gas-phase formation for comparison with the measured one has been computed on the bases of the inflow solutions without consideration of any sources or sinks for dissolved gases within the columns. The calculated gas phases contain between 57 (OR 70 °C) and 95 % (BS 25 °C) of nitrogen whereupon the share of nitrogen decreases towards higher temperatures (Fig. 2.5). In contrast, the share of water vapour increases from 3 % at BS 25 °C to 18 % at BS 70 °C. Oxygen, although on a smaller scale, shows a pattern similar to nitrogen as its share also decreases with temperature from 14 (OR 40 °C) to 12 % (OR 70 °C). In contrast the share of CO_2 increases with temperature but is restricted to a maximum of 5 % (BS 70 °C, Fig. 2.5). Partition of N_2 or water vapour into the gas phase will not cause considerable changes in the fluid phase´ characteristics. In contrast, degassing of O_2 can facilitate the development of reducing conditions by removing a possible electron acceptor from water. Calculation of the calcite saturation index showed an increase in calcite oversaturation by 1, 1.7 and 2.1 % due to CO_2 degassing in the BS columns heated to 25, 40 and 70 °C compared to heating without considering gas-phase formation (not shown). The compositions of the gas phases would be shifted towards CO_2 and N_2, H_2S or CH_4 in case OC degradation would be considered (not shown).

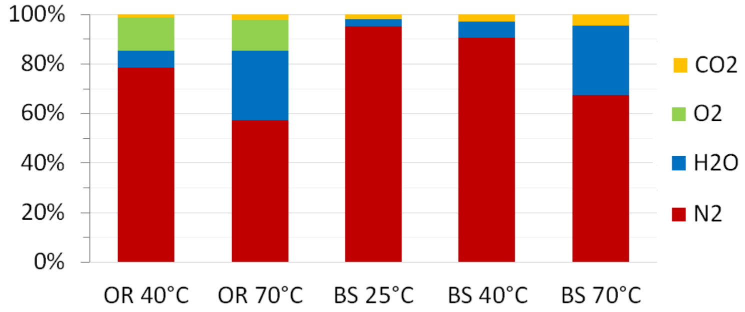

Fig. 2.5: Composition of the calculated gas phases for the OR and BS column experiments.

2.4.2. Monitoring of gas-phase formation by geoelectrical measurements

The base measurements of the electrical behaviour for the BS columns started on Sunday, the 8th of November 2015. However, the groundwater circulation was started two days later at the 11th of November. Fig. 2.6a illustrates the variation of the electrical bulk resistivity during the two months of the base line monitoring. Without groundwater flow the measured resistivities were very low and varied in the differing measuring segments (from 40 to 70 Ωm) without significant relation to the column heights. In each column, increased resistivity values (70-85 Ωm) were observed in the lowest segment of the columns. Since these anomalies disappear after the water infiltration, these values cannot be explained by the special commercial quartz in the lowest centimetres of the columns. Moreover, this indicates gas-phase entrapment particularly at these regions while filling the columns. After the start of percolation with groundwater from the bottom to the top of the columns, the resistivities increased up to 80-120 Ωm. Resistivity increases of the upper column segments lag systematically behind those of lower column segments. This suggests a differing chemical composition of the groundwater in contrast to the filled columns with the saturated sediment. The high values above 140 Ωm (up to approximately 600 Ωm) in the lowest measurement segment of the first column (Fig. 2.6a, 10 °C) at the 13th to 28th of November lead to the suggestion of gas-phase infiltration with the groundwater flow. Using equation 2.6 (Ch. 2.3.2) leads to the suggestion of a gas-phase saturation of almost 65 %. Indeed, the gas phase is transported upwards with the groundwater flow illustrated by the red to orange fan in Fig. 2.6a (10 °C). At the end of the base line measurements almost equal resistivity values indicating equal temperature and measurement conditions with an almost homogeneous sediment infill were found.

Fig. 2.6b shows the transition from the base line monitoring to the heating process of the three columns (Fig. 2.6b: 25, 40 and 70 °C) and the reference column remained at 10 °C (Fig. 2.6b, 10 °C). The heating process started at the 13th of January. For the necessary technical installations and reorganisation of the columns the measurements had to be interrupted one day before. Already the first measurements after the interruption show that the resistivities were affected by the temperature changes (Fig. 2.6b). Since no significant resistivity variations over time and segment height, analogue to those observed after starting the water circulation, were observed, the heating process was proven to be fast and affected the columns equally. The resistivities decreased proportional to the different temperature values in each column. While the resistivity values for the column at 25 °C decreased down to 70-80 Ωm, the values for the column at 40 °C decreased down to 50 Ωm and for the column at 70 °C down to 40 Ωm, approximately (Fig. 2.6b).

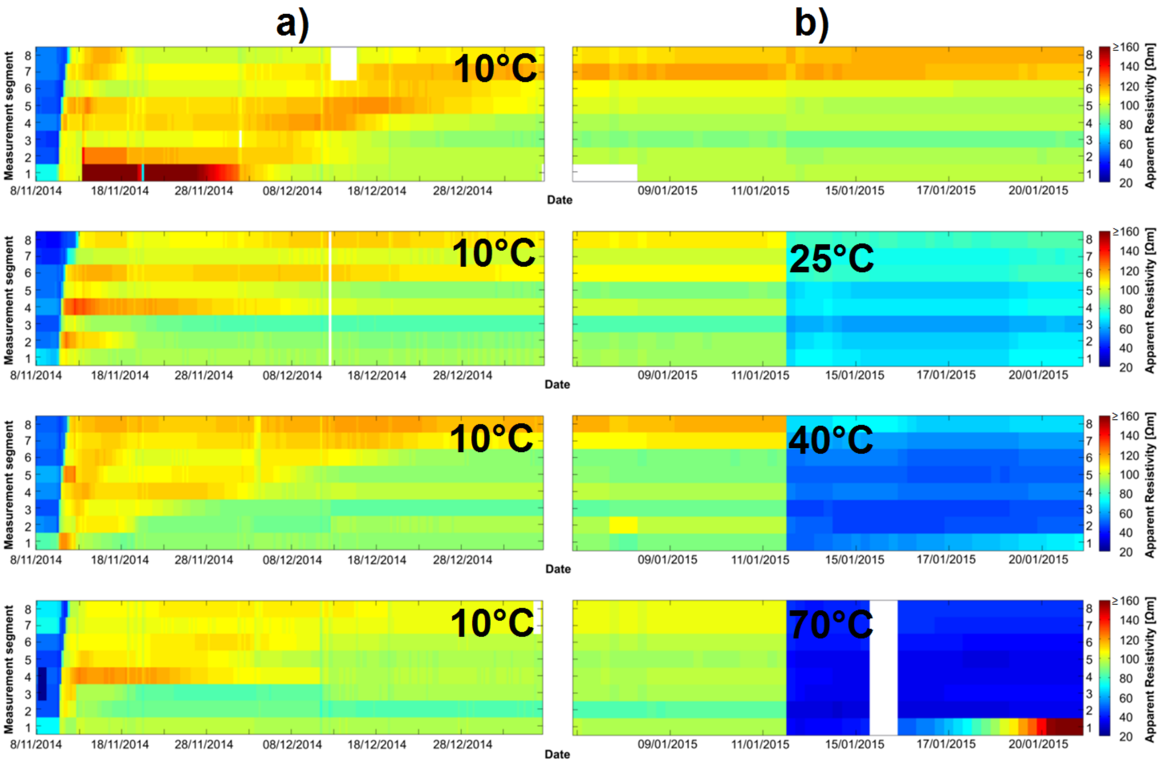

Fig. 2.6: Electrical resistivity results of each of the four columns in the first two months in the freezer at a temperature of 10 °C. After the first three days with relative low electrical resistivity results (between 60 to 80 Ohmm) the switch on of the groundwater circulation induced an increase of the resistivity values up to 110 Ohmm (a). Electrical resistivity results of each of the four columns in the switchover of the base line monitoring to the heating phase (b). Erroneous values are coloured white.

To prove the influence of the temperature and to exclude possible gas-phase influence, the measured values of the first two days after starting the heating period were compared to the model of Dachnov (1962) (Ch. 2.3.2, Eq. 2.4). Fig. 2.7 shows all measured values from 13th to 15th of January, over the whole range with its minimum and maximum values, for all four columns (10 °C, 25 °C, 40 °C and 70 °C) and the values calculated based on Dachnov (1962). Even with the outliers in the segments at the top of the column at 10 °C and 40 °C (Fig. 2.7) the plotted measured values show a good agreement with the calculated values according to the model of Dachnov (1962).

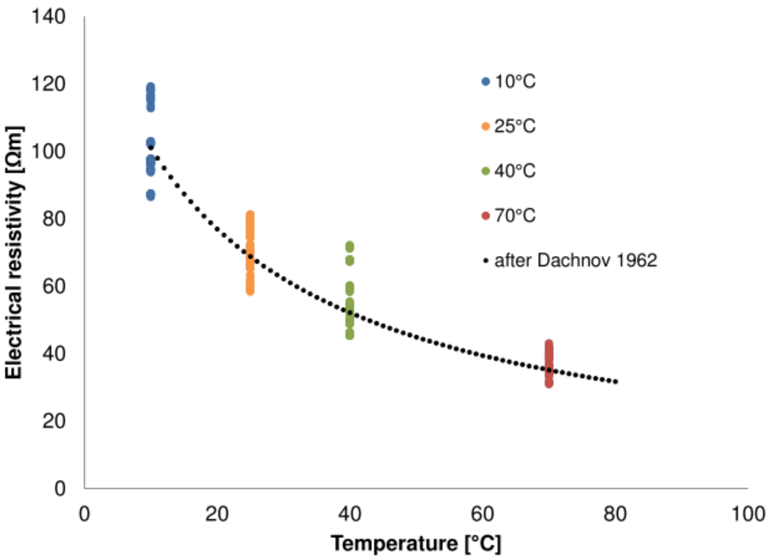

Fig. 2.7: The measured resistivity values of the four columns of every segment in the differing heights from 13th-14th January in comparison to the calculated values based on the model of Dachnov (1962).

However, anomalies were found in the lowest measurement segment in the column heated up to 70 °C starting at the 17th of January (Fig. 2.6b: 70 °C). Since these high electrical resistivity values reach up to 200-500 Ωm, these anomalies cannot be explained by the temperature influence anymore. Consequently there must be changes in the pore filling such as displacement of the pore water by gas-phase formation. Thus, based on equation 2.6 (Ch. 2.3.2) a gas-phase saturation of 55-70 % was calculated for this measurement segment depending on the measured resistivity values. In the column heated up to 40 °C, little anomalies were found starting in the end of January, high anomalies with similar values (150-350 Ωm) analogue to the lowest segment of the column at 70 °C were found at the end of March. Corresponding to equation 2.6 (Ch. 2.3.2) we found a gas-phase saturation between 40-60 % varying over time based on the measured resistivity values. In the lowest segment of the column heated up to 25 °C, smaller anomalies (up to 150 Ωm) have been observed starting in June (Fig. 2.8: 25 °C). Here, a gas-phase saturation of approximately up to 25 % was calculated.

Moreover, after the first occurrences of these anomalies in each column, the high electrical resistivity values did not persist constantly. Fig. 2.8 illustrates the behaviour of the electrical resistivity of the columns from 5th of February until 6th of March and later in June. The changes of the electrical resistivity in the lowest measurement segment proceed heterogeneously instead of a continuous drift leading to the suggestion of outgassing phases. Since these changes occur almost simultaneously over the entire term of the experiment (here only presented for the stated time from February to March and June, cf. Fig. 2.8), a manual impulse based on the water sampling can be assumed. However, the measured values in the segments above do not represent similar anomalies that would indicate a drift of the gas fraction towards the upper measured segments as we could observe for in the base measurements with the illustrated fans (Fig. 2.6a).

Based on the assumption that gaseous bubbles should migrate upwards and accumulate at the top of the columns, higher resistivity values in the upper measurements segments should be monitored from time to time compared to the central measurement segments. Occasionally, in the upper measurement segment of the column at 40 °C increased resistivity values have been observed (Fig. 2.8: 40 °C, June). In response to equation 2.6, for the upper segment a gas-phase saturation of approximately 15 % was calculated. This effect was not measured at the other columns. However, as introduced in chapter 2.3.2 (and cf. Fig. 2.1) based on the arrangement of the cannulas, the most upper 15 cm of the columns could not be monitored by the electrical measurements. Thus, the results here give no information about possible gaseous accumulation in the upper segments of the columns as given in the literature (Istok et al., 2007; Ye et al., 2009).

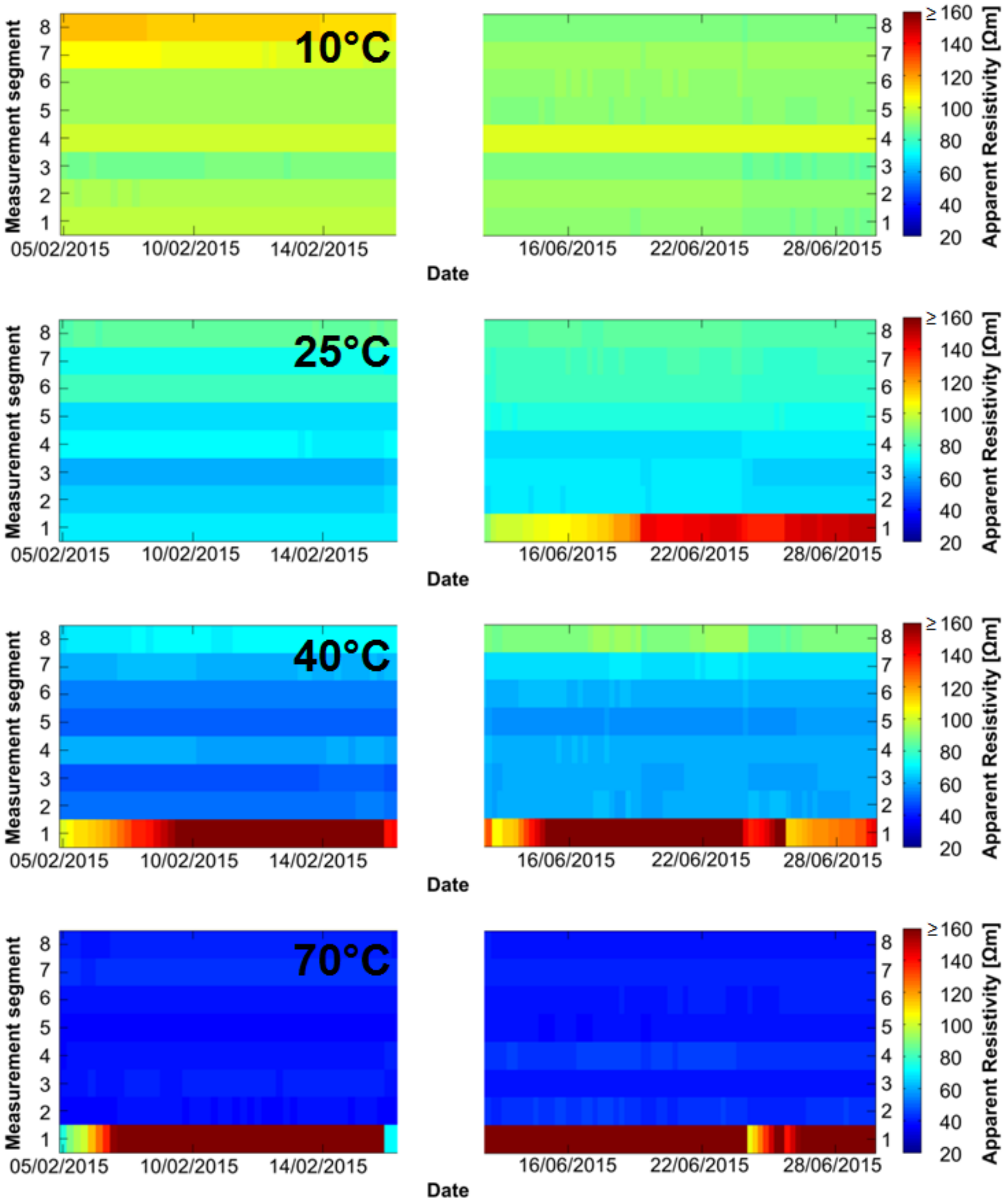

Fig. 2.8: The measured resistivity values of the four columns from 5th-16th of February and from 14th to 29th of June. The data present the variation of these anomalies during the experiment. These anomalies started in column set to 40 °C and 70 °C already in January while the anomalies for the column set to 25 °C were first registered in the middle of June. Further, the data present the increased resistivity values in the upper measurement segment of the column set to 40 °C in the end of the experimental runtime corresponding to the assumption of an accumulation of the gas bubbles at the top of the columns.

2.4.3. Calculated gas-phase formation at different pressures, temperatures and dissolved gas concentrations

Formation of a separated gas phase can be expected up to water saturated depths between 3 and 15 m when the temperature of BS site water in equilibrium with atmospheric N_2, O_2, Ar and CO_2 partial pressures is increased to temperatures between 25 and 85 °C, respectively (Fig. 2.9a). In case the CO_2 partial pressure of infiltrating water is increased to 0.05 atm due to aerobic respiration, the O_2 partial pressure needs to be reduced accordingly about the same partial pressure to keep the sum of partial pressures below the atmospheric pressure conditions of 1 atm. This leads to a gas-phase formation that extends maximum one meter deeper for the same increases in temperature (Fig. 2.9b). Averaged over the whole pressure range, the increase in gas-phase formation due to an increased CO_2 partial pressure in the soil air is more pronounced at lower- (88±4 % at 25 °C) than at higher temperatures (68±9 % at 85 °C, Fig. 2.9).

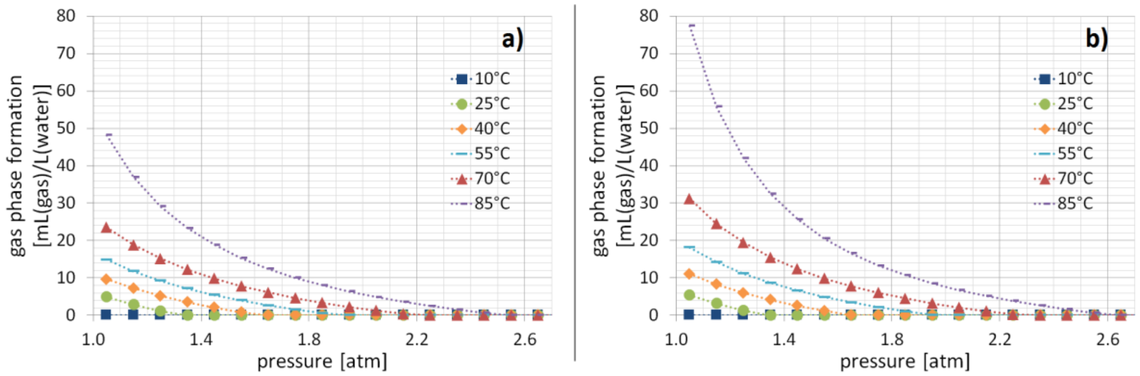

Fig. 2.9: Calculated gas volume at temperatures up to 85 °C and total pressures between 1 and 2.7 atm for near surface aquifer conditions represented by BS site water set to equilibrium with atmospheric partial pressures (a) or with atmospheric partial pressures but increased CO_2- (to 0.05 atm) and accordingly decreased O_2 (to 0.16 atm) partial pressures (b), whereby the initial total gas pressure was 1 atm in a) and b).

A gas-phase formation at higher hydrostatic pressures may also occur in case the groundwater contains additionally dissolved gases as e.g. H_2S, CO_2, CH_4, O_2, N_2 or H_2. Considering only a single gas component saturated at a particular pressure and temperature and by assuming ideal gas behaviour, a definite temperature increase at constant pressure will lead to the formation of a gas phase with a constant volume, independent from the pressure head. At initial conditions (temperature = T_{ini}, gas pressure = $p(Gas)_{ini}$ = P_{total}) the dissolved gas concentration ($c(Gas)_{ini}$ mol L^{-1}) depends on the Henry coefficient and gas pressure (Eq. 3.1):

$$c(Gas)_{T_{ini}} = K_{H_{T_{ini}}} \cdot p(Gas)_{ini} \qquad (Eq. 3.1)$$

Eq. 3.2 describes the dissolved gas concentration after heating and equilibration ($c(Gas)_{end}$ mol L^{-1}):

$$c(Gas)_{T_{end}} = K_{H_{T_{end}}} \cdot p(Gas)_{end} \qquad (Eq. 3.2)$$

With $p(Gas)_{end}$ = $p(Gas)_{ini}$ = P_{total} the variation of the dissolved gas concentration ($\Delta c(Gas) = c(Gas)_{ini} - c(Gas)_{end}$) is calculated by Eq. 3.3:

$$\Delta c(Gas) = \Delta K_H \cdot P_{total} \qquad (Eq. 3.3)$$

The amount of molecules portioning into the evolving gas phase ($n = -\Delta c(Gas)$) is linearly related to the partial pressure (= total pressure) and also linearly related to the difference in the Henry coefficients (ΔK_H) for the examined temperature increase. Thus, the number of moles in the evolving gas phase is related to the solubility as well as to the reaction enthalpy, both combined defining the ΔK_H. At a particular ΔT the ΔK_H remains constant and therefore the number of moles entering the gas phase becomes only related to the partial pressure (= total pressure). Using the ideal gas law for calculating the gas volume yields (Eq. 3.4):

$$V = \frac{n \cdot R \cdot T_{end}}{P} = \frac{-\Delta c(Gas) \cdot R \cdot T_{end}}{P} = \frac{-\Delta K_H \cdot P_{total} \cdot R \cdot T_{end}}{P}$$
$$= -\Delta K_H \cdot R \cdot T_{end} \qquad (Eq. 3.4)$$

Equation 3.4 indicates that the gas volume remains constant over the whole pressure range because of the linear relation between pressure, number of moles and gas volume in the ideal gas law. Overall, the evolving gas volume is mainly related to the gas solubility at these boundary conditions, because of only minor differences in reaction enthalpy. The solid lines in Fig. 2.10a indicate the evolving single component gas volume for heating one litre of the initial solution up to 55 °C at constant pressure conditions between 1 to 10 atm. The volume ranges from 0.0041 to 0.025 L(gas)/L(water) for H_2, N_2, O_2 and CH_4 while the one of CO_2 and H_2S ranges from 0.86 to 1.9 L(gas)/L(water), illustrating the importance of the gas solubility for the evolving gas volume. PhreeqC v3.15 (Parkhurst and Appelo, 2013) uses the Peng–Robinson equation of state instead of the ideal gas law for calculating the activity of gases in the gas phase and this results in a slightly decreasing gas volume at increasing pressure within the considered pressure range between 1 and 10 atm.

The dashed lines in Fig. 2.10 represent the evolving gas volume in case water vapour is allowed as an additional gas component in the gas phase (Fig. 2.10a). The gas-phase volume considering water vapour at lower P_{total} increases considerably compared to the single gas-phase case but with increasing P_{total} the difference becomes smaller. Eq. 3.5 describes that the partial pressure of water vapour after heating ($p(\text{H}_2\text{O})_{\text{end}}$) depends only on the temperature adjusted Henry coefficient ($\text{K}_{\text{water, T\_end}}$), assuming the activity of liquid water is equal to one:

$$\left(K_{water_{T_{end}}}\right)^{-1} = p(H_2O)_{end} \qquad (Eq. 3.5)$$

Eq. 3.5 indicates that the water vapour pressure is independent from the total pressure. Taking into account that the partial pressure of the dissolved gas after heating is now $p(\text{Gas})_{\text{end}} = P_{\text{total}}\text{-}p(\text{H}_2\text{O})_{\text{end}}$, Eq. 3.2 yields:

$$c(Gas)_{T_{end}} = K_{H_{T_{end}}} \cdot p(Gas)_{end} = K_{H_{T_{end}}} \cdot (P_{total} - p(H_2O)_{end}) \qquad (Eq. 3.6)$$

Eq. 3.6 indicates that the dissolved gas concentration after heating becomes smaller compared to the single gas-phase case because the introduction of the water vapour pressure lowers the partial pressure of the gas phase. Therefore, more molecules of the dissolved gas (H_2S, CO_2, CH_4, O_2, N_2 or H_2) will enter the gas phase and consequently a larger gas volume will establish at equal total pressure. Additionally water vapour in the gas phase increases its volume, but with a minor effect. Eq. 3.6 shows also that the relative effect of the water vapour on the final partial pressure of the dissolved gas becomes smaller at increasing total pressure. That explains the convergence of the evolving gas volume between the single gas approach and the gas-water vapour approach visible in Fig. 2.10a. Therefore, the increase of the gas volume, compared to the single gas approach, is highest at 1 atm (47 %) and lowest at 10 atm (4.1 %).

The effect of allowing water vapour as a gas-phase component on the gas-phase volume is lower at 25 °C (mean increase of 15 % (1.5 %)) and higher at 85 °C (mean increase of 338 % (16 %)) at 1 atm (10 atm) due to temperature dependency in water vapour partial pressure (data attached). In the scenario calculations (Ch. 2.3.4, 2.4.4) water vapour has to be considered as a gas-phase component as the effect cannot be neglected below 4 atm and at temperatures up to 60 °C. In the scenario calculations a multicomponent gas phase is used due to the initial dissolved gas components whereby including water vapour has an influence on all of the other partial gas pressures.

The onset for the concentration controlled gas-phase formation of H_2S, CO_2, CH_4, O_2, N_2 and H_2 is at 37, 34, 47, 50, 57 and 77 % of the saturation concentration at fixed boundary conditions of 2 atm total pressure and an exemplary temperature increase to 55 °C, corresponding to dissolved gas concentrations of 98, 36, 1.8, 1.7, 1.4 and 0.96 mmol/L, respectively (Fig. 2.10b). The gas-phase formation for H_2, N_2, O_2 and CH_4 ranges from 0.0002 to 0.031 L(gas)/L(water) while the one of CO_2 and H_2S ranges from 0.029 to 2.5 L(gas)/L(water) (Fig. 2.10b). The values stated for CO_2 represent the volume of gas-phase formation in an unbuffered aquifer (initial pH of 3.7-4.5). The initial pH is increased to 5.8-6.8 and thus the solubility of CO_2 at 2 atm is increased from 106 to

137 mmol/L by assuming a calcite buffered aquifer (CO_2-buff. in Fig. 2.10b). The volume of gas-phase formation is between 80 and 12 % higher in the buffered system compared to the unbuffered system between 37 and 100 % of the saturation concentration, respectively (Fig. 2.10b). In the calculations for scenario C CO_2 is dissolved up to saturation and as a northern German, quartz rich, carbonate poor aquifer (Table 2.2) is used as background for the scenario calculations, the unbuffered case was assumed.

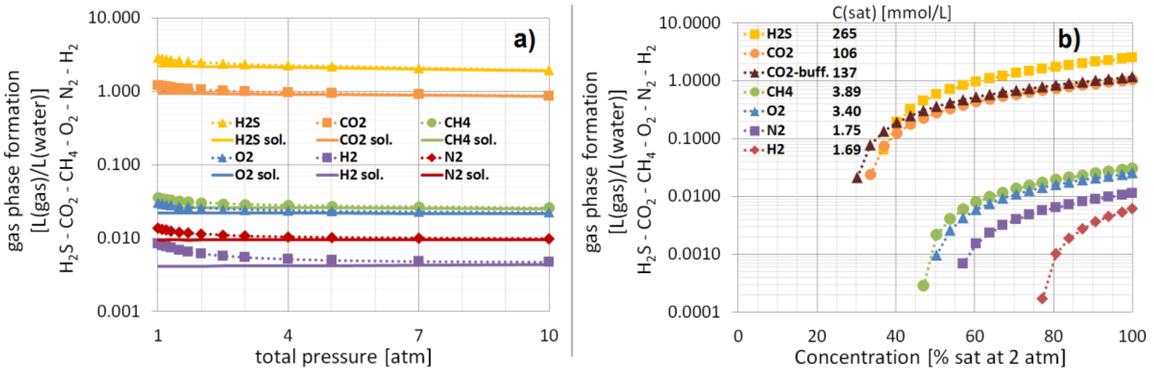

Fig. 2.10: Influence of gas-phase assemblage and pressure conditions (a) and dissolved gas concentrations at a fixed total pressure of 2 atm (b) on the formation of a separate gas phase in L(gas)/L(water) exemplarily shown for 55 °C (data for 25, 40, 70 and 85 °C is supplemented in Fig. S.2.17) - Note: uppermost data point in (b) represents C(sat) and is equivalent to the 2 atm datapoints in (a).

Water in equilibrium to atmospheric partial pressures or to a soil air enriched in CO_2 revealed temperature induced gas-phase formation only in the range of tens of mL gas per L water at its maximum (Fig. 2.9). To assess potential impacts of such a gas-phase formation, an accumulation of the gas phase with time due to the groundwater flow has to be considered. The volume of a temperature induced gas-phase formation slightly decreases with pressure (depth) and thereby approaches a stable value due to a diminishing contribution by water vapour, even in case a source leads to saturated dissolved gas concentrations. Hence the formation of a separate gas phase cannot be excluded solely by the fact of high aquifer pressures without knowledge about the physical and geochemical site conditions.

Degradation of organic carbon or pollutants, which might be intensified at higher temperatures (Bonte et al., 2013a; Jesußek et al., 2013a), can increase dissolved concentrations of reaction products as CO_2, N_2, H_2S and CH_4. Threshold dissolved gas concentration which trigger the onset of a gas-phase formation for N_2 and CH_4 are comparably smaller as for H_2S or CO_2 (Fig. 2.10b), thus at sites containing a lot of degradable organic carbon (natural or pollutant), the formation of a separate gas phase can depend on the preferential degradation pathway. In terms of estimating the extent of a gas-phase formation, the predominant degradation process has to be considered temperature dependent as well (Bonte et al., 2013a; Jesußek et al., 2013a).

2.4.4. Effects on gas-phase saturation and hydraulic conductivity in the zone of maximum residual gas-phase saturation (S_{grm}) by scenario calculations

In the heat storage model used as background for the scenario calculation the temperature gradient gets steeper with decreasing distance to the field of borehole heat exchangers (Fig. 2.2). The ratio of gas-phase formation per litre water follows the temperature gradient and so most of the gas phase forms in the direct vicinity of the BHE´s. To account for the lateral differences in gas-phase formation, the scenario field was divided into five sections (S_5 shown in red (closest), S_4 in yellow, S_3 in green, S_2 in blue and S_1 not shown (furthest)). Within these sections the gas-phase formation is horizontally averaged. Gas-phase formation in S_1 is distributed over 63 m in flow direction resulting in only six exchanged pore volumes over 30 years of runtime. The wide extent of this S_1 together with a temperature increase of only 5.5°K leads to a very flat temperature gradient and thus only neglectable effects arise which are not further discussed. Forming gas phase is assumed to accumulate where it is produced due to immobility as long as gas-phase saturation is below the S_{grm}. Further generated gas phase is assumed to horizontally and/or vertically migrate out of the zone of gas-phase formation (Ch. 2.4.5).

The average gas-phase saturation in S_5 of the 10 m thick aquifer increases up to ~25 % for a S_{grm} of 30 % (Fig. 2.11a) or ~30 % for a S_{grm} of 50 % (Fig. 2.11b) after 30 years of runtime in case oxygen is consumed and nitrogen is produced up to saturated dissolved gas concentrations under atmospheric pressure conditions by aerobic respiration and nitrate reduction (scenario A). Already in S_4 the gas-phase saturation is less than 10 % after 30 years of runtime while the farther away S_3 and S_2 are even less affected (Fig. 2.11a/b). In S_5 the increase in gas-phase saturation is limited to ~5 % (Fig. 2.11a/b) within the first five years. This results in a decrease in hydraulic conductivity of ~20 % with a remaining hydraulic conductivity still nearly double as high as the initial hydraulic conductivity at 10 °C (Fig. 2.11c/d). The depth averaged hydraulic conductivity remains increased over most of the runtime as the reduced density and viscosity outweigh the decreasing water saturation (Fig. 2.11c/d). This would lead to an increased groundwater flow velocity in the heated zone (Popp et al., 2015). Hydraulic conductivity in S_5 decreases below the value of undisturbed groundwater at 10 °C only after ~23.5 years runtime and in case S_{grm} is 50 % (Fig. 2.11d).

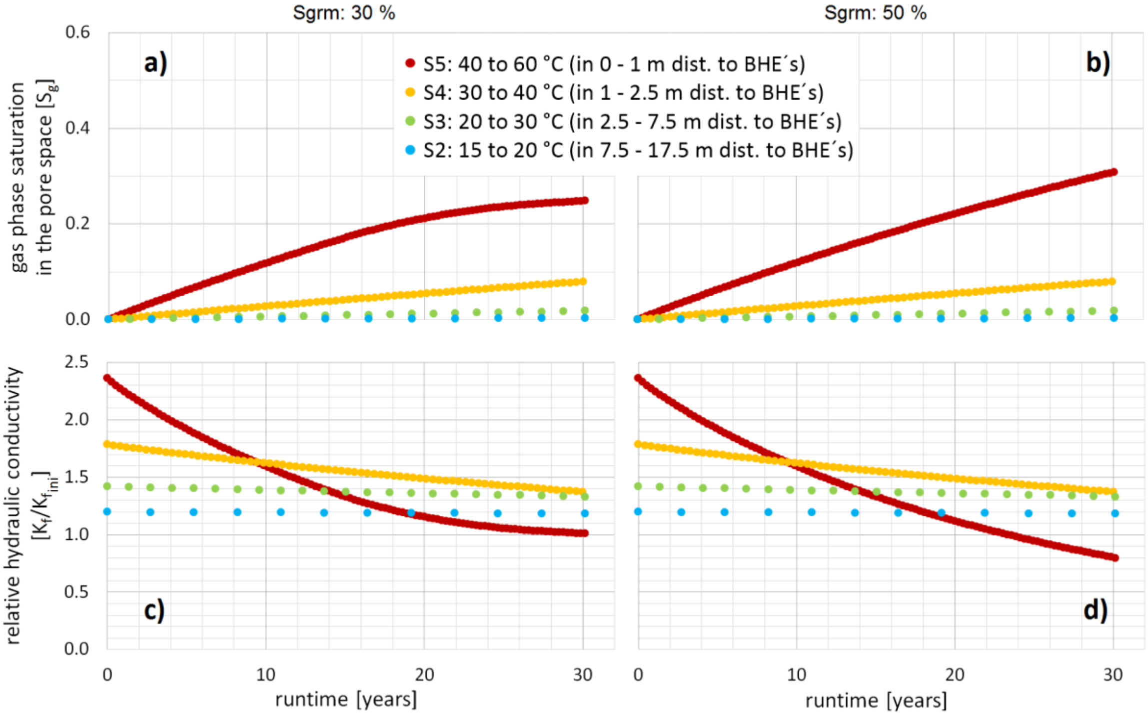

Fig. 2.11: Development of gas-phase saturation in the pore space (a, b) and relative hydraulic conductivity (c, d) averaged over the 10 m thick aquifer in 30 years of runtime as a seasonal heat storage under conditions of scenario A with a S_{grm} of 30 (a, c) or 50 % (b, d).

The assumption of a vertically homogeneous distribution of the gas-phase formation from the top to the bottom of the 10 m thick aquifer in scenario A, is a simplification. For the most affected S_5, the increase in gas-phase saturation (Fig. 2.12a/b) and the decrease in hydraulic conductivity (Fig. 2.12c/d) were therefore additionally calculated depth specifically. Gas-phase saturation increases up to the assumed S_{grm} of 30 % in water saturated depths of 0 to 7 m (Fig. 2.12a). The amount of volume-based gas-phase formation decreases with pressure and depth in a comparable way as it was shown for BS site water equilibrated with atmospheric partial pressures (Fig. 2.9). As a consequence, with each meter in depth from 0 to 7 m it takes longer to reach a S_{grm} of 30 %. At depths between 7 and 10 m 30 % gas-phase saturation is not reached at all within the 30 years runtime (Fig. 2.12a). Hydraulic conductivity in the upper 7 m decreases below initial values (Fig. 2.12c/d) which is not apparent from the depth averaged results in case S_{grm} is 30 % (Fig. 2.11c). Gas phase being generated after S_{grm} is reached, will start to migrate out of the zone of gas-phase formation (Ch. 2.4.5). A S_{grm} of 50 % is not even reached at the top of the aquifer within 30 years runtime (Fig. 2.12b), so probably no or very limited gas-phase migration can be expected in this case.

Nitrogen partial pressures in the soil air are reported to remain about constant on an atmospheric level (Matthes, 1990), though the data available (e.g. Andrews et al., 2005) and also the measurements done within this study imply high dissolved concentrations near equilibrium to a pure N_2 gas phase being more the rule than the exception. Already temperatures in a range of 40 to 60 °C can cause the formation of a separate gas phase to an extent that lowers hydraulic conductivity below initial values, even if no further dissolved gases in addition to N_2 are present in considerable amounts. So especially in near surface aquifers situated in water saturated depths of less than 10 m, as in scenario A, heat storage application design needs to consider the interaction between pressure, operating temperature and dissolved gas concentrations.

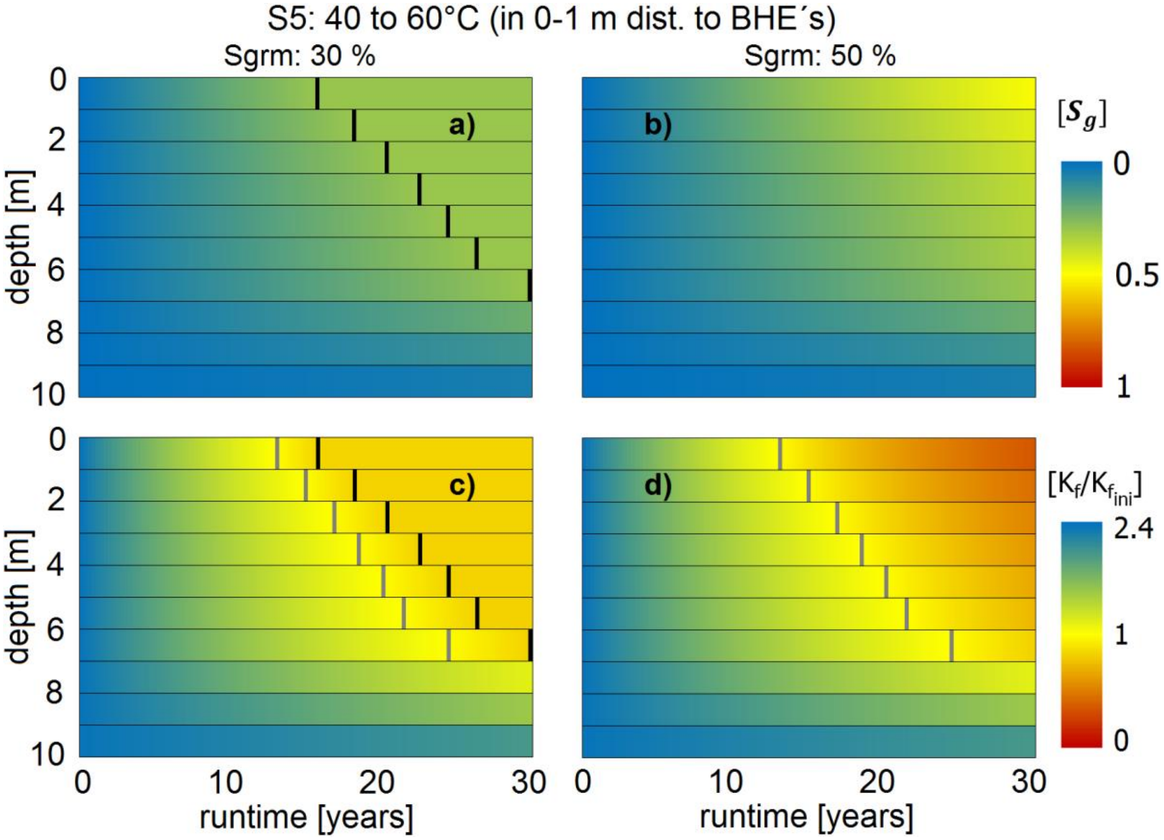

Fig. 2.12: Depth specific resolution of changes in gas-phase saturation in the pore space (a, b) and relative hydraulic conductivity (c, d) for scenario A with assumed S_{grm}´s of 30 % (a, c) or 50 % (b, d) inS5; markers in black indicate runtime when S_{grm} is reached, markers in grey indicate runtime when hydraulic conductivity is equivalent to the initial value at 10 °C.

If methane is dissolved up to saturation due to the presence of a methane source in addition to dissolved N_2 (scenario B), the average gas-phase saturation in the 10 m thick aquifer S_5 increases up to assumed S_{grm}´s of 30 or 50 % in 14 or 29 years, respectively (Fig. 2.13a/b). In S_4 gas-phase saturation reaches 24 % after 30 years of runtime (Fig. 2.13a/b). In this scenario it lasts 12 and 21 years until the hydraulic conductivity in S_5 and S_4 decreases below the initial hydraulic conductivity (Fig. 2.13c/d). If the increased hydraulic conductivity due to viscosity and density effects is set as basis, over the whole runtime of 30 years, the depth averaged hydraulic conductivity decreases about 65 and 86 % in S_5 for assumed S_{grm}´s of 30 and 50 % (Fig. 2.13c/d). Gas-phase saturations are limited to 10 % or even less in the farther away S_3 and S_2 (Fig. 2.13a/b). In S_5, gas-phase saturation increases to 11 % and hydraulic conductivity decreases by 31 % within the first five years of runtime (Fig. 2.13a-d). This corresponds to an intensification of the increase in gas-phase saturation and decrease in hydraulic conductivity of ~100 and ~50 % compared to scenario A, respectively.

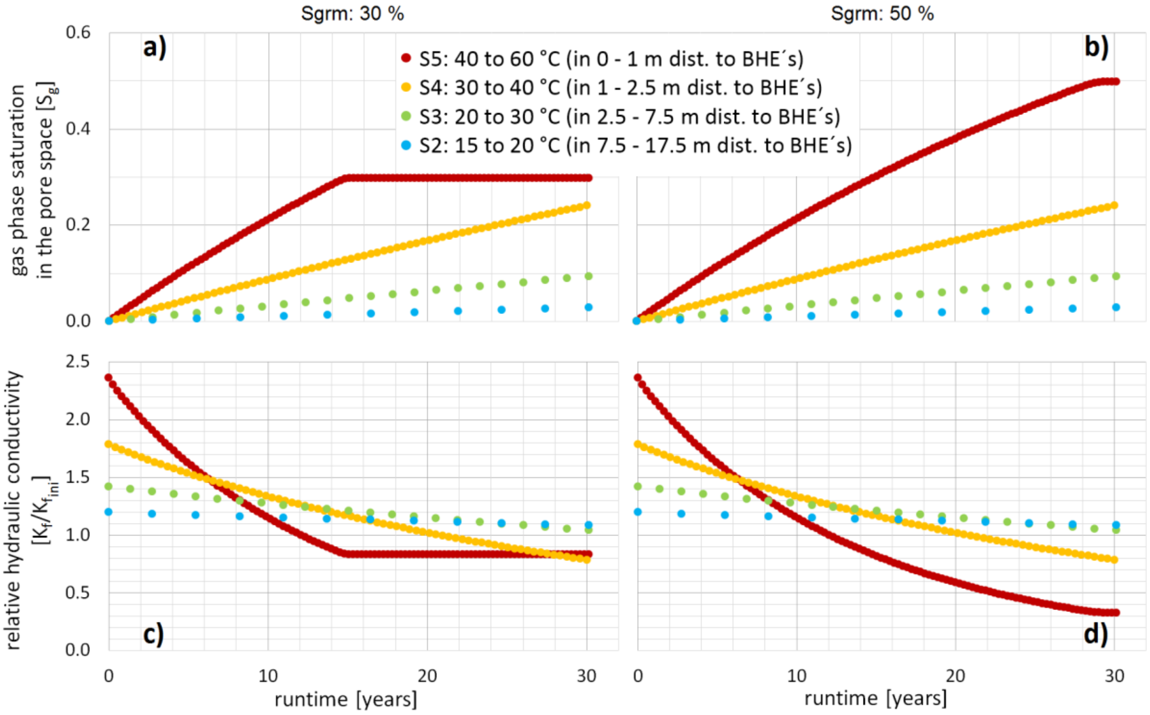

Fig. 2.13: Development of gas-phase saturation in the pore space (a, b) and relative hydraulic conductivity (c, d) averaged over the 10 m thick aquifer in 30 years of runtime as a seasonal heat storage under conditions of scenario B with a S_{grm} of 30 (a, c) or 50 % (b, d).

Again, the most affected S_5 closest to the BHE´s is further investigated depth-specifically in 1 m units. But differences in gas-phase formation and thus changes in gas-phase saturation and hydraulic conductivity with depth are very limited (Fig. 2.14a-d) as methane is dissolved up to the dissolved saturation concentration in each depth (under the precondition of the N_2 concentrations of scenario A). This homogeneous gas-phase formation with depth can be traced back to the small changes in temperature induced gas-phase formation shown for individual gases dissolved up to saturation at total pressures between 2 and 3 atm (Fig. 2.10a). So the main findings of the depth averaged calculations for S_5 (S_{grm} is reached after 14 and 29 years, decrease of hydraulic conductivity of 65 and 86 %, both for a S_{grm} of 30 and 50 %, respectively; Fig. 2.13a-d) also apply for each specific depth (Fig. 2.14a-d). Gas phase generated after S_{grm} has been reached will contribute to the excess gas volume (Ch. 2.4.5).

Possible sources for dissolved methane concentrations as assumed for scenario B are degradation processes of natural or pollutant OC (e.g. Appelo and Postma, 2005), natural migration from deeper layers (Coldewey and Melchers, 2011; McIntosh et al., 2014) or leakages from production (or storage) wells (van Stempvoort et al., 2005). The latter is not known to be a widespread problem in Germany but in case of increasing utilisation of the subsurface including gas storage in porous formations in the future (Pfeiffer and Bauer, 2015), the possible impacts of leakages on the geochemistry of near surface aquifers are already being investigated for ambient groundwater temperatures (Berta, 2017; Berta et al., 2018, 2016, 2015).

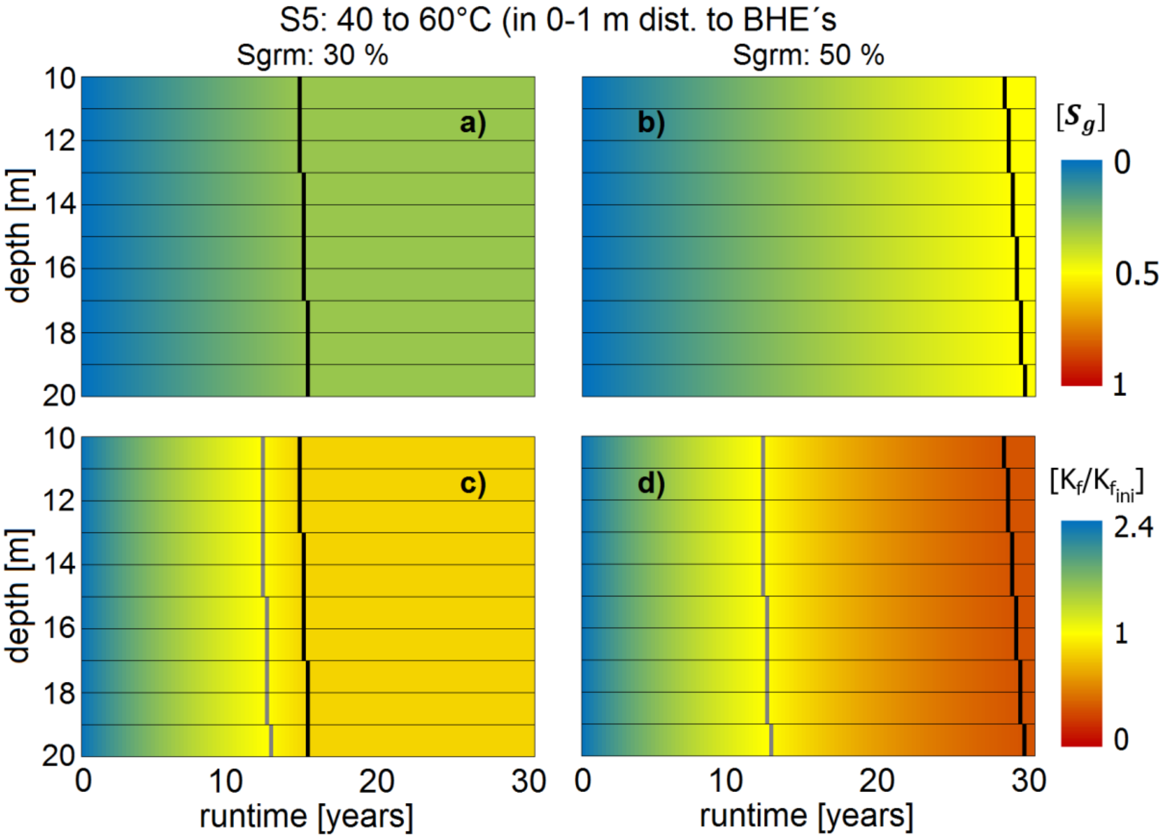

Fig. 2.14: Depth specific resolution of changes in gas-phase saturation in the pore space (a, b) and relative hydraulic conductivity (c, d) for scenario B with assumed S_{grm}´s of 30 % (a, c) or 50 % (b, d) in S5; markers in black indicate runtime when S_{grm} is reached, markers in grey indicate runtime when hydraulic conductivity is equivalent to the initial value at 10 °C.

A S_{grm} of 30 (or 50) % in S_5 and S_4 is reached within the first (two) year(s) if CO_2 is dissolved up to saturation in addition to dissolved N_2 (scenario C) (Fig. 2.15a/b). Basically the same pattern is visible for the hydraulic conductivity whereas the discrepancies between the different sections result from the deviation in the temperature effect on viscosity and density (Fig. 2.15c/d).

Dissolved CO_2 concentrations need to be about a magnitude higher to cause the formation of a separate gas phase compared to those of N_2 or CH_4. Such CO_2 concentrations probably only occur under special geochemical conditions as a natural upward migration of CO_2 bearing fluids (Battani et al., 2010; Fig. 2.10b). But under these special conditions CO_2 exemplifies how fast gas-phase saturation can reach S_{grm} in S_3 to S_5 (Fig. 2.15a/b). Gas being generated in these sections will migrate out of the zone of gas-phase formation for most of the 30 years runtime and contribute to the, accordingly huge, excess gas volume (Ch. 2.4.5).

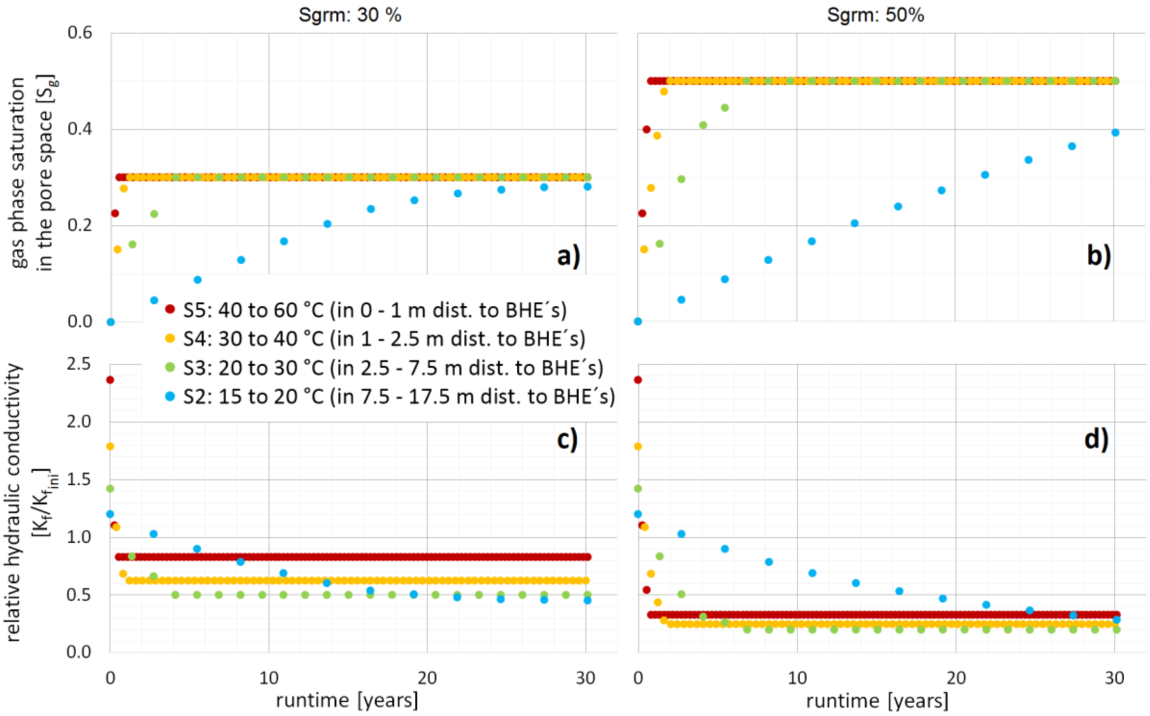

Fig. 2.15: Depth averaged (over a 10 m thick aquifer) development of gas-phase saturation in the pore space (a, b) and relative hydraulic conductivity (c, d) over 30 years of runtime as seasonal heat storage in case CO_2 is dissolved up to saturation in each depth (scenario C) with a S_{grm} of 30 (a, c) or 50 % (b, d).

2.4.5. Effects on gas-phase saturation, heat conductivity and heat capacity in the zone of gas-phase accumulation by scenario calculations

The gas-phase migration and thereby accumulation or degassing of a gas phase not trapped within the sediment starts after 16 (>30), 14 (28) and 0.5 (0.8) years of runtime for S_{grm}´s of 30 (or 50) % in scenarios A, B and C, respectively (Fig. 2.16a). Under the corresponding total pressure conditions of 1.05, 2.05 and 3.05 atm for the top of the aquifer in scenarios A, B, C, the volume of the gas phase exceeding S_{grm} is limited to 1.4 and 5.7 m³ in scenarios A and B while in scenario C the gas-phase volume sums up to ~900 and ~650 m³ for S_{grm}´s of 30 and 50 % (Fig. 2.16a). The aquifers upper boundary morphology will control the migration pathway and potential accumulation in morphological traps of this excess gas phase.

During upward migration the excess gas phase could be laterally diverted by the groundwater flow and thereby partly migrate into the heat storage site, which in the studied case extends 16 m in flow direction (2880 m³ bulk volume). To estimate the maximum possible effects on the heat storage site itself, a case in which all excess gas phase migrates into the heat storage site was assumed. Thereby, average gas-phase saturation inside the heat storage site does not exceed 0.5 and 2 % in scenarios A and B. In contrast, the excess gas volume generated in scenario C would exceed the accessible (effective) pore space (288 m³) inside the heat storage site within 10 or 14 years of runtime for S_{grm}´s of 30 or 50 % (Fig. 2.16a). These values result in a decrease in heat capacity by less than 0.1 and 0.4 % in scenarios A and B at most. Heat capacity in Scenario C decreases by a maximum of ~16 % (Fig. 2.16b). The same pattern repeats in the evolution of heat conductivity as this is decreasing by less than 0.2 and 0.6 ‰ in scenarios A and B, scenario C with 3 % again shows a higher maximum decrease (Fig. 2.16b).

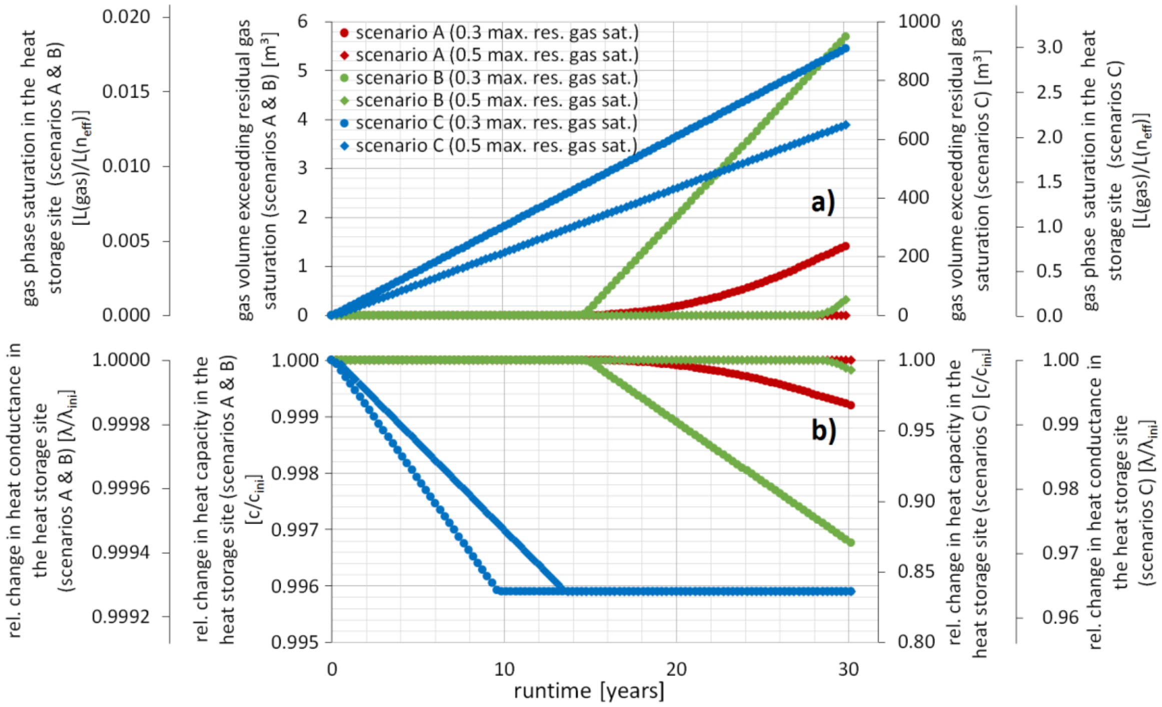

Fig. 2.16: Evolution of the excess gas-phase volume and the corresponding gas-phase saturation inside the heat storage site (a); evolution of relative changes in heat capacity and heat conductivity (b) a gas-phase saturation within the heat storage site as displayed in (a) would cause; note that Scenario A and B are always displayed on the left y-axis while scenario C is displayed on the right y-axis.

If only 0.85 mmol/L N_2 (equilibrium to a 1 atm N_2 gas phase) is present as a dissolved gas, effects of a gas-phase formation on the gas-phase saturation and thus hydraulic conductivity are limited to the uppermost meters of the aquifer. Depending on the S_{grm} of an aquifer, the S_{grm} may be reached within the 30 years runtime or not. Even by assuming that all gas-phase formation after S_{grm} is reached is laterally shifted into the field of BHE, overall effects on porous media properties within the heat storage site as e.g. heat capacity and heat conductivity remain on the per ten thousand scale and are therefore most likely negligible.

The formation of a gas phase is not restricted to the upper meters of an aquifer but may go on also in deeper regions in case additional gases (as e.g. CH_4) are dissolved up to saturation due to an assumed source beside N_2. Nevertheless, in the short term, the effects on gas-phase saturation and hydraulic conductivity will still be limited while in the long-term scale of 30 years, groundwater flow might be influenced considerably due to higher gas-phase saturations compared to the case when only N_2 is present as a dissolved gas. But impact on heat capacity and heat conductivity inside the heat storage site will still remain on the per mille scale.

Gas-phase formation in case CO_2 or H_2S are present in concentrations near solubility is on a higher scale: S_{grm} is reached within a year in the direct vicinity of the BHE and is also reached within a few years in the farther away sections. In case further generated gas phase migrates out of the zone of gas-phase formation, gas-phase formation will go on over the whole 30 years runtime resulting in the build up of a large excess gas volume, probably either spreading widely at the top of the aquifer or accumulating in morphological traps. Also the impact on heat capacity and -conductivity inside the heat storage site might reach values that considerably affect sites efficiency.

2.5. Discussion

Column experiments as conducted within this study are a direct but time- and resource consuming method to determine gas-phase formation ratios. Thermodynamic calculations reproduced the high experimental gas-phase formation ratios at 70 °C with less than 2.5 % deviation. Thus thermodynamic calculations are a feasible approach to assess, at least high, gas-phase formation ratios and enable to state necessity of additional experimental investigations.

Groundwater in equilibrium with atmospheric partial pressures or with an increased CO_2 partial pressure of soil air (Matthes, 1990) causes a gas-phase formation only down to water saturated depths of 12 or 13 m, respectively, in case of heating to 70 °C. A gas-phase formation at greater depths is only initiated if initial dissolved gas concentrations are increased, which might either be caused by natural upward migration of CH_4 or CO_2 from deeper layers or by degradation of natural or pollutant OC. However, degradation of OC probably will not play a major role for dissolved gas concentrations in the highly permeable, poor in OC, northern German aquifers used as background for calculations within this study unless there is e.g. a source zone of organic pollutants (e.g. Feisthauer et al., 2012). Considerable contribution of OC degradation to dissolved gas concentrations occurs in limnic sediments with CH_4 concentrations going up to 1 mmol/L (Juutinen et al., 2009; Schulz and Conrad, 1995) or with even higher CH_4 concentrations in marine sediments (Reeburgh, 2007). Thus, especially at increased temperatures (Bonte et al., 2013a; Jesußek et al., 2013a) and in OC rich, cohesive sediments, increased dissolved gas concentrations due to degradation processes can be expected. Though, in contrast to limnic- or marine sediments beside CH_4 also dissolved N_2 concentrations can be increased in case of high nitrate concentrations caused by agricultural land use (Puckett and Cowdery, 2002; Visser et al., 2009; Wendland et al., 1998).

Appearing gas-phase saturations and subsequent decreases in hydraulic conductivity in the heat storage setting used here vary from very restricted to more substantial in the three scenario calculations. For a frequent setting like scenario A, gas-phase saturation only slowly increases with time, which results in comparable small effects on aquifer hydraulics in the first years of runtime. But as the gas phase accumulates over time, a S_{grm} of 30 % in the most affected S_5 is reached during 30 years in the upper 7 meters. Independently from the S_{grm} or the applied scenario, the temperature induced focused flow due to viscosity and density effects is at least counterbalanced in the direct vicinity of the BHE´s (S_5). In consequence, also a gas-phase formation appearing marginal in the first year(s) of operation should be quantified to estimate long term evolution. Back dissolution of former generated gas phase could occur in periods without heating if the inflowing water is not saturated with dissolved gases. Thereby gas-phase accumulation would slow down in scenario A, but would not change in scenarios B and C due to gas saturated conditions.

Gas-phase accumulation over time is considerably controlled by the groundwater flow velocity as this linearly corresponds to pore water replacement in the heated zone of an aquifer. Van Loon (1991) states a groundwater flow velocity <0.03 m/d or <0.11 m/d as suitable for small (25 m^3/h) or large ATES projects (500 m^3/h), respectively. Nevertheless, groundwater flow velocities one or two magnitudes higher may occur in aquifers mainly consisting of middle or coarse grained sands (Pannike et al., 2006). In Addition to the correspondingly faster gas-phase accumulation due to the increased groundwater flow velocity the temperature profile upstream of the heat storage site would become steeper due to a shift in heat propagation from more diffusive controlled to more advective controlled. This would result in an even more focused gas-phase formation, accumulation and subsequent migration directly upstream the heat storage site.

Another crucial factor for the spatiotemporal distribution of a forming gas phase is the S_{grm} of a sediment as this value controls whether a smaller or larger amount of gas phase stays within the zone of gas-phase formation or starts to migrate. Values for S_{grm}´s reported in the literature show a wide range from 14 % to 55 % (Fry et al., 1997) with other studies lying in between (Istok et al., (2007), 20 % or Ye et al., (2009), 40-50 %). Krol et al. (2011) attributed the difference in S_{grm} of different sediments or sands to pore- and grain size distribution. The column experiments done within this study showed S_{grm} of ~25, ~60 and ~70 % in the zone of gas-phase formation in the columns heated to 25, 40 and 70 °C indicating an influence of the temperature dependent fluid- and gas-phase properties on the S_{grm}. In settings where due to the interplay between temperature, pressure and dissolved gas concentrations a considerable gas-phase formation can be expected, S_{grm} should be site-specifically estimated, as the S_{grm} controls the maximum decrease in hydraulic conductivity. Accumulation of a gas phase does not only lead to subsequent changes in hydraulic conductivity but will also effect porous media properties as heat conductivity, heat capacity and geotechnical behaviour. Overall effects on heat conductivity and heat capacity of a heat storage site will remain rather low in this study´s aquifer settings in case no dissolved gas concentrations near saturation of CO_2 (or H_2S), as used in scenario C, are present. This might be different in OC-rich, cohesive sediments as gas-phase formation can be enhanced by degradation processes. Furthermore, low permeability can limit gas-phase migration causing an accumulation of gas phase exceeding S_{grm} within the zone of gas-phase formation and thus intensify impact on heat conductivity, -capacity and geotechnical behaviour. Especially for near surface heat storage applications within urban areas, the question how subsurface geotechnical behaviour is affected by gas-phase saturations up to 70 % has to be addressed in the future.

However, the formation of a gas phase cannot be seen particularly positive or negative in general in terms of efficiency. In a heat storage site where heat is injected and extracted by a field of borehole heat exchangers (BTES), any decrease in groundwater flow, due to wide-ranging flow deflection caused by the formation of a gas phase directly upstream of a heat storage site, will reduce the advective loss of heat to the surrounding aquifer and thus can increase the sites efficiency. On the contrary, in any heat storage site where water is injected and extracted to store heat (ATES), a gas phase would lead to a wider distribution of the injected water and thus probably lower the sites efficiency by reducing recoverability of the heated water. By aiming at disposal of heat from e.g. industrial processes or building climatisation, a wide-ranging flow deflection would lower heat dissipation and thus efficiency.

Degassing of O_2 or CO_2 can facilitate the development of reducing conditions or increase carbonate (over)saturation. In contaminated aquifers also pollutants can partition into a gas phase and might be transported into former uncontaminated zones. Collapsing of a gas phase by redissolution in case of migration into cooler areas of the aquifer could induce the reverse impacts on groundwater properties and thus in case of pollutants enlarge the contaminated area (Krol et al., 2011). Further, gas-phase formation due to heat storage in a contaminated aquifer (e.g. Picone et al., 2019; Popp et al., 2015; Slenders et al., 2010; Sommer et al., 2013) can lower mass discharge or supply of electron acceptors for microbial degradation processes by deflection of the groundwater flow.

Due to the lack of efficient high spatial resolution monitoring methods in field, the geophysical approach of electrical resistivity measurements was tested here. Since increasing temperatures and gas-phase accumulation affect the electrical behaviour of sediments antithetically, time-lapse electrical resistivity measurements should enable to derive these effects differentiated from base-line measurements. In this study the successful application monitoring of the temperature variations in the eight measurement segments based on the arrangement of the cannulas was demonstrated. Thus, the resistivity changes could be monitored in the vertical axes and ensure a spatial resolution to localise possible differing processes such as gas-phase formation and outgassing pathways. The results showed the strong and immediate onset of the effect of the different temperatures for each column after the base line measurements. The resistivity changes correlated to empirical equations for the temperature dependence based on established literature. In contrast, the influence of the temperature induced chemical reactions can be negligible for the electrical resistivity variations. Further, anomalies detected in the lowest measurement segments of each of the different heated columns in the experimental runtime could not be explained by the increased temperature since the electrical resistivities indeed increased. These increased resistivity values can be explained by decreased water saturation. This suggestion corresponds to the studies of Istok et al. (2007) and Ye et al. (2009) as the gas phase is formed in the lowest part of the columns where the cooler infiltrated water is mostly affected by the heating process. However, since no resistivity anomalies could have been observed for the central measurement segments, the monitoring do not show any outgassing phases of the collected gas in the gas trapping bottles. Further, based on the arrangement of the cannulas the upper 15 cm of the columns could not have been monitored and thus, the measurements do not observe possible gas accumulations in the upper segments of the heated columns. Therefore, further work on laboratory scale should include different electrode arrangements and configurations for an optimised spatial resolution and the possible gas-phase accumulations at the top of the columns. Since the electrode layout in the presented study was entailed due to the arrangement of the cannulas, more electrodes should be used at the sidewalls and circular around the columns, as well as at the bases of the columns in order to have a complete 3D monitoring as shown by Comina et al. (2010).

To summarise, the interplay between dissolved gas content, surrounding pressure and applied temperature increase determines if thermal energy storage causes gas-phase formation and if so also its extent. Generally spoken, if the groundwater’s gas content and the increase in temperature is low while the surrounding pressure is high, a gas-phase formation is unlikely. In contrast, a gas-phase formation is likely in case the groundwater´s gas content and the increase in temperature is high while the surrounding pressure is low. In case of gas-phase formation, groundwater flow velocity and temperature gradient in the aquifer control the gas phase’s spatiotemporal accumulation and distribution. Since all these boundary conditions can site-specifically vary to a considerable extent and the type (ATES/BTES) and dimensioning of an application additionally plays a vital role on the gas-phase formation potential, the possibility for a gas-phase formation and its effects should generally be examined during planning of thermal energy storage applications.

Acknowledgments: *We would like to thank the waterworks Odderade and the LKN Schleswig-Holstein for providing sediment samples and for giving access to wells for groundwater extraction. Further, we thank the 2 anonymous reviewers for helping us in improving the paper with their valuable comments.*

Funding: *This study is part of the ANGUS+ project (03EK3022A) funded by the German Ministry of Education and Research, which had no role in study design; the collection, analysis and interpretation of data; in writing of the report; and in the decision to submit the article for publication.*

2.6. Supplementary Material

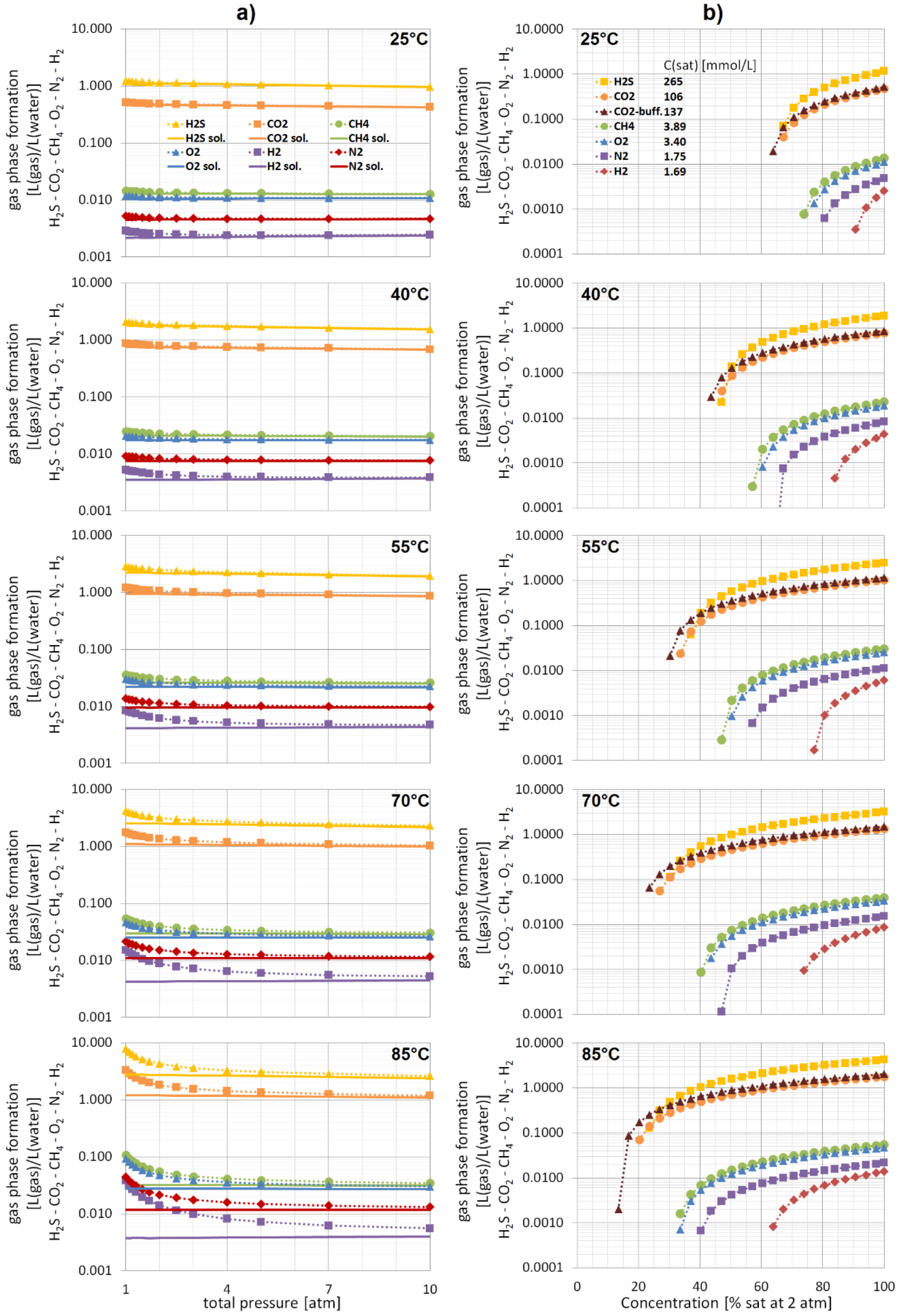

Fig. S.2.17: Influence of gas-phase assemblage and pressure conditions (a) and dissolved gas concentrations at a fixed total pressure of 2 atm (b) on the formation of a separate gas phase in L(gas)/L(water) shown for 25, 40, 55, 70 and 85 °C. Note: uppermost data point in (b) represents C(sat) and is equivalent to the 2 atm datapoints in (a).

3. Temperature influence on mobilisation and (re)fixation of trace elements and heavy metals in column tests with aquifer sediments from 10 to 70 °C

This chapter is based on a paper published 2020 by Lüders, K., Dahmke, A., Fiedler, M. & Köber, R. in Water Research 169 – 115266. https://doi.org/10.1016/j.watres.2019.115266

3.1. Abstract

The operation of seasonal underground thermal energy storages (UTES) as part of renewed heat supply systems can cause amplified temperature variations in the urban subsurface. Therefore, long-term environmental consequences for water extractions by trace elements and heavy metals (TEHMs) are a key point of concern regarding temperature effects on aquifer hydrogeochemistry. To address this issue, we report the results of flow-through and circular-flow column tests conducted with four anoxic northern German aquifer sediments, tempered to 10, 25, 40 and 70 °C and analysed for 20 TEHMs. Increased temperatures in column tests caused increasing Li, As, Mo, Sb and Ba concentrations and decreasing Ni concentrations in all of the sediments with a sediment-specific extent, whereas effects on V, Mn, Co, Tl and U concentrations varied sediment-specifically. Apart from Ba, all these components were released as a pulse in the initial heating phase, indicating a temperature dependent, finite, elutable pool. Re-cooling of the previously heated circular-flow column tests to 10 °C caused reversals of concentration changes by 30 to 95 %. This indicates a return to initial hydrochemical conditions after termination of heat storage operation and downstream from heat storages during the operations. The latter was approximated for As with a simplified analytical 1-dimensional approach, presuming transferability from a laboratory to a field scale. This reversal in concentration changes enables active cooling as a countermeasure in cases of unexpected, adverse TEHM progression. From the perspective of our findings, TEHM concentration changes appear to be temporally and spatially limited.

3.2. Introduction

The subsurface space of urban areas is increasingly affected by usage influencing predominant temperature fields. Intensified use of the urban subsurface by installing and operating seasonal underground thermal energy storages (UTES) as a component for the transformation of heat supply systems (Henning and Palzer, 2012) causes amplified temperature variations up to 90 °C (Bauer et al., 2013; Jenne et al., 1992). In addition, subsurface temperatures are affected by groundwater heat pumps used for heating or cooling purposes (García-Gil et al., 2016b), (sub)surface infrastructure in urban areas (Taniguchi et al., 2007), a combination of both (Epting et al., 2013), or thermal remediation applications for treating groundwater pollution (Beyke and Fleming, 2005). As the numbers of installed geothermal (Bayer et al., 2012) and UTES systems (Bonte et al., 2011) have steadily risen in several countries, concerns about potential conflicts with groundwater quality have arisen due to a lack of knowledge regarding their long-term environmental consequences (Bonte et al., 2011; Hähnlein et al., 2013).

Several UTES studies and field tests in the 1980s and early 1990s focussed on investigating operational aspects such as enhanced corrosion, induced precipitation of Fe and Mn (hydr)oxides in and around source and injection wells, carbonate scaling within heat exchangers and pipes, as well as technical solutions to prevent precipitations (Andersson, 1990; Jenne et al., 1992). Within aquifers, dissolution of amorphic SiO_2 and feldspars (Holm et al., 1987), precipitation of carbonates (Griffioen and Appelo, 1993), the release of organic carbon and an associated shift towards more reductive conditions (Bonte et al., 2013a; Brons et al., 1991; Jesußek et al., 2013a) are expected to be the main hydrogeochemical processes. The latter includes potential reductive dissolution of Fe and Mn (hydr)oxides and the precipitation of sulphides. Associated with these processes, trace elements and heavy metals (TEHMs) can be mobilised and fixated due to (reductive) dissolution or precipitation of minerals that incorporate TEHMs or provide sorption sites, or changes in pH and Eh conditions and subsequent changes to the speciation of solutes or charges on mineral surfaces. Bonte et al. (2013b) found significantly increased concentrations of As at 25 and 60 °C and of P, Mo, V, B and F at 60 °C by heating column tests filled with three quaternary sands. García-Gil et al. (2016) showed that B, Cd and Ni concentrations decreased and Ba concentrations increased with increasing temperatures in a current geothermal field site with groundwater temperatures up to 40 °C. Moreover, elevated temperatures of up to 25 °C with a maximum ΔT of 7 °C in a Holocene aquifer caused increasing concentrations of B and Li, which returned to baseline during re-cooling (Saito et al., 2016). With regard to temporally or spatially decreasing temperatures, Saito et al. (2016) and van Breukelen and Bonte (2016) emphasise the unknown degree of reversibility of TEHM concentration changes, which significantly controls their spatial propagation downstream from heated areas and the return to initial conditions after the end of UTES operations.

Together, these previous studies indicate that concentration changes of groundwater components, especially TEHMs, induced by temperature variations can differ considerably depending on the sediment and experimental setup. This lack of transferability between different sediments may be traced to various, interacting and hard to separate, processes that cause concentration changes to single groundwater components. Consequently, there is no profound basis for a quantifying discussion on the hydrochemical impact of temporally and spatially varying temperature fields in the range of 10 to 70 °C or higher. Therefore, this work focusses on characterising the net-concentration changes of TEHMs at varying temperature conditions in the range of 10 to 70 °C for 4 typical northern German aquifer sediments in flow-through and circular-flow column tests. Essential questions investigated include:

- Which component-specific and temporal relations between temperature conditions and TEHM concentration changes exist for the investigated sediments? Moreover, how reversible are TEHM concentration changes at varying temperature conditions?
- How do concentration changes due to elevated temperatures compare to TEHM concentration variations at ambient groundwater temperatures in different aquifer sediments?
- Which elements can be identified as of primary concern within preliminary hydrogeochemical investigations of UTES project development?

3.3. Materials and Methods

3.3.1. Sediment characterisation

Four natural sediments from anoxic aquifers in Kuden (A), Odderade (B) and Bönebüttel (C+D) in Schleswig-Holstein, Germany were obtained from waterworks drillings (see supplemental map showing sediment locations; Fig. S.3.6). Liners of sediments B, C and D remained sealed until further processing in the laboratory. Liners of sediment A were open and the sediment was exposed to the atmosphere, potentially causing oxidation of sulphides and formation of oxides. Thus, a redistribution of TEHMs before the sediment was geochemically characterised and tempered in the heating experiments cannot be excluded. For each sediment, several metres of drilling cores were homogenised by mixing them in a barrel under an argon atmosphere to minimise the effects of heterogeneity on the results. The homogenised sediment samples were characterised by geochemical analysis (Table 3.1) and stored under an argon atmosphere until needed. To obtain the total element composition of the sediments, acid-pressure digestions were used. The Si content was not directly measurable with this method. Therefore, to obtain the share of SiO_2, the oxides of all measured elements, and the loss of carbon due to ignition (Table 3.1), were subtracted from 100 %. The elemental composition of the sediments determined by acid-pressure digestions showed sediment D having the lowest total TEHM content, followed by sediments A, C, and B (Table 3.1). The sum of the main elements Na, K, Mg, Ca, and Fe followed the same order, for Si this was reversed. Sediment B contained the highest content of organic carbon and sediment C the highest carbonate content (Table 3.1). Sediment-specific contents of individual TEHMs are listed in the supplementals (Table S.3.5).

Table 3.1: Characteristics of the sediments used in the flow-through and circular-flow column tests.

	A: Kuden	***B: Odderade***	***C: Bönebüttel-shallow***	***D: Bönebüttel-deep***
sediment	Pleistocene sand	Pleistocene sand	Pleistocene sand	Tertiary lignite sand
extraction depth *[m below ground surface]*	58-74	66-68 and 69-72	4-12	67-68, 69-73 and 74-77
grain fraction d60 *[µm]*; ***d10*** *[µm]*; ***d60/d10***	326; 145; 2.2	109; 39; 2.8	343; 128; 2.7	448; 158; 2.8
silt *[%]*; ***sand*** *[%]*; ***gravel*** *[%]*	-; 99.2; 0.8	28.6; 71.3; 0.1	1.0; 96.2; 2.8	0.4; 98.5; 1.1
$C_{org.}$[1] *[mg/kg]*	343	1830	142	1070
$C_{carb.}$[1] *[mg/kg]*	55	2322	5711	63
sulphides[2] *[mg/kg]*	262	1208	221	723
Fe bound in amorphous phases[3] *[mg/kg]*	90	3000	800	600
Mn bound in amorphous phases[3] *[mg/kg]*	0.46	48	7.4	0.34
∑Na, K, Mg, Ca and Fe *[mmol/kg(sed.)]*	383	1163	1068	135
∑TEHMs *[mmol/kg(sed.)]*	5.8	16	7.8	2.5
water in use	site water (C)	site water (C)	site water (C)	site water (D)

[1] determined as chrome reducible sulphides by Dethlefsen (2015; personal communication of unpublished data)

[2] determined coulometrically by Dethlefsen (2015; personal communication of unpublished data)

[3] determined by digestion with 0.2 mole per litre ammonium oxalate at a pH of 3 adjusted with oxalic acid following the procedure described in Keon et al. (2001)

3.3.2. Water procurement and characterisation

The groundwater used for the experiments with the Pleistocene sediments A, B and C was pumped from wells in the Pleistocene aquifer (corresponding to sediment C; screened at 8-12 m). Water used with the Tertiary sediment D came from the Tertiary aquifer (corresponding to sediment D; screened at 68-72 m) in Bönebüttel, Schleswig-Holstein, Germany (Table 3.2). Water storage took place in gas-tight bags (PET/Al/PE-composite) to avoid the intrusion of oxygen. To verify the plausibility of assumed processes (e.g. dissolution of a mineral or preferential sorption of divalent over monovalent species), the speciation of solutes and saturation of minerals were calculated for the corresponding waters at the applied temperatures with the hydrochemical modelling program PhreeqC (v3; phreeqc/minteq.v4 databases; Parkhurst and Appelo, 2013).

Table 3.2: Average composition of the water in use, partially taken from Lüders et al. (2016).

		site water C	***site water D***
pH	*[-]*	7.23±0.16	7.57±0.14
TIC	*[mg/L]*	64.6±2.9	31.9±6.5
NPOC	*[mg/L]*	4.44±1.32	1.44±0.48
K^+	*[mg/L]*	1.56±0.04	1.06±0.04
Na^+	*[mg/L]*	16.6±0.7	7.36±0.23
Ca^{2+}	*[mg/L]*	140±2	55.3±0.8
Mg^{2+}	*[mg/L]*	5.59±0.24	1.56±0.02
Fe_{diss}	*[mg/L]*	1.84±0.39	0.73±0.06
Mn_{diss}	*[µg/L]*	209±5	88±2
Si_{diss}	*[mg/L]*	13.2±0.3	11.2±0.3
Al_{diss}	*[µg/L]*	4.05±1.62	6.21±1.35
Cl^-	*[mg/L]*	28.4±1.1	10.7±0.4
NO_3^-	*[mg/L]*	<0.502	<0.502
SO_4^{2-}	*[mg/L]*	91.3±2.9	14.4±1.0
O_2	*[mg/L]*	0.70±0.42	0.70±0.26
N_2	*[mg/L]*	26±1	17±3
CH_4	*[µg/L]*	51±21	21±11
Li	*[µg/L]*	3.7±0.1	2.1±0.2
V	*[µg/L]*	0.21±0.04	0.13±0.03
Cr	*[µg/L]*	0.19±0.05	0.11±0.02
Co	*[µg/L]*	1.3±0.7	0.36±0.13
Ni	*[µg/L]*	67±40	119±84
Cu	*[µg/L]*	0.39±0.16	0.96±0.72
Zn	*[µg/L]*	4.5±3.0	7.9±6.4
As	*[µg/L]*	0.25±0.05	0.13±0.07
Se	*[µg/L]*	0.16±0.01	0.12±0.02
Sr	*[µg/L]*	254±2	105±2
Mo	*[µg/L]*	0.36±0.01	0.55±0.02
Cd	*[µg/L]*	0.014±0.001	0.10±0.08
Sn	*[µg/L]*	0.010±0.003	0.011±0.005
Sb	*[µg/L]*	0.019±0.007	0.011±0.007
Ba	*[µg/L]*	80±1	29±2
Tl	*[µg/L]*	0.008±0.004	0.005±0.001
Pb	*[µg/L]*	0.082±0.023	0.082±0.034
U	*[µg/L]*	0.014±0.001	0.013±0.006

3.3.3. Experimental setups

3.3.3.1. Long-term flow-through column tests

Long-term flow-through column tests were used to examine the temporal development of TEHM elution behaviour (Table 3.3). They were also used to quantify the total elutable amount of TEHMs over the experimental runtime. Therefore, sediment C filled 110 cm long HDPE columns (internal diameter: 10 cm), were percolated with site water (Table 3.2) and tempered to 10, 25, 40 and 70 °C for 10 months using a refrigerator and heating tapes. A flow rate of 1 mL/min led to an initial residence time within the column of 36 h, which shortened at higher temperatures over the experimental runtime due to gas-phase formation and entrapment (Lüders et al., 2016). Water samples for TEHM analyses were taken at the in and outflow. A detailed description of an identical setup is included in Lüders et al. (2016).

Table 3.3: Listing and comparison of the applied experimental approaches.

experimental approaches	**attributes**	**target issues**
flow-through column tests *[4 columns; sediment C; 10, 25, 40 and 70 °C]*	• natural sediment-water ratio and flow speed • limited sediment-water contact time (36 h)	• temporal TEHM elution behaviour (continuous or time-limited release?)
circular-flow column tests α-series *[16 circuits; sediments A, B, C and D; 10, 25, 40 and 70 °C]*	• increased sediment-water contact time (~25 d) • approaching of steady state conditions • ~tenfold lowered sediment-water ratio	• determination of TEHM concentrations for steady state conditions • relation of temperature induced concentration changes to the variability between different (investigated) sediments at 10 °C
circular-flow column tests β-series *[6 circuits, sediments A and D; 25, 40 and 70 °C]*	• as α-series above • heating and subsequent cooling of the same sediment-water-system	• quantification of the reversible share of temperature induced concentration changes in the centre of a heat storage
circular-flow column tests γ-series *[12 circuits, sediments A and D; 10, 25, 40 and 70 °C]*	• as α-series above • water of heated system combined with unheated sediment for the cooling phase	• quantification of the reversible share of temperature induced concentration changes downstream from a heat storage

3.3.3.2. Circular-flow column tests

34 circuits, divided into three different experimental series, were set up (Table 3.3 and supplemental Fig. S.3.7). An α-series consisting of 16 circuits, four for each sediment, tempered to 10, 25, 40 and 70 °C, were run for eight weeks to determine TEHM concentrations at steady-state conditions. To evaluate concentration changes due to increased temperatures, these were set in relation to the concentration variations between the different sediments at 10 °C. The β- and γ-series investigated the reversible share of element-specific concentration changes (subsequently referred to as "reversibilities") in a heat storage cycle with increasing and then decreasing temperatures. These were performed for one week at increased temperatures and one week at the initial 10 °C. The β-series consisted of 6 circuits, three filled with sediment A and three with sediment D. One circuit per sediment was tempered to 25, 40 and 70 °C for one week. Afterwards, all six circuits were re-cooled to 10 °C and operated for another week, which represented a simplified heating and re-cooling phase in the centre of a heat storage without considerable advective loss of heated water. The γ-series consisted of 12 circuits, again the half filled with sediment A and the half with sediment D. Three circuits per sediment were run at 10 °C and one of the other three circuits per sediment at 25, 40 or 70 °C, respectively. After one week of operation, the columns were disconnected from the reservoir bags. Subsequently, the reservoir bag of a heated circuit was connected to a column

that was previously run at 10 °C to simulate an advective transport of thermally affected water to cooler down-gradient surroundings e.g. induced by background regional groundwater flow or mismatches in injected and extracted water volumes. The three new circuits per sediment were run for another week at 10 °C. So consequently, in the β-series, reversibility of TEHM concentration changes was tested by heating and cooling the same water-sediment system, while in the γ-series, reversibility was tested by displacing the water from the heated water-sediment system to a sediment that had remained at ambient temperatures of 10 °C. All three series were run under anoxic conditions (supplemental Fig. S.3.8 and Fig. S.3.9). A detailed description of the experimental setup and calculations of element-specific reversibilities is included in Appendix A (Ch. 0).

3.3.4. Analytics of aqueous samples

On-site parameters, main cations, main anions, TIC (total inorganic carbon), NPOC (non purgeable organic carbon) and dissolved methane were analysed by using geochemical standard methods. Dissolved O_2 was measured with an optode (NEOFOX-GT, FOSPOR-sensor; Ocean Optics, Inc., Largo, FL, USA). TEHM samples were filtered with 0.2 µm RC-filters and analysed by an inductively coupled plasma mass spectrometer (7500cs; Agilent Technologies, Inc., Santa Clara, CA, USA) following the measurement routine described in Garbe-Schönberg (1993) for the elements Li, V, Cr, Co, Ni, Cu, Zn, As, Se, Sr, Mo, Cd, Sn, Sb, Ba, Tl, Pb and U. When applicable, ICP-OES (Vista AX CCD; Varian, Inc., Palo Alto, CA, USA) measurements for As, Co and Ba were performed to improve measurement density for the flow-through column tests.

3.3.5. Estimation of potential plumes with increased TEHM concentrations around UTES sites

To address concerns regarding the geochemical effects of UTES sites on water extractions, information about the extent of potential plumes with increased TEHM concentrations are helpful. Existing complex models either focus on technical issues such as clogging (García-Gil et al., 2016a) or the redistribution of As between and around the hot and cold wells of an aquifer thermal energy storage (ATES) system based on temperature dependent surface complexation (Bonte et al., 2014).

Due to insufficient understanding of TEHM release and fixation process details and associated parameterisation deficits, we developed a simplified analytical 1-dimensional (1D) approach to estimate the progression of TEHM concentrations based on existing data. The following destails of this approach are supported by a step-by-step description for the calculations in Appendix A (Ch. 3.6.1.2).

TEHM concentrations and reversibilities were taken from the circular-flow column experiments (Chs. 3.3.3.2, 3.4.1.2 and 3.4.2). Assuming TEHM concentration changes induced by changes in temperatures are reversible (Ch. 3.4.2), TEHMs advectively transported out of thermally affected spaces at borehole thermal energy storage (BTES) sites should be re-fixated downstream. BTES fields would likely be installed in cohesive sediments whose temperature dependent TEHM release behaviour has not yet been investigated, hence data from this study´s loose sediments were used as a substitute. In ATES systems, TEHMs released around the “hot well” during the injection cycle would be partially pumped out in the subsequent hot water extraction cycle and, after reinjection, re-fixated both around and downstream from the corresponding “cold well”. This back and forth pumping of water with increased TEHM concentrations also occurs in the following storage cycles, where the exact share of TEHMs transported to the “cold well” and the share of TEHMs being re-fixated downstream from the “hot” or “cold” well depicts site specifically. However, consideration of various TEHM distributions between the “hot” and “cold” wells go beyond the scope and capabilities of this simplified 1D approach, as these calculations only consider refixation downstream from the “hot well” following the initial injection cycle. Thus, compared to a real site where re-fixation of released TEHMs is distributed to the downstream direction of the "hot" and "cold" wells, the TEHM affected distance downstream from the ATES site as a whole will rather be overestimated with these calculations.

Processes not covered, such as contact of pumped water to surface installations and associated mineral precipitation or TEHM sorption as wells as a potential gas-phase formation with effects on the flow field were also neglected in this simplified approach. Exemplarily this estimation was done for As, as As appeared to be the most relevant TEHM (Ch. 3.4.3 and Bonte et al., 2013b).

3.4. Results and Discussion

3.4.1. TEHM concentration changes due to increased temperatures: Relation to background hydrogeochemistry and associated release processes

3.4.1.1. Flow-through column tests

In the flow-through column test with sediment C heated to 70 °C, the pH decreased slightly from ~7.2 to ~7.0 within the first 10 exchanged pore volumes (PVs). Afterwards, pH conditions remained largely stable around 7.2 (see supplemental Fig. S.3.10, also for the following main groundwater components). Na and K concentrations increased with the start of heating during the first 4 PVs. The release then declined over the experimental runtime and terminated after 6 and 170 PVs, respectively. Ca and Mg decreased with the start of heating and, after ~25 PVs, the concentration decrease stabilised at a lower level. The TIC concentrations also decreased during the entire time the column was heated, indicating carbonate precipitation, which was supported by a decreasing oversaturation of calcite along the flow path. Si was released over the entire experimental heating runtime, but after a maximum at approximately 50 PVs, the release slowly declined. For the first 50 PVs, a stronger, and then declining release of organic carbon was accompanied by Eh values decreasing by 250 mV to ~200 mV with increasing Fe and decreasing sulphate concentrations, indicating iron and sulphate reducing conditions. At the lower temperatures, these effects were either occurring to a lesser extent (e.g. Na, K or C_{org} release) or not at all (e.g. sulphate reduction).

The observed TEHM concentration changes at increased temperatures can be divided into four categories. First, elements that showed a strong release after the start of heating that then diminished with ongoing experimental runtime (Li, As, Mo and Sb). Second, elements that showed lowered concentrations at increased temperatures (Co, Ni, Cu, Zn, Cd and Sn). Third, elements that exhibited continuous release over the experimental runtime (Ba). Fourth, elements whose concentrations were not substantially affected by increased temperatures (Al, V, Cr, Mn, Se, Sr, Tl and Pb). The release behaviour observed for Li, Mo and Sb was similar to that exemplarily shown for As (Fig. 3.1), where release was strongest at 70 °C for Li, As and Mo and at 40 °C for Sb. The time-limited release of these elements indicates an elution from temperature dependent, finite pools. Thus, under unchanged temperature conditions, and after depletion of the corresponding pools, further release of these elements should not occur. The total eluted amount per element over the experimental runtime in the column test at 70 °C compared to the element content in sediment C (supplemental Table S.3.5) yielded an elutable share of 0.1, 10, 15 and 2.1 % for Li, As, Mo and Sb, respectively. The elutable share of As at 10 % is within the range of the mean share of the non and specifically adsorbed As fraction (9.2 %) that were determined for 20 different soils by Wenzel et al. (2001), suggesting this fraction is a temperature dependent, elutable pool. The elements of the second category showed lower concentrations at elevated temperatures compared to the 10 °C reference experiment. For Co (Fig. 3.1), and Cu and Cd, this is related to decreasing concentrations at higher temperatures. For Ni, Zn and Sn, increasing concentrations in the 10 °C reference experiment over experimental runtime (that did not occur as strongly at elevated temperatures) were responsible. Concentrations changes of Co, Cu and Cd appeared to be longer lasting than those of the first category, although potentially stronger concentration changes in the initial heating phase might be prevented by limited starting concentrations. Ba showed a stable, continuous release at increased temperatures, which decreased slightly towards the end of the experimental runtime (Fig. 3.1). This indicates a much larger pool with differing properties compared to elements with time-limited releases (Li, As, Mo and Sb).

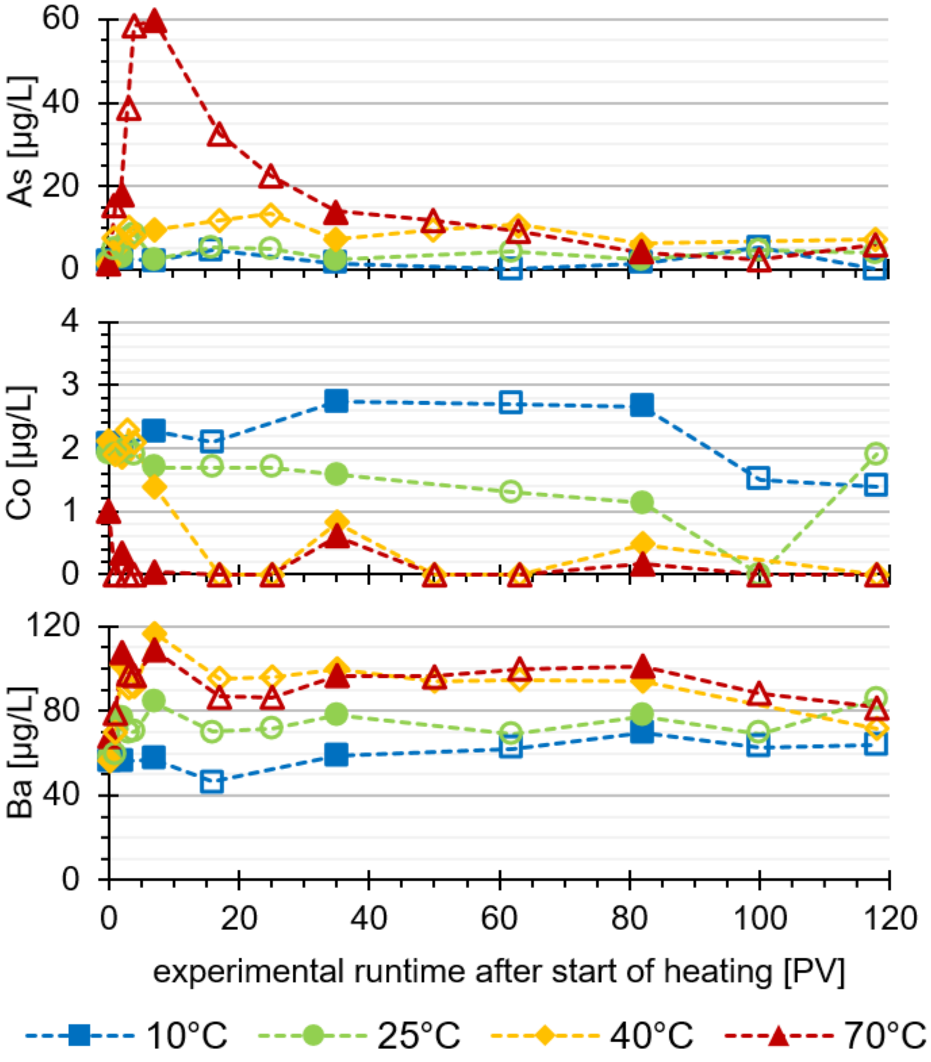

Fig. 3.1: As, Co and Ba effluent concentrations of flow-through column tests with sediment C at 10, 25, 40 and 70 °C. Full and half symbols indicate measurement by ICP-MS or ICP-OES, respectively.

3.4.1.2. Circular-flow column tests

In the α-series of circular-flow column tests (see supplemental Fig. S.3.11 to Fig. S.3.25 for graphs that show pH, Eh and concentrations of main groundwater components over experimental runtime), pH values started at ~7.3 to 7.5 for sediments A, B and C, and at ~7.7 for sediment D. At 10, 25 and 40 °C the pH values remained stable. At 70 °C the pH decreased by approximately 0.2 units within the first week, then slightly decreased further and stabilised at pH values between 6.5 and 6.7 (for sediments A, B and C) and approximately 7.4 (for sediment D). Ca and Mg concentrations decreased in sediments A and C, increased with sediment B and were stable with sediment D. TIC concentrations strongly increased at higher temperatures for all sediments, probably caused by a stronger organic carbon release and respiration. Na and K concentrations generally increased at higher temperatures, whereas Si concentrations increased over experimental runtime only at 70 and partially at 40 °C. For Na and K, this indicates desorption as the main source, while at higher temperatures the dissolution of silicates may have also contributed to increasing Na and K concentrations. Organic carbon concentrations increased over the entire experimental runtime at 25, 40 and 70 °C. Eh values fluctuated, but overall they were stable at 300 to 350 mV within the first week. After one to two weeks of experimental runtime, Eh values started to decrease to between 50 and 250 mV, with no obvious temperature trend. This drop was accompanied by decreasing sulphate concentrations at 70 °C in all sediments, at 40 °C in sediments A, C and D and at 25 °C in sediment D. Fe concentrations partially increased at 10 (C and D), 25 (A, B and D) and 40 °C (D). Mn concentration slightly increased at 10 and 25 °C with sediments A and C and were increasing stronger for sediment B at all elevated temperatures.

Comparison of circular-flow column eluate concentrations of the α-series after one and eight weeks of circuit operations at 70 °C revealed that for most TEHMs concentration changes were significantly larger in the first week of heating than in the subsequent seven weeks (supplemental Fig. S.3.26). This can be explained by discontinuous TEHM release behaviour (Ch. 3.4.1.1) or by relatively fast reaching of steady-state conditions. V, Sb and Tl concentrations decreased after concentration increases in the first week of heating, indicating a subsequent fixation process.

Examining TEHM concentrations after the initial week of heating, and before the onset of stronger reducing conditions, showed that Li, As, Mo, Sb and Ba concentrations increased with temperature in all four investigated sediments in the circular-flow column experiments; and, the extent was sediment-specific (Fig. 3.2). Depending on the sediment used, V, Mn, Co, Cu, Zn, Sn, Tl, Pb and U concentrations increased, decreased or went unchanged with increasing temperatures (Fig. 3.2). Ni concentrations decreased with temperature, but partially only after a maximum concentration at 25 °C (Fig. 3.2). The elements Al, Cr, Se, Sr, Cd and Pb were unaffected by changes in temperature (supplemental Fig. S.3.27). For sediment C, which was investigated in both the flow-through and the circular-flow column tests, the direction of concentration changes for the individual elements was equal in both setups. However, in contrast to the flow-through column tests, concentrations of Co, Ni, Cu, Zn and Sn showed a maximum concentration at 25 °C instead of 10 °C before decreasing with increasing temperatures. As several elements were affected, this behaviour might be linked to a regulating parameter such as pH, which was slightly higher (~7.6) in the circular-flow than in the flow-through column tests (~7.4) heated to 25 °C.

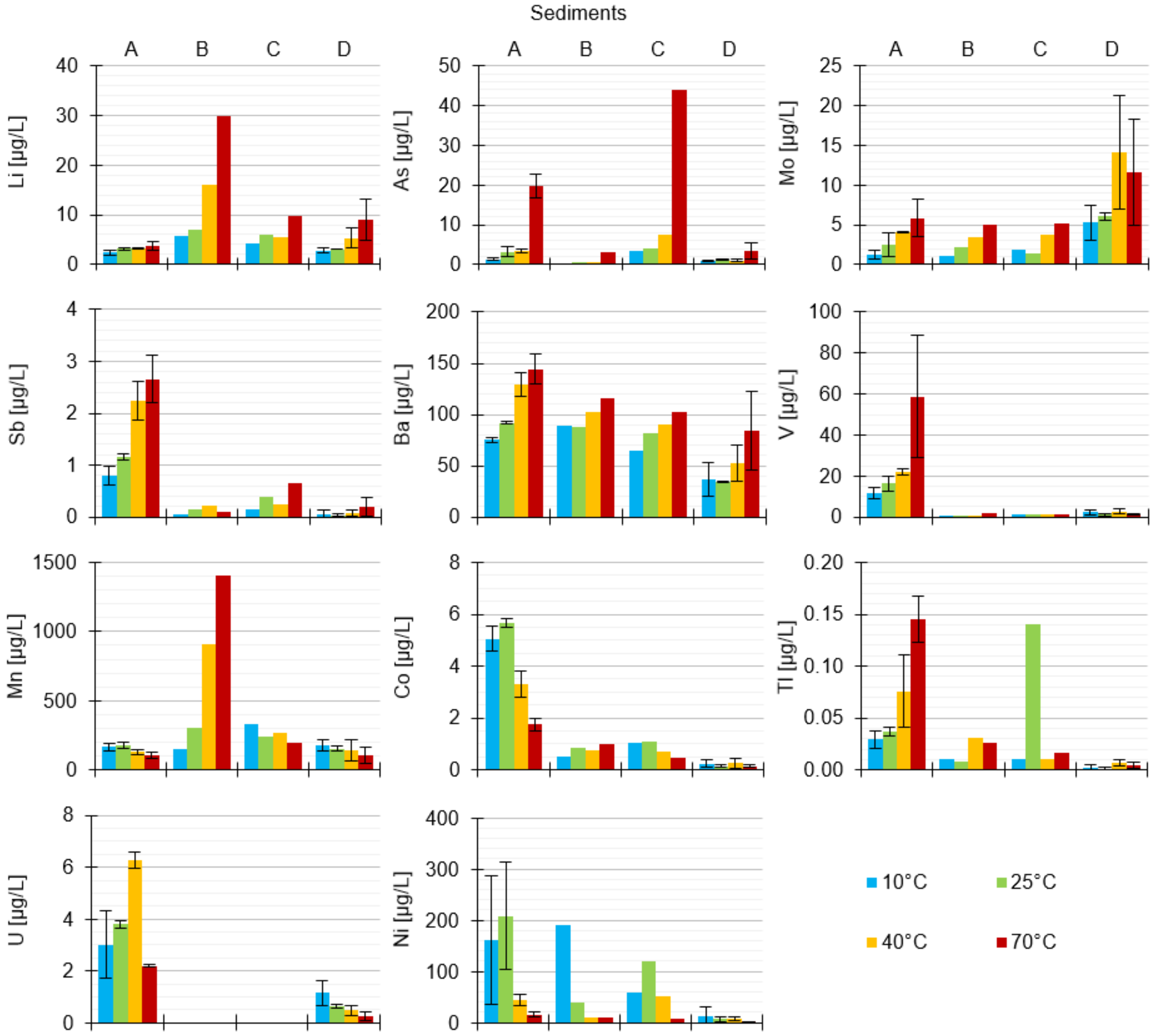

Fig. 3.2: Concentrations of Li, As, V, Mo, Sb, Ba, V, Mn, Co, Tl, U and Ni in eluates of sediments A, B, C and D after one week of tempering to 10, 25, 40 or 70 °C in circular-flow column tests. For sediments A and D the measurements after one week of heating from the α-, β- and γ-series were included, error bars indicate the standard deviation; for sediments B and C the measurements from the α-series are displayed. Equivalent graphs of Al, Cr, Cu, Zn, Se, Sr, Cd, Sn and Pb (Fig. S.3.27) and graphs for circular-flow column tests α-series including measurements after eight weeks (Fig. S.3.26) are supplemented.

3.4.1.3. Hydrochemical processes regulating TEHM concentration changes

Several TEHMs released at increased temperatures exist as oxyanions under the respective conditions. In the flow-through and circular-flow column experiments, this included the concentration increases of As, Mo, Sb (in all sediments, Fig. 3.1 and Fig. 3.2) and V (sediment-specific, Fig. 3.2). A preferential release of oxyanions has already been observed (Bonte et al., 2013b) and corresponded to the weaker sorption of anions such as arsenate, arsenite, selenate, selenite and silicate at increased temperatures (Kersten and Vlasova, 2013, 2009a, 2009b; Maji et al., 2007; Parida and Das, 1997). This weaker sorption of anions was likely caused by a decrease in the point of zero charge with increasing temperatures, predominantly coupled to a change in the dissociation constant of water (Álvarez-Merino et al., 2008; Tewari and McLean, 1972), and an associated negative enthalpy of surface complexation reactions for anions (Bonte et al., 2014; Kersten and Vlasova, 2009a). In contrast, individual studies on marine clayey material found decreasing concentrations of arsenate and arsenite at increasing temperatures (Genç-Fuhrman et al., 2004). These authors assumed this was due to better accessibility to inner surfaces caused by a widening of the grain structure and accelerated diffusion at higher temperatures, which could superpose the weaker sorption of anions in fine-grained sediments. For cations, a decrease in the point of zero charge can cause stronger sorption on variable charge surfaces as reported for Cu^{2+}, Pb^{2+}, Zn^{2+}, Ni^{2+}, Cd^{2+} and Co^{2+} (Angove et al., 1999; Echeverría et al., 2003; Rodda et al., 1993). This corresponds with the observed decreases in Co (sediment-specific, Fig. 3.1 and Fig. 3.2) and Ni concentrations (in all sediments, Fig. 3.2) with increasing temperatures and reported positive enthalpies of surface complexation reactions for cations (Bonte et al., 2014). Changes in pH can cause diverse effects, however, pH conditions show no general change due to increasing temperatures (supplemental Fig. S.3.28; Bonte et al., 2013b and Brons et al., 1991), hence, the decrease in the point of zero charge appears to be the dominant process.

A second temperature dependent process affecting TEHM concentrations may be the preferential sorption of divalent in exchange for monovalent ions at increased temperatures, as has been shown for Ca^{2+}, Mg^{2+}, Cu^{2+} and Ni^{2+} in exchange for K^+ and Na^+ by Bansal (1982), El-Batouti et al. (2003), Ogwada and Sparks (1986) and Udo (1978). When these studies presented enthalpies for the sorption reactions, they reported lower enthalpy values for the sorption of monovalent cations, suggesting a similar mechanism as for the exchange between anions and cations, as less positively charged monovalent ions were preferentially desorbed. Although not observable for all of the elements in combination with all examined sediments, cations with monovalent speciation tended to show increasing concentrations (Na^+ and K^+ in supplemental Fig. S.3.10, Fig. S.3.15 and Fig. S.3.16 as well as Li^+ and Tl^+ in Fig. 3.2), while cations with divalent speciation showed rather decreasing concentrations (Ca^{2+} and Mg^{2+} in supplemental Fig. S.3.10, Fig. S.3.17 and Fig. S.3.18; as well as Co^{2+} and Ni^{2+} in Fig. 3.1 and Fig. 3.2).

A third potential process controlling TEHM concentrations is the reductive dissolution of Mn and Fe (hydr)oxides (Bonte et al., 2013b). Their dissolution is associated with an increase in organic carbon availability and biodegradation at higher temperatures that causes a shift towards stronger reducing conditions, including potential sulphate reduction (Chs. 3.4.1.1 and 3.4.1.2; as well as Bonte et al., 2013a and Jesußek et al., 2013a). Thus, TEHMs incorporated into or sorbed on Mn- and Fe-(hydr)oxides can be released, while newly precipitated sulphides can incorporate or adsorb TEHMs at the same time and in close spatial proximity (Bonte et al., 2013b; Kabata-Pendias, 2010). Aside from sulphides, also carbonates, frequently precipitated at increased temperatures, can incorporate Fe and Mn (Griffioen and Appelo, 1993) and potentially further TEHMs associated with Fe or Mn. Consequently, decreasing concentrations of V, Sb and Tl after the shift towards sulphate reducing conditions in the circular-flow column tests (Ch. 3.4.1.2, supplemental Fig. S.3.26) were likely associated with the fixation in or on newly precipitated sulphides or carbonates.

With Ba as a divalent cation, decreasing concentrations would be expected (Katz et al., 2013). However, Ba concentrations increased (Fig. 3.1 and Fig. 3.2). In contrast to those elements being released by desorption (Li, As, Mo and Sb; 3.4.1.1), continuously released Ba (Fig. 3.1) likely originated from longer lasting mineral dissolution. This assumption is supported by observations made at an ongoing geothermally used aquifer with temperatures up to 40 °C, where Ba concentrations were positively correlated with temperature changes (García-Gil et al., 2016b), given that relatively fast sorption processes were probably already near a steady state.

In agreement with the work of Bonte et al. (2013b), there was no general correlation between released TEHMs and sediment characteristics related to sorption of TEHMs such as bulk Fe content or amorphic Fe phases for the investigated sediments.

3.4.2. Reversibility of temperature induced TEHM concentration changes

Reversibility of TEHM concentration changes was investigated with 18 circular-flow column tests of the β and γ-series for TEHMs whose concentrations were affected by increased temperatures (Li, V, Mn, Co, Ni, As, Mo, Sb, Ba, Tl and U; 3.4.1.2). Mo showed the lowest (30 %) and Tl the highest

(95 %) overall reversibility, with all other elemental reversibilities lying between 47 and 77 % (Fig. 3.3a). To investigate whether element-specific reversibilities were influenced by the heating temperature, sediment, or experimental setting, reversibilities were displayed separately for these categories. Element-specific reversibilities were averaged for experiments with equal temperatures, equal sediments and equal experimental settings and plotted against an overall average (Fig. 3.3b-d). Average reversibility at 40 °C (74 %) was only slightly higher than at 25 °C and 70 °C (57 and 59 %). The element-specific deviation in reversibility between the three temperatures ranged from 9 % (Tl) to 67 % (U), highlighting the importance of element-specific differences (Fig. 3.3b). Overall, no consistent trend between reversibility with temperature was apparent. Average reversibility in sediment A (65 %) was only slightly higher than in sediment D (62 %). Average reversibilities of Li, V, Mn, Co and Ni were higher in sediment A, whereas As, Mo, Sb, Ba, Tl and U showed a higher average reversibility in sediment D. The differences in reversibility between the two sediments reached 41 % for V, but stayed below 10 % for Mn, As, Sb and Tl (Fig. 3.3c). Average reversibilities in the γ-series (69 %) were higher than in the β-series (58 %). Only Li, As and U showed higher reversibilities in the β-series experiments (Fig. 3.3d). Similar reversibilities for the experiments with sediments from which TEHMs were released in the preceding heating phase (β-series) and for those that were not heated previously (γ-series) suggests that fixation of TEHMs due to (re)cooling was largely independent from the initial release process.

Reversibility of concentration changes with one week of re-cooling to 10 °C after a one-week phase of heating to 25, 40 or 70 °C was incomplete for all analysed TEHMs. Given the overall complexity of the systems, quantifying reversibilities was the main attempt. However, in relation to main element hydrogeochemistry and the literature, there are clues regarding the potential processes limiting reversibility. In the β-series, incomplete reversibility might be partially explained by the dissolution of Mn or Fe (hydr)oxides due to increased temperatures (Ch. 3.4.1.2) and a thermally enhanced aging of remaining Fe (hydr)oxides (Ford et al., 1997) with an associated decline in sorption capacity. However, this does not explain incomplete reversibilities in the γ-series, as the sediment in contact with the water during the re-cooling phase had not been heated. Based on the equal duration of the heating and re-cooling phases in this study, slower sorption kinetics at 10 °C, as opposed to desorption kinetics at elevated temperatures, as observed by Bruemmer et al. (1988) and Scheckel and Sparks (2001) are a likely explanation for incomplete reversibilities in both series. This should be further addressed in future studies by applying a longer re-cooling phase and, if applicable, by measuring a time series of concentrations during the heating and re-cooling phases.

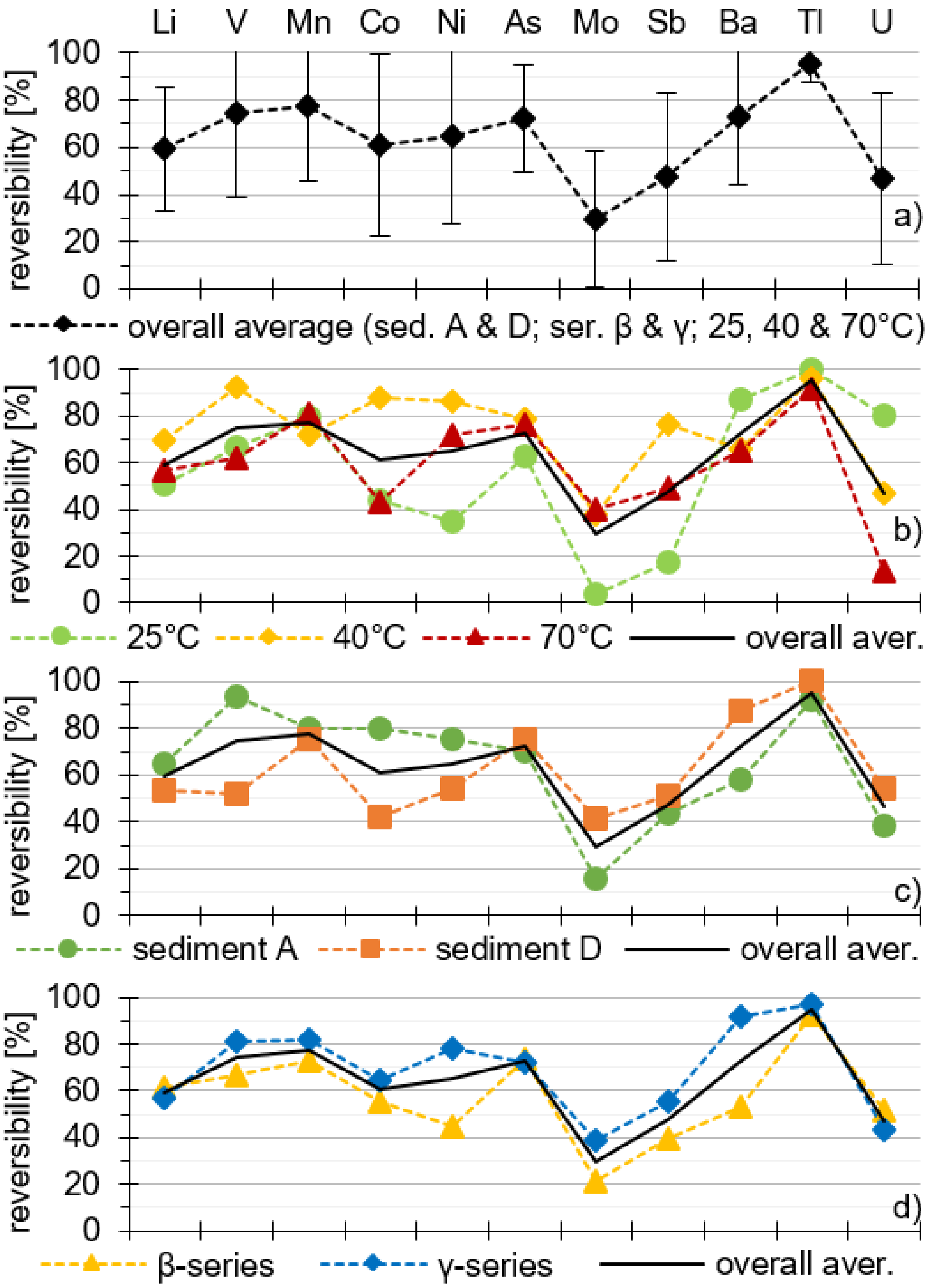

Fig. 3.3: Element-specific reversibilities of temperature induced concentration changes after re-cooling down to 10 °C for one week in circular-flow column tests; a) overall average reversibilities with the error bars indicating standard deviation; b) average reversibilities for equal temperatures in the heating phase; c) average reversibilities for equal sediments; and d) average reversibilities for equal experimental settings; in b)-d) also the overall reversibility is shown as reference.

3.4.3. Evaluation of TEHM concentration changes

The extent and frequency of pronounced TEHM concentration changes were evaluated to identify elements of primary concern for preliminary investigations of UTES project development. Three criteria were evaluated: First, concentration changes between 10 and 70 °C in the circular-flow column tests normalised to the concentration of the respective element at 10 °C, which was taken as the initial state, were used to assess the extent of relative, element-specific TEHM concentration changes (Fig. 3.4; blue bars, left axis). Second, the same concentration changes normalised to the standard deviation of concentrations measured in circular-flow column tests with all four sediments tempered to 10 °C were used to relate temperature induced changes to the variability (standard deviation) in the initial state between the different sediments (Fig. 3.4; yellow bars, right axis). Third, a review of increasing or decreasing concentrations at higher temperatures, including results published in this context.

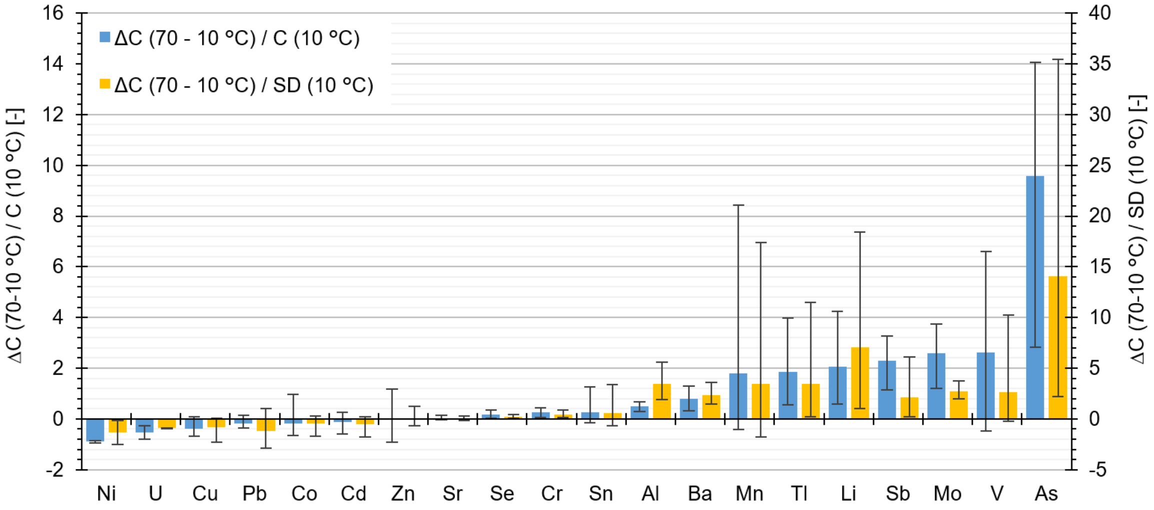

Fig. 3.4: TEHM concentration changes between 10 and 70 °C normalised to either the concentrations measured in the corresponding circular-flow column tests with the same sediment tempered to 10 °C (left axis) or the standard deviation (SD) of concentrations measured in column tests with all four sediments tempered to 10 °C (right axis). Displayed are the mean values, error bars indicate minimum- and maximum values for normalised concentration increases.

By focussing on the first and second criteria, Mn, Tl, Li, Sb, Mo, V and As showed comparatively high values in both aspects, indicating that these elements show strong temperature effects that exceed variations at ambient temperatures of 10 °C. However, to evaluate which elements should be of primary focus in future investigations, all available laboratory and field studies in this context were reviewed (Bonte et al., 2013b; García-Gil et al., 2016b; Jesußek et al., 2013a; Saito et al., 2016). TEHMs were assigned to a category from 1 to 5 representing descending relevance in preliminary hydrogeochemical investigations for UTES projects (Table 3.4) and depending on whether a specific TEHM demonstrated sediment-specifically, or for all sediments, increased or decreased concentrations at elevated temperatures, or only negligible changes. It was noted that field studies are only available for temperatures up to 25 and 41 °C, whereas laboratory work covered temperatures up to 60 and 70 °C. In the laboratory study by Bonte et al. (2013b) and in this study, As concentrations increased with temperature in all sediments and partially increased already at 25 °C. In contrast, the field studies revealed no evidence for increasing As concentrations (García-Gil et al., 2016b; Saito et al., 2016). Explanations may include differences in sediment composition, lack of data from the initial phase of heating (García-Gil et al., 2016b) when the strongest TEHM concentration changes occur in laboratory experiments (Ch. 3.4.1.1 and Bonte et al., 2013b), or an insufficient temperature increase for measurable concentration changes (Saito et al., 2016). Furthermore, sediments investigated in laboratory experiments are typically disturbed. Sediments are usually obtained from drillings, moved to the laboratory, homogenised and placed in columns. This process might cause the activation of mineral surfaces and potentially intensifies concentration changes under laboratory conditions. This is in contrast to field studies, as indicated by the concentration increases in this study´s column tests at 10 °C compared to the respective site water (supplemental Fig. S.3.29). How results from laboratory investigations are scalable to field conditions in terms of the influence of temperatures up to 70 °C on hydrogeochemistry, especially for TEHM behaviour, to our knowledge, has not yet been investigated. This issue is not further elaborated on here, but is addressed in the TestUM-Aquifer project, which combines a field heat storage test with laboratory experiments with sediment samples from the test site (see Ch. 4 for details).

Using the currently available dataset as a basis, three groups of elements (category 1-3, Table 3.4) revealed a combined concentration limit for ground or drinking water by (inter)national regulations (supplemental Table S.3.6) with increasing concentrations due to elevated temperatures in some of the investigated sediments. The first group comprises only As, which showed the strongest relative concentration increases at higher temperatures, increases that exceeded the standard deviation of As concentrations at 10 °C in most of the sediments. The second group, consisting of V, Mn and Mo, still exhibited considerable relative concentration increases at higher temperatures in several sediments that also exceeded the variability of concentrations at 10 °C, but, on average, to a lesser extent than As. The third group of elements (B, F, Cr, Co, Sb, Ba, Tl and U) was released from a limited share of the sediments at increased temperatures, and the relative concentration changes only partially exceeded the standard deviation of concentrations measured at 10 °C. For the fourth group of elements (Al, Ni, Cu, Zn, Se, Cd, Hg and Pb) no or negligible concentration increases due to elevated temperature were observed. For the fifth group of elements (Li, Be, P, Sc, Ga, Sr, Sn, La, Eu, Ho, Yb and Th) there were no concentration limits for ground- or drinking water in place, which indicates the innocuousness of concentration changes for these elements. Therefore, the elements As, V, Mn, Mo, B, F, Cr, Co, Sb, Ba, Tl and U should be treated with particular care for preliminary investigations of UTES project development. However, due to the lack of TEHM data from high-temperature field tests, the unproven transferability from the laboratory to the field and the overall limited database, this assessment of elements should be continuously verified with data from future laboratory and field/pilot studies.

Table 3.4: Overview of expectable TEHM behaviour due to increasing temperatures. Categorisation based on TEHM concentration changes in a: Jesußek et al. (2013a; one sediment, 10-70 °C), b: Bonte et al. (2013b; three sediments, 5-60 °C), c: García-Gil et al. (2016b; one field area, up to 41 °C), d: Saito et al. (2016; one field test site, up to 25 °C) and e: this study (four sediments, 10-70 °C). References a, b and e represent experimental- and c and d field studies.
Category 1: concentrations increased considerably in most sediments;
Category 2: concentrations increased in several sediments;
Category 3: concentrations increased partially to a limited extent;
Category 4: concentrations were decreasing or unaffected by changes in temperature;
Category 5: no threshold values for groundwater quality are in place (supplemental Table S.3.6).
Where necessary, subscripts indicate specific references for differentiation.

Category		**1**	**2**			**3**								**4**								**5**												
increasing temperatures lead to…		**As**	**V**	**Mn**	**Mo**	**B**	**F**	**Cr**	**Co**	**Sb**	**Ba**	**Tl**	**U**	**Al**	**Ni**	**Cu**	**Zn**	**Se**	**Cd**	**Hg**	**Pb**	**Li**	**Be**	**P**	**Sc**	**Ga**	**Sr**	**Sn**	**La**	**Eu**	**Ho**	**Yb**	**Th**	$\sum$
…increasing concentrations	*in all tested sediments*[1]	$x_{b/e}$	x_b	x_a	$x_{b/e}$	$x_{b/d}$	x			x_e	$x_{c/e}$											x		x										10
	sediment-specific[1]		x_e	x_e				x_b	x_e			x	x										x					x						7
…decreasing concentrations	*in all tested sediments*[1]														$x_{c/e}$																			1
	sediment-specific[1]			x_e		x_c			x_e				x						x_c															5
…comparatively small or no concentration changes	*in all tested sediments*[1]	$x_{c/d}$		$x_{b/c/d}$	x_c			$x_{c/d/e}$	$x_{b/c}$	$x_{b/d}$	x_b			x	$x_{b/d}$	x	x	x	$x_{b/d/e}$		x				x	x	x		x	x	x	x	x	23
	sediment-specific[1]		x_e					x_b	x_e			x											x					x						5
references: *(a: Jesußek et al. 2013;* *b: Bonte et al. 2013b;* *c: García-Gil et al. 2016a;* *d: Saito et al. 2016; e: this study)*		b, c, d, e	b, c, e	a, b, c, d, e	b, c, e	b, c, d	a, b	b, c, d, e	b, c, e	b, d, e	b, c, e	e	e	b, c, d, e	b, c, d, e	b, c, d, e	b, c, d, e	c, d, e	b, c, d, e	-	b, c, d, e	d, e	b	a, b	b	b	b, d, e	e	b	b	b	b	b	

[1] within the respective study

3.4.4. Estimated spreading of plumes with increased TEHM concentrations around UTES facilities during the initial heating phase

Although there are still uncertainties regarding process, parametrisation and transferability of concentration changes from laboratory experiments to field applications, the size ratios between an aquifer section used to store heat and potential plumes of increased TEHM concentrations were estimated to obtain an assessment concerning their potential spreading. This was done for As by calculating the distribution of As concentrations both up and downstream from numerical UTES sites. The estimated As concentrations were placed in context using a legal threshold value to deduce distances downstream from heat storages potentially affected by critical TEHM concentrations, depending on site and sediment-specific characteristics. For the generic boundary conditions of the numerical UTES sites examined here, the drinking water limit of As (10 µg/L, Table S.3.6) taken as an exemple threshold value would be undercut by two sediments with relatively high As discharges ~25 or ~45 m downstream from the the BTES field and ~200 or ~400 m downstream from the ATES injection well for sediment A or C (Fig. 3.5). In cross section, these distances are approximately 1.2 or 2.5 (ATES) and 1.8 or 3 (BTES) times larger than the yellow framed 170 m (ATES) or 14 m (BTES) aquifer section used for heat extraction (Fig. 3.5). As most TEHMs released in the column tests appeared to originate from a finite pool (Ch. 3.4.1.1), this estimation yielded the maximum expected concentrations and distances for initial heat storage cycles, which should decline and shrink after the initial operating phase, respectively. In instances where a heat storage operation is terminated before TEHMs are completely eluted, TEHM concentrations should decrease when linked to decreasing temperatures over time, as demonstrated in this study for decreasing temperatures over distance. Although, to refine and increase the robustness of such estimations, further research is required to test whether longer heating phases or multiple heating and cooling cycles can cause enhanced (reductive) dissolution or aging of sorbing minerals and an associated decline in reversibility. However, the performed estimations illustrate that even for sediments with relatively high TEHM discharge, only narrowly restricted areas with increased TEHM concentrations should develop during the initial heating phase.

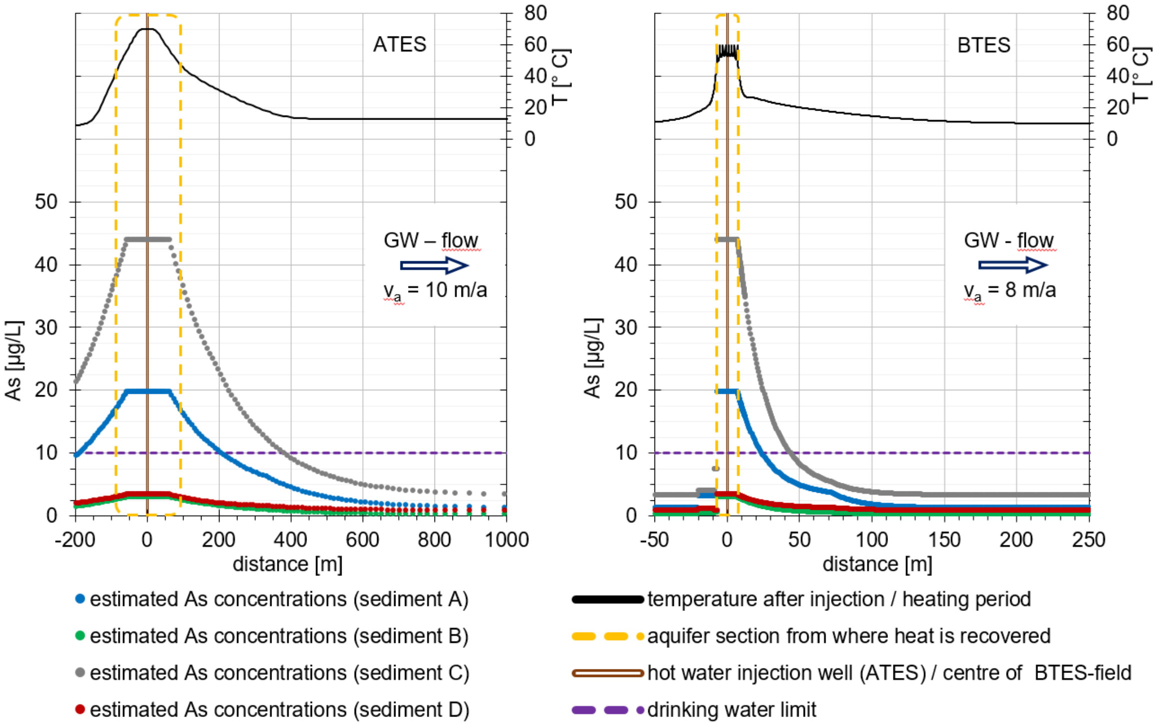

Fig. 3.5: Estimated As concentrations up and downstream from generic numerical BTES and ATES sites for the initial operation phase (derived from the measured As concentrations and corresponding reversibilities for sediments A, B, C and D; see 3.4.1and 3.4.2). For reference, the temperature profiles, the aquifer sections from where heat is recovered and the drinking water limit for As (see supplemental Table S.3.6) are shown.

3.5. Conclusions

Flow-through and circular-flow column tests with four typical, anoxic, northern German aquifer sediments showed increasing Li, As, Mo, Sb and Ba concentrations and decreasing Ni concentrations at elevated temperatures in all of the investigated sediments, whereas temperature effects on V, Mn, Co, Tl and U concentrations varied sediment-specifically. Apart from Ba, all these components showing increased concentrations at higher temperatures were temporally released, indicating a temperature dependent, finite TEHM pool, which limited the released mass and duration. However, in the short term, elevated temperatures of 70 °C caused concentration changes in As, V, Mn, Li and Tl to exceed variations between the sediments at 10 °C considerably. Since these concentration changes varied considerably between the sediments, preliminary, site-specific hydrochemical investigations for planned heat storage sites remain necessary to assess TEHM behaviour.

Processes triggered or intensified by a temperature increase that are believed to be largely responsible for the TEHM release include:

- a decrease in the point of zero charge and an associated negative enthalpy for surface complexation reactions of anions leading to desorption of TEHMs present as (oxy)anions (e.g. vanadate, chromate, arsenate/arsenite, molybdate and antimonate)
- preferential desorption of monovalent ions (e.g. Li and Tl) in exchange for divalent (e.g. Co and Ni) ions
- the (reductive) dissolution of minerals such as Mn and Fe (hydr)oxides, whereby potentially further TEHMs (Ba) are released.

Re-cooling down to 10 °C demonstrated the TEHM release to be element-specifically reversible between 30 and 95 %. The degree of reversibility seemed to be somewhat unaffected by the applied temperature, the sediment or the experimental setting. If higher kinetic sorption rates at higher temperatures are responsible for incomplete reversibility, then higher reversibilities could be presumed in the field with longer contact times.

In general, the observed reversibility of TEHM concentration changes:

- allows for estimating distances around heat storage sites affected by increased TEHM concentrations, as shown for As with a 1D approach based on the experimental data and temperature profiles from existing numerical UTES sites
- allows for the application of active cooling as a countermeasure in cases of an unexpected adverse progression of TEHM concentrations
- will lead to successive redevelopment of initial natural groundwater conditions with reversals to natural ambient temperatures downstream or after the termination of UTES operations.

Currently, it appears impossible to relate TEHM releases due to heating of a sediment to easily obtainable hydrogeochemical parameters as contents of specific metal-oxides or sulphides. Therefore, further research in identifying and quantifying the involved processes could enable developing methods for faster preliminary site investigations with limited temporal and financial efforts, as well as the development of more detailed, process-based models for predicting TEHM behaviour under varying temperatures. Together with the verification of transferability of laboratory results to the field, this would promote a more widespread application of subsurface heat storages.

Beyond the processes discussed here, future evaluation procedures should focus on a balanced consideration of groundwater protection and sustainable use of the geologic underground. In this sense, and for streamlining of UTES authorisation procedures, the possibility of assessing the impact area as a subterranean technical facility, for which criteria are different than for groundwater, and allow time-limited deviations from the surrounding area inside the facility, should be assessed juridically.

Acknowledgments:
We thank our colleagues Markus Ebert and Frank Dethlefsen for their cooperation and valuable comments throughout the preparation of this study as well as several student assistants who helped in conducting the laboratory experiments. Further, we thank the ICP-MS laboratory at Kiel University's Institute of Geosciences that conducted TEHM analysis on the basis of scientific cooperation as well as the waterworks Kuden and Odderade and the LKN Schleswig-Holstein for providing sediment samples and for giving access to wells for groundwater extraction. Finally, we thank the three anonymous reviewers for their constructive comments that helped to improve the quality of this paper.

Funding:
This study is part of the ANGUS-projects funded by the German Federal Ministry of Education and Research (Angus+: 03EK3022A) and the German Federal Ministry for Economic Affairs and Energy (Angus II: 03ET6122A), which both had no role in study design; the collection, analysis and interpretation of data; in writing of the report; and in the decision to submit the article for publication.

3.6. Supplementary Material

3.6.1. Appendix A - Materials and Methods

Providing further background data and detailed descriptions of the experimental setups and the calculations for estimating potential plumes with increased TEHM concentrations around UTES sites:

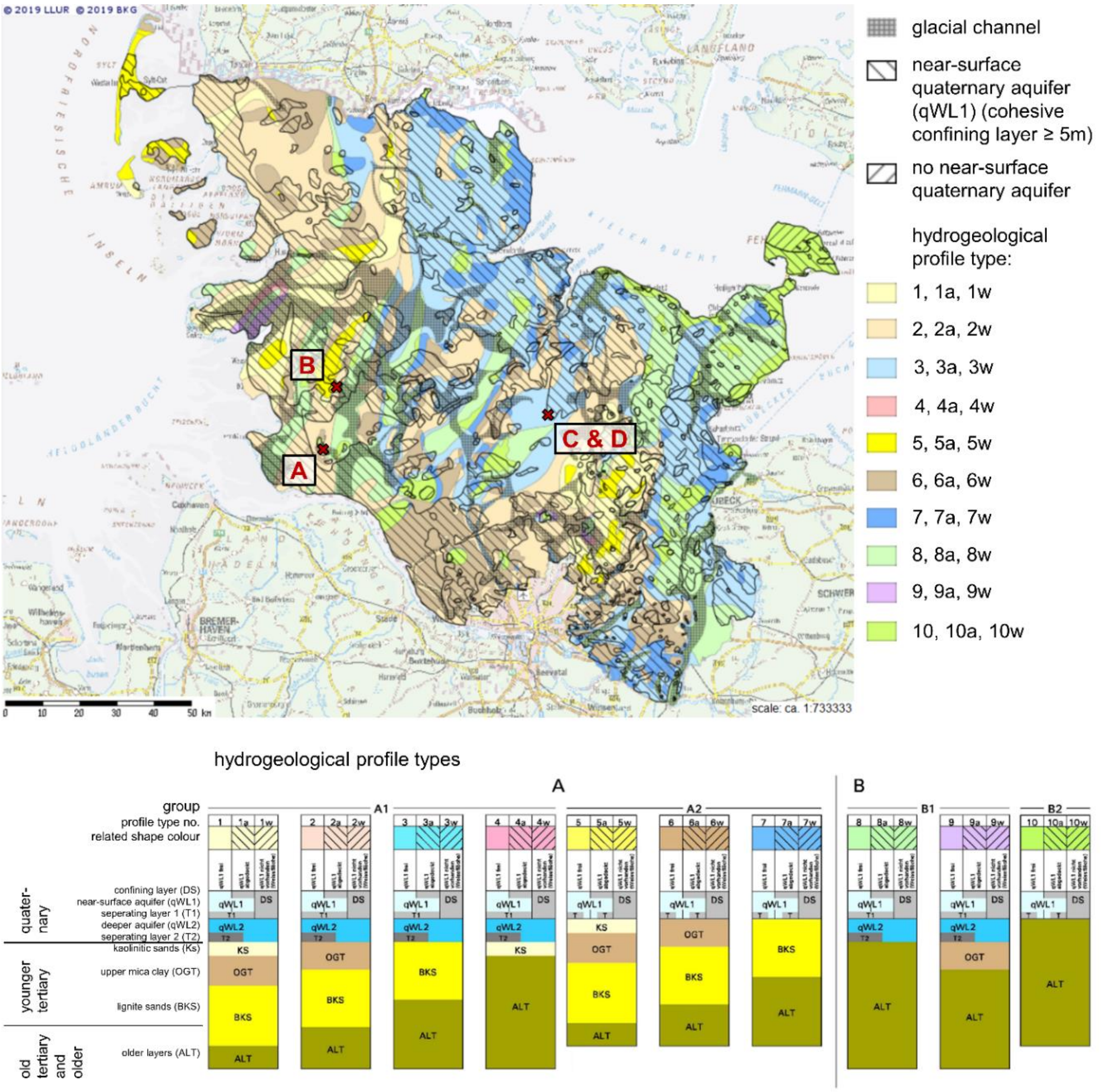

Fig. S.3.6: Hydrogeological map of the German State Schleswig-Holstein showing the locations of the four sediments investigated in the laboratory experiments (modified from LLUR, 2019).

Table S.3.5: Element contents of the examined sediments.

		A: Kuden	***B: Odderade***	***C: Bönebüttel-shallow***	***D: Bönebüttel-deep***
Si	*[mol/kg(sed.)]*	16.0	14.6	15.1	16.1
Na	*[mmol/kg(sed.)]*	94	139	160	15
K	*[mmol/kg(sed.)]*	197	325	225	90
Ca	*[mmol/kg(sed.)]*	27	341	580	8.7
Mg	*[mmol/kg(sed.)]*	15	117	33	2.9
Fe	*[mmol/kg(sed.)]*	50	241	70	18
∑ Na-Fe	*[mmol/kg(sed.)]*	383	1163	1068	135
Li	*[mmol/kg(sed.)]*	0.72	2.2	0.67	0.54
V	*[mmol/kg(sed.)]*	0.20	0.67	0.16	0.049
Cr	*[mmol/kg(sed.)]*	0.21	0.59	0.16	0.077
Mn	*[mmol/kg(sed.)]*	0.81	4.8	2.7	0.20
Co	*[mmol/kg(sed.)]*	0.022	0.068	0.021	0.0040
Ni	*[mmol/kg(sed.)]*	0.062	0.16	0.047	0.013
Cu	*[mmol/kg(sed.)]*	0.072	0.11	0.067	0.049
Zn	*[mmol/kg(sed.)]*	0.14	0.40	0.15	0.053
As	*[mmol/kg(sed.)]*	0.017	0.090	0.031	0.014
Se	*[mmol/kg(sed.)]*	0.15	0.27	0.16	0.071
Sr	*[mmol/kg(sed.)]*	0.43	1.0	0.89	0.15
Mo	*[mmol/kg(sed.)]*	0.0013	0.0030	0.0021	0.0030
Cd	*[mmol/kg(sed.)]*	0.00090	0.0014	0.00093	0.00085
Sn	*[mmol/kg(sed.)]*	0.0072	0.016	0.0048	0.0051
Sb	*[mmol/kg(sed.)]*	0.0015	0.0024	0.0012	0.00076
Ba	*[mmol/kg(sed.)]*	1.6	2.3	1.7	0.78
Tl	*[mmol/kg(sed.)]*	0.0010	0.0015	0.0010	0.00050
Pb	*[mmol/kg(sed.)]*	0.073	0.092	0.053	0.052
U	*[mmol/kg(sed.)]*	0.0027	0.0053	0.0027	0.0018
∑TEHM	*[mmol/kg(sed.)]*	5.8	16	7.8	2.5

3.6.1.1. Detailed experimental setup of α-, β- and γ-series of circular-flow column tests and an explanation of calculations for quantifying the reversible share of concentration changes

Each circuit consisted of a 40 cm long stainless-steel column (internal diameter: 6 cm), a stainless-steel 3-way valve to retrieve water samples, a 1 L gas-tight reservoir bag (PET/AL/PE-composite) functioning as a supply and collector for the water percolating through the columns, a peristaltic pump with a viton pumping-tube and a set of stainless-steel capillaries as connections (Fig. S.3.7). As no replacement of solutions occurred, contact time between sediment and water continuously increased , which allowed for the assessment of TEHM concentrations while approaching steady-state conditions. To minimise the intrusion of oxygen into the systems, build-up was done step-by-step: first reservoir bags, pump and columns were connected and flushed with argon. Next, the site water was pumped from the storage bags into the reservoir bags and further into the columns, thereby replacing the argon. Under continuous pumping of water from below, covered with inflowing argon from above, and the addition of the prior homogenised sediment from above, the columns were filled under repeated compaction of the sediment. Before closing the circuits, the sediments were equilibrated with the corresponding inflow solution by running the columns as flow-through systems using a flow rate of 0.75 mL/min (corresponding to 6.3 h residence time) for a minimum of three days at 10 °C until steady-state conditions were established. This was done to minimise potential effects on the starting conditions such as increased pore water concentrations due to potential diffusive intrusion of oxygen during storage, or DOC mobilisation by re-wetting dry parts of the sediment. Subsequently, the circuits were closed by connecting the column outflows to the reservoir bag inflows. During circuit operation, the columns were tempered using a refrigerator and heating chambers while the flow rate was kept at 0.75 mL/min. Water samples for TEHM analyses were retrieved from 3-way valves between the columns and the reservoir bags.

For the interpretation of the β- and γ-series, the reversibilities were calculated in several steps: for the β-series, the concentrations in the circuits remaining at 10 °C (from the γ-series) were subtracted from the concentrations in the circuits with the same sediment heated to 25, 40 or 70 °C (β-series) to calculate the concentration changes during the initial heating phase. Subsequently, the concentration changes caused by re-cooling were calculated by subtracting the concentrations after one week of re-cooling from the concentrations in the corresponding circuits after the heating phase. For the γ-series, the dilution by connecting parts of the heated and non-heated circuits had to be considered, therefore, the concentration changes after the heating phase were adjusted according to the share of water contributed by the column and capillaries of the circuits conducted at 10 °C (Eq. A.1). Then, the concentration changes caused by re-cooling were calculated by subtracting the concentrations after one week of re-cooling from the corresponding calculated circuit's starting concentrations after dilution. Thus, element-specific reversibilities were calculated by relating concentration increases (or decreases) in the heating phase to subsequent concentration decreases (or increases) in the re-cooling phase.

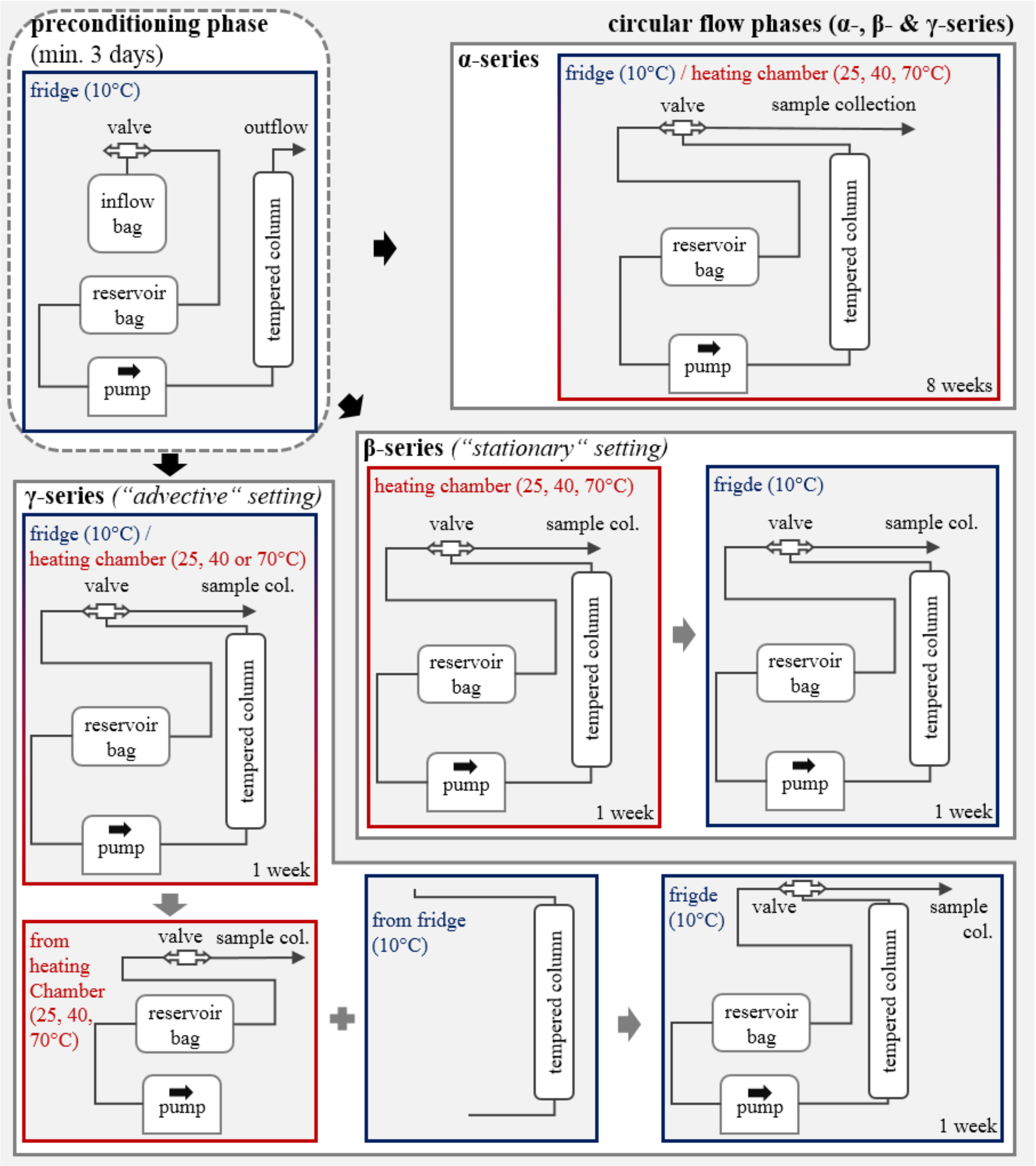

Fig. S.3.7: Setup of α-, β- and γ-series of circular-flow column tests.

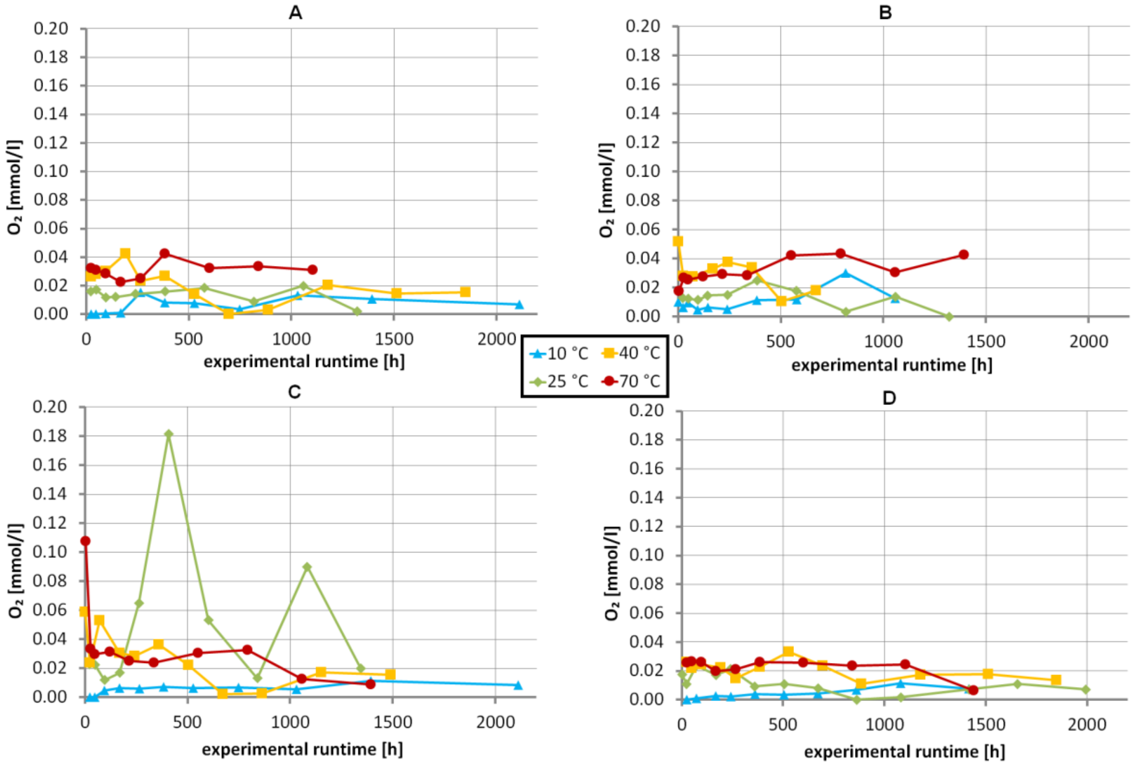

Fig. S.3.8: Progression of O_2 concentrations over experimental runtime in the α-series of circular-flow column tests with sediments A, B, C and D at 10, 25, 40 and 70 °C (modified from Kempermann, 2015). Note, measurements were not conducted within the closed circuits, instead extracted water samples were directly measured under normal atmosphere conditions, which potentially caused dissolution of small amounts of oxygen depending on the exact time between water extraction and measurement.

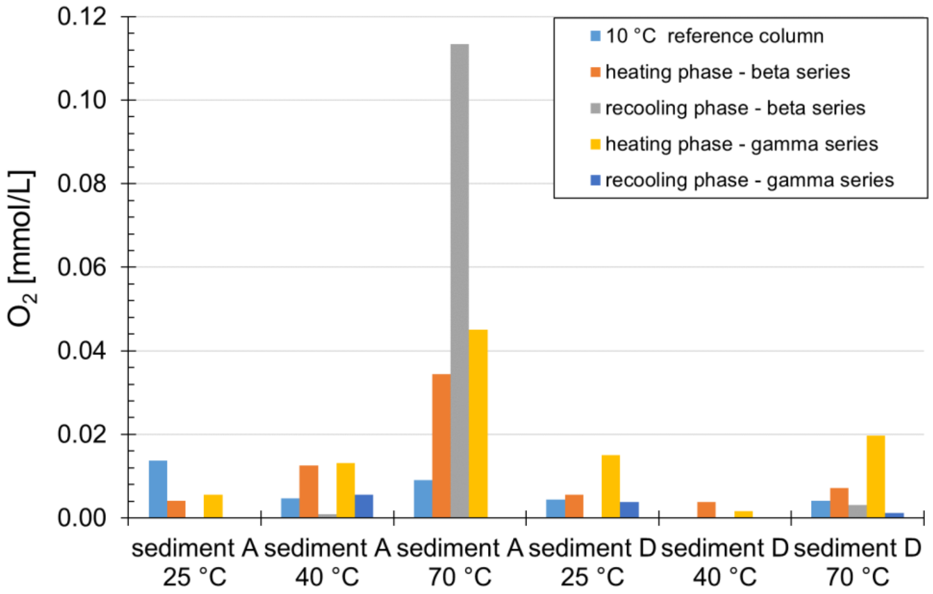

Fig. S.3.9: O_2 concentrations in the β- and γ-series of circular-flow column tests. Note, measurements were not conducted within the closed circuits, instead extracted water samples were directly measured under normal atmosphere conditions, which potentially caused dissolution of small amounts of oxygen depending on the exact time between water extraction and measurement.

Eq. S.1: Calculation of concentrations before re-cooling in γ-series of circular-flow column tests.

$$C(before\ recooling) = C(heated) \times share\ of\ heated\ water + C(10\ °C) \times share\ of\ 10°C\ water$$

3.6.1.2. Estimation of potential plumes with increased TEHM concentrations around UTES sites

The estimation of As concentrations along the flow path downstream of generic ATES and BTES sites is described step-by-step. Underlying temperature profiles from the end of the last simulated heat injection cycle were taken from existing numerical ATES (Meier-Ewert, 2018) and BTES models (Popp et al., 2015) with similar background groundwater flow velocities of 10 and 8 m/a, respectively. For BTES sites in cohesive sediments, slower groundwater flow velocities can be expected. Due to variations in the grid spacing of the underlying numerical models, the distances of temperature data points ranged from 1.5 to 56 m for the ATES and from 0.1 to 1 for the BTES model, which were taken into account in the following calculations. While only four temperatures, 10, 25, 40 and 70 °C, were investigated in the laboratory experiments, the calculations required assigned concentration values for the entire examined temperature range. For this reason, the concentrations measured at 10, 25, 40 and 70 °C were evenly assigned to the corresponding temperature ranges ‘below 17.5 °C’ [$C(T_{<17.5\,°C})$], ‘17.5-32.5 °C’ [$C(T_{17.5\text{-}32.5\,°C})$], ‘32.5-55 °C’ [$C(T_{32.5\text{-}55\,°C})$] and ‘above 55 °C’ [$C(T_{>55\,°C})$], respectively. Arithmetic mean values between the investigated temperatures were taken as boundaries for the temperature ranges.

For the BTES site, the spatial propagation of As concentrations along the groundwater flow path are described from upstream to downstream as follows: Upstream and in the centre of the BTES field the concentrations measured at 10, 25, 40 and 70 °C were directly assigned to their corresponding temperature ranges ($T_{<17.5\,°C}$, $T_{17.5\text{-}32.5\,°C}$, $T_{32.5\text{-}55\,°C}$ and $T_{>55\,°C}$. Downstream from the BTES site, where temperature starts to decrease below 55 °C (which is the lower limit of the highest temperature range), As re-fixation was assumed to start. The decrease in As concentration was calculated from one temperature data point in the downstream flow direction to the next (max. ΔK of 2.6 for the ATES-site and 7.6 for the BTES-site), subsequently referred to as T_i for the higher temperature (closer to the heat storage) and T_{i+1} for the next lowest temperature (farther away from the heat storage). Therefore, $C(T_i)$ and $C(T_{i+1})$ represent the concentrations corresponding to the temperature data points (Eq. A.2). First, a potential concentration difference, ΔC_{pot}, between T_i and T_{i+1} was calculated, which characterised the concentration difference if the pore water solution of a defined volume of up-gradient sediment with a defined porosity was equilibrated with the same volume of down-gradient sediment with the same porosity at the respective temperatures under the assumption of complete reversibility. Therefore, to gain ΔC_{pot}, the measured concentration according to the temperature range of T_{i+1} (so $C(T_{<17.5\,°C})$, $C(T_{17.5\text{-}32.5\,°C})$, $C(T_{32.5\text{-}55\,°C})$ or $C(T_{>55\,°C})$) was subtracted from $C(T_i)$. Second, considering that temperature dependencies for concentrations during re-cooling are, to a certain extent, different from temperature dependencies during heating, which expressed in incomplete reversabilities in the laboratory experiments, ΔC_{pot} was multiplied with the reversibility [R] for each calculation step. For sediments A (0.73) and D (0.71) reversibility values for As were taken from the experimental γ-series, and for sediments B and C the average (0.72) was used. Third, considering that the effect of process reversibilities on concentrations in spatially separated areas depend on the volume ratio of both areas, ΔC_{pot} was multiplied by the ratio of the distance $|T_iT_{i+1}|$ between the two temperature points T_i and T_{i+1} and the distance heated to above 55 °C [|>55 °C|]. Finally, this effective concentration decrease between T_i and T_{i+1} was then subtracted from $C(T_i)$ to gain $C(T_{i+1})$ (Eq. A.2). For the BTES site, only the downstream concentration decreases needed to be calculated. For the ATES site, overprinting of the background groundwater flow field by injection and extraction of the water needed to be considered. This required calculating As concentrations for decreasing temperatures in both the up and downstream directions by applying the scheme for the downstream part of the BTES site (see above). The resulting concentration profiles are roughly similar in both directions and only slightly elongated in the background groundwater flow direction for the ATES site.

Eq. S.2: Calculation of decreasing As concentrations due to recooling downstream (BTES) or down- and upstream (ATES) a heat storage site. See the text for a detailed explanation of the formula symbols.

$$C(T_{i+1}) = C(T_i) - \left(\Delta C_{pot} \times R \times \frac{|\mathrm{T}_i T_{i+1}|}{|> 55\ °C|}\right)$$

$C(T_{i+1})$: calculated concentration at the next lower temperature data point T_{i+1}
$C(T_i)$: starting concentration at the temperature data point T_i
ΔC_{pot}: potential concentration difference between T_i and T_{i+1} under assumption of complete reversibility
R: sediment and element specific reversibility obtained from laboratory experiments
$|T_iT_{i+1}|$: distance between the two temperature points T_i and T_{i+1}
|>55 °C|: distance heated to above 55 °C

3.6.2. Appendix B - Results and Discussion

Additional figures of experimental results and background data regarding (groundwater quality guidelines:

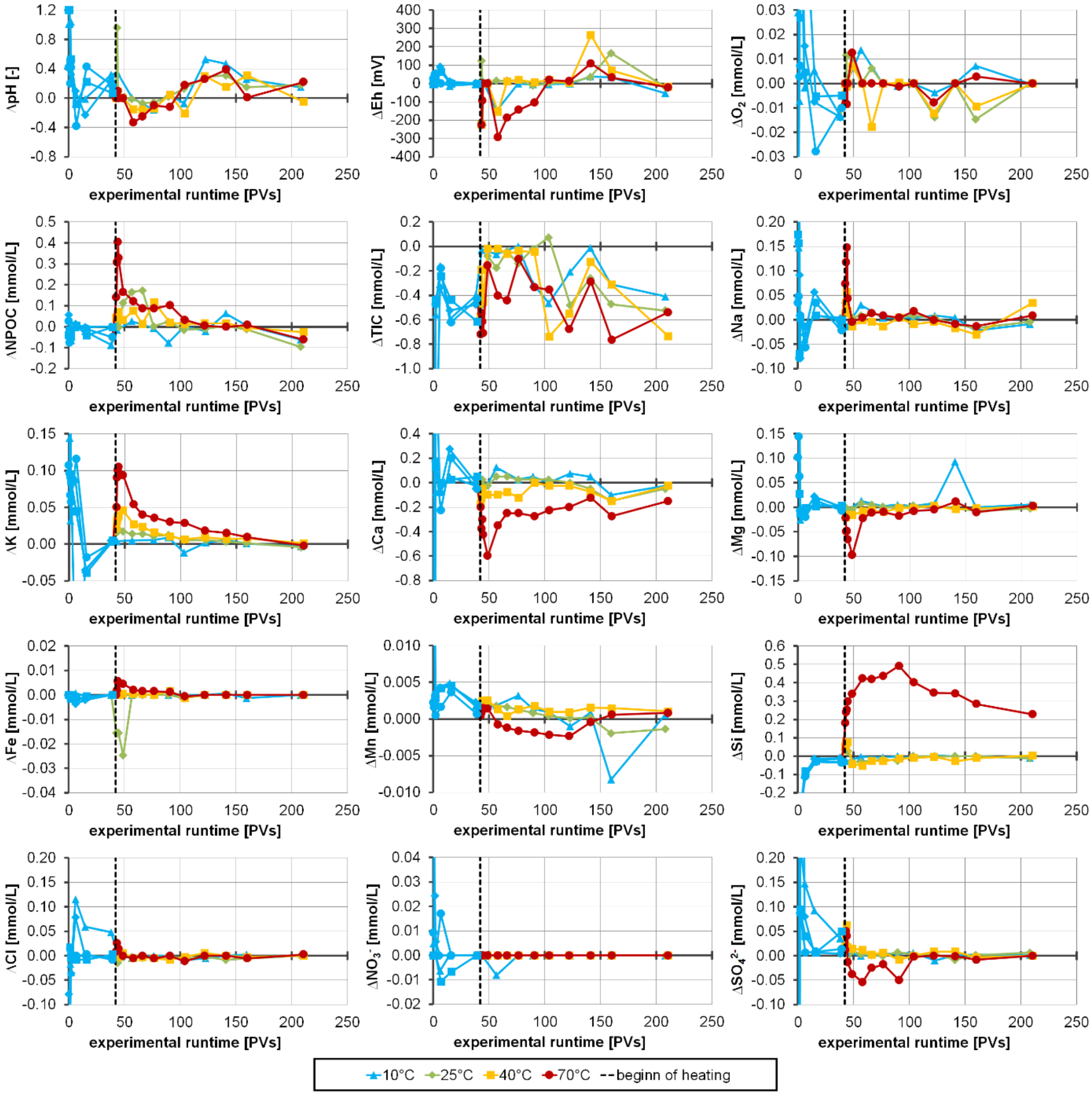

Fig. S.3.10: Changes in pH, Eh and concentrations of main groundwater components between inflow and outflow over the experimental runtime in exchanged pore volumes (PVs) of flow-through column tests with sediment C.

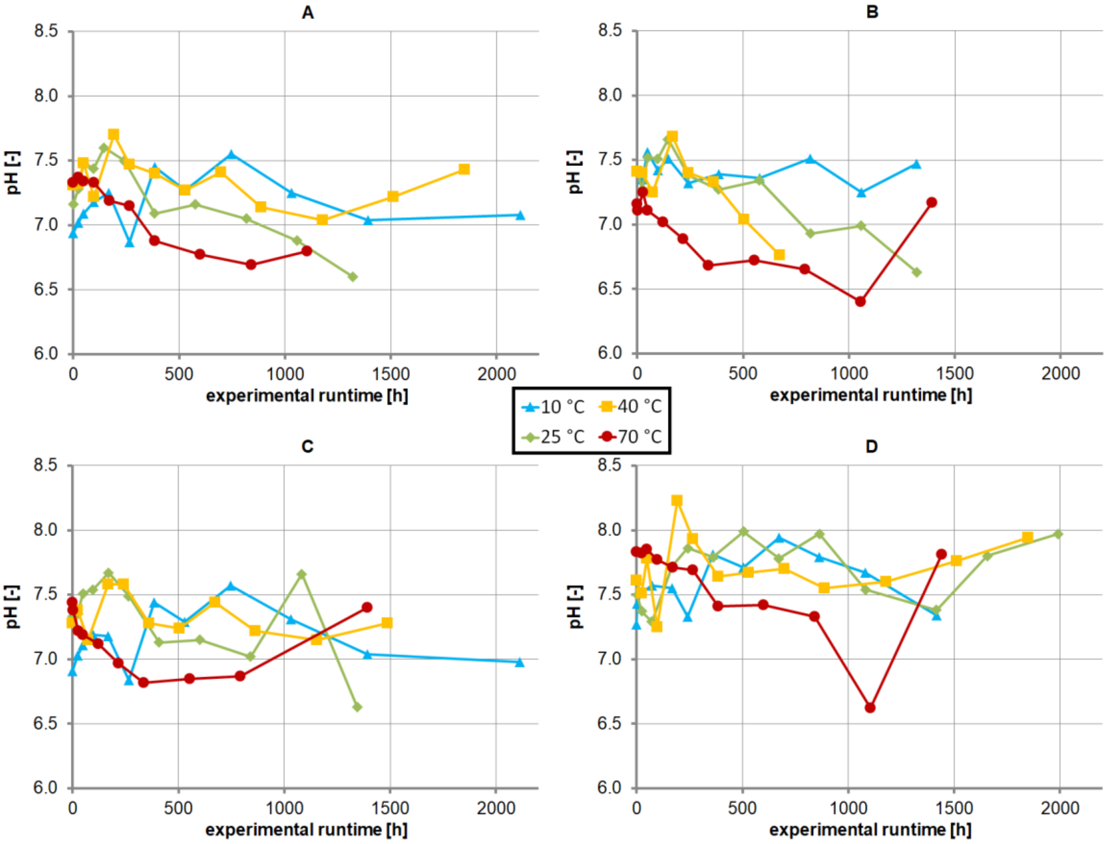

Fig. S.3.11: Progression of pH values over experimental runtime in the α-series of circular-flow column tests with sediments A, B, C and D at 10, 25, 40 and 70 °C (modified from Kempermann, 2015).

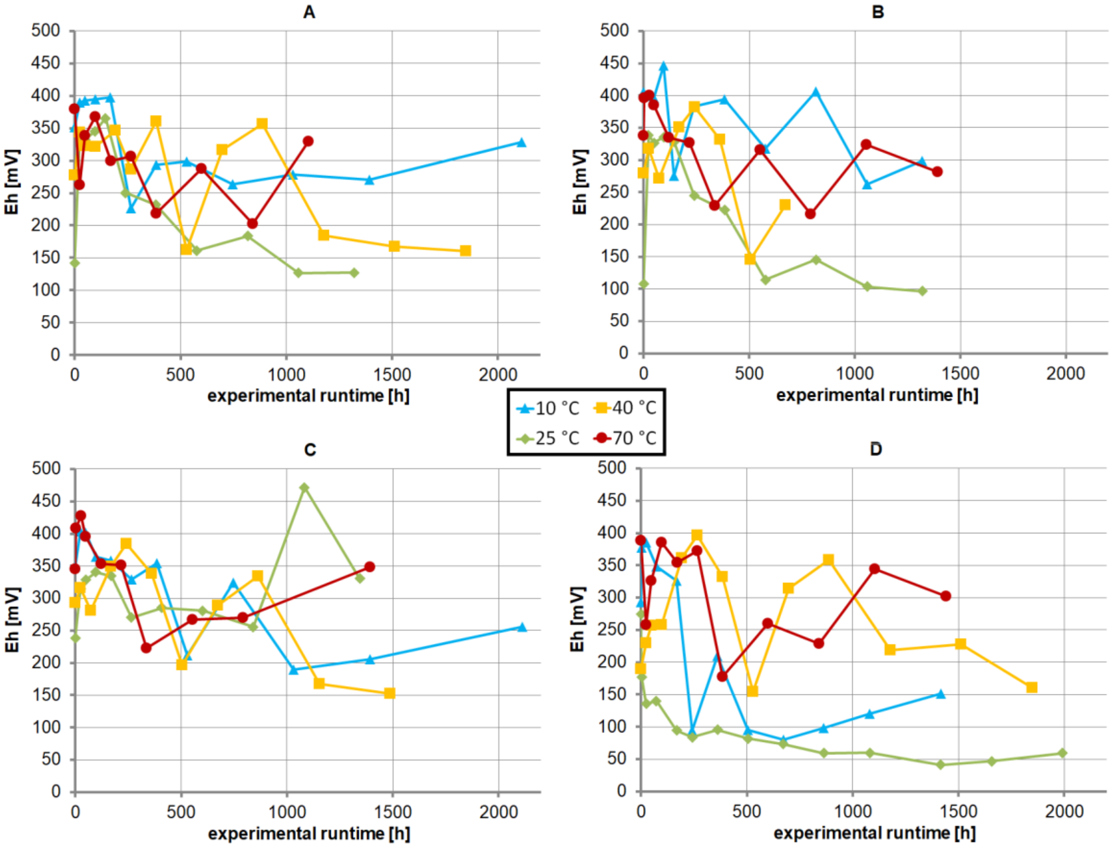

Fig. S.3.12: Progression of Eh values over experimental runtime in the α-series of circular-flow column tests with sediments A, B, C and D at 10, 25, 40 and 70 °C (modified from Kempermann, 2015).

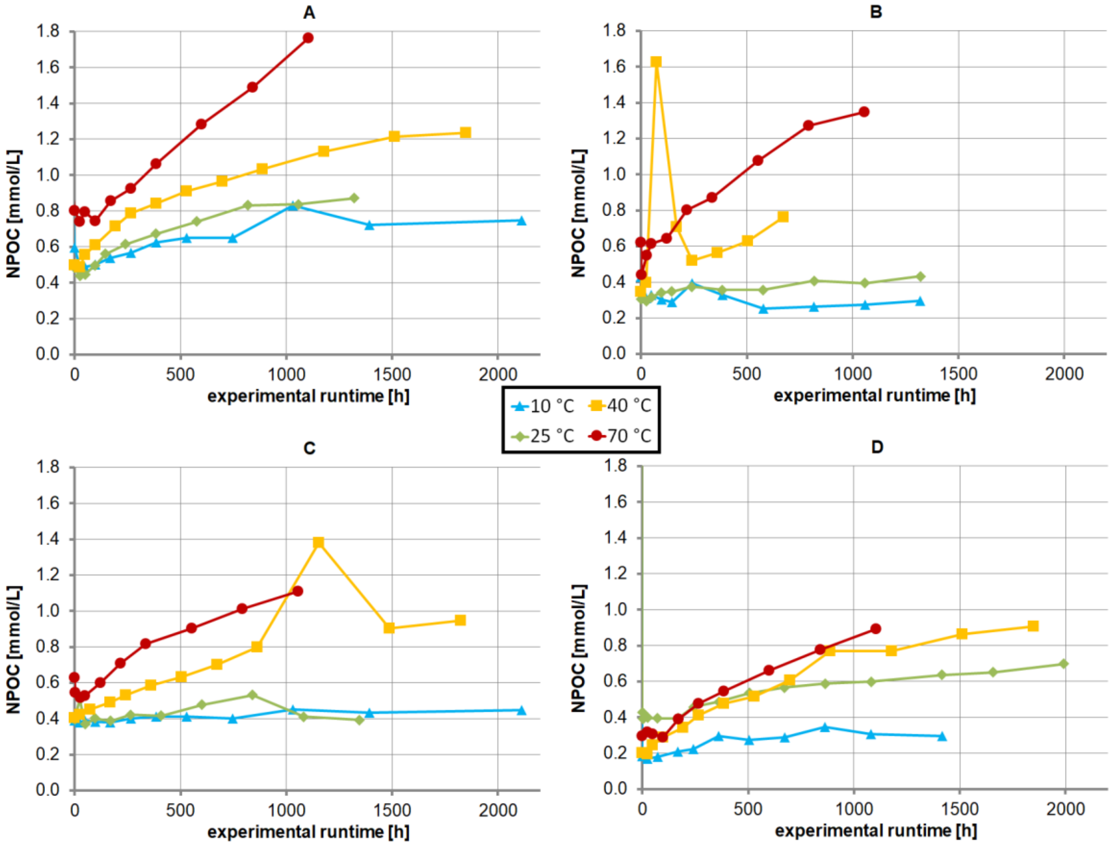

Fig. S.3.13: Progression of NPOC concentrations over experimental runtime in the α-series of circular-flow column tests with sediments A, B, C and D at 10, 25, 40 and 70 °C (modified from Kempermann, 2015).

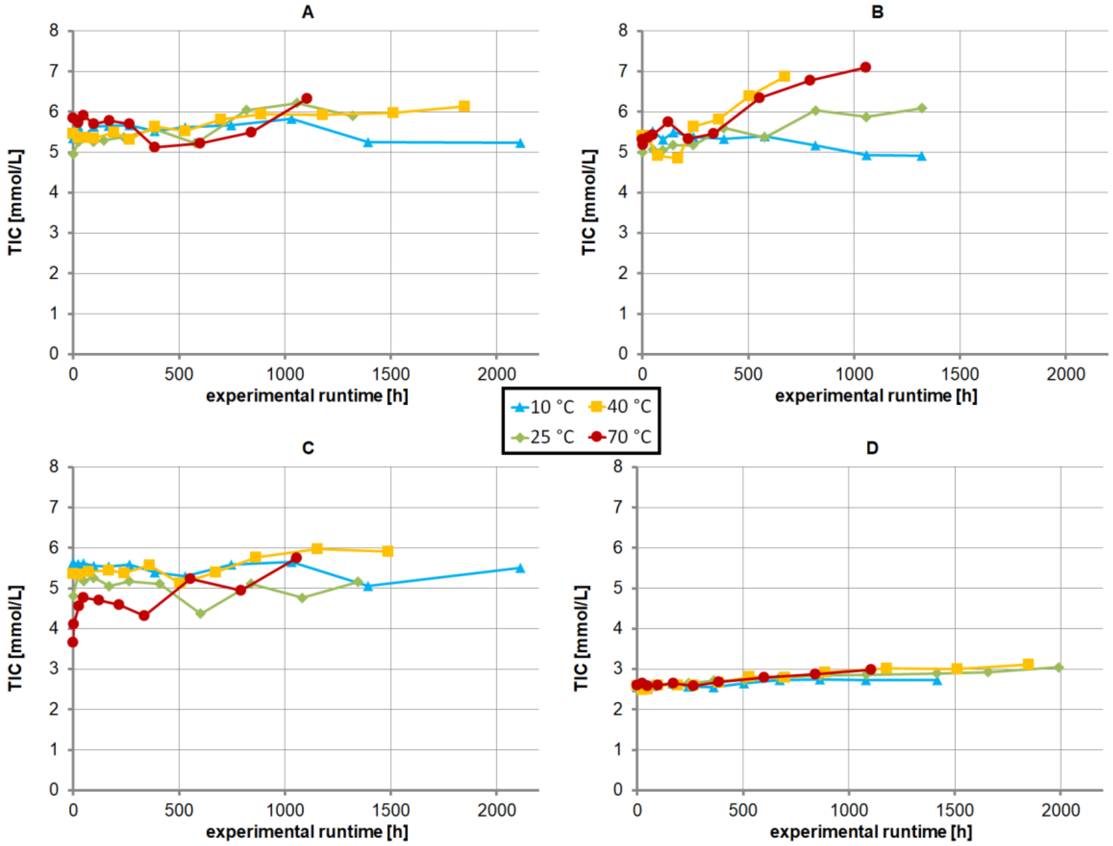

Fig. S.3.14: Progression of TIC concentrations over experimental runtime in the α-series of circular-flow column tests with sediments A, B, C and D at 10, 25, 40 and 70 °C (modified from Kempermann, 2015).

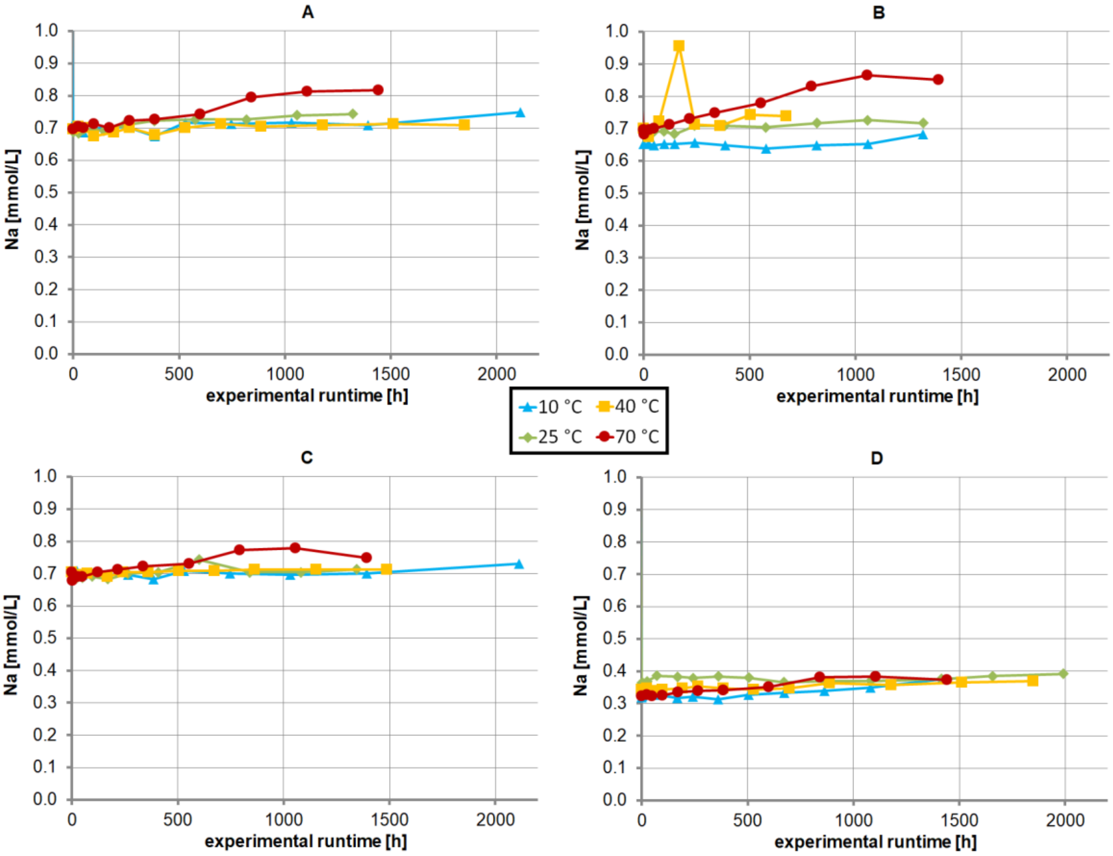

Fig. S.3.15: Progression of Na concentrations over experimental runtime in the α-series of circular-flow column tests with sediments A, B, C and D at 10, 25, 40 and 70 °C (modified from Kempermann, 2015).

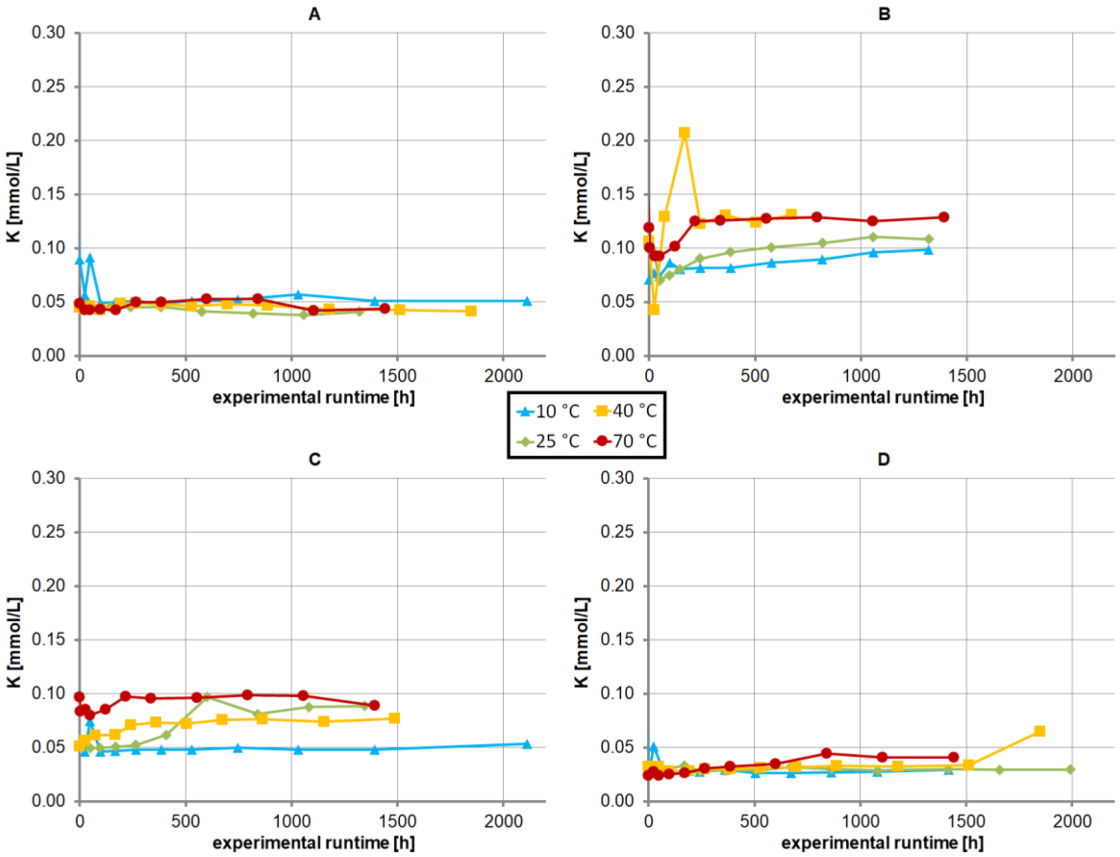

Fig. S.3.16: Progression of K concentrations over experimental runtime in the α-series of circular-flow column tests with sediments A, B, C and D at 10, 25, 40 and 70 °C (modified from Kempermann, 2015).

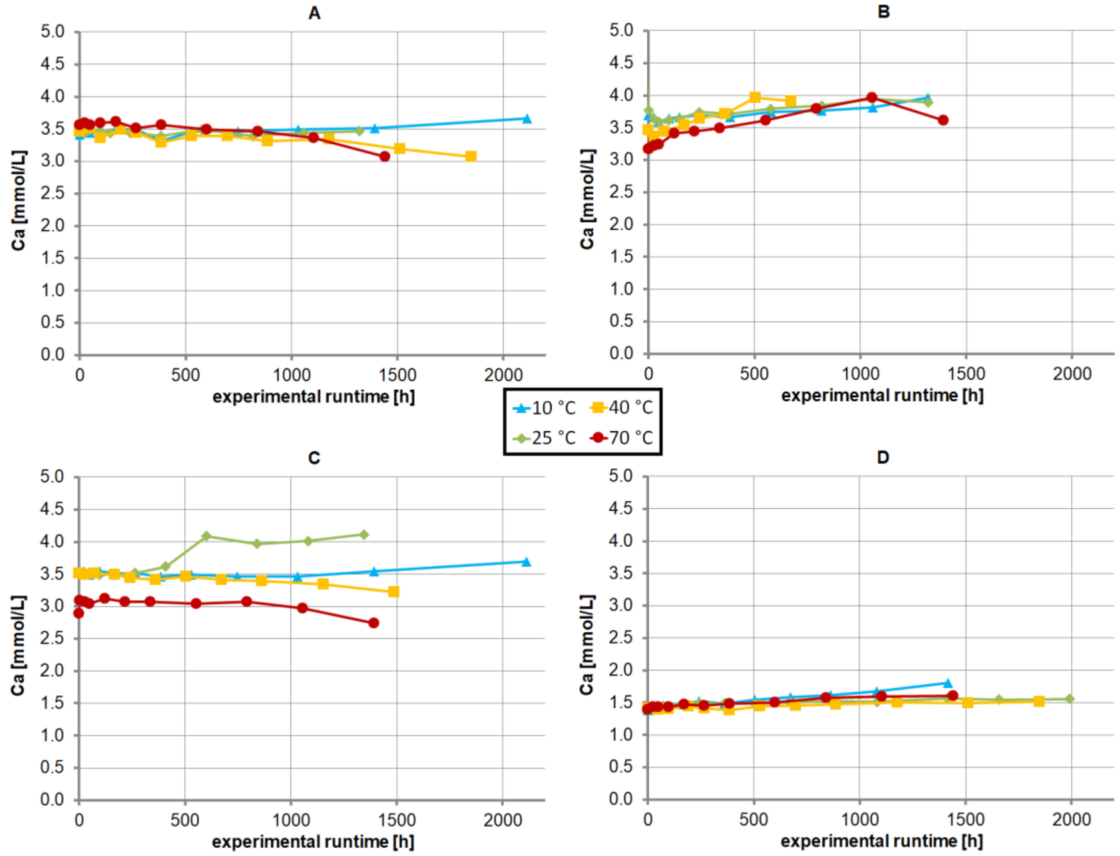

Fig. S.3.17: Progression of Ca concentrations over experimental runtime in the α-series of circular-flow column tests with sediments A, B, C and D at 10, 25, 40 and 70 °C (modified from Kempermann, 2015).

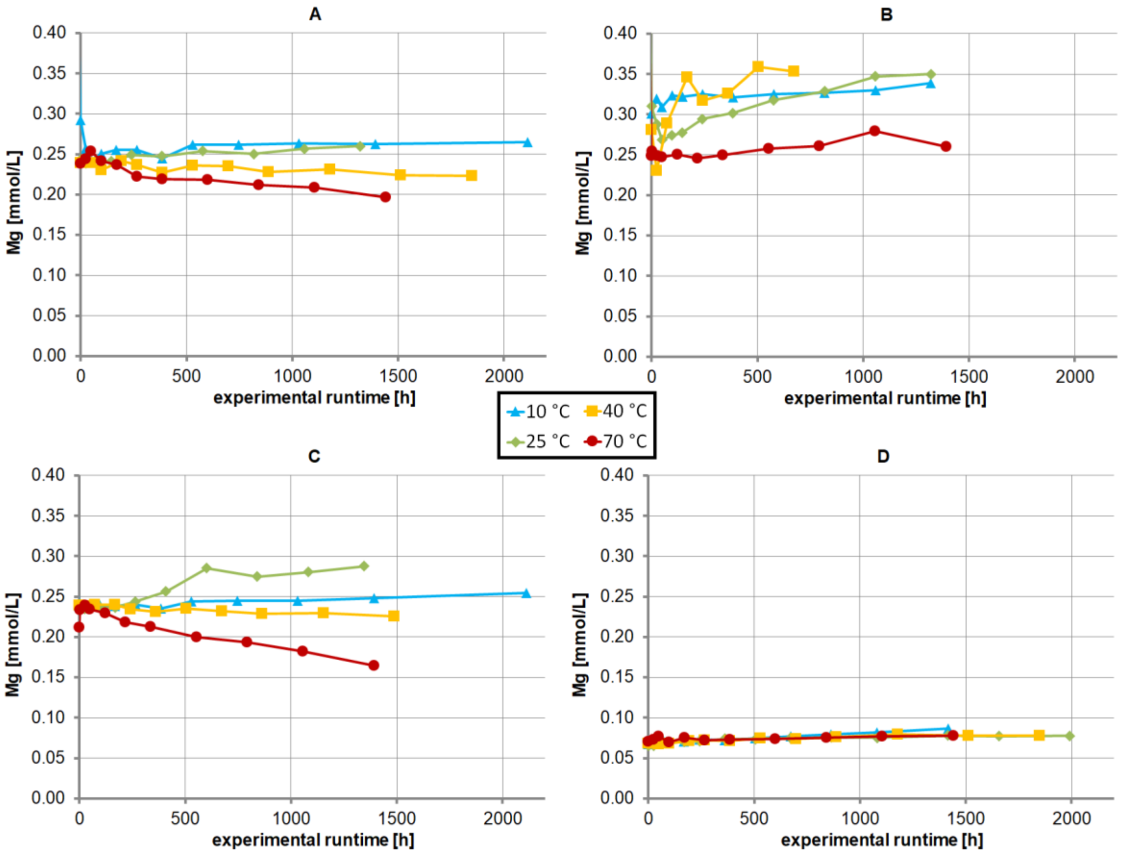

Fig. S.3.18: Progression of Mg concentrations over experimental runtime in the α-series of circular-flow column tests with sediments A, B, C and D at 10, 25, 40 and 70 °C (modified from Kempermann, 2015)

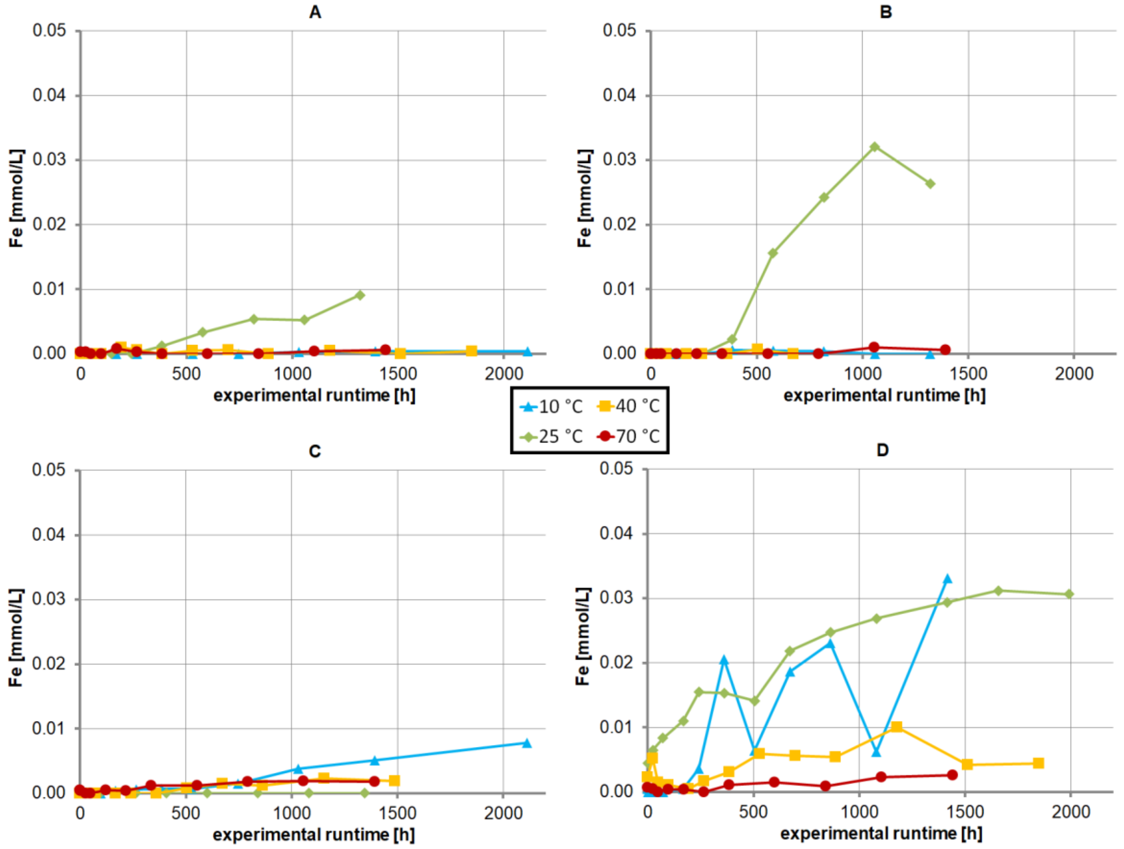

Fig. S.3.19: Progression of Fe concentrations over experimental runtime in the α-series of circular-flow column tests with sediments A, B, C and D at 10, 25, 40 and 70 °C (modified from Kempermann, 2015).

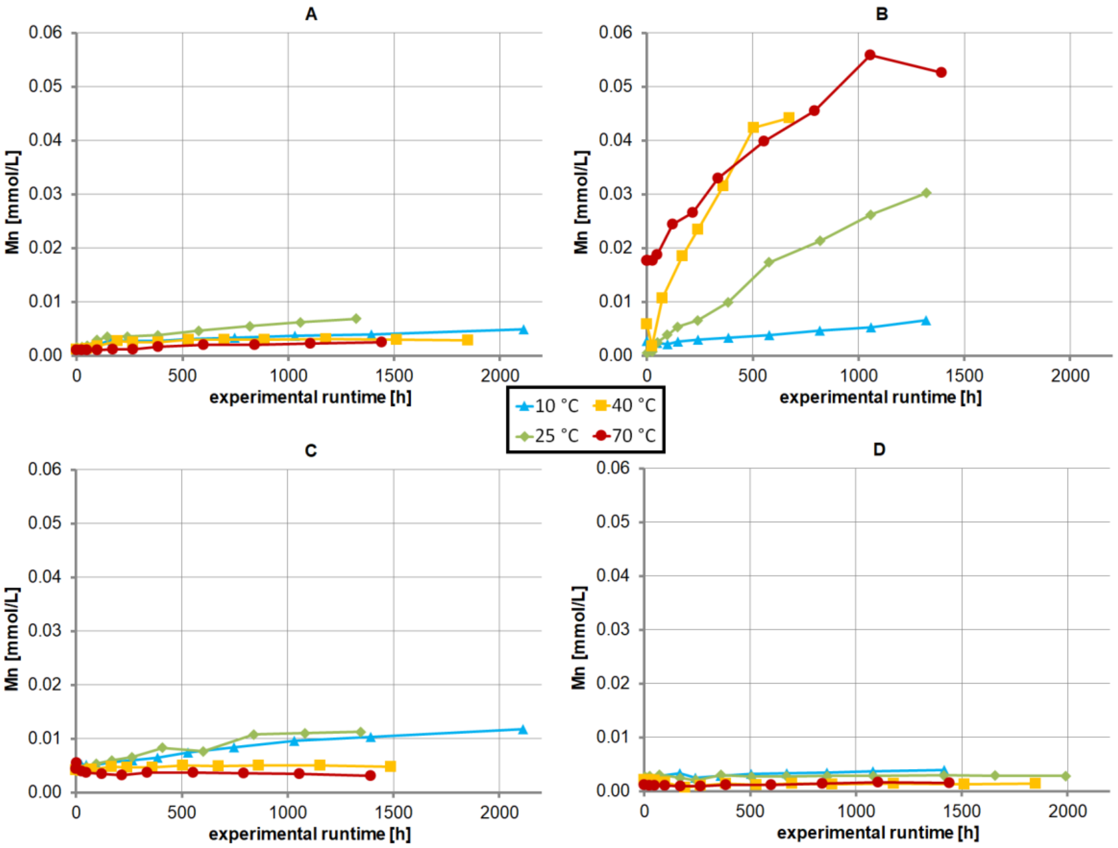

Fig. S.3.20: Progression of Mn concentrations over experimental runtime in the α-series of circular-flow column tests with sediments A, B, C and D at 10, 25, 40 and 70 °C (modified from Kempermann, 2015).

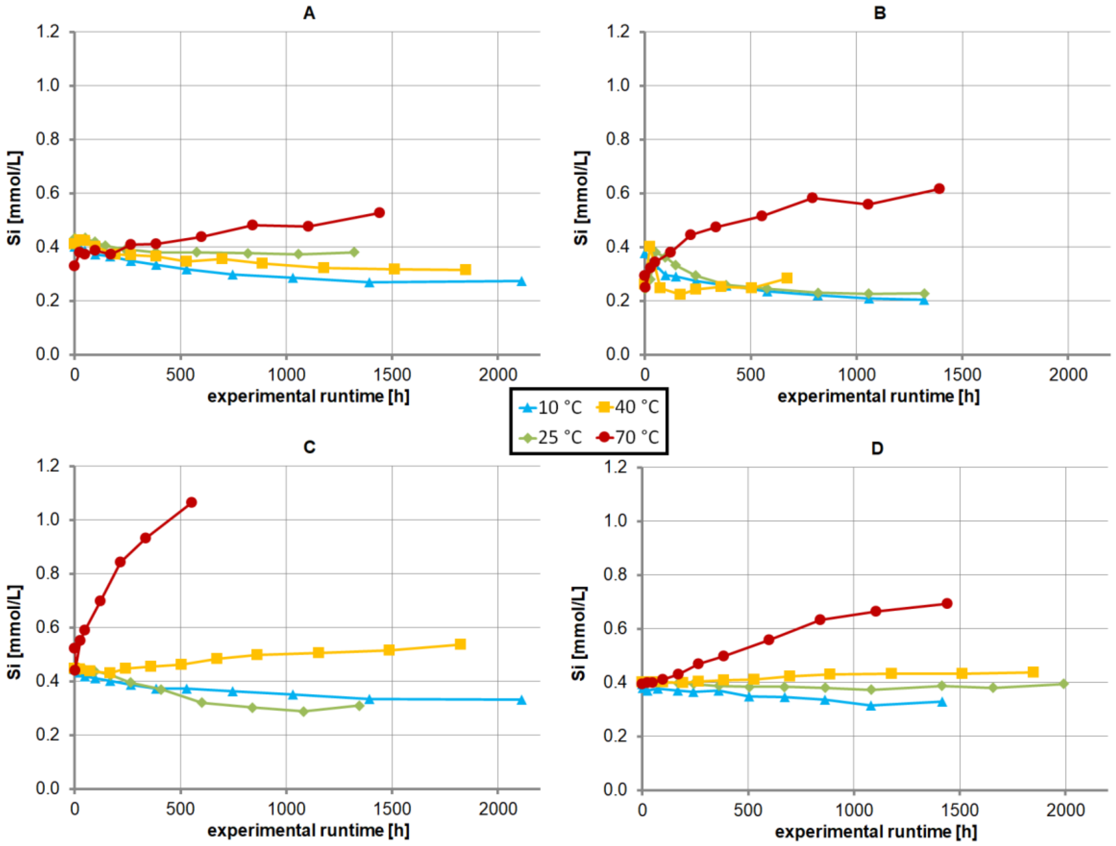

Fig. S.3.21: Progression of Si concentrations over experimental runtime in the α-series of circular-flow column tests with sediments A, B, C and D at 10, 25, 40 and 70 °C (modified from Kempermann, 2015).

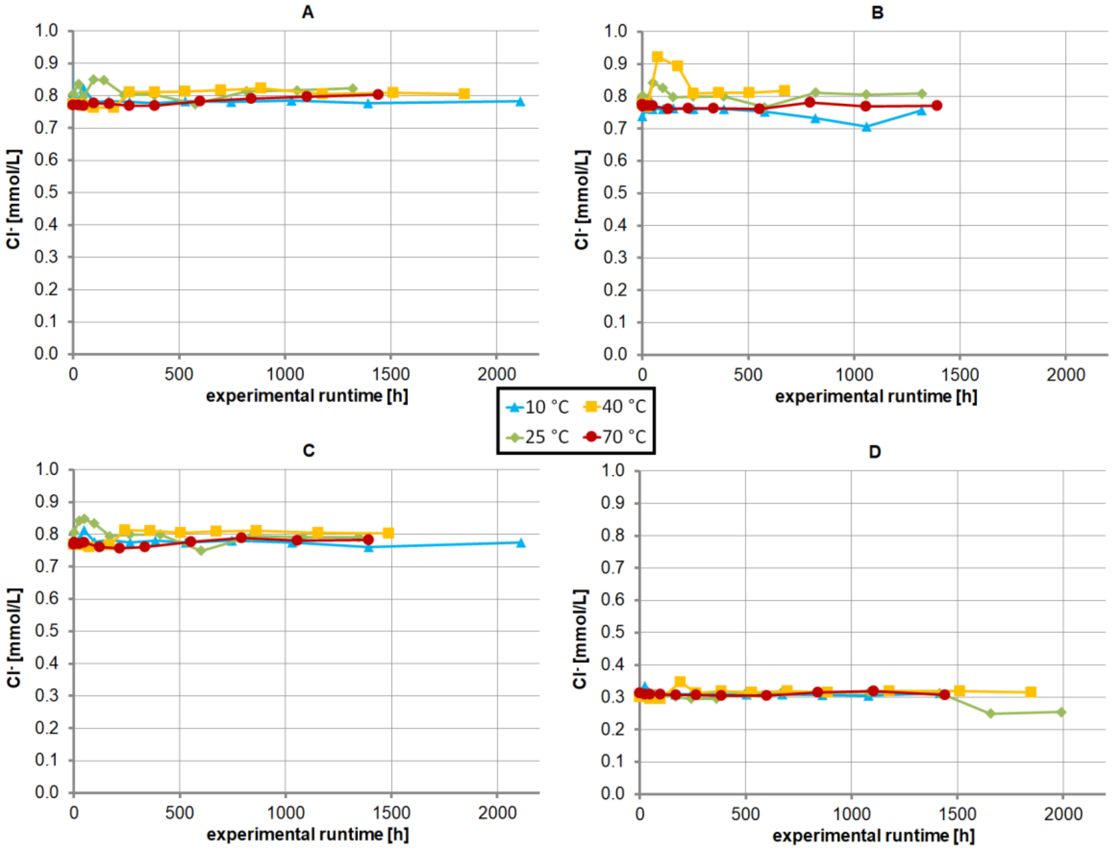

Fig. 3.22: Progression Cl$^-$ concentrations over experimental runtime in the α-series of circular-flow column tests with sediments A, B, C and D at 10, 25, 40 and 70 °C (modified from Kempermann, 2015).

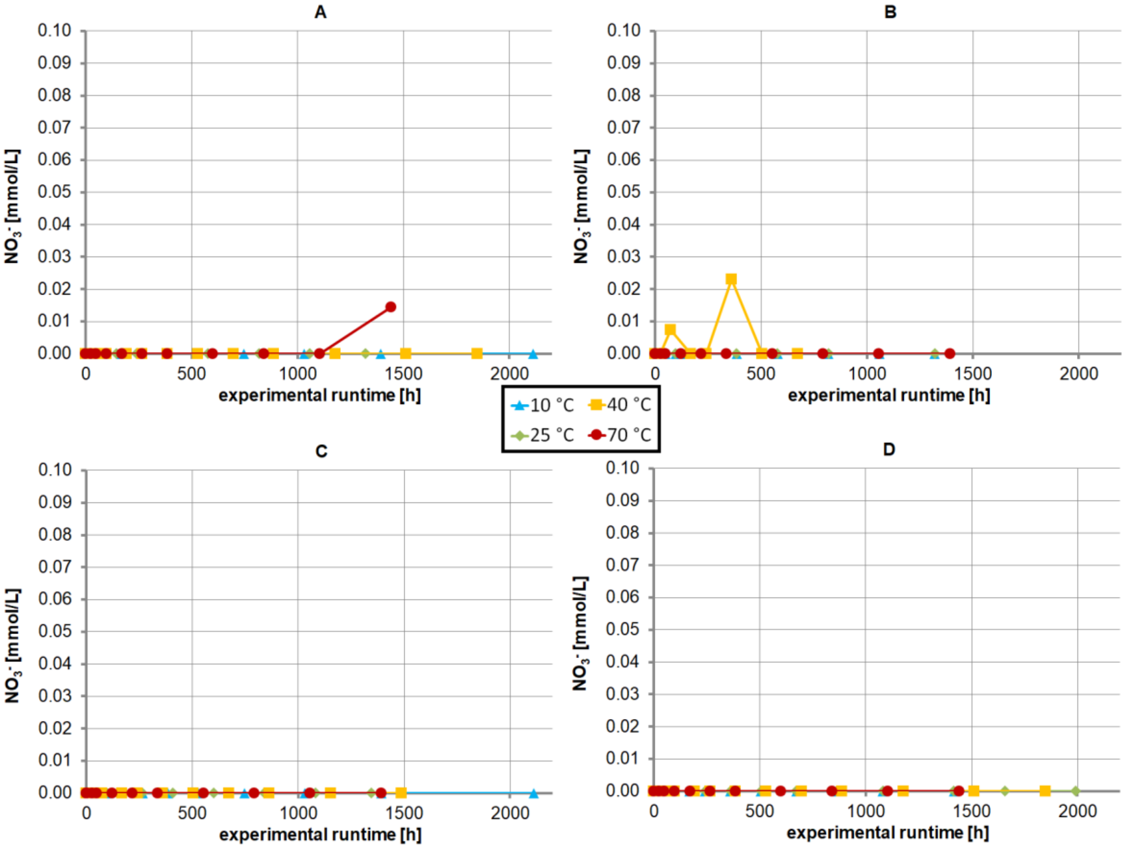

Fig. S.3.23: Progression of NO_3^- concentrations over experimental runtime in the α-series of circular-flow column tests with sediments A, B, C and D at 10, 25, 40 and 70 °C (modified from Kempermann, 2015).

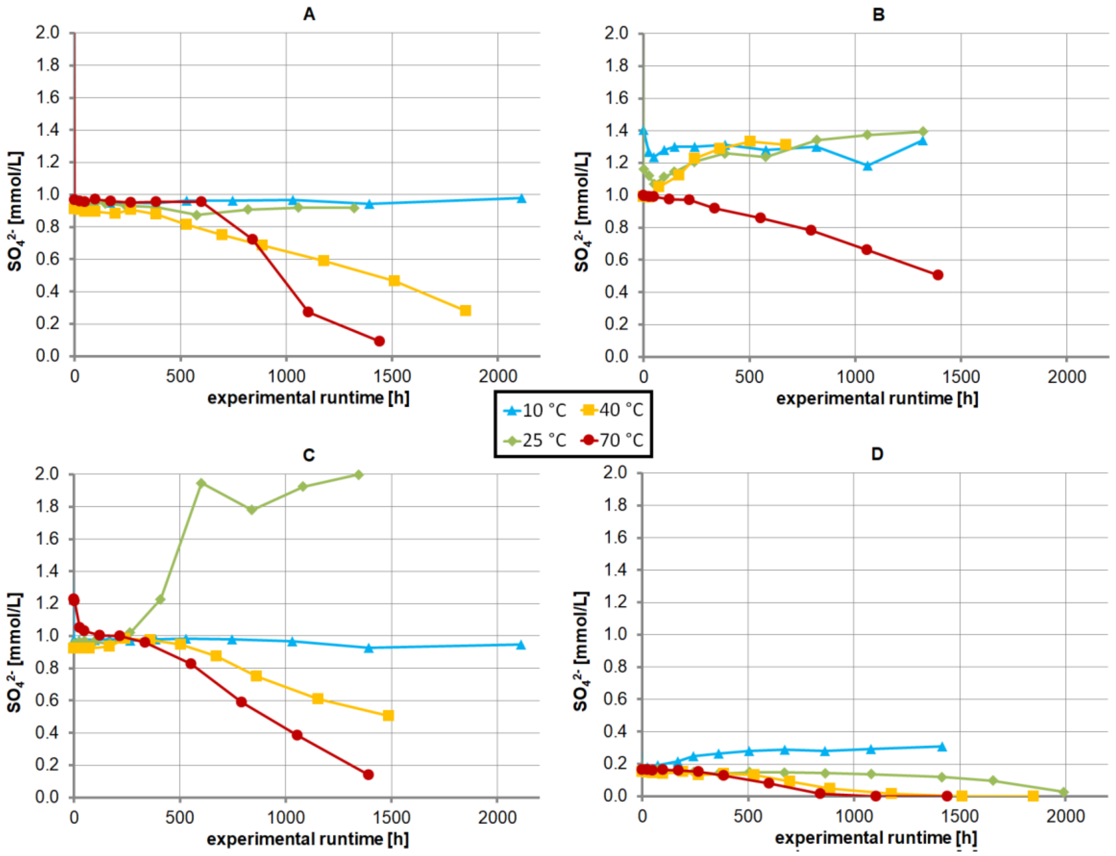

Fig. S.3.24: Progression of SO_4^{2-} concentrations over experimental runtime in the α-series of circular-flow column tests with sediments A, B, C and D at 10, 25, 40 and 70 °C (modified from Kempermann, 2015).

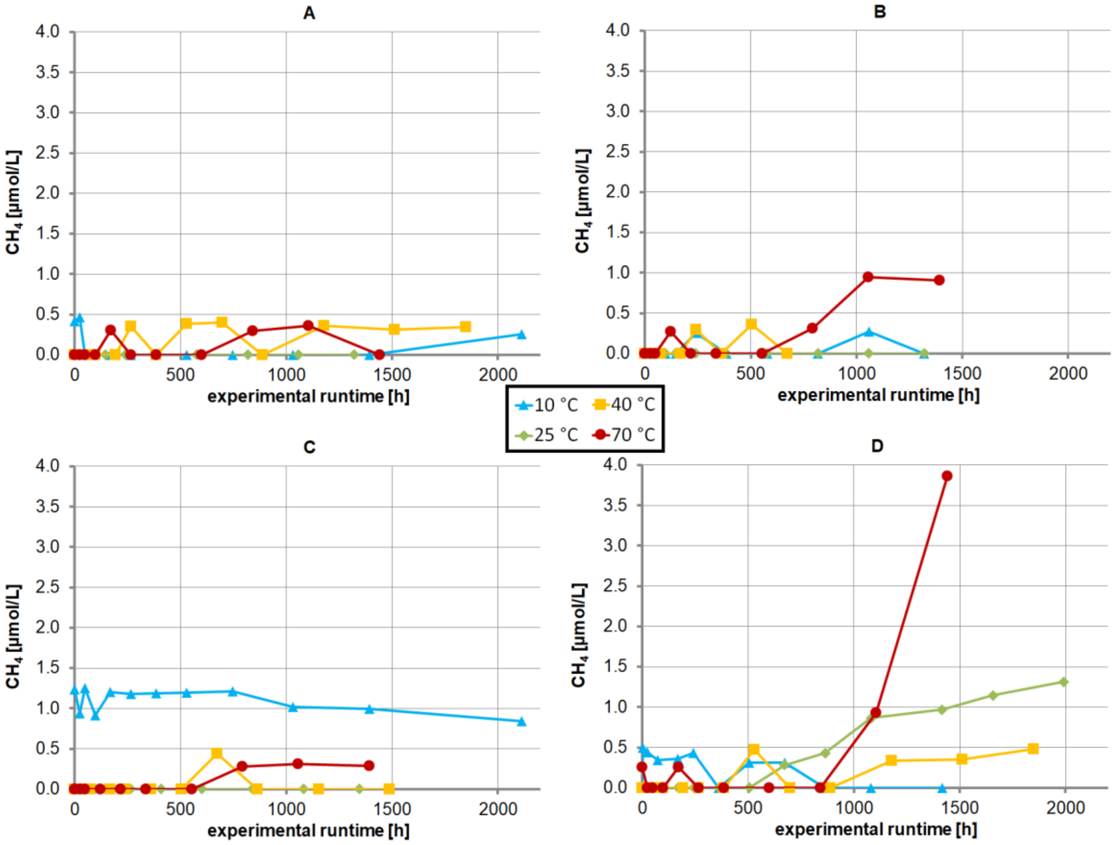

Fig. S.3.25: Progression of CH_4 concentrations over experimental runtime in the α-series of circular-flow column tests with sediments A, B, C and D at 10, 25, 40 and 70 °C (modified from Kempermann, 2015).

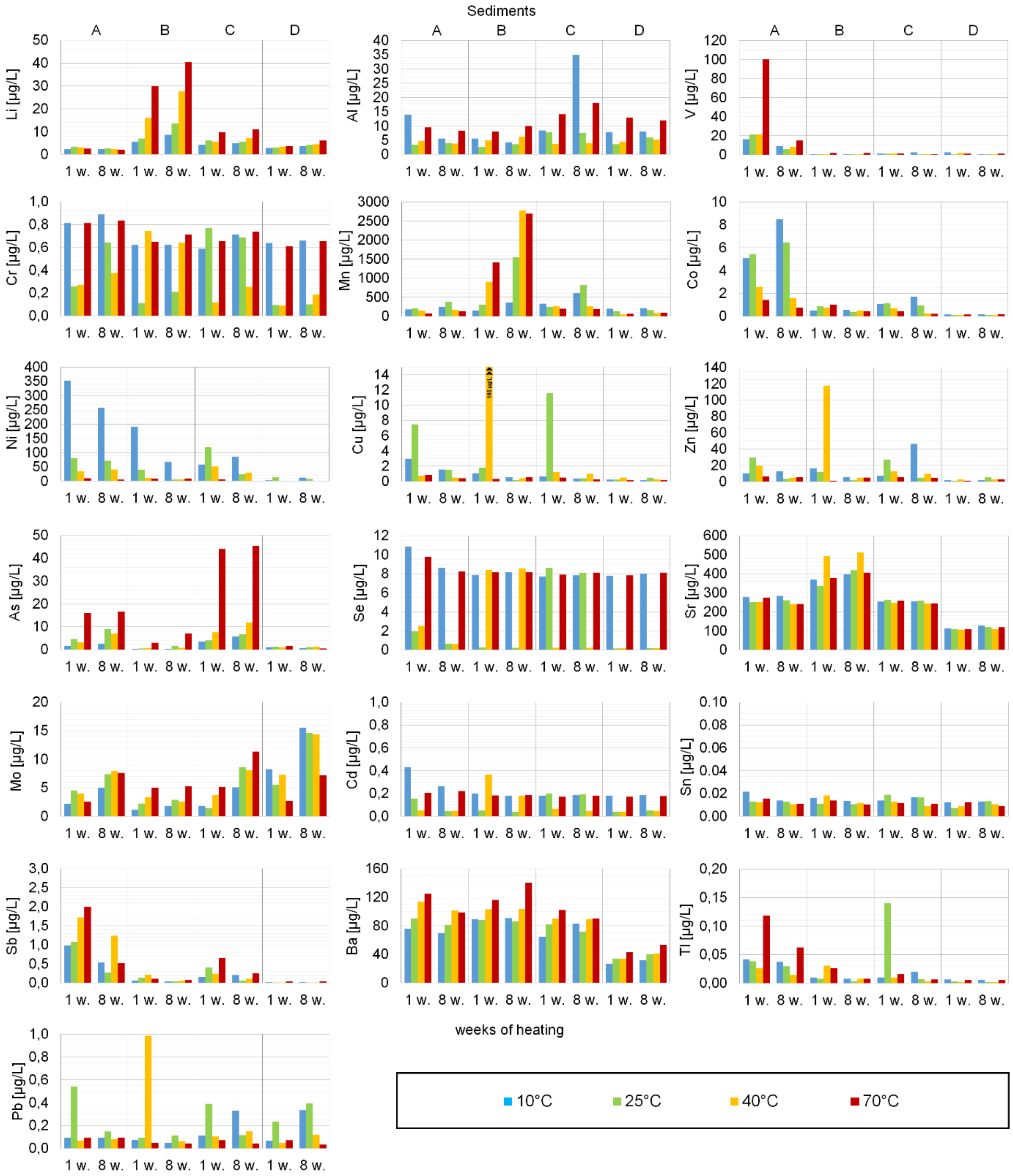

Fig. S.3.26: Concentrations of Li, Al, V, Cr, Mn, Co, Ni, Cu, Zn, As, Se, Sr, Mo, Cd, Sn, Sb, Ba, Tl and Pb in eluates of the α-series circular-flow column tests with sediments A, B, C and D after one and eight weeks of tempering to 10, 25, 40 or 70 °C.

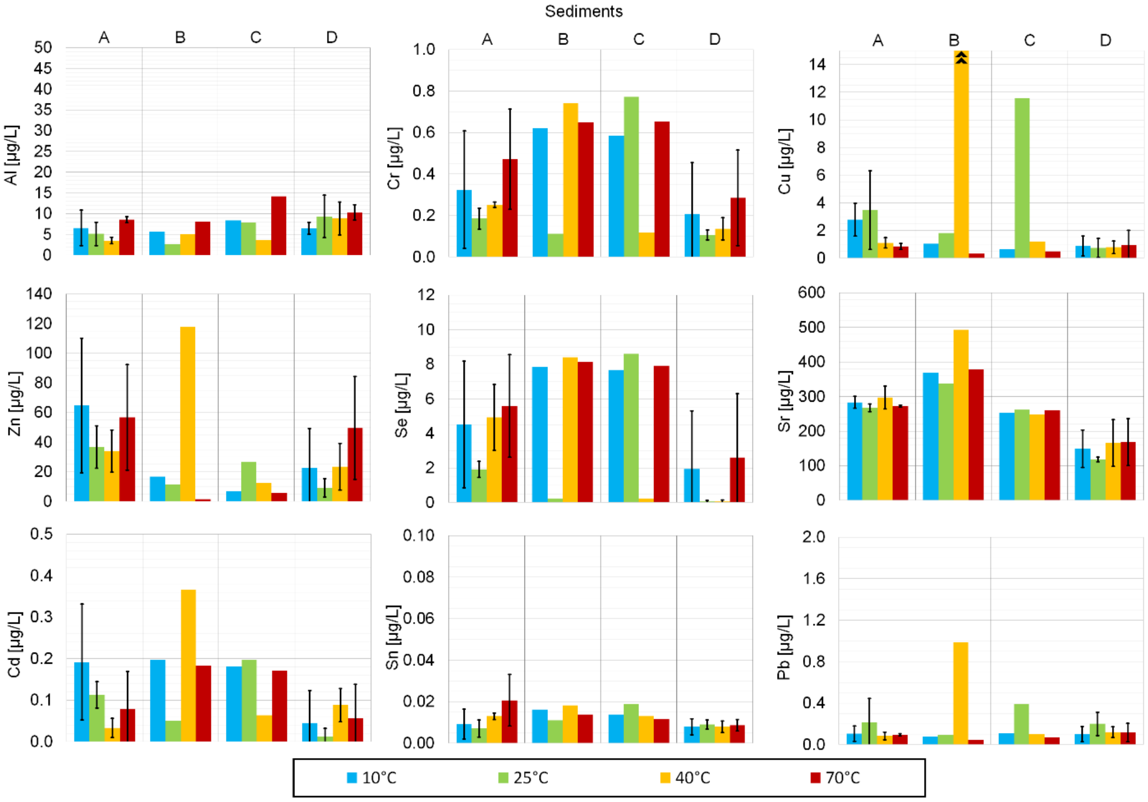

Fig. S.3.27: Concentrations of Al, Cr, Cu, Zn, Se, Sr, Cd, Sn and Pb in eluates of sediments A, B, C and D after one week of tempering to 10, 25, 40 or 70 °C in circular-flow column tests. For sediments A and D data from the alpha, beta and gamma series were used, error bars indicate the standard deviation; sediments B and C were only investigated in the alpha series.

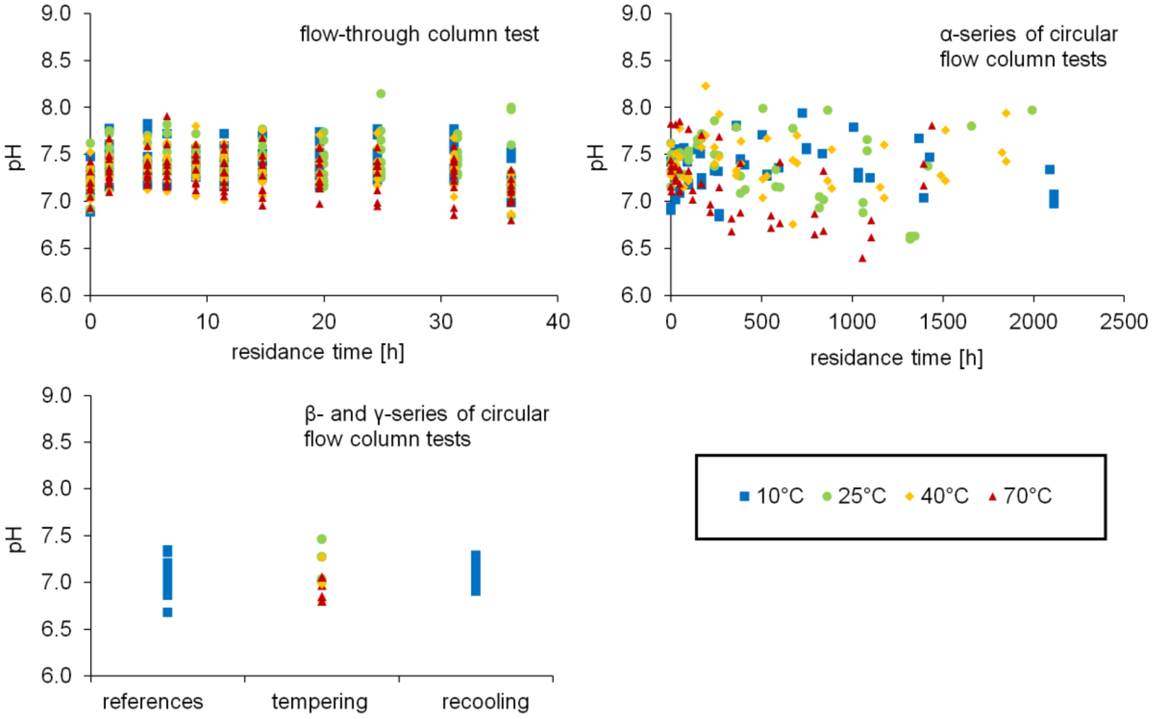

Fig. S.3.28: Measured pH values in the flow-through- and circular-flow column tests at 10, 25, 40 and 70 °C.

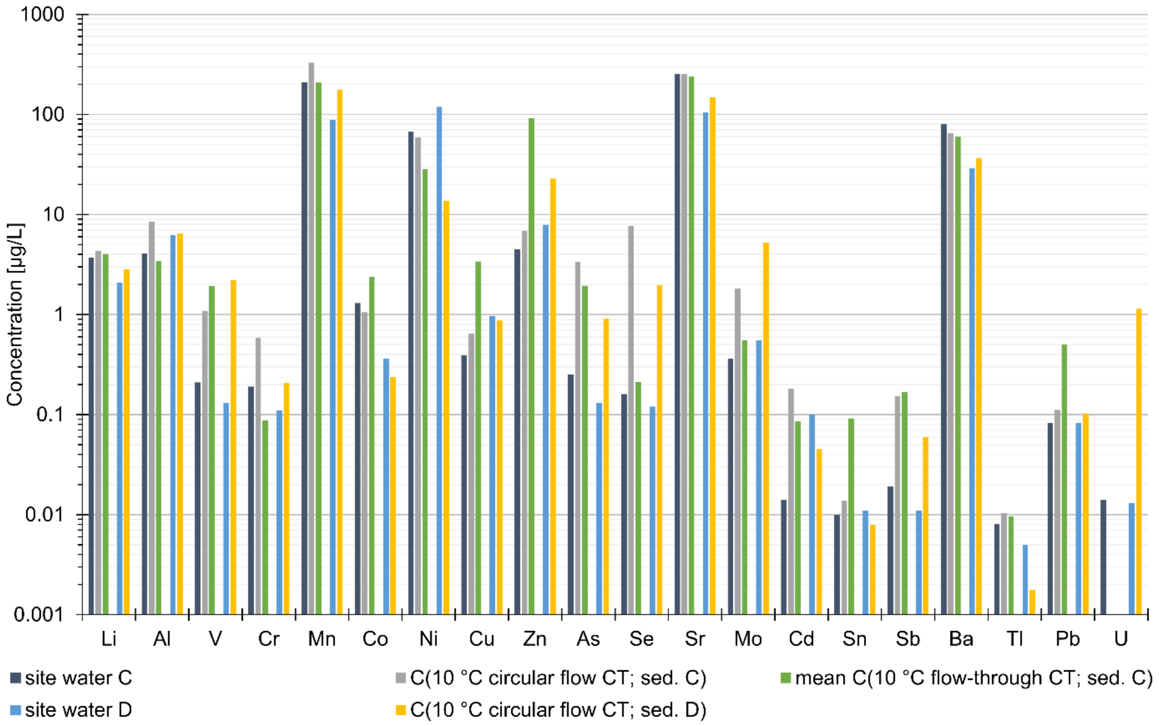

Fig. S.3.29: Comparison of site water concentrations with laboratory column tests (CT) with the respective sediment conducted at 10 °C.

Table S.3.6: Current drinking water limits and (insignificance-)threshold-values for trace elements and heavy metals in Germany, as well as the respective (provisional) guideline values for drinking water quality of the WHO.

		drinking water limits [TrinkwV] *(BMJ, 2001)*	***threshold-values [GrwV]*** (BMJ, 2010)	***insignificance-threshold-values*** *(LAWA, 2017)*	***(provisional) guideline values*** *(WHO, 2017)*
B	*[µg/L]*	1000	-	180	2400
Al	*[µg/L]*	200	-	-	-
V	*[µg/L]*	-	-	4	-
Cr	*[µg/L]*	50	-	3.4	50
Mn	*[µg/L]*	50	-	-	-
Co	*[µg/L]*	-	-	2	-
Ni	*[µg/L]*	20	-	7	70
Cu	*[µg/L]*	2000	-	5.4	2000
Zn	*[µg/L]*	-	-	60	-
As	*[µg/L]*	10	10	3.2	10
Se	*[µg/L]*	10	-	3	40
Mo	*[µg/L]*	-	-	35	-
Cd	*[µg/L]*	3	0.5	0.3	3
Sb	*[µg/L]*	5	-	5	20
Ba	*[µg/L]*	-	-	175	1300
Hg	*[µg/L]*	1	0.2	0.1	6
Tl	*[µg/L]*	-	-	0.2	-
Pb	*[µg/L]*	10	10	1.2	10
U	*[µg/L]*	10	-	-	30

4. Predictability of initial hydrogeochemical effects induced by short-term infiltration of ~75 °C hot water into a shallow glaciogenic aquifer

This chapter is based on a paper published 2021 by Lüders, K., Hornbruch, G., Zarrabi, N., Heldt, S., Dahmke, A. & Köber, R. in Water Research X 13 – 100121. https://doi.org/10.1016/j.wroa.2021.100121

4.1. Abstract

Despite their potential in heating supply systems, thus far high-temperature aquifer thermal energy storages (HT-ATES) currently lack widespread application. Reducing the potential risks by improving the predictability of hydrogeochemical processes accelerated or initiated at elevated temperatures might promote the development of this technology. Therefore, we report the results of a short-term hot water infiltration field test with subsurface temperatures above 70 °C, along with associated laboratory batch tests at 10, 40 and 70 °C for 28 sediment samples to determine their usability for geochemical prediction.

Most groundwater components had lower maximal concentrations and smaller concentration ranges in field samples compared to the batch tests. This indicates that the strongest geochemical effects observed in laboratory tests with sufficient site-specific sediment samples will likely be attenuated at the field scale. A comparison of field measurements with predicted concentration ranges, based on temperature induced relative concentration changes from the batch tests, revealed that the predictive power was greatest, where the hot infiltrated water had cooled least and the strongest geochemical effects occurred. The batch test-based predictions showed the best accordance with field data for components, with significant temperature-induced concentration changes related to ion exchange and (de)sorption processes. However, accurate prediction of concentration changes based on other processes, e.g. mineral dissolution, and downstream reversals in concentrations, requires further investigation.

The here presented procedure enables the prediction of maximal expectable temperature-dependent concentration changes for most environmentally relevant ancillary groundwater components, e.g. As, with limited effort.

4.2. Introduction

Seasonal high-temperature aquifer thermal energy storages (HT-ATES) in urban areas have the potential to be a key technology in the transformation of the heating sector energy system away from the use of fossil fuels (Henning and Palzer, 2012). However, thus far, the wider application of ATES systems with temperatures above 50 °C has been hampered by technical, financial, social, political and legal risks (Fleuchaus et al., 2020). One aspect, that causes potential technical or legal issues, is the various hydrogeochemical processes accelerated or initiated by elevated temperatures of up to 90 °C, and the induced changes to the flow regime (Bauer et al., 2013; Jenne et al., 1992).

This includes processes associated with operational issues, such as i) accelerated corrosion (Andersson, 1990; Jenne et al., 1992); ii) the precipitation of carbonates (Griffioen and Appelo, 1993) and Fe and Mn (hydr)oxides (Andersson, 1990; Willemsen, 1990) that can cause scaling within heat exchangers, pipes and in and around wells; iii) the formation of a separate gas phase (Lüders et al., 2016) that can block pipes or parts of the near-well pore space and iv) the dissolution of amorphous silica and silicates at increased temperatures (Arning et al., 2006; Bonte et al., 2013b; Holm et al., 1987) that can precipitate when the water is cooled in the surface installations during heat recovery (Gunnarsson and Arnórsson, 2005). There are also processes associated with potential changes in groundwater quality, such as i) the release of dissolved organic carbon (DOC) and associated redox processes (Bonte et al., 2013a; Brons et al., 1991; Jesußek et al., 2013a, 2013b); ii) the release and fixation of trace elements and heavy metals (Bonte et al., 2013b; García-Gil et al., 2016b; Lüders et al., 2020; Saito et al., 2016) and iii) increased or decreased solubility (Koproch et al., 2019), volatilisation (Schwardt et al., 2021) and degradation (Men and Cheng, 2011; Něměček et al., 2018; Zuurbier et al., 2013) of organic contaminants.

These hydrogeochemical processes have been investigated in laboratory studies using batch (Arning et al., 2006; Jesußek et al., 2013a; Koproch et al., 2019; Men and Cheng, 2011; Schwardt et al., 2021), flow-through (Bonte et al., 2013b, 2013a; Griffioen and Appelo, 1993; Jesußek et al., 2013b, 2013a; Lüders et al., 2016) and circular flow column tests (Lüders et al., 2020). Furthermore, attempts have been made to empirically categorise trace elements and heavy metals relevant for administrative approval (Lüders et al., 2020). Previous HT-ATES field tests, installed in depths varying from below 10 to above 200 m below ground surface (bgs), have mainly focussed only on processes that potentially damage the ATES operation itself, as well as on technical solutions to prevent these processes (Andersson, 1990; Jenne et al., 1992; Molz et al., 1981; Opel et al., 2014; Perlinger et al., 1987; Ueckert and Baumann, 2019). Initial hydrogeochemical effects with potential environmental consequences relevant for administrative approval (Bonte et al., 2011; Hähnlein et al., 2013; Possemiers et al., 2014) and observations of geochemical effects downstream of the infiltration well have not been in focus of HT-ATES field tests so far. Furthermore, all the aforementioned studies focus either on laboratory investigations or on field observations. Thus, whether laboratory investigations with site material and water can yield reliable predictions regarding temperature-dependent (initial) hydrogeochemical effects at the aquifer scale is largely undetermined.

Therefore, this work combines a short-term hot water infiltration field test with temperatures of up to 78 °C, with preceding laboratory batch tests for 28 sediment samples from the field test site. Essential questions investigated by this approach include:

- Which initial component-specific, temperature-dependent geochemical effects observed in the hot water infiltration field test can be predicted by the laboratory investigations, and to what extent?
- How does the geochemical heterogeneity of the sediments affect variances in geochemical behaviour at the laboratory and field scale?

4.3. Materials and Methods

4.3.1. “TestUM” field test site

The “TestUM” field test site is located near Wittstock, Brandenburg, Germany [53°11'40"N, 12°30'18"E], on an abandoned airfield. Subsurface exploration during an earlier CO_2 injection test on the same site, a few metres away (Lamert et al., 2012; Peter et al., 2012), showed that the shallow subsurface consists of typical northern German glacio-fluviatile Quaternary sediments, with alternating layers of sandy and cohesive sediments of variable thickness. Based on further drill logs and geophysical investigation with an electric conductivity (EC) and a hydraulic-profiling-tool (HPT), an area featuring a ~9 m thick sandy layer, 6–15 m bgs, overlaid by a 2-3 m thick cohesive layer was chosen for the hot water infiltration test (see also Heldt et al., 2021; Hornbruch et al., in prep.; Keller et al., 2021). Groundwater head measurements between 2.9 and 3.5 m bgs showed that the sandy layer used for infiltration is confined. Locally, groundwater flowed in west-southwest direction, with a mean hydraulic gradient of 0.0011 and a mean groundwater flow velocity of 0.09 m/d (Heldt et al., 2021a).

For setting up the test field, one 2” extraction and one 2” infiltration well screened in 7-14 m bgs, five 2” monitoring wells each screened at 7–8, 10–11 and 13–14 m bgs and 12 multi-level CMT®-wells (Continuous Multichannel Tubing; Solinst Canada Ltd., Georgetown, Ontario, CA) screened at 5 (partial), 7.5, 10.5, 13.5 and 17 m bgs were installed with sonic drilling (see Fig. 4.1 for a map of the field tests monitoring network). This resulted in 71 groundwater-monitoring points distributed over 17 wells.

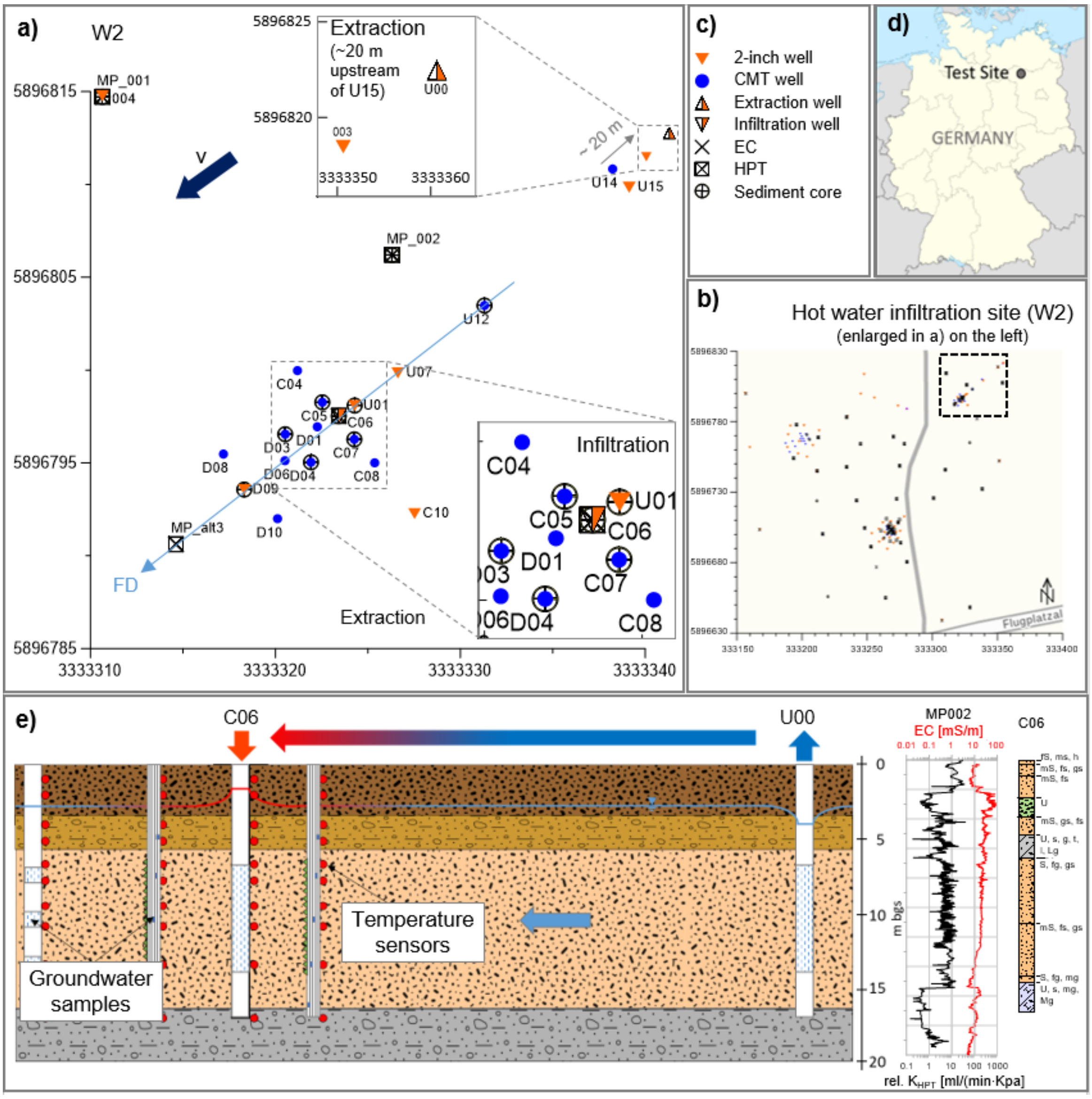

Fig. 4.1: Monitoring network of the hot water infiltration field test site (a; profile FD is used in Fig. 4.3 for illustrating temperature changes) and the wider TestUM field test area with the framed hot water infiltration site (b); the respective legend (c); the location of the TestUM field test site (d); and a simplified subsurface structure and test setup along a selection of hydraulic-profiling tool (HPT), electrical conductivity (EC) and drill log exploration data (e; data curve colours are equal to the axis label); partly from Heldt et al., 2021 and Keller et al., 2021).

4.3.2. Laboratory experiments

4.3.2.1. Sediment and water procurement and characterisation

Before installing the monitoring wells, ~100 kg of sediment samples from 0-18 m bgs were obtained from nine different bore holes (at positions U01, U12, C05, C06, C07, D03, D04, D09 and MP002; Fig. 4.1) by either macro-core® or sonic drilling (Geoprobe Systems®, Salina, Kansas, US). Macro-core® drilling yields sediment samples with minimal physical and chemical disturbance (EPA, 1997), in contrast, sonic drilling can cause elevated temperatures at the drill core interface and thus might potentially affect temperature dependent geochemical behaviour in subsequent laboratory investigations. However, there were no noticeable deviations in the temperature-induced geochemical effects of the different sediment samples depending on the used drilling technique, wherefore no further differentiation regarding the drilling technique was made. Each half-metre drill core, consisting of, on average, 1733 g sediment, was mixed and split into three parts: 1) a 400 g individual sediment sample, specific to the respective well location and half metre depth range; 2) half of the remaining sediment was mixed to a homogenised composite sample of the infiltration layer and 3) the rest was kept in the drill cores as backup material. The individual sediment samples were used to investigate the heterogeneity in hydrogeochemical behaviour at elevated temperatures. The homogenised composite sample of the infiltration layer was used for geochemical characterisation (with triplicates, Table 4.1) and for further laboratory investigations with a higher sediment demand not part of this study.

Table 4.1: Sediment characteristics of the target aquifer for the hot water infiltration test. Data of the different carbon and iron contents for the individual sediment samples, as well as data of the individual trace elements and heavy metals that are ionically bound are included in the supplementary material (Table S.4.3 and Table S.4.4, respectively).

	Composite sample
Sediment	Pleistocene sand
Extraction depth *[metres below ground surface]*	6-14
Grain fraction ***d60*** *[µm]****; d10*** *[µm]****; d60/d10***	347±69; 117±40; 3.3±1.0
silt *[%]*; ***sand*** *[%]*; ***gravel*** *[%]*	11±8; 86±8; 3±3
C[1] *[mg/kg]*	1035±225
$C_{org.}$[1] *[mg/kg]*	560±265
$C_{carb.}$[1] *[mg/kg]*	517±306
reactive Fe[2] *[mg/kg]*	407±38
Fe bound in crystalline iron oxides, siderite and magnetite[3] *[mg/kg]*	1032±245
∑ ionically bound trace elements and heavy metals (listed in section 2.4)[4] *[mg/kg]*	65±22

[1] determined with a Multi N/C 2100 Analyser with HT-1300 oven (Analytik Jena AG, Jena, Germany); total carbon (C) directly, total organic carbon ($C_{org.}$) after removal of total inorganic carbon ($C_{carb.}$) with 2 M HCL, $C_{carb.}$ was calculated from the difference between C and $C_{org.}$.

[2] determined by extraction with 1 M HCL according to Leventhal and Taylor (1990) and subsequent photometric analysis of the extracts according to the ferrozine method (Stookey, 1970) with hydroxylammonium chloride as the reductive agent.

[3] determined by extraction with 5 M HCL according to Heron et al. (1994) and subsequent photometric analysis of the extracts according to the ferrozine method (Stookey, 1970) with hydroxylammonium chloride as the reductive agent.

[4] determined by digestion with 1 M sodium dihydrogen phosphate at pH 5 adjusted with sodium hydroxide following the procedure described in Keon et al. (2001).

All sediment samples were stored under argon atmosphere in refrigerators at 10 °C until further use. The water used for the laboratory experiments was repeatedly pumped from the extraction well and well 004 (Fig. 4.1) and stored at 10 °C in a refrigerator in gas-tight bags (PET/Al/PE-composite) to avoid gas exchange with the atmosphere (Table 4.2).

Sediment samples from the same wells, but from the low permeable layers above and below the target aquifer utilised for the hot water infiltration have been investigated in a separate study (Meier zu Beerentrup et al., in prep.).

Table 4.2: Initial composition of the water used for laboratory experiments.

		site water from extraction well U00	***site water from well 004***
pH	*[-]*	6.24±0.27	6.48±0.18
O_2	*[mg/L]*	1.12±0.36	2.66±0.98
electrical conductivity	*[µS/cm]*	535±2	427±17
redox potential	*[mV]*	355±235	373±9
alkalinity	*[mmol/L]*	2.39±0.29	-
NPOC	*[mg/L]*	2.89±0.61	3.13±1.27
TIC	*[mg/L]*	-	30.2±5.1
K^+	*[mg/L]*	2.12±0.38	1.30±0.14
Na^+	*[mg/L]*	19.2±1.2	9.80±0.30
Ca^{2+}	*[mg/L]*	91.8±5.9	75.3±3.2
Mg^{2+}	*[mg/L]*	5.62±0.22	5.06±0.17
Fe_{diss}	*[µg/L]*	30.4±17.9	43.7±75.3
Mn_{diss}	*[µg/L]*	76.0±9.5	2.97±0.93
Si_{diss}	*[mg/L]*	4.88±0.10	4.67±0.12
Al_{diss}	*[µg/L]*	8.16±4.17	6.17±3.05
Cl^-	*[mg/L]*	9.05±2.34	3.69±0.42
NO_2^-	*[mg/L]*	<0.4	<0.2
NO_3^-	*[mg/L]*	6.67±3.31	7.28±0.81
SO_4^{2-}	*[mg/L]*	143±18	100±8
CH_4	*[µg/L]*	4.04±1.77	0.60±0.22
TCE	*[µg/L]*	5.51±1.94	6.92±2.05
Li	*[µg/L]*	1.64±0.39	0.72±0.05
V	*[µg/L]*	0.90±0.22	0.68±0.06
Cr	*[µg/L]*	0.12±0.05	0.19±0.07
Co	*[µg/L]*	0.79±0.26	0.77±0.69
Ni	*[µg/L]*	3.14±1.60	2.17±0.37
Cu	*[µg/L]*	2.71±1.83	3.45±1.84
Zn	*[µg/L]*	23.2±10.2	29.1±24.3
As	*[µg/L]*	0.29±0.11	0.16±0.01
Se	*[µg/L]*	0.48±0.07	0.20±0.10
Sr	*[µg/L]*	204±7	164±7
Mo	*[µg/L]*	0.22±0.09	0.12±0.04
Cd	*[µg/L]*	0.41±0.15	0.09±0.01
Sn	*[µg/L]*	0.012±0.005	0.009±0.005
Sb	*[µg/L]*	0.157±0.016	0.039±0.003
Ba	*[µg/L]*	61.8±10.0	29.0±0.5
Tl	*[µg/L]*	0.012±0.002	0.005±0.001
Pb	*[µg/L]*	0.274±0.299	0.184±0.076
U	*[µg/L]*	1.47±1.13	0.091±0.010

4.3.2.2. Batch tests

Batch tests were used to determine the heterogeneity in hydrogeochemical behaviour of individual sediment samples at elevated temperatures and to consider the observed variance for the subsequent predictive calculations (Ch. 4.3.5), due to their low sample volume requirements. Sediment samples (n=28), from the sandy aquifer section into which the hot water was infiltrated (6-15 m bgs), were tempered for one week at 60 rpm in a shaking chamber to 10 and 40 °C, and in a custom build heating chamber on a shaker to 70 °C. For each of the 84 batches, 40 g of sediment and 80 mL of site water were filled into 200 mL HDPE vials (sediment samples from C, D and U wells, with site water from extraction well U00) or 100 mL glass vials (sediment samples from MP002 drill core, with site water from well 004) in an argon filled glove box (Table 4.2), to avoid oxygen intrusion. The vials were closed with HDPE screw caps or aluminium crimp caps with butyl septa, respectively. The potential degassing of CO_2 while filling the vials cannot be prevented with this procedure. To identify concentration changes induced by the vial material, blank tests with both vial materials and site water, but without sediment, were applied at each temperature (see Table S.4.5 in the supplementary material). Due to the high ratio between the concentrations resulting from the releases from the blank vials versus the respective mean concentration increase in the sediment batch tests for Si_{diss} with the glass vials (up to 1.31) and non-purgeable organic carbon (NPOC) with the HDPE vials (up to 0.81), only the data from the sediment batch tests with the other vial material were used for further data evaluation for these two components. After one week, the vials were reopened and the water was separated from the sediment using 7 µm cellulose round filters, and then filled into the analytical vials (Ch. 4.3.4).

4.3.3. Short-term hot water infiltration field test

To identify the geochemical effects of elevated temperatures, the initial hydrogeochemical state and natural variations in the target aquifer were characterised in six baseline sampling campaigns, conducted between October 2018 and April 2019 (224, 183, 128, 93, 64 and 28 days before the start of the hot water infiltration; Fig. S.4.10). Over the whole monitoring period from autumn 2018 to summer 2019, the groundwater heads increased by up to 40 cm, similarly in all the different monitoring wells. Thus, there are no indications for significant changes in the hydraulic gradient or the groundwater flow direction over time.

Hot water infiltration started on the 23rd of May 2019 and finished on the 29th of May 2019. A submersible pump pumped cold water from extraction well U00 into a cold-water buffer tank. There, the water was covered with argon to avoid oxygen intrusion; however, concomitant equilibration of CO_2 between the water phase and the argon coverage may have facilitated subsequent carbonate precipitation at elevated temperatures. From the cold-water buffer tank, the water was pumped through a plate heat exchanger, where it was heated to approximately 85 °C, then into a hot water buffer tank where the hot water could degas to minimise potential tube or well clogging by gas bubbles. To eliminate traces of the organic contaminant trichloroethylene (TCE; Table 4.2, Fig. S.4.10), the formed gas phase was dissipated over an activated carbon filter before being released. From the hot water buffer tank, the water flowed by gravity at ~14.5 L/min into the infiltration well. Towards the end of the hot water infiltration, the infiltration rate decreased to below 1 L/min (Heldt et al., 2021a), presumably due to clogging of tubes and the well screen caused by a combination of transported fines from the extraction well, precipitates and gas bubbles. In total, ~86 m³ of ~75 °C hot water was infiltrated over a period of 4.5 days. Water extraction and infiltration superimposed the natural hydraulic conditions around the respective wells during operation, but the induced hydraulic signal faded away within a few hours (data not shown).

Subsequently, eight sampling campaigns (4, 12, 15, 20, 33, 48, 68 and 104 days after the start of infiltration) were conducted to monitor the hydrogeochemical effects in the post hot water infiltration phase. In each monitoring campaign, water samples were taken from 40 to 70 monitoring points (3 to 5 per well). To minimise hydraulic effects of the sampling campaigns, groundwater samples from the 2-inch wells were retrieved with low pumping rates of ~4 L/min by submersible pumps (MP1, Grundfos GmbH, Erkrath, Germany; or Whale submersible electric galley pump, Munster Simms Engineering Ltd., Bangor, Northern Ireland). The water samples from the different screened depths in the 2-inch wells (7-8, 10-11 and 13-14 m bgs) were separated by using packers above and below the pump submerged to the respective monitoring depths. The water then flowed through a PVC tube into a mixing cell, where probes for the on-site parameters (Ch. 4.3.4) were installed. To pump groundwater from the CMT-wells into the mixing cell (~100 mL/min), peristaltic pumps, stainless steel capillaries and viton (pumping) tubes were utilised, which allowed to minimise intrusion of oxygen, despite a relatively long residence time in the pumping system. In both setups, water samples for the analytical vials (Ch. 4.3.4) were taken at a three-way-valve directly before the mixing cell. Keller et al. (2021) used several baseline and post hot water infiltration sampling campaigns to also take water samples for investigating the potential effects of elevated temperatures on the microbial diversity and total cell counts to mutually support data interpretation.

4.3.4. Analytics of aqueous samples

On-site parameters (pH, Eh, electrical conductivity and O_2 concentration), main cations, main anions, NPOC, total inorganic carbon (TIC; laboratory tests), ammonium and dissolved methane and trichloroethylene (TCE) were analysed using standard geochemical methods. Alkalinity was determined by acid titration. Trace element and heavy metal samples were filtered with 0.2 mm RC-filters and analysed by an inductively coupled plasma mass spectrometer (7500cs; Agilent Technologies, Inc., Santa Clara, CA, USA) following the method described in Garbe-Schönberg (1993) for the elements Li, Al, V, Cr, Co, Ni, Cu, Zn, As, Se, Sr, Mo, Cd, Sn, Sb, Ba, Tl, Pb and U.

4.3.5. Prediction of potential concentration changes in the hot water infiltration field test based on laboratory investigations

The concentration changes between the laboratory batch tests at 10, 40 and 70 °C were used to predict temperature-dependent potential concentration changes in the hot water infiltration field test. First, the component-specific relative concentration changes, between the batch tests at increased temperatures of 40 and 70 °C and the reference batch tests at 10 °C, were calculated for all 28 sediment samples and plotted against temperature (as shown for V in Fig. S.4.11). Relative changes were chosen over absolute values as they allow for better consideration of different base concentration levels. Then, the 0th, 25th, 50th, 75th and 100th percentile of the 28 component-specific relative concentration changes between 10 and 40 °C and 40 and 70 °C were approximated by linear or exponential regression functions. Whether linear or exponential regression functions were applied for a component was determined by the higher coefficient of determination for the median concentrations (50th percentile) over the whole temperature range (from 10, to 40 and 70 °C). The two temperature ranges were calculated separately to prevent over- or underestimations of concentrations around the temperatures actually investigated in the laboratory batch tests, while enabling the prediction of concentrations in between. To calculate well and depth-specific potential concentration changes, the corresponding baseline concentrations and temperature measurements completed the equation (as shown in Eqs. A.1 and A.2; Ch. 4.6).

This procedure resulted in a component-specific potential concentration range calculated from the heterogeneity of the sediment samples investigated in the laboratory batch tests, linked with the temperatures measured in the hot water infiltration field test.

4.4. Results and Discussion

4.4.1. Geochemical effects in laboratory experiments

Overall, temperature-induced geochemical effects in the laboratory tests followed the pattern expected from previous studies: for the main groundwater constituents, an increase in temperature caused a release of organic carbon (Brons et al., 1991; Jesußek et al., 2013a), silica and potassium (Arning et al., 2006; Holm et al., 1987), whereas concentrations of inorganic carbon, calcium and magnesium decreased (Griffioen and Appelo, 1993; Fig. 4.2a). Despite the elevated NPOC concentrations, microbial catalysed redox reactions appeared to be limited within the one-week sediment-water contact time, as expected from lag phases of microbial growth (Mellefont and Ross, 2003). This resulted in negligible effects on median concentrations of redox sensitive parameters, such as nitrate and sulphate. Also, the median concentrations of trace elements and heavy metals mostly behaved as expected from the literature: increasing concentrations with increasing temperature were observed for monovalent cations (Li and Tl) and those components likely present as oxyanions (e.g. V, As, Se and Mo). Concentrations of divalent cations (e.g. Co, Ni and Zn) rather decreased (Bonte et al., 2013b; Lüders et al., 2020; Fig. 4.2b). Unlike afore cited studies, concentrations of Cu and Al increased in several sediment samples at 70 °C.

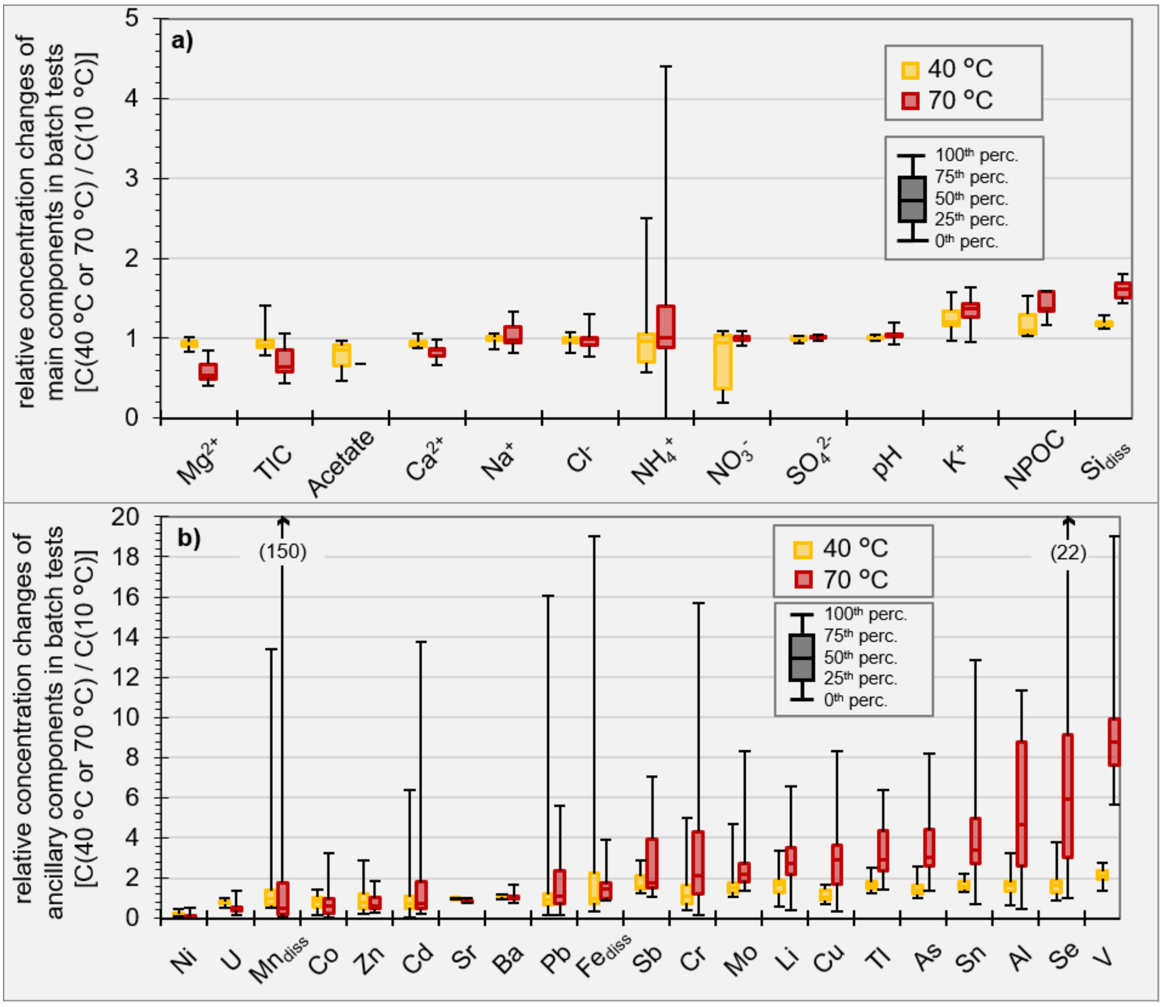

Fig. 4.2 Impact of temperature on concentrations of main (a) and ancillary (b) groundwater components in one-week batch tests at 10, 40 and 70 °C. Shown are the 0th, 25th, 50th, 75th and 100th percentile of relative concentration changes at 40 and 70 °C compared to those at 10 °C from the 28 sediment samples; sorted from the strongest relative decrease in median concentrations between 10 and 70 °C on the left towards the respective strongest increase on the right.

Most of the components, which showed elevated concentrations at increased temperatures, also demonstrated a greater concentration variation at 40 and even more at 70 °C, compared to 10 °C (e.g. Si_{diss}, Li, V, Cr, As, Se and Sb). A similar wider scattering of concentrations at higher temperatures has also been reported by Bonte et al. (2013b) and Lüders et al. (2020). Taken together, the small-scale heterogeneity in groundwater chemistry at ambient temperatures observed in the baseline monitoring for the hot water infiltration test (Fig. 4.4, Fig. S.4.10, Hornbruch et al., in prep.), can be expected to increase when temperatures rise. This would result in, not only shifted, but also wider concentration ranges at elevated temperatures.

4.4.2. Effects of the hot-water infiltration field test on aquifer hydrochemistry

4.4.2.1. Temporal evolution of induced temperature changes

The infiltration of the hot water caused elevated temperatures, up to ~70 °C in close proximity to the infiltration well. Higher temperatures at the top of the aquifer than at the bottom (Fig. 4.3) can be attributed to temperature induced vertical convection, as shown by coupled numerical simulations (Heldt et al., 2021a), with local variations in hydraulic permeability (see HPT-logs in Fig. 4.1) contributing to spatial variations. Around the first monitoring campaign, 4-5 days after the start of the hot water infiltration, maximal temperatures of 72 °C were recorded at the monitoring points 7.5 m bgs in wells C05 and D01, 1-1.5 m away from the infiltration well (see Fig. 4.1 for positions). In monitoring wells C04, C08, D03, D04 and D06, all 3-4 m away from the infiltration well, the highest temperatures (30-41 °C) at 7.5 m bgs were recorded around the second monitoring campaign, 12-13 days after infiltration start. The monitoring wells further downstream (D08, D09, D10; 6.5 m away from the infiltration well) showed the highest temperatures of 14-15 °C around the 5th and 6th monitoring campaigns, 48-68 days after the start of the infiltration. A more detailed insight into temporal and spatial evolution of temperatures is presented in Heldt et al. (2021a, 2021b).

4.4.2.2. Overview of geochemical effects induced by hot water infiltration

To determine the geochemical effects induced by the hot water infiltration, the average concentrations, including standard deviations, in wells around and downstream from the infiltration well were compared for the baseline period and the first (first month) and second (from second month onwards) post-infiltration periods. These average concentrations represent several monitoring wells and campaigns and, therefore, the effects of a mixture of reached temperatures. However, increased concentrations of NO_2^-, K^+, Si_{diss}, Li, V, Cr, As, Se, Mo, Sb, Ba, Tl, U and CH_4 during the post-infiltration period(s) can be attributed to the elevated temperatures as they exceeded the natural variations during baseline monitoring and the potential mixing effects of original and infiltrated water (Fig. 4.4). For all components, apart from NO_2^- and CH_4, which were not detected and U, which was not significantly affected, the trend of increasing concentration with increasing temperature is also apparent in the laboratory batch tests (Fig. 4.2). Conversely, not all expected concentration changes apparent in the batch tests (e.g. for Co) were obvious and distinguishable from water mixing in the field measurements. The decreasing Cl^- concentrations and increasing U concentrations in the field measurements (Fig. 4.4) do not fit the expectations based on the laboratory batch tests (Fig. 4.2) and cannot be fully explained by water mixing processes between original and infiltrated water and therefore, for now, must be attributed to an unidentified process. Beside the quantitatively limited concentration changes of NO_2^- and CH_4 (<15 µmol/L), there were no indications of an intensification of microbially catalysed redox processes in the field measurements. This fits with expectations, as elevated temperatures were sustained only for a couple of days, and is also supported by the observation of only minor temperature-induced changes in the microbial community (Keller et al., 2021).

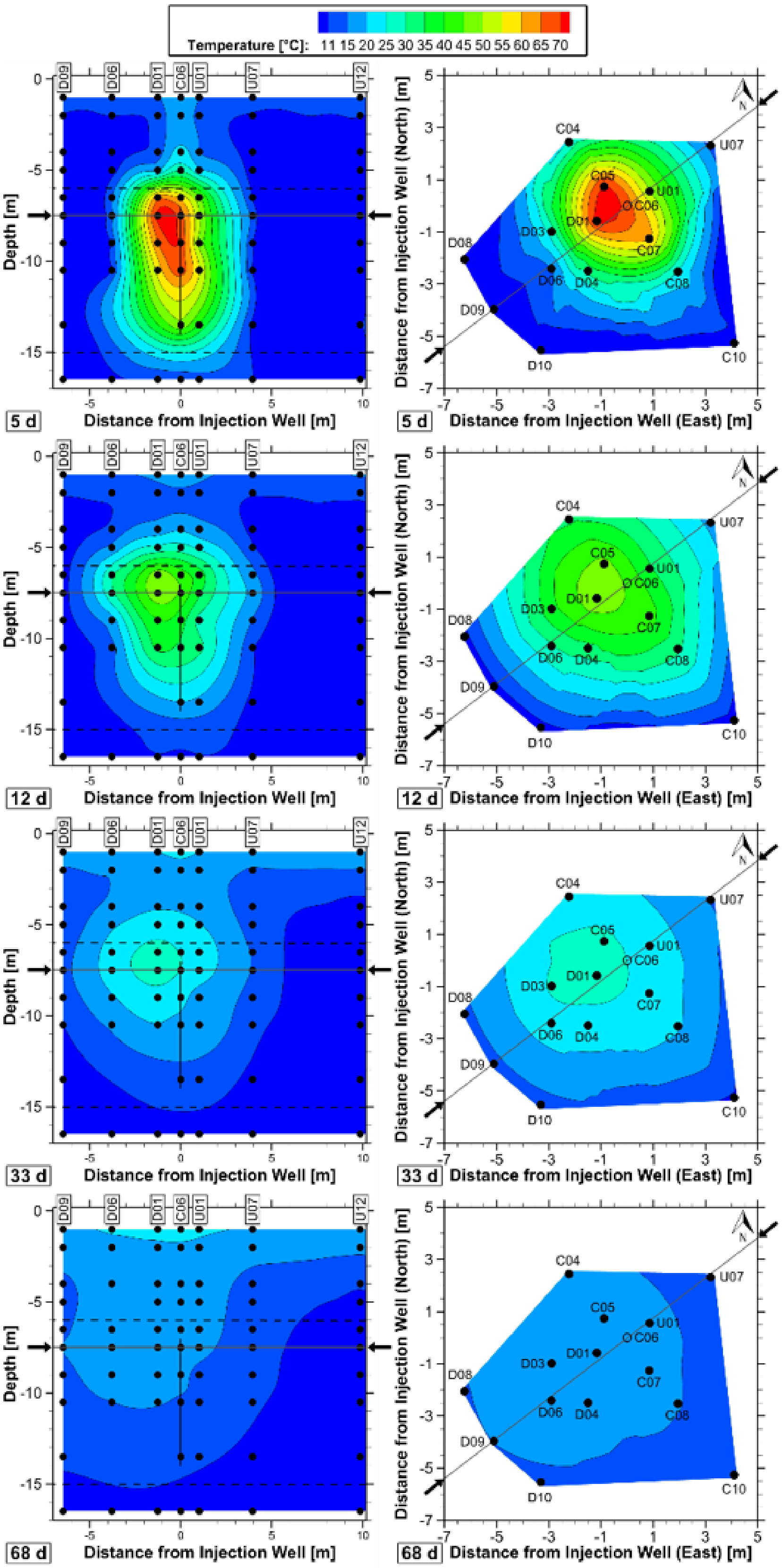

Fig. 4.3: Interpolated temperatures on a vertical (left column) and horizontal (right column) cross-section through the field test area at 5, 12, 33 and 68 days after start of the hot water infiltration (top to bottom rows). The vertical section is taken along the profile "FD (Flow Direction)" in Fig. 4.1, with groundwater flow from the top right to the lower left along the indicated profile. The horizontal section is shown for a depth of 7.5 m below ground surface, i.e. near the top of the aquifer. Black dots indicate temperature measuring points. The interpolated temperature distributions were derived by kriging using Tecplot 360 (Tecplot, Inc., WA, USA) with a range value of 0.3, a zero value of 0, a linear drift and taking into account the eight nearest points for the horizontal plane and all the points for the vertical cross section.

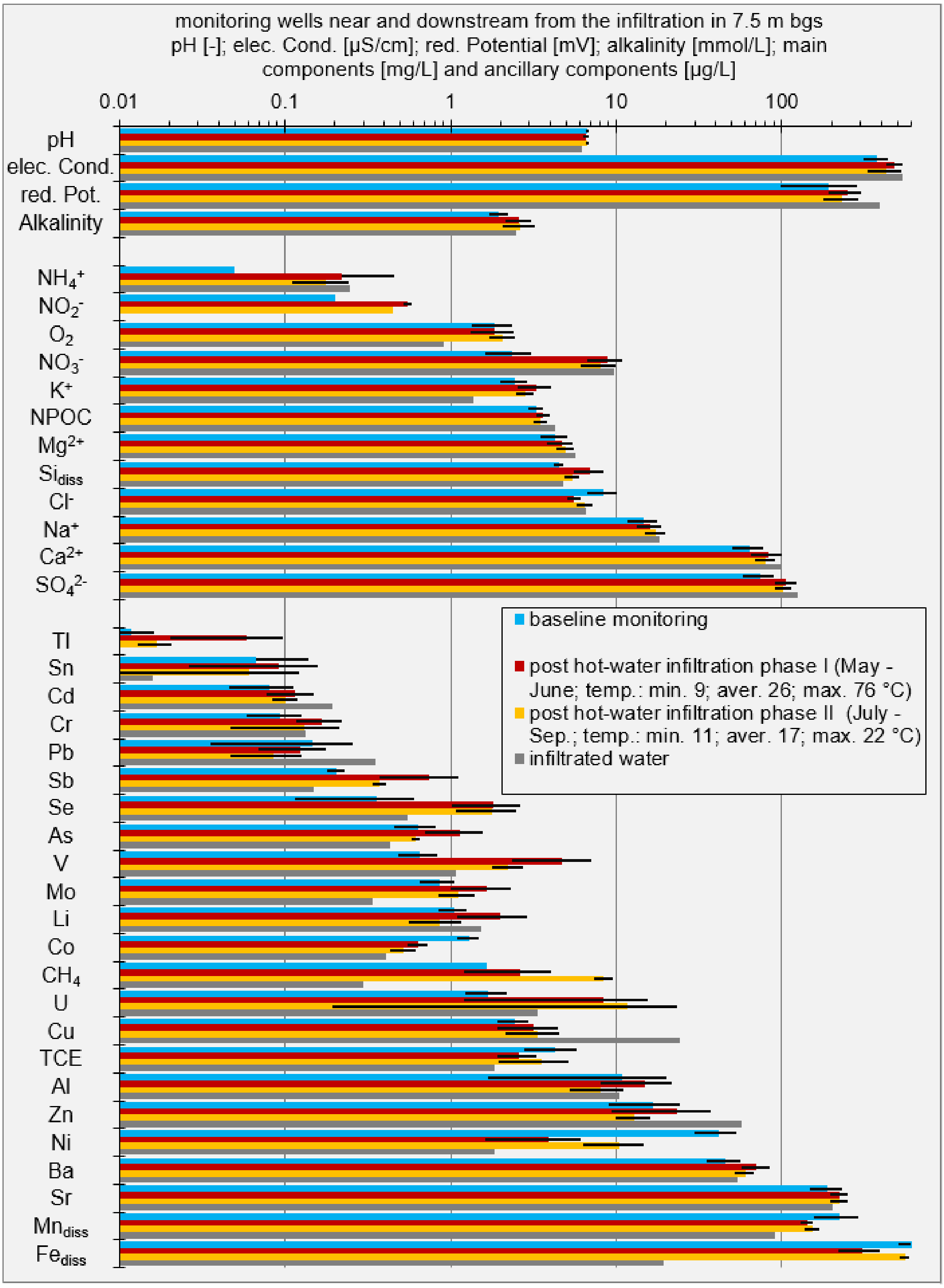

Fig. 4.4: Overview of field data for monitoring wells U01, C04, C05, C07, C08, D01, D03, D04, D06, D08, D09 and D10 (in 7.5 m below ground surface (bgs); see Fig. 4.1 for positions), separated after sampling during baseline monitoring, the first month after hot water infiltration, the further post infiltration phase and the infiltrated water. Average values and standard deviations are shown; main and ancillary components are sorted by ascending concentration, after the average baseline concentration within their group.

4.4.2.3. Reversibility of concentration changes in the field test

In ATES systems, geochemical reversibility characterises how aquifer hydrogeochemistry affected by elevated temperatures returns to initial conditions when temperatures decrease: a) around/downstream of the “hot well” during hot water infiltration and the storage period; b) due to heat extraction between hot water recovery and water re-infiltration into the “cold well” and c) after termination of ATES operation. To investigate how far the geochemical effects of elevated temperatures persist, maximal concentrations of K^+, Si_{diss}, Li, V, As, Mo and Se, that all showed increased concentrations near the infiltration well, were observed downstream. With increasing distance from the infiltration well (T_{max}=78 °C), maximal temperatures decreased from 73 to 41 °C and down to 15 °C at 1 m (D01), 3 m (D03) and 6.5 m (D09) from the well, respectively. Similar behaviour was observed for the maximal concentrations of Li, V, As, Mo and Se, as they returned to values within or near the geogenic range (Fig. 4.5). Thus, the field test data validated the rapid concentration changes with declining temperatures for components which concentration changes are related to temperature-dependent ion exchange and (de)sorption processes (e.g. Li, V, As, Mo and Se; Fig. 4.5) as has been shown in previous laboratory (Lüders et al., 2020) and modelling (Bonte et al., 2014) studies. As expected, reversal concentration changes related to mineral dissolution and precipitation (Si_{diss} and K^+) were slower (Fig. 4.5).

In case of longer sustained elevated temperatures, induced reductive dissolution of Fe- and Mn (hydr)oxides may reduce sorption capacity and thus reversibility (Bonte et al., 2013b; Lüders et al., 2020). Oxidative dissolution to a relevant extent is unlikely in this field test, as the oxygen concentration of the infiltrated water (0.9 mg/L; Fig. 4.4) was below the median oxygen concentrations in all monitored depths in the baseline monitoring (Fig. S.4.10), which also indicated a rather oxidised state of the sediment. However, in settings with larger oxygen infiltration, also oxidative dissolution reactions might play a role. Further, in a cyclic heat storage operation, groundwater constituents released at elevated temperatures will partly also be extracted with the hot water and fixated around the cold well after reinfiltration (as modelled by Bonte et al., 2014), or in potential mineral precipitates e.g. in the surface installations. Thus, the overall effect on the (re)distribution of released groundwater constituents is controlled by the interplay of the aforementioned processes and requires further research.

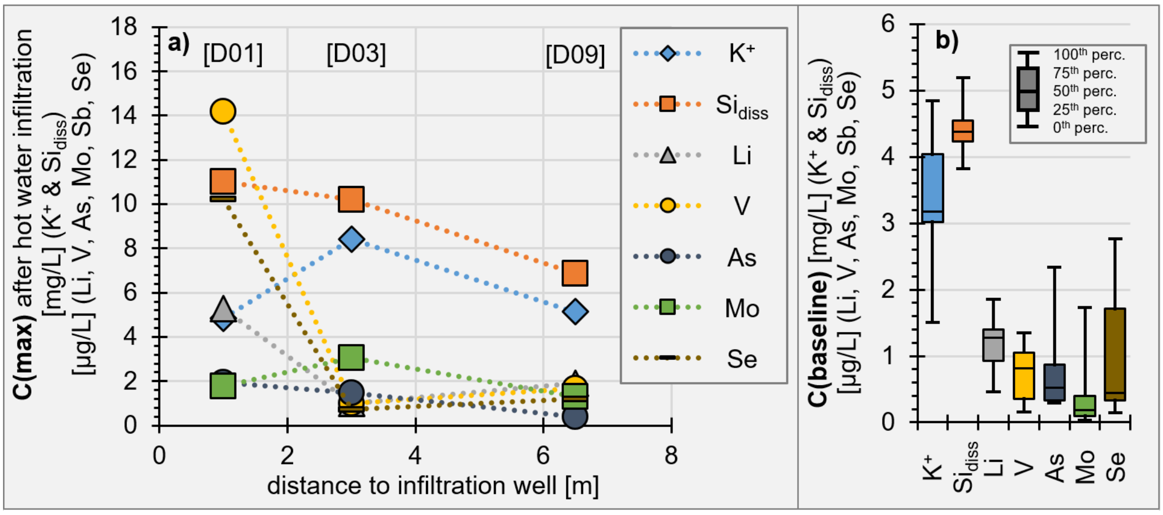

Fig. 4.5: Downstream development of K^+, Si_{diss}, Li, V, As, Mo and Se concentrations (a) that were increased due to hot water infiltration; compared to baseline concentrations in the respective monitoring wells D01, D03 & D09 (b).

4.4.3. Direct comparison of concentrations between the laboratory batch tests and the field test

For a primary comparison of concentrations between the field and the laboratory data at high temperatures, the data from the batch tests at 70 °C and monitoring points sampled at temperatures >55 °C were directly compared (the comparison of data from monitoring points sampled between 25 and 55 °C and associated batch tests at 40 °C is in the supplementary information; Fig. S.4.12). After the five-day hot water infiltration, five monitoring points, all from the central monitoring wells C05, C07 and D01 which are within a 1.5 m radius around the infiltration well, fit this criterion.

The maximal concentrations of components in the field samples >55 °C were within or below the concentration range of the laboratory batch tests at 70 °C for 24 of 31 components (all but NPOC, TIC, NO_3^-, Si_{diss}, Co, Ba and Tl). Overall, environmentally relevant concentration increases of most ancillary components seemed to be well represented. Moreover, despite the larger temperature range of the field samples (59–72 °C), the field data concentration range was smaller than the laboratory data concentration range for 26 of 31 components (all but NPOC, Co, Ni, Ba and Tl; Fig. 4.6). Both aspects are plausible, as the sediment samples investigated in the batch tests, originated from a wider area than the three central monitoring wells (Fig. 4.1). Thus, within the central hot zone around the infiltration well, the water may have only been in contact with a limited range of sedimentary compositions. Another possible explanation for this observation may also lie in the flow path of the water from the infiltration until the respective monitoring well; the water can encounter sediments of slightly different compositions, which potentially counterbalances the strongest effects. Both explanations indicate that considering a (preferably wide) variety of individual small-scale sediment samples in laboratory tests might serve as a safety buffer for concentrations expectable on the field scale.

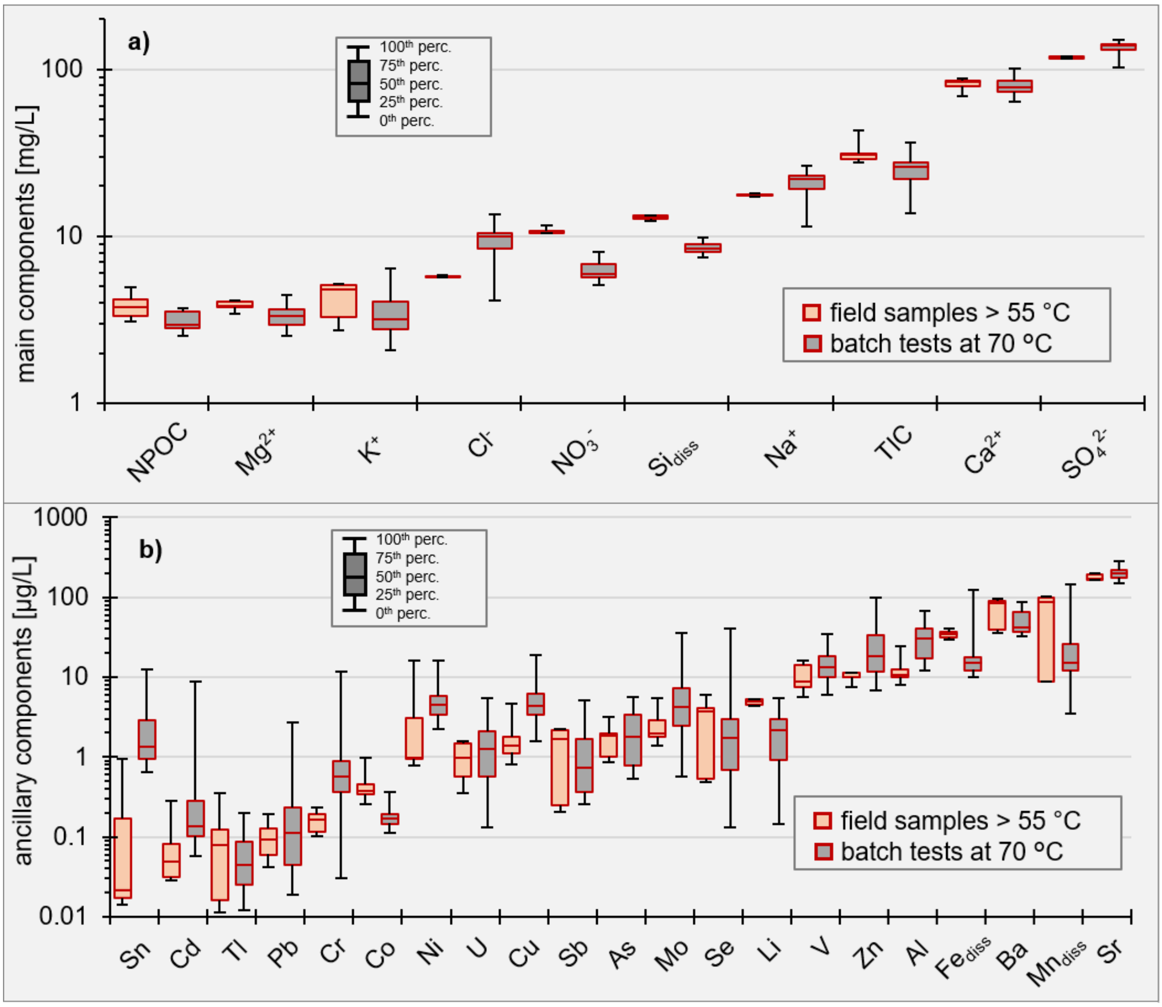

Fig. 4.6: Comparison of (a) main and (b) ancillary components concentrations in field samples from monitoring points C05 (7.5 and 10.5 m below ground surface[bgs]), C07 (7.5 bgs) and D01 (7.5 and 10.5 m bgs) in the temperature range 55-75 °C (n=5) and the concentrations in samples from the 70 °C batch tests (n=28). Components are sorted after median concentrations (50th percentile) in the field measurements; data for field samples in the temperature range from 25 to 55 °C (n=10) in comparison to the batch tests at 40 °C (n=28; Fig. S.4.12).

4.4.4. Comparison of field concentrations with the predicted concentration range from laboratory batch tests

With focus on the initial concentration changes caused by the highest temperatures attained in the field test, the predictive power of the laboratory batch tests was evaluated temporally by the first monitoring campaign after hot water infiltration, and spatially by the three central monitoring wells nearest to the infiltration well (C05, C07 and D01; each with three sampled depths). Overall, 33 % and 68 % of the concentrations of main and ancillary groundwater components measured in these wells, respectively, were between the 0th and 100th percentile of the predicted concentration range based on the temperature-induced concentration changes in the laboratory batch tests (Fig. 4.7; see Fig. S.4.11 for explanation). With 43 % and 40 % of concentrations of main and ancillary components laying below the 50th percentile, respectively, there appeared to be a slight overall underestimation of concentrations by the laboratory-based predictions.

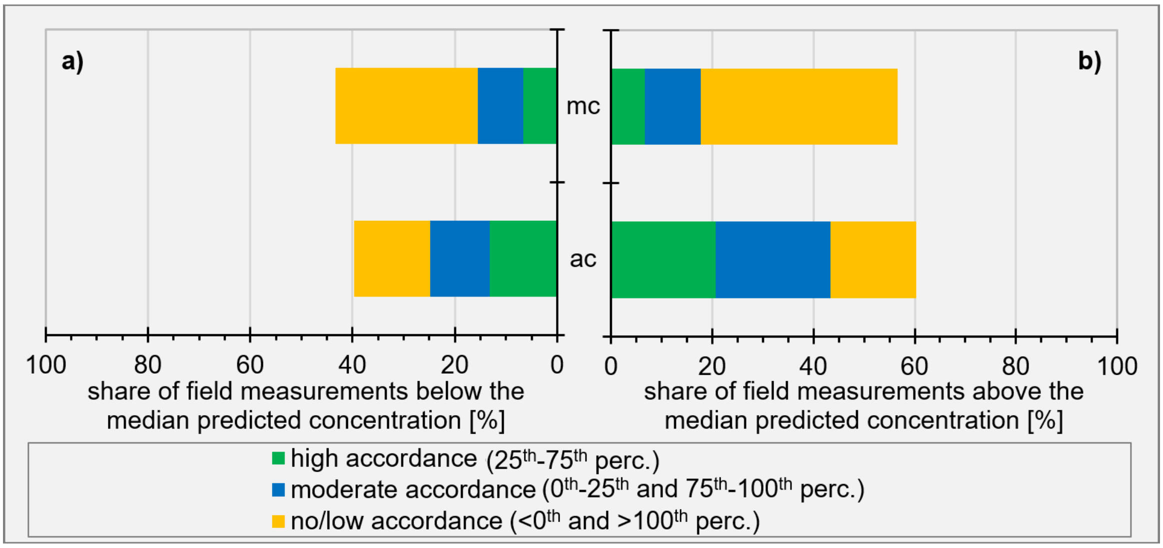

Fig. 4.7: Average accordance of main (mc) and ancillary components (ac) concentrations measured in wells C05, C07 and D01 during the first monitoring campaign after the hot water infiltration, with the predicted concentrations based on the temperature-induced concentration changes in the laboratory batch tests. The shares of field measurements (a) below and (b) above the median predicted concentrations are shown, separated for the intervals below, between and above the 0th, 25th, 50th, 75th and 100th percentile of predicted concentrations on the respective side of the figure.

To determine whether the temperature during monitoring had an effect on the agreement between measured concentrations and the predicted concentration range, the comparison between measured and predicted concentrations was broken down to the individual monitoring points of the wells C05, C07, D01 and D03 (n=12) including their respective sampling temperatures. Thereby, the overall accordance between measured and predicted concentrations was greatest, where the hot infiltrated water had cooled least prior to monitoring (Fig. 4.8a). The laboratory batch tests yielded the best results, in terms of predictive power, when the hottest temperature, and thus the largest change in concentration occurred, suggesting that the target infiltration temperature could be utilised as a basis for predicting the maximal expected temperature-induced concentration changes. On the on hand, maximal expectable concentration changes could be used as input parameters for scenario calculation that estimate the attenuated concentration changes in the wider surroundings (as e.g. shown in Lüders et al., 2020). On the other hand, the maximal expectable concentrations of environmentally relevant groundwater components are important for administrative approval procedures.

Furthermore, components with increased concentrations at elevated temperatures (K^+, Si_{diss}, Li, V, Cr, As, Se, Mo, Sb, Ba, Tl and U) also had a higher proportion of concentrations above the 100th percentile of predicted concentrations the further temperatures declined (Fig. 4.8b) which implies a retarded adaption of concentrations to decreasing temperatures.

Despite the similar trend for main and ancillary components, there is a significant gap in the accordance between these groups (Fig. 4.8a), indicating different behaviour of individual (groups of) components. To address this, the underlying data of Fig. 4.7 was broken down to the individual groundwater constituents (Fig. 4.9). From the main groundwater components, the measured concentrations of Mg^{2+}, TIC, Ca^{2+}, NO_3^-, Na^+, K^+, Cl^-, SO_4^{2-} and Si_{diss} were within the predicted concentration range for less than 50 % of the monitoring wells C05, C07 and D01. Considering the data in Fig. 4.2, Fig. 4.4 and Fig. 4.6, three distinct groups of these components can be identified. For Na^+, Cl^-, NO_3^- and SO_4^{2-} with comparatively small temperature-dependent concentration changes in the laboratory batch tests (Fig. 4.2), concentration changes due to mixing of infiltrated water (Fig. 4.4) with residual water from around the infiltration well probably exceeded any potential temperature-related concentration changes. Concentrations of TIC, Ca^{2+}, Mg^{2+} and Sr that were predominantly affected by temperature-dependent precipitation of carbonates (Griffioen and Appelo, 1993; Reddy and Nancollas, 1976) behave differently: to reach the target infiltration temperatures of 75 to 80 °C, temperatures in the surface installations (heat exchanger, tubes and tanks) must be even higher, and reached temperatures between 80 and 90 °C. This had no impact on geochemical processes that demand sediment-water contact, though mineral precipitation processes related to elevated temperatures can be affected. Therefore, the higher temperatures before infiltration probably caused stronger carbonate precipitation than expected based on the logged in-aquifer temperatures, which is not considered in the predicted concentration range calculations. Concentrations of TIC, Ca^{2+} and Mg^{2+} in the extracted water (Table 4.2) deviated from the values around the infiltration well in the baseline monitoring (Fig. 4.4;Fig. S.4.10), adding the mixing of the different waters as an additional source of uncertainty. Si_{diss}, Tl and, to a lesser extent K^{+}, showed increasing concentrations at elevated temperatures in the laboratory batch tests (Fig. 4.2), that were also visible in the field data (Fig. 4.4). However, the Si_{diss} and K^{+} concentrations declined slower than other components when temperatures decreased (Fig. 4.5), and Si_{diss} concentrations measured in the monitoring wells exceeded those observed in the laboratory tests (Fig. 4.6). The conducted batch tests seem to slightly underestimate concentration changes for silica, potassium and thallium (substituting potassium in silicates; Shaw, 1952), which is probably related to mineral dissolution of potassium bearing silicates and amorphous silica being the underlying release processes (Arning et al., 2006; Bonte et al., 2013b).

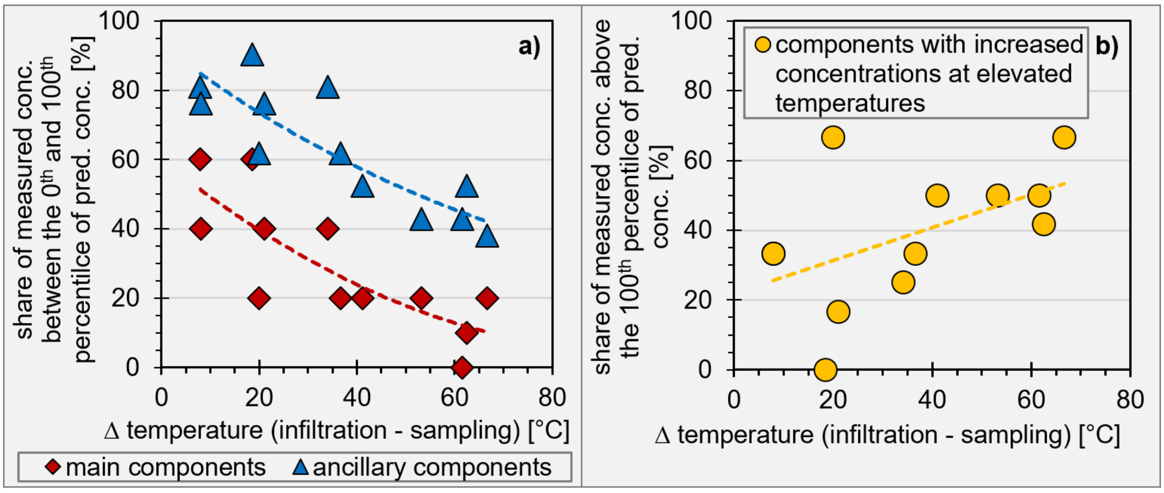

Fig. 4.8: (a) Share of main and ancillary components concentrations measured at 7.5, 10.5 and 13.5 m below ground surface (bgs) in wells C05, C07, D01 and D03 that were between the 0th and the 100th percentile of predicted concentrations; and (b) share of concentration of components with increased concentrations at elevated temperatures (Ch. 4.4.2.2) measured at 7.5, 10.5 and 13.5 m bgs in wells C05, C07, D01 and D03 that were above the 100th percentile of predicted concentrations; in relation to both the temperature deviation between infiltrated water and the temperature of the monitoring well during sampling in the respective depth. Data were taken from the monitoring campaign after the hot water infiltration with the highest temperatures (first campaign for C05, C07 and D01; second for D03).

Overall, ancillary components showed a better agreement between measured and predicted concentrations than the main components. Ion exchange is the controlling process for most ancillary components (Bonte et al., 2013b; Lüders et al., 2020); therefore, their temperature-induced concentration changes are apparently more directly affected by elevated temperatures, and relatively less by auxiliary effects, such as water mixing, mineral precipitation and dissolution. However, the concentrations of the ancillary components measured in the monitoring wells C05, C07 and D01 that were within the predicted concentration ranges to more than 50 % (from Cd to Ni in Fig. 4.9), were rather in the upper range (50th to 100th percentile) of predicted concentrations (Fig. 4.9). This indicates a slight underestimation of their concentration changes by the conducted batch tests. U, Cu, Tl, NH_4^+, Sr and Sn showed an accordance between measured and predicted concentrations of less than 50 % for the referred monitoring wells (Fig. 4.9). In contrast to most other component concentrations, U, Cu, NH_4^+ and Sn were changing erratically, rather than gradually over time, starting from the baseline monitoring. Thus, the actual effect of elevated temperatures on concentrations of these components, as well as their predictability, remains uncertain.

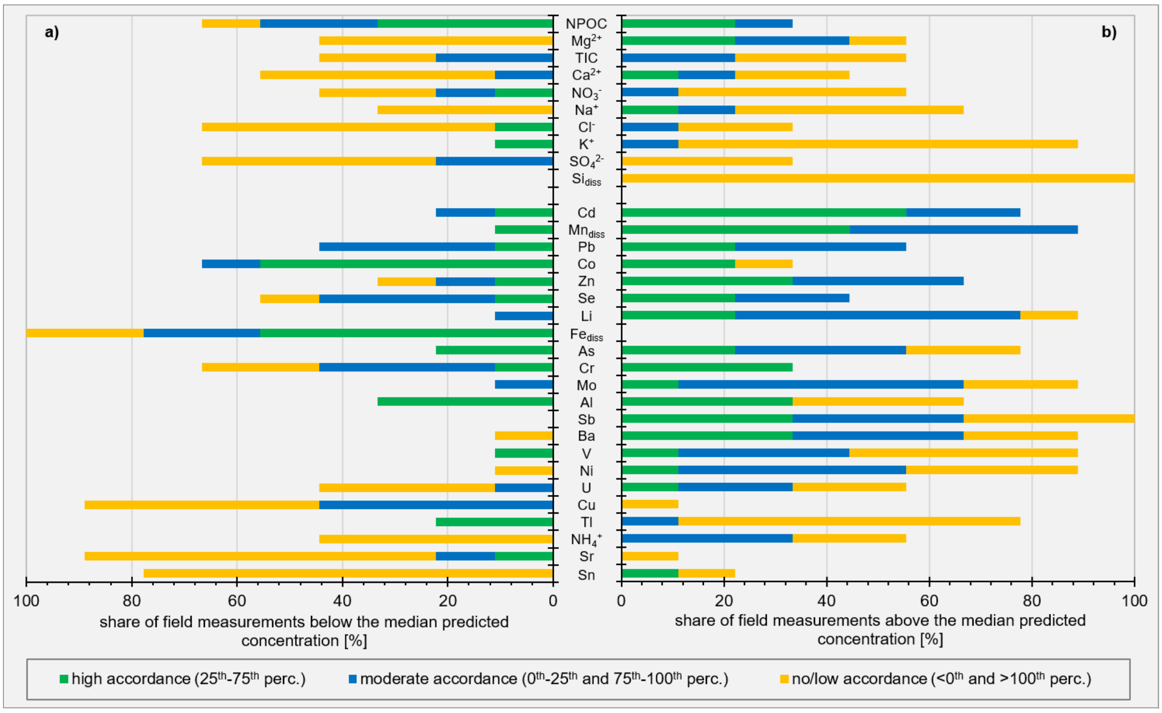

Fig. 4.9: Average component specific accordance of concentrations measured in wells C05, C07 and D01 during the first monitoring campaign after the hot water infiltration with the predicted concentrations based on the temperature induced concentration changes in the laboratory batch tests. Shown are the shares of field measurements (a) below and (b) above the median predicted concentrations, separated for the intervals below, between and above the 0th, 25th, 50th, 75th and 100th percentile of predicted concentrations on the respective figure side.

4.5. Conclusions

A short-term hot water infiltration field test for simulating the hydrogeochemical effects caused by an initial heating phase of a HT-ATES system led to temperatures above 70° C near the infiltration. Frequent sampling of 17 monitoring wells tracked hydrochemical changes with high spatial and temporal resolution, enabling an evaluation of the predictive power of laboratory batch tests, conducted with 28 individual sediment samples from the field test site at 10, 40 and 70 °C.

In monitoring wells around the hot-water infiltration well, elevated temperatures caused increased concentrations of NO_2^-, K^+, Si_{diss}, Li, V, Cr, As, Se, Mo, Sb, Ba, Tl, U and CH_4. Changes in other groundwater constituents were either indistinguishable from the concentration range observed during baseline monitoring or from mixing effects of infiltrated and original water (O_2, NPOC, NH_4^+, NO_3^-, SO_4^{2-}, Na^+, Mg^{2+}, Ca^{2+}, Fe_{diss}, Mn_{diss}, Al, Co, Ni, Cu, Zn, Sr, Cd, Sn, Pb and TCE). A direct comparison with the laboratory batch test data identified the following:

- the trend of increasing concentrations with increasing temperature in the field measurements of the aforementioned components, except for NO_2^-, CH_4 and U, is as predicted by the laboratory batch tests.
- conversely, not all concentration changes expected from the batch tests were observed in the field measurements, partly due to superimposition by water mixing in the field.
- the maximal concentrations in field measurements above 55 °C were within or below the concentration range in the laboratory batch tests at 70 °C, for 24 out of 31 components (all but NPOC, TIC, NO_3^-, Si_{diss}, Co, Ba and Tl).

Furthermore, for 26 out of 31 viewed components the concentration ranges in the batch tests at 70 °C were larger than the concentration ranges measured in the five monitoring points sampled at temperatures above 55 °C. For this field test site, the concentration changes observed in the laboratory tests were attenuated at the field scale.

A comparison of field measurements from the three central monitoring wells C05, C07 and D01 with predicted concentration ranges based on the temperature-induced relative concentration changes in the laboratory batch tests revealed the following:

- overall agreement of field measurements with the predicted concentration ranges is better for components that showed pronounced temperature-induced concentration changes related to ion exchange and (de)sorption processes (which is true for most environmentally relevant ancillary groundwater components).
- the conducted batch tests are less suitable for predicting temperature-induced concentration changes related to mineral dissolution.
- the accordance of the field measurements with predicted concentration ranges is greatest, where the least cooling between the hot water infiltration and the sampling occurred, indicating:
    - a retarded adaption of concentrations to decreasing temperatures.
    - that the maximal temperature-induced concentration changes of many ancillary components can be well predicted.
    - that the target infiltration temperature of the hot water can be used to estimate maximal expectable concentration changes.

This procedure, for component-specific predictions of potential concentration changes induced by elevated temperatures, is suitable for components related to ion exchange and (de)sorption processes in the vicinity of a hot water infiltration. Thus, utilising the maximal expected temperatures allows prediction of maximal expectable concentration changes for most of the environmentally relevant ancillary groundwater components. However, as temperatures decline with distance to the infiltration well, most of the surrounding aquifer will only be exposed to attenuated concentration changes. Both aspects will play a major role in authorisation procedures, from a geochemical point of view.

Successive shifts in the redox state towards stronger reducing conditions and associated concentration changes in redox sensitive components, as expected from prolonged high subsurface temperatures, and their predictability at the field scale, were not investigated here. The same applies for cyclic operation, apart from the initial heating phase, simulating the operating phase of a subsurface heat storage and its induced (bio)geochemical effects. Thus, both aspects are in focus of consecutive investigations. Finally, predicting the geochemically affected space around ATES systems also requires future association of laboratory data characterising potentially delayed or incomplete reversibility of heat-induced concentration changes with the evolution of temperatures at the field scale.

Acknowledgments: *We thank our colleagues Markus Ebert and Frank Dethlefsen for their cooperation, improvements in analytics and valuable comments throughout the preparation of this study as well as Marco Mahnecke, Jens Wemhöner, Lena-Sophie Kuhr, Jan Gustmann, Nina-Sophie Keller and all other helping hands for supporting the field and/or laboratory investigations. Furthermore, we thank the project partners from UFZ-MET for geophysical exploration and installation of the monitoring wells, the ICP-MS laboratory at Kiel University's Institute of Geosciences for conducting the analysis of trace elements and heavy metals on the basis of scientific cooperation, as well as the municipality of Wittstock/Dosse and the Brandenburgische Boden GmbH for supporting the project. In addition, we would like to mention the Angus-projects (https://www.angus-projekt.de/de?set_language=en), in which the experimental basis for the here presented study was laid. Finally, we thank the two anonymous reviewers for their constructive comments that helped to improve the quality of this paper.*

Funding: *This study is part of the TestUM-Aquifer project funded by the German Federal Ministry of Education and Research (03G0875A), which had no role in study design; the collection, analysis and interpretation of data; in writing of the report; and in the decision to submit the article for publication.*

4.6. Supplementary material

Table S.4.3: Geochemical characteristics of individual sediment samples from the target aquifer for the hot water infiltration.

sediment sample		***C*[1]**	***$C_{org.}$*[1]**	***$C_{carb.}$*[1]**	***reactive Fe*[2]**	**Fe bound in crystalline iron oxides, siderite and magnetite[3]**
[well]	*[m bgs]*	*[mg/kg]*	*[mg/kg]*	*[mg/kg]*	*[mg/kg]*	*[mg/kg]*
U01	7.5	1169	958	210	0.42	0.98
U01	10.5	544	488	56	0.35	0.97
U01	13.5	3040	362	2678	0.46	1.14
C05	7.5	546	471	75	0.44	1.02
C05	10.5	410	391	20	0.40	0.86
C05	13.5	2019	524	1495	0.43	1.24
C06	7.5	713	593	120	0.55	1.53
C06	10.5	330	360	0	0.38	1.04
C06	13.5	6503	278	6225	0.48	0.97
C07	7.5	553	490	63	0.38	0.87
C07	10.5	432	424	8	0.35	0.94
C07	13.5	1582	376	1206	0.41	1.32
D03	7.5	585	509	76	0.60	1.69
D03	10.5	455	432	23	0.35	0.83
D03	13.5	438	370	68	0.45	1.25
D04	7.5	880	1116	0	0.48	0.84
D04	10.5	419	537	0	0.29	0.66
D04	13.5	4121	296	3824	0.33	0.72
D09	7.5	571	583	0	0.63	1.21
D09	10.5	556	662	0	0.36	0.75
D09	13.5	2063	490	1573	0.45	1.14

[1] determined with a Multi N/C 2100 Analyser with HT-1300 oven (Analytik Jena AG, Jena, Germany); total carbon (C) directly, total organic carbon ($C_{org.}$) after removal of total inorganic carbon ($C_{carb.}$) with 2 M HCL, $C_{carb.}$ was calculated from the difference between C and $C_{org.}$, and was set to zero in case measured $C_{org.}$ was larger than measured C.

[2] determined by extraction with 1 M HCL according to Leventhal and Taylor (1990) and subsequent photometric analysis of the extracts according to the ferrozine method (Stookey, 1970) with hydroxylammonium chloride as the reductive agent.

[3] determined by extraction with 5 M HCL according to Heron et al. (1994) and subsequent photometric analysis of the extracts according to the ferrozine method (Stookey, 1970) with hydroxylammonium chloride as the reductive agent.

Table S.4.4: Concentrations of ionically bound trace elements and heavy metals. Determined by digestion with 1.0 mol/L sodium dihydrogen phosphate at pH 5 adjusted with sodium hydroxide, following the procedure of Keon et al. (2001).

	mean value [µg/kg]	***standard deviation [µg/kg]***
Li	<17	<17
Al	33600	17000
V	584	325
Cr	147	124
Mn	9850	8010
Co	103	36
Ni	147	56
Cu	864	908
Zn	8100	13700
As	138	57
Se	<69	<69
Sr	1830	1930
Mo	<94	<94
Cd	34	37
Sn	26	14
Sb	814	1420
Ba	4900	1530
Tl	103	21
Pb	289	135
U	99	91

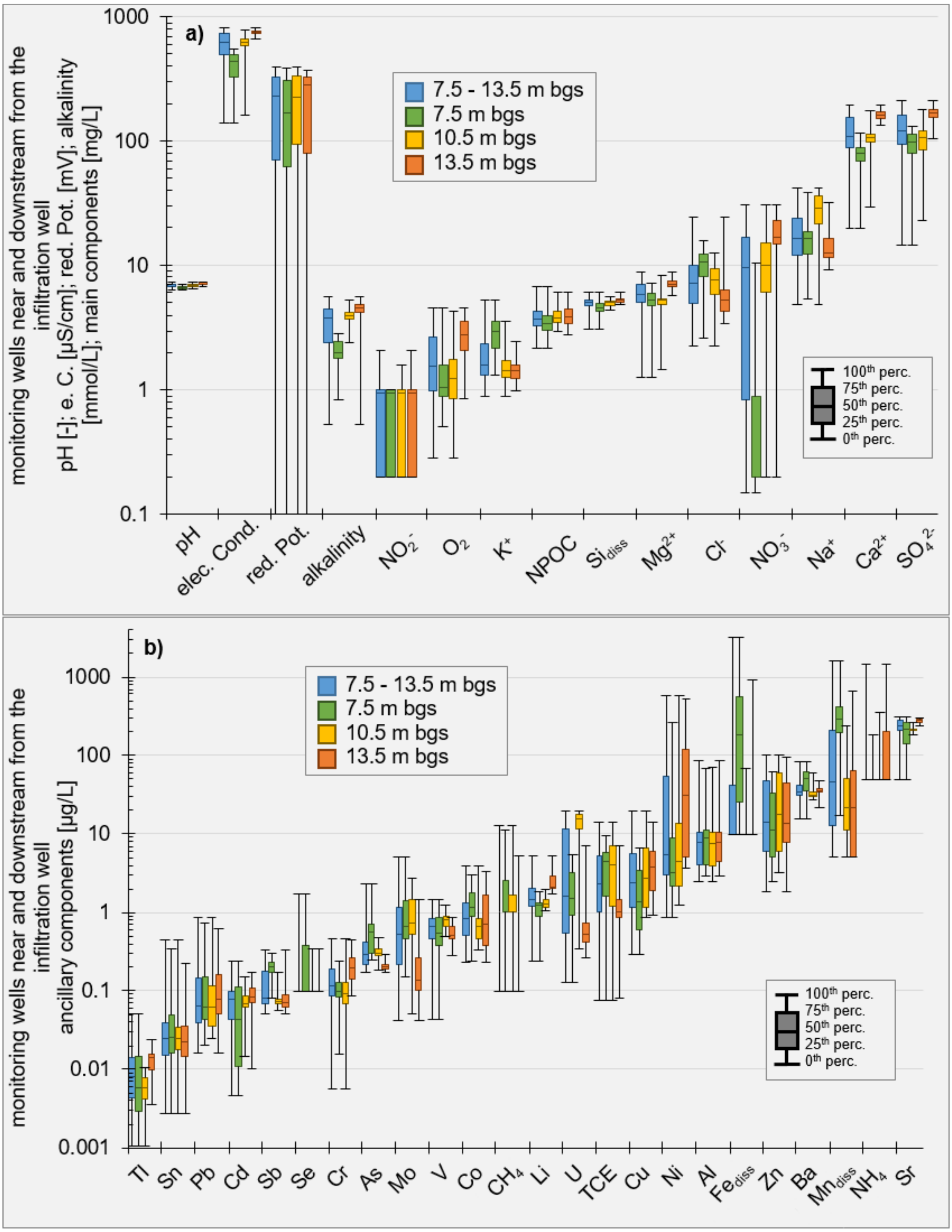

Fig. S.4.10: Geochemical baseline data for (a) main and (b) ancillary groundwater components from six monitoring campaigns in sampling wells U01, C04, C05, C07, C08, D01, D03, D04, D06, D08, D09 and D10 in the various filtered depths.

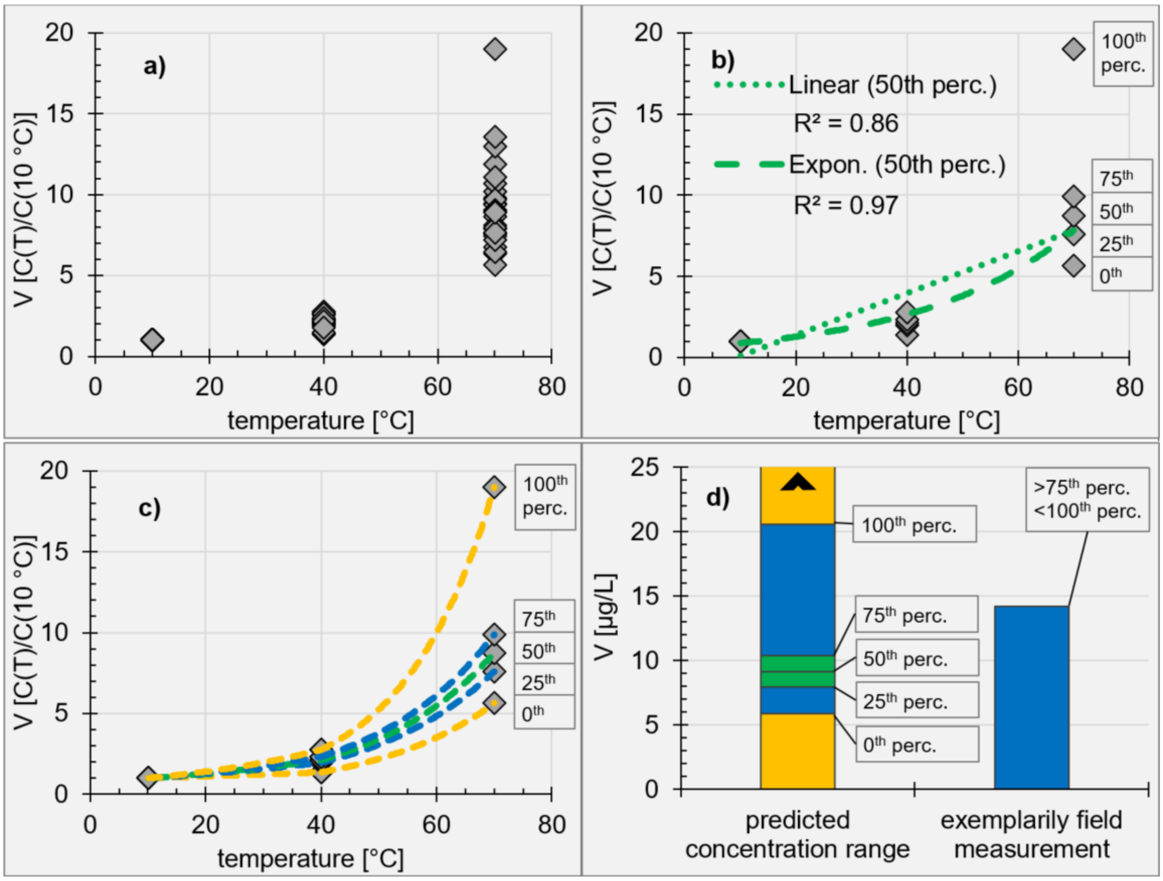

Fig. S.4.11: (a) course from the laboratory batch test data (relative concentration change at elevated temperatures of 40 and 70 °C referred to the concentration measured in the 10 °C batch test with the respective sediment sample; (b) component-specific choice of linear or exponential regression function (based on the better coefficient of determination for the 50th percentile of relative concentration changes; (c) over displaying of the 0th, 25th, 50th, 75th and 100th percentile regression functions linking temperature with relative concentration change (separated for the temperature intervals 10-40 °C and 40-70 °C; (d) the final comparison of the predicted concentration range (using the regression functions from (c) and the measured temperature at the viewed monitoring point) and the concentration measured in the field sample. The determined applicable category (here '>75th perc. <100th perc.) is the basis for the Fig. 4.7 to Fig. 4.9, the colours of which correspond to the respective categories here. All shown examples are for V, the comparison with field data is done for the first sampling after start of hot water infiltration in monitoring point 7.5 m below ground surface (bgs) in well D01.

Eq. S.4.1: Calculation of the multiplication factor (M) for the 0th, 25th, 50th, 75th and 100th percentile (nth perc.) of component specific relative concentration changes in the laboratory batch tests using the respective exponential (a) or linear (b) regression function parameters (X) and (Y) as wells as the temperature (T) measured at the examined monitoring point (mp). Regression parameters were either obtained for the temperature range 10-40 °C or for the temperature range 40-70 °C, depending on the monitoring point temperature).

a) $M_{n^{th}perc.} = X_{n^{th}perc.} \times e^{Y_{n^{th}perc.} \times T_{mp}}$

b) $M_{n^{th}perc.} = X_{n^{th}perc.} \times T_{mp} + Y_{n^{th}perc.}$

Eq. S.4.2: Calculation of a component and monitoring point (mp) specific 0th to 25th, 50th, 75th and 100th percentile (nth perc.) concentration (C) by multiplying the respective monitoring points baseline concentration (base) with the component specific multiplication factor (M) describing the temperature dependent relative concentration change.

$$C_{mp_{n^{th}perc.}} = C_{mp_{base}} \times M_{n^{th}perc.}$$

Table S.4.5: Ratio of component specific release from blank material and the mean concentration increase in the sediment batch tests with the respective vial material. Note that the NPOC data from the HDPE vials and the Si$_{diss}$ data from the glass vials were excluded from the further data evaluation of the batch tests, due to the high blank values. In case “n.a.” is stated, samples have not been analysed for the respective value. An “-“ indicates, that there was a release of the respective component in the blank tests, but concentrations in the sediment batch tests decreased, so no ratio was calculable.

		HDPE vial blanks		***glass vial blanks***	
		10 → 40 °C	10 → 70 °C	*10 → 40 °C*	10 → 70 °C
TIC	[-]	<0.01	<0.01	<0.01	<0.01
NPOC	[-]	0.12	0.81	<0.01	<0.01
Na^+	[-]	<0.01	<0.01	<0.01	0.22
K^+	[-]	<0.01	0.07	<0.01	<0.01
Ca^{2+}	[-]	<0.01	<0.01	<0.01	-
Mg^{2+}	[-]	<0.01	-	<0.01	-
Si_{diss}	[-]	<0.01	<0.01	1.31	1.05
Acetate	[-]	-	<0.01	<0.01	<0.01
Cl^-	[-]	<0.01	<0.01	<0.01	<0.01
NO_3^-	[-]	<0.01	<0.01	<0.01	0.04
SO_4^{2-}	[-]	<0.01	<0.01	<0.01	<0.01
Mn_{diss}	[-]	<0.01	<0.01	n.a.	0.04
Fe_{diss}	[-]	<0.01	<0.01	<0.01	<0.01
Li	[-]	<0.01	0.03	n.a.	0.14
Al	[-]	<0.01	0.13	n.a.	0.05
V	[-]	<0.01	<0.01	n.a.	<0.01
Cr	[-]	<0.01	0.02	n.a.	0.13
Co	[-]	<0.01	<0.01	n.a.	-
Ni	[-]	-	<0.01	n.a.	-
Cu	[-]	<0.01	<0.01	n.a.	-
Zn	[-]	<0.01	<0.01	n.a.	-
As	[-]	<0.01	<0.01	n.a.	<0.01
Se	[-]	<0.01	<0.01	n.a.	<0.01
Sr	[-]	<0.01	-	n.a.	-
Mo	[-]	<0.01	<0.01	n.a.	0.15
Cd	[-]	<0.01	<0.01	n.a.	-
Sn	[-]	<0.01	<0.01	n.a.	<0.01
Sb	[-]	0.09	<0.01	n.a.	<0.01
Ba	[-]	<0.01	<0.01	n.a.	0.04
Tl	[-]	0.06	<0.01	n.a.	<0.01
Pb	[-]	<0.01	<0.01	n.a.	<0.01
U	[-]	<0.01	-	n.a.	<0.01

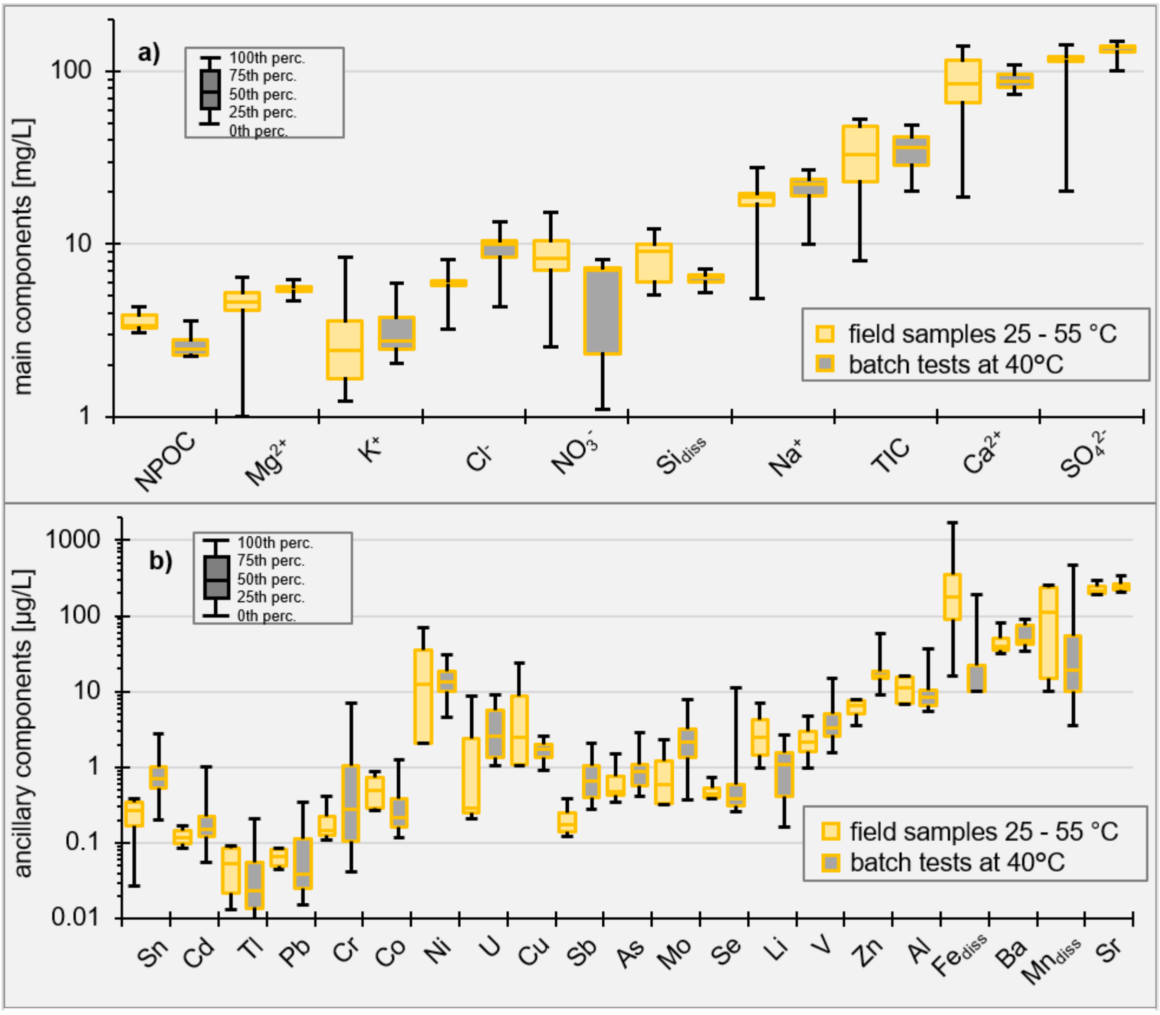

Fig. S.4.12: Comparison of (a) main and (b) ancillary components concentrations in field samples from the first and second monitoring after the hot water infiltration at monitoring points U01 (7.5 and 10.5 m below ground surface [bgs]), C04 (7.5 m bgs), C05 (13.5 m bgs), C07 (10.5 m bgs), C08 (7.5 m bgs), D01 (13.5 m bgs), D03 (7.5 m bgs), D04 (7.5 m bgs) and D06 (7.5 m bgs) in the temperature range 25–55 °C (n=10) and the concentrations in samples from the 40 °C batch tests (n=21). Components are sorted in the same order as in Fig. 4.6 for comparison.

5. Zusammenfassung und Ausblick

5.1. Hintergrund

Durch den hohen Anteil des Sektors Wärme- und Kälteerzeugung am Gesamtenergieverbrauch spielt dessen Transformation eine Schlüsselrolle beim Erreichen der globalen Klimaschutzziele. Die Einbindung saisonal schwankender (bspw. Solarthermie und Umweltwärme) oder ganzjährig anfallender (bspw. tiefe Geothermie und industrielle Abwärme) Wärmequellen in die Versorgungssysteme kann dabei einen wesentlichen Beitrag zur Senkung des Anteils fossiler Energiequellen im Bereich der Wärmeerzeugung erbringen. Um diese alternativen Wärmequellen möglichst effizient in die Wärmeversorgungssysteme einzubinden und so die Dekarbonisierung bestehender Wärmenetze zu beschleunigen, können Wärmespeicher zum saisonalen Ausgleich von Wärmebereitstellung und –bedarf in zentralen Wärmenetzen urbaner Gebiete eingesetzt werden. Wird dies mit einem Ausbau der Wärmenetze und damit einhergehend einer Erhöhung privater und gewerblicher Anschlussraten kombiniert, könnte die netzbasierte Wärmeversorgung auch zurzeit noch fossil betriebene, dezentrale Heizsysteme in oft un- oder nur teilsanierten Bestandsgebäuden ersetzen.

Schritte in diese Richtung gibt es bspw. bei kleineren Wärmenetzen in Dänemark, bei denen verstärkt auf den Ausbau solarthermischer Anlagen in Verbindung mit Erdbeckenwärmespeicher gesetzt wird, wodurch bspw. in Vojens 45 % des jährlichen Wärmebedarfs im Wärmenetz solarthermisch gedeckt werden kann (State of Green, 2020). Aufgrund des höheren saisonalen Speicherbedarfs von Wärmenetzen (größerer) urbaner Gebiete, werden hier jedoch eher grundwasserbasierte-, sprich ATES-Systeme, Verwendung finden (State of Green, 2020), deren Potential bisher jedoch noch weitestgehend ungenutzt geblieben ist. In Anbetracht des bei noch nicht in der breiten Nutzung angekommenen Technologien inhärenten Mangels langfristig erfolgreicher Anwendungsbeispiele, liegt der Fokus bei der Betrachtung von UTES-Systemen jedoch oft auf möglichen Risiken (Fleuchaus et al., 2020) und weniger auf dem möglichen Beitrag zur effizienten netzbasierten Wärmeversorgung breiter Bevölkerungsanteile (State of Green, 2020). Bei den möglichen Risiken von UTES-Systemen spielen unter anderem auch Unsicherheiten hinsichtlich thermisch induzierter hydrogeochemischer Effekte, mit Einfluss auf den technischen Betrieb oder mögliche Umweltauswirkungen, eine Rolle. Hierbei kann ein besseres Verständnis potentiell induzierter Effekte zu einer fundierten Risikobewertung beitragen. Vor diesem Hintergrund wurden in den Kapiteln 2, 3 und 4 dieser Dissertation anhand eines Feld- und verschiedener Laborversuche, sowie geochemischer Modell- bzw. Szenarienrechnungen drei in der bestehenden Literatur als relevant identifizierte, aber bisher noch nicht dementsprechend eingehend untersuchte, Aspekte dieser Unsicherheiten hinsichtlich thermisch induzierter hydrogeochemischer Effekte bei HT-UTES Systemen näher beleuchtet.

5.2. Zusammenfassung

5.2.1. Hydrogeochemische Effekte mit Einfluss auf den Anlagenbetrieb

Mögliche Beeinträchtigungen des technischen Betriebs von ATES-Systemen durch thermisch induzierte hydrogeochemische Effekte waren bereits im Fokus verschiedener Studien in den 80er und 90er Jahren. Dabei wurden unter anderem Ansätze entwickelt und getestet um mit der Ausfällungen von Karbonaten oder einer Gasphasenbildung einhergehende Scaling- und Clogging-Effekte zu verhindern, bzw. deren Effekte auf den technischen Betrieb saisonaler Wärmespeicher zu minimieren (siehe Kap. 1.3.1).

Um hierfür einen Beitrag zu leisten, wird in Kapitel 2 dieser Arbeit beschrieben, welches Ausmaß einer Gasphasenbildung und möglicher hydraulischer Effekte in Abhängigkeit der Konzentrationen gelöst vorliegender Gase, den Druckbedingungen und des Temperaturanstiegs zu erwarten ist und wie eine gebildete Gasphase auf der Laborskala monitoringtechnisch erfasst werden kann. Dabei zeigte ein Vergleich der Gasphasenbildung zwischen experimentellen Säulenversuchen bei 10, 25, 40 und 70 °C mit thermodynamischen Berechnungen auf Basis der Zusammensetzung des Zulaufwassers und den Versuchstemperaturen, dass die mit ~9 bzw. 18 mL(Gas)/L(Wasser) vergleichsweise hohe Gasphasenbildung bei 70 °C mit einer Abweichung von weniger als 2.5 % reproduziert werden konnte (Kap. 2.4.1). Auf dieser Basis wurden die geochemischen Gleichgewichtsberechnungen als geeigneter Ansatz zur Abschätzung der thermisch induzierten Gasphasenbildung betrachtet. Mit Hilfe zeitlich aufgelöster geoelektrischer Widerstandsmessungen konnte die Gasphasenbildung zudem lokalisiert und so der mit Gasphase gefüllte Anteil des Porenraums im Bereich der Gasphasenbildung auf ~25, ~40-60 und ~55-70 % (bei 25, 40 und 70 °C) abgeschätzt werden (Kap. 2.4.1, 2.4.2).

Für Grundwasser welches bei 10 °C im Gleichgewicht mit der Atmosphäre oder auch im Gleichgewicht zu erhöhten CO_2-Partialdrücken der Bodenluft steht, ergaben die geochemischen Gleichgewichtsberechnungen, dass eine Erwärmung auf 70 °C nur bis in wasser-gesättigte Tiefen von 12 oder 13 m u. GOK zu einer Gasphasenbildung führt (Kap. 2.4.3). Bei tieferliegenden Wärmespeichern und dementsprechend höheren Umgebungsdrücken würde eine Erwärmung auf 70 °C hingegen nur zur Bildung einer Gasphase führen, wenn bspw. durch die Umwandlung von organischen Kohlenstoffverbindungen oder der Zugabe von CO_2 zur Verhinderung einer Karbonatfällung in ATES-Systemen entsprechend gegenüber einem Gleichgewicht mit der Bodenluft erhöhte gelöste Gaskonzentrationen vorlägen.

Kontrollierend für die räumliche und zeitliche Akkumulation einer gebildeten Gasphase wirken u. a. die Nachführung thermisch unbeeinflussten Wassers, potentielle Rücklösungsprozesse der Gasphase bei Abkühlung, sowie Migrationsprozesse der gebildeten Gasphase im porösen Medium. Die durchgeführten Szenarienrechnungen adressieren diese Aspekte allerdings nur vereinfacht (feste Grundwasserfließgeschwindigkeit bzw. Gasphasenaufstieg bei Überschreitung einer angenommenen maximalen residualen Gasphasensättigung) oder vernachlässigen sie (Rücklösung; vgl. Kap. 2.3.4). Dennoch können solche Szenarienrechnungen für verschiedene gelöste Gaskonzentrationen (Table 2.4) eine Orientierung hinsichtlich möglicher Gasphasensättigungen und damit dem Ausmaß von Änderungen in der Permeabilität (Kap. 2.4.4) und in der Wärmeleitfähigkeit bzw. –kapazität (Kap. 2.4.5) liefern, um so die Notwendigkeit umfangreicherer Modellsimulation zu prüfen.

Insgesamt deuten die Ergebnisse der betrachteten Szenarien darauf hin, dass eine thermisch induzierte Gasphasenbildung in gut durchlässigen, organikarmen Lockersedimenten bei einem druckhaltenden Speicherbetrieb häufig vernachlässigbar sein wird. Inwieweit mitunter temperaturinduziert verstärkte Umwandlungsprozesse von organischen Kohlenstoffverbindungen (Kap. 1.3.2, 1.3.3.2 bzw. 2.5) bspw. bei organikreichen Sedimenten im Speicherhorizont oder als Deckschicht gegebenenfalls zu einer im Ausmaß für den Speicherbetrieb relevanten Gasphasenbildung führen können, bedarf jedoch weiterer Untersuchungen.

5.2.2. Hydrogeochemische Effekte mit Einfluss auf die Grundwasserqualität

Ein Aspekt bei der Genehmigung von UTES-Systemen sind potentielle Auswirkungen erhöhter Temperaturen auf die Grundwasserqualität (Bonte et al., 2011; Hähnlein et al., 2013; VDI, 2010). Aus hydrogeochemischer Sicht liegt der Fokus in bestehender Literatur dabei im Wesentlichen auf einer bei erhöhten Temperaturen verstärkten Freisetzung und Umwandlung von organischem Kohlenstoff und ggf. damit einhergehender Ausbildung reduzierenderer Bedingungen, sowie der möglichen Mobilisierung von Spurenkomponenten und Schwermetallen (Kap. 1.3.2). Insbesondere mit Blick auf Spurenkomponenten und Schwermetalle betonen Saito et al. (2016) und van Breukelen und Bonte (2016) die Relevanz der Reversibilität thermisch induzierter Konzentrationsänderungen, um deren Effekte auf die Grundwasserqualität unter Einbeziehung der räumlichen Ausdehnung induzierter Konzentrationsänderungen im Falle wieder abnehmender Temperaturen insgesamt abschätzen zu können.

Vor diesem Hintergrund charakterisiert Kapitel 3 dieser Arbeit anhand von mit drei pleistozänen und einem tertiären norddeutschen Aquifersediment befüllten Durchfluss- und Kreislaufsäulenversuchen die Mobilisierung und (Re)fixierung von Spurenkomponenten und Schwermetallen unter variierenden Temperaturbedingungen zwischen 10 und 70 °C.

Dabei stiegen bei Temperaturen von 70 und teils auch 40 °C im Vergleich zu den Versuchen bei 10 °C in allen untersuchten Sedimenten die Li-, As-, Mo-, Sb- und Ba-Konzentrationen an, bzw. nahmen die Ni-Konzentrationen ab. Demgegenüber variierten die temperaturinduzierten Konzentrationsänderungen bei V, Mn, Co, Tl und U sedimentspezifisch (Kap. 3.4.1.2). Die im Versuchsverlauf abnehmende Freisetzungsintensität wies bei allen Komponenten, außer Ba, auf zeitlich begrenzte temperaturinduzierte Konzentrationsanstiege und damit einen in Abhängigkeit der Temperatur endlichen Freisetzungspool hin (3.4.1.1). In einigen der untersuchten Sedimente überstiegen die initialen Konzentrationsänderungen von As, V, Mn, Li und Tl bei 70 °C dabei deutlich die Konzentrationsunterschiede zwischen den verschiedenen untersuchten Sedimenten bei 10 °C (Kap. 3.4.3). Zu mindestens auf Basis der hier betrachteten Sedimente überwog somit der Temperatureffekt auf die Konzentrationen von einigen Spurenkomponenten und Schwermetalle bei Erwärmung auf 70 °C gegenüber deren natürlicher Variabilität bei 10 °C.

Die durch die Temperaturerhöhungen ausgelösten Konzentrationsänderungen lassen sich dabei im Wesentlichen auf drei Prozesse zurückführen (Kap. 3.4.1.3):

a) eine Abnahme des Ladungsnullpunktes und eine damit einhergehende Desorption von als Oxyanionen gebundenen Schwermetallen und Spurenkomponenten (z. B. Vanadat, Arsenat/Arsenit, Molybdat, Antimonat);
b) eine präferentielle Desorption monovalenter- (z. B. Li und Tl) im Austausch für divalente Kationen und
c) die (reduktive) Lösung von Mineralen, wie Mn(IV)- und Fe(III)-(Hydr)Oxiden, unter Freisetzung eingebauter, bzw. daran sorbierter Spurenkomponenten und Schwermetalle.

Mit der Rückkühlung zuvor auf 25, 40 oder 70 °C temperierter Versuche auf 10 °C konnte zudem im Mittel der untersuchten Sedimente und Temperaturen eine Reversibilität in den elementspezifischen Konzentrationsänderungen zwischen 30 und 95 % gezeigt werden (Kap. 3.4.2). Grundsätzlich führt diese beobachtete Reversibilität der Konzentrationsänderungen von Spurenelementen und Schwermetallen zu einer sukzessiven Wiederherstellung der entsprechenden initialen, natürlichen Konzentrationsniveaus, sobald sich das Temperaturniveau saisonal im zyklischen Betrieb, abstromig einer UTES-Anlage oder nach Beendigung des Speicherbetriebs wieder natürlichen Umgebungswerten annähert.

Ohne auf der Feldskala u. a. zu erwartende Vermischungsprozesse und der Verlagerung von Wassermassen zwischen warmer und kalter Seite im zyklischen Speicherbetrieb bei ATES-Systemen, betrachten die hier im Labor durchgeführten Durchfluss- und Kreislaufsäulenversuche jedoch nur Teilaspekte von Wärmespeicher-Systemen. So werden in den Durchflusssäulenversuchen durch das stetige Nachströmen unbeeinflussten Wassers bspw. Rückkoppelungseffekte durch eine sich im zyklischen Betrieb sukzessive verändernde Wasserbeschaffenheit vernachlässigt. Dennoch lässt sich auf Basis der mit zunehmenden ausgetauschten Porenvolumen in den Durchflusssäulenversuchen abnehmenden Konzentrationsänderungen ableiten, dass auch im zyklischen Speicherbetrieb die Konzentrationsspitzen durch eine Erschöpfung der verfügbaren Freisetzungspools mit zunehmender Zyklenzahl tendenziell abnehmen werden. Die Reversibilitätsuntersuchungen in den Kreislaufsäulenversuchen bilden hingegen in einem der beiden betrachteten Versuchsszenarien die Abkühlung des Wassers in einem zuvor nicht erwärmten Sedimentbereich ab und simulieren so eine Verlagerung des Wassers, jedoch werden auch hierbei Vermischungsprozesse oder die Entwicklung in weiteren Speicherzyklen nicht mitbetrachtet.

Um auf Basis der erhobenen experimentellen Daten exemplarisch abzuschätzen in welcher Entfernung zu einer UTES-Anlage zuvor temperaturinduziert angestiegene (hier As-)Konzentrationen wieder unter einen Schwellenwert fallen, bedarf es somit einiger Annahmen (vgl. Kap. 3.3.5). So wird für diese Abschätzung in Kap. 3.4.4 ein analytischer 1D-Ansatz vorgestellt, welcher auf den Temperaturprofilen existierender numerischer UTES-Anlagen basiert. Über diese Temperaturprofile gehen so indirekt auch Einflüsse von Vermischungsprozessen und der Wasserverlagerung zwischen warmer und kalter Seite im zyklischen Speicherbetrieb bei ATES-Systemen mit in die Betrachtung ein. Allerdings hat der in den 1D-Ansatz integrierte Volumenbezug bei der auf den experimentell bestimmten Reversibilitäten basierenden Berechnung der Wiederfestlegung zur Folge, dass die Ausbreitung temperaturinduzierter Konzentrationsänderungen für ATES-Systeme im Abstrom der warmen Seite überschätzt wird, da die anteilige Wiederfestlegung auf der kalten Seite des Wärmespeichers nicht mitbetrachtet wird.

5.2.3. Prognostizierbarkeit initialer hydrogeochemischer Effekte

In Ermangelung einer breiten hydrogeochemischen Datenlage von umgesetzten und in Betrieb befindlichen HT-ATES-Anlagen können prognostische Voruntersuchungen sowohl für die Auslegung der technischen Anlagenbestandteile bzw. einer ggf. benötigten Wasserbehandlung, als auch für die Einordnung genehmigungsrechtlicher Fragen einen Beitrag leisten. Mit Blick auf die Verhinderung von Scaling- und Cloggingeffekten führte Sanner (2004) dafür bspw. Versuche mit einem Teststand durch, wobei anhand gepumpten Wassers potentielle Maximaltemperaturen für die entsprechenden Aquifere bestimmt wurden, bei denen noch keine Mineralausfällungen zu erwartend sind. Des Weiteren entwickelten Vail et al. (1992) einen Ansatz für eine modellbasierte Anpassung der zur Verhinderung von Scaling und Clogging nötigen Wasserbehandlung. Beide zuvor genannten Ansätze, wie auch die in Kap. 2 dieser Arbeit gezeigten Berechnungen einer möglichen Gasphasenbildung, verwenden als Eingangsparameter aus dem geplanten Wärmespeicherhorizont lediglich die Wasserzusammensetzung. Zugängliche Brunnen vorausgesetzt, sind erste Einschätzungen zu diesen, ggf. den technischen Anlagenbetrieb beeinflussenden, temperaturinduzierten Effekten somit mit vergleichsweise geringem Aufwand verbunden.

Demgegenüber rücken bei potentiellen temperaturinduzierten hydrogeochemischen Einflüssen auf die Grundwasserqualität Sediment-Wasser-Wechselwirkungen in den Fokus, bei denen standortspezifische Unterschiede in der Sedimentzusammensetzung wesentlich das Ausmaß und die Dauer induzierter Konzentrationsänderungen beeinflussen (Kap. 3; Bonte et al., 2013b). Hinsichtlich deren Prognostizierung führen verschiedene Aspekte zu Unsicherheiten inwieweit sich Laborergebnisse für eine Abschätzung auf der Feldskala zu erwartender temperaturinduzierter Konzentrationsänderungen eignen: So besteht zunächst geostatistisch allgemein eine Unsicherheit über die räumliche Repräsentanz einzelner Sedimentproben, bei denen darüber hinaus im Zuge von Kernbohrung, Transport und ggf. Homogenisierung auch die Zugänglichkeit reaktiver Oberflächen beeinflusst sein kann. Hinzu kommen verschiedene Versuchsansätze mit unterschiedlichen Sediment-Wasser-Verhältnissen und -Kontaktzeiten (vgl. Kap. 1.4).

Da die größten Konzentrationsänderungen bei den allermeisten Komponenten initial nach einer Temperaturerhöhung auftreten (Kap. 3; Bonte et al., 2013b), wurde der Fokus in Kapitel 4 zunächst hierauf gelegt. Einerseits wurde dafür ein Feldversuch, bei dem über 4,5 Tage Wasser mit bis zu 78 °C in einen glaziogenen Lockergesteins-Aquifer infiltriert wurde, hydrochemisch mit 17 in mindestens drei Tiefen verfilterten Beobachtungspegeln räumlich und zeitlich eng überwacht (Kap. 4.3.3). Andererseits wurden 28 verschiedene Sedimentproben von der Testfeldlokation in einwöchigen Batchversuchen auf jeweils 10, 40 und 70 °C temperiert und die dabei induzierten Konzentrationsänderungen untersucht (Kap. 4.3.2).

Im Bereich der in 1-1.5 m Entfernung zur Infiltration nahegelegensten Beobachtungspegel führte die Wasserinfiltration zu maximalen Temperaturen von 72 °C. In 3-4 m Entfernung traten noch

Maximaltemperaturen von 30-41 °C auf (Kap. 4.4.2.1). Die erhöhten Temperaturen hatten Konzentrationsanstiege von NO_2^-, K^+, Si_{diss}, Li, V, Cr, As, Se, Mo, Sb, Ba, Tl, U und CH_4 zur Folge. Konzentrationsänderungen der weiteren Grundwasserkomponenten waren nicht von den Konzentrationen im Baseline-Monitoring oder Mischungsprozessen mit dem infiltrierten Wasser zu unterscheiden (Kap. 4.4.2.2). Die temperaturinduzierten Konzentrationsanstiege wurden für alle Komponenten, außer NO_2^-, CH_4 und U, auch in den Batchversuchen beobachtet. Im Gegensatz konnten jedoch nicht alle in den Batchversuchen beobachteten Konzentrationsänderungen auch in den Felddaten einem Temperatureffekt zugeordnet werden, da diese im Feld vermutlich teilweise durch Mischungseffekte überlagert wurden (Kap. 4.4.2.2). Sowohl die maximalen Konzentrationen, als auch die beobachteten Konzentrationsspannbreiten, waren bei Feldproben aus Messstellen mit mehr als 55 °C für 24 bzw. 26 von 31 betrachteten Grundwasserkomponenten kleiner als in den Batchversuchen bei 70 °C. Dies deutet darauf hin, dass die Betrachtung mehrerer (hier 28) einzelner Sedimentproben in Laborversuchen zu einer eher konservativen Abschätzung von auf der Feldskala zu erwartenden Konzentrationen führt (Kap. 4.4.3). Zudem bestätigten abstromig bei geringeren Temperaturen wieder abnehmende Konzentrationen auch in den Felddaten die zuvor in Laborversuchen beobachtete Reversibilität temperaturinduzierter Konzentrationsänderungen (vgl. Kap. 3.4.2, 4.4.2.3).

Neben dem voranstehenden direkten Vergleich der Labor- und Felddaten erfolgte auch ein Vergleich zwischen den Feldmessungen der drei zentralen Beobachtungspegel mit auf Basis der temperaturinduzierten relativen Konzentrationsänderungen in den Batchversuchen prognostizierten Konzentrationsspannbreiten. Der gewählte Prognoseansatz eignete sich dabei in erster Linie für Grundwasserkomponenten, deren temperaturinduzierten Konzentrationsänderungen weitestgehend durch Ionenaustausch und (De)sorptionsprozesse kontrolliert werden (Kap. 4.4.4), was auf die meisten umweltrelevanten Nebenkomponenten im Grundwasser zutrifft (Kap. 3.4.1.3). Des Weiteren war die Übereinstimmung zwischen den Feldmessungen und den prognostizierten Konzentrationsspannbreiten umso größer, je näher die Temperaturen des beprobten Wassers noch an denen des mit bis zu ~78 °C infiltrierten Wassers waren (Kap. 4.4.4). Dies kann auf eine retardierte Anpassung der Konzentrationen an die durch Abkühlung und Vermischungsprozesse wieder geringeren Temperaturen zurückgeführt werden, worauf auch die vorherigen Untersuchungen zur Reversibilität der Konzentrationsänderungen von Spurenkomponenten und Schwermetallen bereits hindeuteten (Kap. 3.4.2). Zum anderen zeigt es aber auch, dass maximale temperaturinduzierte Konzentrationsänderungen der meisten Nebenkomponenten gut prognostizierbar sind und die Infiltrationstemperatur für eine Abschätzung dieser geeignet ist.

Liegt der Fokus jedoch nicht auf der Abschätzung maximal bei einer Temperaturerhöhung zu erwartender Konzentrationen, sondern auf dem räumlichen Ausbreitungsverhalten von Konzentrationsänderungen, stößt der vorgestellte Prognoseansatz an seine Grenzen. Hierfür könnte eine Kombination der Prognose maximal zu erwartender Konzentrationen (Kap. 4.3.5) mit der Prognose gegenüber wieder abnehmender Temperaturen im Abstrom eines Speichers retardierter Konzentrationsrückgänge (Kap. 3.3.5) eine orientierende Abschätzung liefern. Wie in Kap. 5.2.2 diskutiert, dürften die Annahmen dieses Ansatzes jedoch insbesondere für ATES-Systeme zu einer tendenziellen Überschätzung der Ausbreitung temperaturinduzierter Konzentrationsänderungen führen.

5.3. Ausblick

Im Winter mit der überschüssigen Wärme des Sommers zu heizen und im Sommer mit der Kälte des Winters zu kühlen: Gegenüber dem Einsatz von Strom in Klimaanlagen im Sommer und fossilen Brennstoffen in Heizungen im Winter zeigt dieser plakativ vereinfachte Grundgedanke saisonaler Wärme- bzw. Kältespeicher deren Potential für Wärmeversorgungssysteme auf. Weder die grundlegend dahinterstehende Argumentation, noch, dass sich insbesondere Aquifere für großvolumige saisonale Speicher eignen würden, hat sich dabei in den letzten knapp 40 Jahren wesentlich geändert; so schrieb bereits Hydén (1985): „Natural groundwater aquifers are being considered as a possible solution to the problem of economic seasonal heat storage. Aquifers may provide large storage volumes at low cost. The availability of a seasonal heat storage facility could be of value in a number of situations, for example, in connection with the utilization of industrial waste heat or solar energy. One possibility of obtaining large storage facilities would be to utilize natural aquifers with suitable properties and dimensions.” Lediglich die Motivation für die Nutzung saisonaler Wärmespeicher dürfte sich seit 1985 von einer vermutlich ökonomisch geprägten Betrachtung im Nachgang der Ölpreiskrisen der 70er Jahre um den möglichen Beitrag bei der Dekarbonisierung des Wärmesektors erweitert haben.

Gleichzeitig hat der Mangel an langfristig erfolgreichen Demonstrationsvorhaben gerade in Anbetracht dieser inzwischen mehreren Jahrzehnten Forschungshistorie zu einer Grundskepsis gegenüber dem Potenzial der Technologie geführt. Dies mag dazu beitragen, dass sich die breitere Anwendung der Technologie, trotz des vielfach beschriebenen Bedarfs an saisonalen Wärmespeicheroptionen (BMWi, 2021; Henning and Palzer, 2012), weiter verzögert. Dabei betonen bspw. Fleuchaus et al. (2020), dass es hinsichtlich der weitestgehend technisch geprägten Schwierigkeiten bei HT-ATES-Systemen im Bereich Clogging und Scaling in den 80er Jahren (Jenne et al., 1992) durchaus Fortschritte gegeben hat. So kann im Bereich der je nach Standort ggf. nötigen Wasserbehandlung zur Verhinderung von Clogging- und Scalingeffekten inzwischen in Abhängigkeit der hydrogeochemischen Standortbedingungen auf verschiedene erprobte Gegenmaßnahmen zurückgegriffen werden (Nielsen und Vangkilde-Pedersen, 2019). Alternativ besteht zudem die Möglichkeit durch Vorabtests maximale Speichertemperaturen zu bestimmen, bei denen keine Wasserbehandlung nötig ist, wobei diese mit zum Teil 60-70 °C (Sanner, 2004) durchaus in einem wahrscheinlich häufig effizient nutzbaren Temperaturbereich liegen können (Nielsen und Vangkilde-Pedersen, 2019). Erweitert man diesen Ansatz hin zu einer Kartierung maximal ohne eine Wasserbehandlung anwendbarer Speichertemperaturen in Aquiferen im Umkreis bestehender Wärmenetzte, ergäbe sich eine Planungsgrundlage, mit der sich der technische Aufwand reduzieren und so eine einfachere und schnellere Umsetzung von Wärmespeicherprojekten begünstigen ließe.

Hinsichtlich möglicher umweltrelevanter hydrochemischer Effekte erhöhter Aquifertemperaturen bei der Wärmespeicherung zeigen sowohl die im Rahmen dieser Arbeit, als auch die in vorrangegangenen Studien untersuchten Sedimente, insbesondere bezogen auf Spurenkomponenten und Schwermetalle, ein breites komponentenspezifisches Spektrum temperaturinduzierter Konzentrationsänderungen. Hervorzuheben ist hierbei jedoch deren zeitliche und räumliche Begrenzung sowie Reversibilität bei Abkühlung: Für einen effizienten zyklischen Speicherbetrieb wird ein möglichst großer Anteil des erwärmten bzw. abgekühlten Wassers lediglich zwischen der warmen und kalten Seite des Speichers hin und her gepumpt und verbleibt somit innerhalb des Systems. Dadurch ist auf Basis der beobachteten Reversibilität der temperaturinduzierten Konzentrationsänderungen (Kap. 3.4.2) hauptsächlich von einer Verlagerung freigesetzter Komponenten von der warmen zur kalten Seite des ATES-Systems auszugehen, welche vor dem Hintergrund begrenzter Freisetzungspools (Kap. 3.4.1.1) mit zunehmender Zyklenzahl zudem tendenziell abnehmen wird. Lediglich mit dem nicht zurückgewonnenen erwärmten Wasser, kann somit anteilig durch temperaturinduzierte Effekte beeinflusstes Wasser aus dem Speichersystem hinaustransportiert werden, wobei auch hier die beobachtete Reversibilität im Zuge der Abkühlung des Wassers zu einer sukzessiven Wiederherstellung der natürlichen Grundwasserbeschaffenheit führen wird. Im Zusammenspiel mit der, für einen gegebenen Wärmebedarf, geringeren Raumbeanspruchung von HT-ATES-Systemen gegenüber Speichern mit einem geringerem Temperaturniveau (Wang et al., 2021), sollten daher auch mögliche stärkere initiale Konzentrationsänderungen innerhalb des ATES-Systems keinen grundsätzlichen genehmigungsrechtlichen Hinderungsgrund darstellen. Dies wird auch durch entsprechende Möglichkeiten zur abwägenden Bewertung im Wasserhaushaltsgesetzt adressiert, indem eine Abweichung vom allgemeinen Bewirtschaftungsziel eines guten mengenmäßigen und chemischen Zustandes zulässig ist, wenn der Nutzen der veränderten Grundwasserbeschaffenheit „…für die nachhaltige Entwicklung größer ist als der Nutzen, den die Erreichung der Bewirtschaftungsziele für die Umwelt und die Allgemeinheit hat,…“ (vergl. §31 und §47 WHG; BMJ, 2009). In diesem Zusammenhang sollte entsprechend beachtet werden, dass auch andere klimaneutrale Wärmeversorgungskonzepte mit Umweltbelastungen einhergehen (Bünger und Matthey, 2018; Matthey und Bünger, 2019), welche mit einer vermehrten Nutzung von UTES-Systemen teils vermieden werden könnten.

Insgesamt geht es somit allerdings wieder auf die Frage zurück, wieso eine breitere Anwendung von UTES-Systemen trotz der von vielen Akteuren beschriebenen Notwendigkeit saisonaler Wärmespeicher (BMWi, 2021; Engelmann et al., 2021; State of Green, 2020; Thamling et al., 2020) bisher kaum erfolgt ist. Hierbei kann ein Blick auf die in den letzten Jahren neu in Betrieb genommenen, saisonal betriebenen, HT-Erdbeckenspeicher helfen, welche in direkter Kombination mit solarthermischen Anlagen zur Wärmeversorgung in kleineren und mittleren kommunalen Wärmenetzen in Dänemark eingesetzt werden (Johansen and Werner, 2022). Zum einen ist die Wärmeversorgung über Wärmenetze in Dänemark schlicht weiter verbreitet als in Deutschland und vielen anderen europäischen Ländern (Abb. 1.3a), sodass es Wärmenetze auf verschiedenen Größenskalen gibt, deren Dekarbonisierung von der Kombination mit einem Wärmespeicher profitieren kann; zum anderen gibt es durch mehrere Jahrzehnte Erfahrung in der Planung der Wärmeversorgung (Johansen and Werner, 2022) aber auch Grund zur Annahme, dass die Wärmenachfrage entsprechend belastbar für eine langfristig effiziente Nutzung von Wärmespeichern prognostiziert ist. Doch selbst der größte dieser Erdbeckenspeicher ermöglicht bisher nur die solarthermische Wärmeversorgung von etwa 2000 Haushalten (Ramboll, 2015; State of Green, 2014), sodass auch dänische Akteure darauf hinweisen, dass saisonale Speicher für größere Fernwärmenetze in urbanen Gebieten vermutlich rein aus Platzgründen nicht als Erdbeckenspeicher umsetzbar sind, sondern als ATES-Systeme geplant werden müssten (State of Green, 2020).

Nimmt man die belastbare Prognose nutzbarer Wärmequellen und zukünftiger Wärmenachfrage als entscheidendes Kriterium für einen sowohl energetisch als auch wirtschaftlich effizienten Speicherbetrieb (Fleuchaus et al., 2020), besteht vermutlich erst mit der nun in Vorbereitung befindlichen verpflichtenden kommunalen Wärmeplanung (BMWK, 2022) auch in Deutschland auf Sicht die Möglichkeit bessere Rahmenbedingungen für die Nutzung von Synergieeffekten zwischen ausgebauten bzw. verdichteten Wärmenetzen und zentralen saisonalen Wärmespeichern zu schaffen. Voraussetzung dafür wäre allerdings eine frühzeitige Koordinierung der gesamtsystemisch möglichst effizienten Nutzung begrenzter Ressourcen wie Biomasse oder klimaneutralem Wasserstoff. Da deren verstärkter Einsatz bereits in bestehenden Dekarbonisierungsstrategien von Wärmenetzbetreibern vorgesehen wird (Agora Energiewende, 2019), dürfte eine der dezentralen kommunalen Wärmeplanung nachgeschaltete Überprüfung auf gesamtsystemische Kompatibilität des Einsatzes dieser begrenzten Ressourcen (BMWK, 2022) weitere Verzögerungen bei der Transformation zentraler Wärmeversorgungsysteme zur Folge haben. Lassen sich Biomasse und Wasserstoff in anderen Anwendungsszenarien sinnvoller einsetzen, müssten Wärmenetzbetreiber die Einbindung weiterer alternativer Wärmequellen in die Wärmenetze forcieren und wären dabei voraussichtlich auch auf den vermehrten Einsatz saisonaler Wärmespeicher angewiesen.

In diesem Zusammenhang wird häufig Dänemark als Vorbild für eine funktionierende Wärmewende betrachtet (Engelmann et al., 2021; Johansen and Werner, 2022; State of Green, 2020), wo im Gegensatz zu Deutschland jedoch bereits 1979 ein erstes Gesetz zur Wärmeplanung beschlossen wurde (Johansen and Werner, 2022). Gut 40 Jahre später wurde 2020 in Dänemark ein EE-Anteil bei der Wärme- und Kältebereitstellung von 50 % erreicht, wobei der EE-Anteil in den letzten 16 Jahren um 30 % gestiegen ist (Abb. 1.3b). Dies verdeutlicht die Herausforderung der deutschen Klimaschutzziele, die im Wärmesektor eine 30-prozentige Steigerung des EE-Anteils in ~8 Jahren vorsehen (ERK, 2022). Um sich nicht allzu weit von diesem Ziel zu entfernen, wird man möglichst effizient verschiedene erneuerbare Energien in die Wärmeversorgungssysteme einbinden müssen, wozu Hochtemperatur-Wärmespeicher auf verschiedenen Größenskalen einen Beitrag leisten können und aller Voraussicht nach auch erforderlich sein werden.

Für eher grundsätzliche Aspekte bspw. hinsichtlich des Einflusses induzierter Strömungs- und Mischungsprozesse auf die räumliche Ausbreitung hydrogeochemischer Effekte im zyklischen Betrieb eines Hochtemperatur-Wärmespeichers oder auch bezogen auf technische Optimierungen zur Steigerung von Wärme-Rückgewinnungsraten oder zur Verhinderung von Clogging-Effekten können auch weiterhin Feldversuche (wie z. B. im Projekt TestUM-II) einen geeigneten Rahmen darstellen. Allerdings müssen im Zuge einer verbreiteteren Nutzung von Wärmespeichern im geologischen Untergrund vermutlich auch vermehrt weitere geologische Einheiten als Speicherformationen in Betracht gezogen werden, deren Verhalten bei Erwärmung von den hier betrachteten organikarmen norddeutschen Lockersedimente abweichen kann. Auch ist davon auszugehen, dass je nach zeitlichem Verlauf von Wärmeangebot und Nachfrage, sowie den örtlichen Begebenheiten, Speicher für verschiedene Temperaturniveaus und Zeitskalen benötigt werden. Insbesondere die Betrachtung saisonaler Hochtemperatur-Wärmespeicher geht jedoch mit räumlichen und zeitlichen Dimensionen einher, die dazu führen, dass sich entsprechend langfristige hydrogeochemische Effekte wahrscheinlich am besten analog zur angestrebten Vorgehensweise bei den „Reallaboren der Energiewende“ in Kopplung mit Pilotprojekten betriebsbegleitend unter verschiedenen geologischen Begebenheiten untersuchen ließen. Parallel könnten so bereits Erfahrungen und auch sich daraus ergebende Fragestellungen im Regelbetrieb gesammelt werden. Die grundsätzliche Reversibilität temperaturinduzierter hydrogeochemischer Effekte bei Abkühlung kann dabei die Grundlage dafür darstellen, potentielle genehmigungsrechtliche Bedenken durch geeignete, praxistaugliche Monitoring-Auflagen und nicht durch Ablehnung zu adressieren.

Literaturverzeichnis

Adinolfi, M., Ruck, W., 1992. Microbiological and Environmental Effects of Aquifer Thermal Energy Storage, in: Aquifer Thermal Energy (Heat and Chill) Storage: Proceedings of the 27th Intersociety Energy Conversion Engineering Conference. pp. 69–74.

AGEB, 2021. Anwendungsbilanzen zur Energiebilanz Deutschland - Endenergieverbrauch nach Energieträgern und Anwendungszwecken, AG Energiebilanzen e.V.

Agora Energiewende, 2019. Wie werden Wärmenetze grün? Dokumentation zur Diskussionsveranstaltung am 21. Mai 2019 auf den Berliner Energietagen 2019.

Alikhani, J., Deinhart, A.L., Visser, A., Bibby, R.K., Purtschert, R., Moran, J.E., Massoudieh, A., Esser, B.K., 2016. Nitrate vulnerability projections from Bayesian inference of multiple groundwater age tracers. J. Hydrol. https://doi.org/10.1016/j.jhydrol.2016.04.028

Álvarez-Merino, M.A., Fontecha-Cámara, M.A., López-Ramón, M. V, Moreno-Castilla, C., 2008. Temperature dependence of the point of zero charge of oxidized and non-oxidized activated carbons. Carbon N. Y. 46, 778–787. https://doi.org/10.1016/j.carbon.2008.02.002

Amos, R.T., Mayer, K.U., 2006. Investigating the role of gas bubble formation and entrapment in contaminated aquifers: Reactive transport modelling. J. Contam. Hydrol. 87, 123–154. https://doi.org/10.1016/j.jconhyd.2006.04.008

Amos, R.T., Mayer, K.U., Bekins, B.A., Delin, G.N., Williams, R.L., 2005. Use of dissolved and vapor-phase gases to investigate methanogenic degradation of petroleum hydrocarbon contamination in the subsurface. Water Resour. Res. 41, 1–15. https://doi.org/10.1029/2004WR003433

Andersen, L.J., Madsen, B., Bull, N., 1985. Hydrogeological investigations as a basis for heat storage in aquifers, in: Hydrogeology in the Service of Man, Mémoires of the 18th Congress of the International Association of Hydrogcologists. Cambridge, pp. 59–67.

Andersson, O., 1990. Scaling and corrosion in subsurface thermal energy storage systems, in: Hooghart, J.C., Posthumus, C.W.S. (Eds.), Hydrochemistry and Energy Storage in Aquifers. pp. 53–71.

Andersson, O., Sellberg, B., 1992. Swedish ATES Applications: Ten Years of Development Experience, in: Aquifer Thermal Energy (Heat and Chill) Storage: Proceedings of the 27th Intersociety Energy Conversion Engineering Conference.

Andersson, S., Nilsson, S.I., 2001. Influence of pH and temperature on microbial activity, substrate availability of soil-solution bacteria and leaching of dissolved organic carbon in a mor humus. Soil Biol. Biochem. 33, 1181–1191. https://doi.org/10.1016/S0038-0717(01)00022-0

Andrews, W.J., Stark, J.R., Fong, A.L., Fallon, J.D., 2005. Water-Quality Assessment of Part of the Upper Mississippi River Basin, Minnesota and Wisconsin—Ground-Water Quality along a Flow System in the Twin Cities Metropolitan Area, Minnesota, 1997-98. U.S. Geol. Surv. Sci. Investig. Rep. 5120, 44.

Angove, M.J., Wells, J.D., Johnson, B.B., 1999. The Influence of Temperature on the Adsorption of Cadmium(II) and Cobalt(II) on Goethite. J. Colloid Interface Sci. 211, 281–290. https://doi.org/10.1006/jcis.1998.6010

Appelo, C.A.J., Postma, D., 2005. Geochemistry, Groundwater and Pollution, 2nd edn. ed. A.A. Balkema Publishers, Leiden.

Archie, G.E., 1942. The Electrical Resistivity Log as an Aid in Determining Some Reservoir Characteristics. J. Pet. Technol. 5, 54–62.

Arning, E., Kölling, M., Schulz, H.D., Panteleit, B., Reichling, J., 2006. Einfluss oberflächennaher Wärmegewinnung auf geochemische Prozesse im Grundwasserleiter. Grundwasser 11, 27–39. https://doi.org/10.1007/s00767-006-0116-0

Arp, H.P.H., Schmidt, T.C., 2004. Air-water transfer of MTBE, its degradation products, and alternative fuel oxygenates: the role of temperature. Environ. Sci. Technol. 38, 5405–5412.

Bansal, O.P., 1982. Thermodynamics of K-Ni and Ca-Ni exchange reactions on kaolinite clay. J. Soil Sci. 33, 63–71. https://doi.org/10.1111/j.1365-2389.1982.tb01748.x

Bastin, J.-F., Clark, E., Elliott, T., Hart, S., van den Hoogen, J., Hordijk, I., Ma, H., Majumder, S., Manoli, G., Maschler, J., Mo, L., Routh, D., Yu, K., Zohner, C.M., Crowther, T.W., 2019. Understanding climate change from a global analysis of city analogues. PLoS One 14, e0217592. https://doi.org/10.1371/journal.pone.0217592

Battani, A., Deville, E., Faure, J.L., Jeandel, E., Noirez, S., Tocqué, E., Benoît, Y., Schmitz, J., Parlouar, D., Sarda, P., Gal, F., le Pierres, K., Brach, M., Braibant, G., Beny, C., Pokryszka, Z., Charmoille, A., Bentivegna, G., Pironon, J., de Donato, P., Garnier, C., Cailteau, C., Barrès, O., Radilla, G., Bauer, A., 2010. Geochemical study of natural CO2 emissions in the french massif central: How to predict origin, processes and evolution of CO2 leakage. Oil Gas Sci. Technol. 65, 615–633. https://doi.org/10.2516/ogst/2009052

Bauer, S., Beyer, C., Dethlefsen, F., Dietrich, P., Duttmann, R., Ebert, M., Feeser, V., Görke, U., Köber, R., Kolditz, O., Rabbel, W., Schanz, T., Schäfer, D., Würdemann, H., Dahmke, A., 2013. Impacts of the use of the geological subsurface for energy storage: An investigation concept. Environ. Earth Sci. 70, 3935–3943. https://doi.org/10.1007/s12665-013-2883-0

Bauer, S., Pfeiffer, T., Boockmeyer, A., Dahmke, A., Beyer, C., 2015. Quantifying Induced Effects of Subsurface Renewable Energy Storage. Energy Procedia 76, 633–641. https://doi.org/10.1016/j.egypro.2015.07.885

Bayer, P., Saner, D., Bolay, S., Rybach, L., Blum, P., 2012. Greenhouse gas emission savings of ground source heat pump systems in Europe: A review. Renew. Sustain. Energy Rev. 16, 1256–1267. https://doi.org/10.1016/j.rser.2011.09.027

Beaubien, S.E., Ciotoli, G., Lombardi, S., 2003. Carbon dioxide and radon gas hazard in the Alban Hills area (central Italy). J. Volcanol. Geotherm. Res. 123, 63–80. https://doi.org/10.1016/S0377-0273(03)00028-3

Bell, K.Y., LeBoeuf, E.J., 2013. Influence of temperature and macromolecular mobility on sorption of TCE on humic acid coated mineral surfaces. Chemosphere 90, 176–181. https://doi.org/10.1016/j.chemosphere.2012.05.112

Bergmann, P., Schmidt-Hattenberger, C., Kiessling, D., Rücker, C., Labitzke, T., Henninges, J., Baumann, G., Schütt, H., 2012. Surface-downhole electrical resistivity tomography applied to monitoring of CO 2 storage at Ketzin, Germany. GEOPHYSICS 77, B253--B267. https://doi.org/10.1190/geo2011-0515.1

Berta, M., 2017. Experimental investigation of hydrogeochemical consequences of gas leakages into shallow aquifers. PHD-Thesis. Kiel Universtiy.

Berta, M., Becker, A., Dethlefsen, F., Ebert, M., Koch, S., Dahmke, A., 2015. Experiments showed no reactions coupled to methane leaked into shallow aquifers. First Break 33, 93–95.

Berta, M., Dethlefsen, F., Ebert, M., Gundske, K., Dahmke, A., 2016. Surface passivation model explains pyrite oxidation kinetics in column experiments with up to 11 bars p(O2). Environ. Earth Sci. 75, 1–13. https://doi.org/10.1007/s12665-016-5985-7

Berta, M., Dethlefsen, F., Ebert, M., Schäfer, D., Dahmke, A., 2018. Geochemical Effects of Millimolar Hydrogen Concentrations in Groundwater: An Experimental Study in the Context of Subsurface Hydrogen Storage. Environ. Sci. Technol. 52, 4937–4949. https://doi.org/10.1021/acs.est.7b05467

Beyke, G., Fleming, D., 2005. In situ thermal remediation of DNAPL and LNAPL using electrical resistance heating. Remediation 15, 5–22. https://doi.org/10.1002/rem.20047

BiB, 2020. Bevölkerungsdichte in der BRD (2020). Bundesinstitut für Bevölkerungsforschung.

Blicher-Mathiesen, G., McCarty, G.W., Nielsen, L.P., 1998. Denitrification and degassing in groundwater estimated from dissolved dinitrogen and argon. J. Hydrol. 208, 16–24. https://doi.org/10.1016/S0022-1694(98)00142-5

BMJ, 2010. Verordnung zum Schutz des Grundwassers (Grundwasserverordnung - GrwV). Bundesministerium der Justiz.

BMJ, 2009. Gesetz zur Ordnung des Wasserhaushalts (Wasserhaushaltsgesetz - WHG). Bundesministerium der Justiz.

BMJ, 2001. Verordnung über die Qualität von Wasser für den menschlichen Gebrauch - Trinwasserverordnung vom 21.05.2001. Bundesministerium der Justiz.

BMWi, 2021. Dialog Klimaneutrale Wärme 2045, Bundesministerium für Wirtschaft und Energie.

BMWi, 2015. Erneuerbare Energien im Jahr 2014. Bundesministerium für Wirtschaft und Energie.

BMWK, 2023. Mehr Tempo bei der Transformation der Wärmeversorgung - Wärmenetze klimaneutral um- und ausbauen. Gemeinsame Erklärung des Bundesministeriums für Wirtschaft und Klimaschutz, des Bundesbauministeriums, sowie beteiligter Verbände; Stand 12. Juni 2023.

BMWK, 2022. Konzept für die Umsetzung einer flächendeckenden kommunalen Wärmeplanung als zentrales Koordinierungsinstrument für lokale , effiziente Wärmenutzung. Diskussionspapier des Bundesministeriums für Wirtschaft und Klimaschutz, Stand 28. Juli 2022.

Bockelmann, F., Fisch, M.N., Kühl, L., Petruszek, T., Nüßle, F., Sanner, B., 2012. Optimization of ground coupled heating and cooling supply systems in office buildings – reversible heat pump and free cooling, in: Proceedings of the 12th International Conference on Energy Storage, Innostock, Spain, 2012.

Bonte, M., 2013. Impacts of shallow geothermal energy on groundwater quality - A hydrochemical and geomicrobial study of the effects of ground source heat pumps and aquifer thermal energy storage. PHD-Thesis. VU University Amsterdam.

Bonte, M., Röling, W.F.M., Zaura, E., Van Der Wielen, P.W.J.J., Stuyfzand, P.J., Van Breukelen, B.M., 2013a. Impacts of shallow geothermal energy production on redox processes and microbial communities. Environ. Sci. Technol. 47, 14476–14484. https://doi.org/10.1021/es4030244

Bonte, M., Stuyfzand, P.J., Breukelen, B.M. Van, 2014. Reactive Transport Modeling of Thermal Column Experiments to Investigate the Impacts of Aquifer Thermal Energy Storage on Groundwater Quality. Environ. Sci. Technol. 48, 12099–12107. https://doi.org/10.1021/es502477m

Bonte, M., Stuyfzand, P.J., Hulsmann, A., Van Beelen, P., 2011. Underground Thermal Energy Storage : Environmental Risks and Policy Developments in the Netherlands and European Union. Ecol. Soc. 16, 22.

Bonte, M., van Breukelen, B.M., Stuyfzand, P.J., 2013b. Temperature-induced impacts on groundwater quality and arsenic mobility in anoxic aquifer sediments used for both drinking water and shallow geothermal energy production. Water Res. 47, 5088–5100. https://doi.org/10.1016/j.watres.2013.05.049

Bridger, D.W., Allen, D.M., 2005. Designing Aquifer Thermal Energy Storage Systems. Ashrae J. 47, 32–37.

Brielmann, H., Griebler, C., Schmidt, S.I., Michel, R., Lueders, T., 2009. Effects of thermal energy discharge on shallow groundwater ecosystems. FEMS Microbiol. Ecol. 68, 273–286. https://doi.org/10.1111/j.1574-6941.2009.00674.x

Brielmann, H., Lueders, T., Schreglmann, K., Ferraro, F., Avramov, M., Hammerl, V., Blum, P., Bayer, P., Griebler, C., 2011. Oberflächennahe Geothermie und ihre potenziellen Auswirkungen auf Grundwasserökosysteme. Grundwasser 16, 77–91. https://doi.org/10.1007/s00767-011-0166-9

Brons, H.J., 1992. Biogeochemical aspects of aquifer thermal energy storage. PHD-Thesis. LUW-Wageningen.

Brons, H.J., Griffioen, J., Appelo, C.A.J., Zehnder, A.J.B., 1991. (Bio)geochemical reactions in aquifer material from a thermal energy storage site. Water Res. 25, 729–736. https://doi.org/10.1016/0043-1354(91)90048-U

Bruemmer, G.W., Gerth, J., Tiller, K.G., 1988. Reaction kinetics of the adsorption and desorption of nickel, zinc and cadmium by goethite. I. Adsorption and diffusion of metals. J. Soil Sci. 39, 37–52. https://doi.org/10.1111/j.1365-2389.1988.tb01192.x

Brunet, P., Clément, R., Bouvier, C., 2010. Monitoring soil water content and deficit using Electrical Resistivity Tomography (ERT) – A case study in the Cevennes area, France. J. Hydrol. 380, 146–153.

Bünger, B., Matthey, A., 2018. Methodenkonvention 3.0 zur Ermittlung von Umweltkosten - Methodische Grundlagen, Umweltbundesamt. https://doi.org/10.1007/978-3-8348-8657-6_2

Bürger, V., Hesse, T., Palzer, A., Köhler, B., Herkel, S., Engelmann, P., Quack, D., 2017. Klimaneutraler Gebäudebestand 2050, Umweltbundesamt.

Carrigan, C.R., Yang, X., LaBrecque, D.J., Larsen, D., Freeman, D., Ramirez, A.L., Daily, W., Aines, R., Newmark, R., Friedmann, J., Hovorka, S., 2013. Electrical resistance tomographic monitoring of CO2 movement in deep geologic reservoirs. Int. J. Greenh. Gas Control 18, 401–408. https://doi.org/10.1016/j.ijggc.2013.04.016

Chiodini, G., Frondini, F., 2001. Carbon dioxide degassing from the Albani Hills volcanic region, Central Italy. Chem. Geol. 177, 67–83.

Christ, M.J., David, M.B., 1996. Temperature and moisture effects on the production of dissolved organic carbon in a Spodosol. Soil Biol. Biochem. 28, 1191–1199. https://doi.org/10.1016/0038-0717(96)00120-4

Coldewey, W.G., Melchers, C., 2011. Gas im Münsterland – Gefahren und Nutzung, in: 62. Deutsche Brunnenbauertage Und BAW-Baugrundkolloquium „Baugrundaufschlüsse: Planung, Ausschreibung, Durchführung, Überwachung Und Interpretation“ 13. – 15. April 2011 Im Bau-ABC Rostrup / Bad Zwischenahn. Münster, p. 2.

Comina, C., Cosentini, R.M., Della Vecchia, G., Foti, S., Musso, G., 2010. Hydro-chemo-mechanical processes in soil samples: monitoring through electrical resistivity tomography. EPJ Web Conf. 6, 22012. https://doi.org/10.1051/epjconf/20100622012

Cornelissen, G., van Noort, P.C.M., Parsons, J.R., Govers, H. a. J., 1997. Temperature Dependence of Slow Adsorption and Desorption Kinetics of Organic Compounds in Sediments. Environ. Sci. Technol. 31, 454–460.

Corwin, D.L., Lesch, A.M., 2005. Apparent soil electrical conductivity measurements in agriculture. Comput. Electron. Agric. 46, 11–43.

Dachnov, V.N., 1962. Interpretazija resultatov geofiziceskich issledovanij skvazin, 2nd edn. ed. Izdat. Gostoptechizdat, Moscow.

Daily, W., Ramirez, A., LaBreque, D., Nitao, J., 1992. Electrical Resistivity Tomography of Vadose Water Movement. Water Resour. Res. 28, 1429–1442.

Debenedetti, P.G., 1996. Metastable Liquids: Concepts and Principles. Princeton University Press, Princeton.

Dietrich, P., 1999. Konzeption und Auswertung gleichstromgeoelektrischer Tracerversuche unter Verwendung von Sensitivitätskoeffizienten.

Dincer, I., Rosen, M.A., 2010. Thermal Energy Storage: Systems and Applications. John Wiley & Sons, Chichester.

Echeverría, J., Indurain, J., Churio, E., Garrido, J., 2003. Simultaneous effect of pH, temperature, ionic strength, and initial concentration on the retention of Ni on illite. Colloids Surfaces A Physicochem. Eng. Asp. 218, 175–187. https://doi.org/10.1016/S0927-7757(02)00587-3

El-Batouti, M., Sadek, O.M., Assaad, F.F., 2003. Kinetics and thermodynamics studies of copper exchange on Na-montmorillonite clay mineral. J. Colloid Interface Sci. 259, 223–227. https://doi.org/10.1016/S0021-9797(02)00173-X

Engelmann, P., Köhler, B., Meyer, R., Dengler, J., Herkel, S., Kießling, L., Quast, A., Berneiser, J., Bär, C., Sterchele, P., Heilig, J., Bürger, V., Braungardt, S., Hesse, T., Sandrock, M., Maaß, C., Strodel, N., 2021. Systemische Herausforderung der Wärmewende, Climate Change - Umwelt Bundesamt.

EPA, 1997. Superfund Innovative Technology Evaluation Program - Final Demonstration Plan for the Evaluation of Soil Sampling and Soil Gas Sampling Technologies, U.S. Environmental Protection Agency - Archive Document.

Epting, J., Händel, F., Huggenberger, P., 2013. Thermal management of an unconsolidated shallow urban groundwater body. Hydrol. Earth Syst. Sci. 17, 1851–1869. https://doi.org/10.5194/hess-17-1851-2013

ERK, 2022. Zweijahresgutachten 2022. Gutachten zur Entwicklung der Treibhausgasemissionen, Trends der Jahresemissionsmengen und zur Wirksamkeit von Maßnahmen (gemäß § 12 Abs. 4 Bundes-Klimaschutzgesetz). Hg. v. Expertenrat für Klimafragen (ERK).

Eurostat, 2022. Anteil erneuerbarer Energien am Bruttoendenergieverbrauch nach Bereichen.

Evanko, C.R., Dzombak, D.A., 1998. Influence of Structural Features on Sorption of NOM-Analogue Organic Acids to Goethite. Environ. Sci. Technol. 32, 2846–2855. https://doi.org/10.1021/es980256t

Feast, N.A., Hiscock, K.M., Dennis, P.F., Andrews, J.N., 1998. Nitrogen isotope hydrochemistry and denitrification within the Chalk aquifer system of north Norfolk, UK. J. Hydrol. 211, 233–252.

Feisthauer, S., Seidel, M., Bombach, P., Traube, S., Knöller, K., Wange, M., Fachmann, S., Richnow, H.H., 2012. Characterization of the relationship between microbial degradation processes at a hydrocarbon contaminated site using isotopic methods. J. Contam. Hydrol. 133, 17–29. https://doi.org/10.1016/j.jconhyd.2012.03.001

Ferguson, G., 2009. Unfinished Business in Geothermal Energy. Ground Water 47, 167. https://doi.org/10.1111/j.1745-6584.2008.00528.x

Ferguson, R.J., 1984. A Kinetic Model for Calcium Carbonate Deposition. Mater. Perform. November, 25–34.

Filius, J.D., Lumsdon, D.G., Meeussen, J.C.L., Hiemstra, T., Van Riemsdijk, W.H., 2000. Adsorption of fulvic acid on goethite. Geochim. Cosmochim. Acta 64, 51–60. https://doi.org/10.1016/S0016-7037(99)00176-3

Fleiter, T., Steinbach, J., Ragwitz, M., 2016. Mapping and analyses of the current and future (2020 - 2030) heating/cooling fuel deployment (fossil/renewables) - Work package 1: Final energy consumption for the year 2012, European Commission under contract N°ENER/C2/2014-641.

Fleuchaus, P., Godschalk, B., Stober, I., Blum, P., 2018. Worldwide application of aquifer thermal energy storage – A review. Renew. Sustain. Energy Rev. 94, 861–876. https://doi.org/10.1016/j.rser.2018.06.057

Fleuchaus, P., Schüppler, S., Bloemendal, M., Guglielmetti, L., Opel, O., Blum, P., 2020. Risk analysis of High-Temperature Aquifer Thermal Energy Storage (HT-ATES). Renew. Sustain. Energy Rev. 133, 110153. https://doi.org/10.1016/j.rser.2020.110153

Ford, R.G., Bertsch, P.M., Farley, K.J., 1997. Changes in transition and heavy metal partitioning during hydrous iron oxide aging. Environ. Sci. Technol. 31, 2028–2033. https://doi.org/10.1021/es960824+

Friedman, S.P., 2005. Soil properties influencing apparent electrical conductivity: a review. Comput. Electron. Agric. 46, 45–70. https://doi.org/10.1016/j.compag.2004.11.001

Friedman, S.P., Seaton, N.A., 1998. Critical path analysis of the relationship between permeability and electrical conductivity of three-dimensional pore networks. Water Resour. Res. 34, 1703–1710.

Fry, V.A., Selker, J.S., Gorelick, S.M., 1997. Experimental investigations for trapping oxygen gas in saturated porous media for in situ bioremediation. Water Resour. Res. 33, 2687–2696. https://doi.org/10.1029/97WR02428

Garbe-Schönberg, C.-D., 1993. Simultaneous Determination of Thirty-Seven Trace Elements in Twenty-Eight International Rock Standards By ICP-MS. Geostand. Geoanalytical Res. 17, 81–97. https://doi.org/10.1111/j.1751-908X.1993.tb00122.x

García-Gil, A., Epting, J., Ayora, C., Garrido, E., Vázquez-Suñé, E., Huggenberger, P., Gimenez, A.C., 2016a. A reactive transport model for the quantification of risks induced by groundwater heat pump systems in urban aquifers. J. Hydrol. 542, 719–730. https://doi.org/10.1016/j.jhydrol.2016.09.042

García-Gil, A., Epting, J., Garrido, E., Vázquez-Suñé, E., Lázaro, J.M., Navarro, J.Á.S., Huggenberger, P., Calvo, M.Á.M., 2016b. A city scale study on the effects of intensive groundwater heat pump systems on heavy metal contents in groundwater. Sci. Total Environ. 572, 1047–1058. https://doi.org/10.1016/j.scitotenv.2016.08.010

García-Gil, A., Gasco-Cavero, S., Garrido, E., Mejías, M., Epting, J., Navarro-Elipe, M., Alejandre, C., Sevilla-Alcaine, E., 2018. Decreased waterborne pathogenic bacteria in an urban aquifer related to intense shallow geothermal exploitation. Sci. Total Environ. 633, 765–775. https://doi.org/10.1016/j.scitotenv.2018.03.245

GEF Ingenieur AG, casaGeo Data & Services GmbH, geomer GmbH, 2014. Wärmeatlas.

Genç-Fuhrman, H., Tjell, J.C., McConchie, D., 2004. Adsorption of Arsenic from Water Using Activated Neutralized Red Mud. Environ. Sci. Technol. 38, 2428–2434. https://doi.org/10.1021/es035207h

Gerhardt, N., Ganal, I., Jentsch, M., Rodriguez, J., Stroh, K., Buchmann, E.K., 2019. Entwicklung der Gebäudewärme und Rückkoplung mit dem Energiesystem in -95 % THG- Klimaszenarien 1. Teilbericht im Rahmen des Projektes : Sektorkopplung mit dem Fokus Fernwärme mit hohen Anteilen konventioneller KWK-Erzeugung und Rückkopplung.

Gerhardt, N., Zimmermann, B., Ganal, I., Pape, A., Giron, P., Ghosh, D., Dörre, E., Kallert, A., Yu, Y.-J., 2021. Transformationspfade der Fernwärme in Rückkopplung mit dem Energiesystem und notwendige Rahmenbedingungen.

Giordano, N., Comina, C., Mandrone, G., 2015. The First Italian Experimence of Ground Thermal Energy Storage: an Integrated Approach for Design and Monitoring, from Laboratory to Field Scale, in: Proceedings of the World Geothermal Congress, Melbourne, Australia, 2015. Melbourne, Australia.

Giordano, N., Firmbach, L., Comina, C., Dietrich, P., Mandrone, G., Vienken, T., 2013. Laboratory scale electrical resistivity measurements to monitor the heat propagation within porous media for low enthalpy geothermal applications, in: Proceedings of the 32nd Conference of the National Group of Solid Earth Geophysics – GNGTS, Trieste, Italia, 2013. Trieste, Italy.

Gosset, J.M., 1987. Measurement of Henry’s Law Constants for C, and C2 Chlorinated Hydrocarbons. Environ. Sci. Technol. 21, 202–208.

Grellier, S., Bouyé, J.M., Guérin, R., Robain, H., Skhiri, N., 2005. Electrical Resistivity Tomography (ERT) applied to moisture measurements in bioreactor: principles, in situ measurements and results, in: Proceedings of the International Workshop of “Hydro-Physico-Mechanics of Landfills” LIRIGM, Grenoble, France, 2005.

Griebler, C., Brielmann, H., Haberer, C.M., Kaschuba, S., Kellermann, C., Stumpp, C., Hegler, F., Kuntz, D., Walker-Hertkorn, S., Lueders, T., 2016. Potential impacts of geothermal energy use and storage of heat on groundwater quality, biodiversity, and ecosystem processes. Environ. Earth Sci. 75, 1–18. https://doi.org/10.1007/s12665-016-6207-z

Griffioen, J., Appelo, C.A.J., 1993. Nature and extent of carbonate precipitation during aquifer thermal energy storage. Appl. Geochemistry 8, 161–176. https://doi.org/10.1016/0883-2927(93)90032-C

Gunn, D.A., Chambers, J.E., Uhlemann, S., Wilkinson, P.B., Meldrum, P.I., Dijkstra, T.A., Haslam, E., Kirkham, M., Wragg, J., Holyoake, S., Hughes, P.N., Hen-Jones, R., Glendinning, S., 2014. Moisture monitoring in clay embankments using electrical resistivity tomography. Constr. Build. Mater. 92, 82–94.

Gunnarsson, I., Arnórsson, S., 2005. Impact of silica scaling on the efficiency of heat extraction from high-temperature geothermal fluids. Geothermics 34, 320–329. https://doi.org/10.1016/j.geothermics.2005.02.002

Hähnlein, S., Bayer, P., Blum, P., 2010. International legal status of the use of shallow geothermal energy. Renew. Sustain. Energy Rev. 14, 2611–2625. https://doi.org/10.1016/j.rser.2010.07.069

Hähnlein, S., Bayer, P., Ferguson, G., Blum, P., 2013. Sustainability and policy for the thermal use of shallow geothermal energy. Energy Policy 59, 914–925. https://doi.org/10.1016/j.enpol.2013.04.040

Hähnlein, S., Blum, P., Bayer, P., 2011. Oberflächennahe Geothermie – aktuelle rechtliche Situation in Deutschland. Grundwasser 16, 69–75. https://doi.org/10.1007/s00767-011-0162-0

Hegele, P.R., Mumford, K.G., 2014. Gas production and transport during bench-scale electrical resistance heating of water and trichloroethene. J. Contam. Hydrol. 165, 24–36. https://doi.org/10.1016/j.jconhyd.2014.07.002

Heldt, S., Wang, B., Hu, L., Hornbruch, G., Lüders, K., Werban, U., Bauer, S., 2021a. Numerical Investigation of a High Temperature Heat Injection Test. J. Hydrol. 126229. https://doi.org/10.1016/j.jhydrol.2021.126229

Heldt, S., Wang, B., Hu, L., Hornbruch, G., Lüders, K., Werban, U., Bauer, S., 2021b. Data of a high temperature heat injection test. Data Br. 36, 107035. https://doi.org/10.1016/j.dib.2021.107035

Hem, J.D., 1985. Study and Interpretation of the Chemical Characteristics of Natural Water, U.S. Geological Survey Water-Supply Paper. Department of the Interior, US Geological Survey, Reston,Va.

Henning, H.-M., Palzer, A., 2012. 100 % Erneuerbare Energien für Strom und Wärme in Deutschland. Fraunhofer-Institut für Solare Energiesysteme, ISE. Freiburg.

Hermans, T., Vandenbohede, A., Lebbe, L., Nguyen, F., 2012. A shallow geothermal experiment in a sandy aquifer monitored using electric resistivity tomography. Geophysics 77, 11–21.

Hermans, T., Wildemeersch, S., Jamin, P., Orban, P., Broyère, S., Dassargues, A., Nguyen, F., 2015. Quantitative temperature monitoring of heat tracing experiment using cross-borehole ERT. Geothermics 53, 14–26.

Heron, G., Christensen, T.H., Enfield, C.G., 1998. Henry's Law Constant for Trichloroethylene between 10 and 95 °C. Environ. Sci. Technol. 32, 1433–1437.

Heron, G., Crouzet, C., Bourg, A.C.M., Christensen, T.H., 1994. Speciation of Fe(II) and Fe(III) in Contaminated Aquifer Sediments Using Chemical Extraction Techniques. Environ. Sci. Technol. 28, 1698–1705. https://doi.org/10.1021/es00058a023

Hiester, U., Jungk, V., Canzler, W., Poetke, D., Ulrich, K.-U., 2022. Umweltverträgliche Nutzung geothermischer Wärmespeicher - Ermittlung und Bewertung thermischer Veränderungen im Grundwasser.

Hoffmann, R., Dietrich, P., 2004. Geoelektrische Messungen zur Bestimmung von Grundwasserfließrichtungen und -geschwindigkeiten. Grundwasser 3, 194–203.

Holm, T.R., Eisenreich, S.J., Rosenberg, H.L., Holm, N.P., 1987. Groundwater Geochemistry of Short-Term Aquifer Thermal Energy Storage Test Cycles. Water Resour. Res. 23, 1005–1019.

Hornbruch, G. et al. TestUM: A test site for controlled field experiments in a shallow aquifer within the scope of the energy transition research - experimental design and database (in preperation).

Huang, Q., Hong, C.-S., 2002. Aqueous solubilities of non-ortho and mono-ortho PCBs at four temperatures. Water Res. 36, 3543–3552.

Hydén, H., 1985. Seasonal Heat Storage in Shallow Aquifers, in: Downing, R.A., Jones, G.P. (Eds.), Hydrogeology in the Service of Man, Mémoires of the 18th Congress of the International Association of Hydrogcologists. Cambridge, pp. 35–41.

IEA, 2018. The Future of Cooling - Opportunities for energy-efficient air conditioning. International Energy Agency.

IEA, 2015. Energy Technology Perspectives 2015. International Energy Agency. https://doi.org/10.1787/energy_tech-2010-en

Imhoff, P.T., Frizzell, A., Miller, C.T., Hill, C., Carolina, N., 1997. Evaluation of Thermal Effects on the Dissolution of a Nonaqueous Phase Liquid in Porous Media. Environ. Sci. Technol. Technol. 31, 1615–1622.

Istok, J.D., Park, M.M., Peacock, A.D., Oostrom, M., Wietsma, T.W., 2007. An experimental investigation of nitrogen gas produced during denitrification. Ground Water 45, 461–467. https://doi.org/10.1111/j.1745-6584.2007.00319.x

Jenne, E.A., 1990. Aquifer Thermal Energy Storage: the importance of geochemical reactions, in: Hooghart, J., Posthumus, C. (Eds.), Hydrochemistry and Energy Storage in Aquifers. pp. 19–33.

Jenne, E.A., Andersson, O., Willemsen, A., 1992. Well, Hydrology, and Geochemistry Problems Encountered in ATES Systems and Their Solutions, in: Jenne, E.A. (Ed.), Aquifer Thermal Energy (Heat and Chill) Storage: Proceedings of the 27th Intersociety Energy Conversion Engineering Conference. San Diego, CA. https://doi.org/10.4271/929153

Jesußek, A., 2012. Temperaturbedingte Auswirkungen unterirdischer Wärmespeicherung auf hydrogeochemische Sediment-Wasser-Wechselwirkungen in einem oberflächennahen Grundwasserleiter. PHD-Thesis. Kiel University.

Jesußek, A., Grandel, S., Dahmke, A., 2013a. Impacts of subsurface heat storage on aquifer hydrogeochemistry. Environ. Earth Sci. 69, 1999–2012. https://doi.org/10.1007/s12665-012-2037-9

Jesußek, A., Köber, R., Grandel, S., Dahmke, A., 2013b. Aquifer heat storage: Sulphate reduction with acetate at increased temperatures. Environ. Earth Sci. 69, 1763–1771. https://doi.org/10.1007/s12665-012-2009-0

Johansen, K., Werner, S., 2022. Something is sustainable in the state of Denmark: A review of the Danish district heating sector. Renew. Sustain. Energy Rev. 158, 112117. https://doi.org/10.1016/j.rser.2022.112117

Jollien, L., Remonnay, S., Miserez, F., 1992. Heat Storage at SPEOS (Swiss ATES Pilot Plant) Chemical and Microbiological Aspects and Problems, in: Aquifer Thermal Energy (Heat and Chill) Storage: Proceedings of the 27th Intersociety Energy Conversion Engineering Conference. pp. 41–46.

Juutinen, S., Rantakari, M., Kortelainen, P., Huttunen, J.T., Larmola, T., Alm, J., Silvola, J., Martikainen, P.J., 2009. Methane dynamics in different boreal lake types. Biogeosciences 6, 209–223. https://doi.org/10.5194/bg-6-209-2009

Kabata-Pendias, A., 2010. Trace Elements in Soils and Plants, 4th editio. ed. CRC Press, Boca Raton, Fl.

Kabuth, A., Dahmke, A., Beyer, C., Bilke, L., Dethlefsen, F., Dietrich, P., Duttmann, R., Ebert, M., Feeser, V., Görke, U.J., Köber, R., Rabbel, W., Schanz, T., Schäfer, D., Würdemann, H., Bauer, S., 2017. Energy storage in the geological subsurface: dimensioning, risk analysis and spatial planning: the ANGUS+ project. Environ. Earth Sci. 76. https://doi.org/10.1007/s12665-016-6319-5

Katz, L.E., Criscenti, L.J., Chen, C., Larentzos, J.P., Liljestrand, H.M., 2013. Temperature effects on alkaline earth metal ions adsorption on gibbsite: Approaches from macroscopic sorption experiments and molecular dynamics simulations. J. Colloid Interface Sci. 399, 68–76. https://doi.org/10.1016/j.jcis.2012.05.011

Keller, N.S., Hornbruch, G., Lüders, K., Werban, U., Vogt, C., Kallies, R., Dahmke, A., Richnow, H.H., 2021. Monitoring of the effects of a temporally limited heat stress on microbial communities in a shallow aquifer. Sci. Total Environ. 146377. https://doi.org/10.1016/j.scitotenv.2021.146377

Keller, G. V, Frischknecht, F.C., 1966. Electrical Methods in Geophysical Prospecting. Pergamon Press, Oxford.

Kellner, C., Edel, H.-G., Meyer, C., 2016. Unterirdische Enteisenung und Entmanganung – wirtschaftliche Kühlung und Klimatisierung von Gebäuden. Bbr 8.

Kempermann, A., 2015. Weiterentwicklung von Kreislaufsäulenversuchen zur Untersuchung des Temperatureinflusses auf die Geochemie unter anaeroben Bedingungen. Master-Thesis. Kiel University.

Keon, N.E., Swartz, C.H., Brabander, D.J., Harvey, C., Hemond, H.F., 2001. Validation of an Arsenic Seqential Extraction Method for Evaluating Mobility in Sediments. Environ. Sci. Technol. 35, 2778–2784. https://doi.org/10.1021/es001511o

Kersten, M., Vlasova, N., 2013. The influence of temperature on selenate adsorption by goethite. Radiochim. Acta 101, 413–420. https://doi.org/10.1524/ract.2013.2041

Kersten, M., Vlasova, N., 2009a. Arsenite adsorption on goethite at elevated temperatures. Appl. Geochemistry 24, 32–43. https://doi.org/10.1016/j.apgeochem.2008.10.004

Kersten, M., Vlasova, N., 2009b. Silicate adsorption by goethite at elevated temperatures. Chem. Geol. 262, 372–379. https://doi.org/10.1016/j.chemgeo.2009.02.002

Knauss, K.G., Dibley, M.J., Leif, R.N., Mew, D. a, Aines, R.D., 2000. The aqueous solubility of trichloroethene (TCE) and tetrachloroethene (PCE) as a function of temperature. Appl. Geochemistry 15, 501–512.

Knödel, K., Krummel, H., Lange, G., 2005. Handbuch zur Erkundung des Untergrundes von Deponien und Altlasten – Band 3: Geophysik. Springer, Berlin.

Koch, M., Ruck, W., 1992. Injection of CO2 for the Inhibition of Scaling in ATES Systems, in: Aquifer Thermal Energy (Heat and Chill) Storage: Proceedings of the 27th Intersociety Energy Conversion Engineering Conference. pp. 63–68.

Kopernikus-Projekt Ariadne, 2021. Deutschland auf dem Weg zur Klimaneutralität 2045. https://doi.org/10.48485/pik.2021.006

Koproch, N., Dahmke, A., Köber, R., 2019. The aqueous solubility of common organic groundwater contaminants as a function of temperature between 5 and 70 °C. Chemosphere 217, 166–175. https://doi.org/10.1016/j.chemosphere.2018.10.153

Koproch, N., Dahmke, A., Schwardt, A., Köber, R., 2022. Temperature influence on the NAPL-water interfacial area between 10 °C and 60 °C for trichloroethylene. J. Contam. Hydrol. 245, 103932. https://doi.org/10.1016/j.jconhyd.2021.103932

Krol, M.M., Mumford, K.G., Johnson, R.L., Sleep, B.E., 2011. Modeling discrete gas bubble formation and mobilization during subsurface heating of contaminated zones. Adv. Water Resour. 34, 537–549. https://doi.org/10.1016/j.advwatres.2011.01.010

Lamert, H., Geistlinger, H., Werban, U., Schütze, C., Peter, A., Hornbruch, G., Schulz, A., Pohlert, M., Kalia, S., Beyer, M., Großmann, J., Dahmke, A., Dietrich, P., 2012. Feasibility of geoelectrical monitoring and multiphase modeling for process understanding of gaseous CO 2 injection into a shallow aquifer. Environ. Earth Sci. 67, 447–462. https://doi.org/10.1007/s12665-012-1669-0

LAWA, 2017. Bund/Länder-Arbeitsgemeinschaft Wasser. Ableitung von Geringfügigkeitsschwellenwerten für das Grundwasser - Aktualisierte und überarbeitete Fassung 2016.

Lerm, S., Alawi, M., Miethling-Graff, R., Wolfgramm, M., Rauppach, K., Seibt, A., Würdemann, H., 2011. Influence of microbial processes on the operation of a cold store in a shallow aquifer: impact on well injectivity and filter lifetime. Grundwasser 16, 93–104. https://doi.org/10.1007/s00767-011-0165-x

Lerm, S., Westphal, A., Miethling-Graff, R., Alawi, M., Seibt, A., Wolfgramm, M., Würdemann, H., 2013. Thermal effects on microbial composition and microbiologically induced corrosion and mineral precipitation affecting operation of a geothermal plant in a deep saline aquifer. Extremophiles 17, 311–327. https://doi.org/10.1007/s00792-013-0518-8

Leventhal, J., Taylor, C., 1990. Comparison of methods to determine degree of pyritization. Geochim. Cosmochim. Acta 54, 2621–2625. https://doi.org/10.1016/0016-7037(90)90249-K

Levy, R., 1976. Size of sodium—calcium montmorillonite crystallites. J. Colloid Interface Sci. 57, 572–574. https://doi.org/10.1016/0021-9797(76)90235-6

Lide, D.R., 2005. CRC Handbook of Chemistry and Physics, Internet Version. CRC Press, Boca Raton, Fl. https://doi.org/978-1466571143

Lienen, T., Lüders, K., Halm, H., Westphal, A., Köber, R., Würdemann, H., 2017. Effects of thermal energy storage on shallow aerobic aquifer systems: temporary increase in abundance and activity of sulfate-reducing and sulfur-oxidizing bacteria. Environ. Earth Sci. 76, 261. https://doi.org/10.1007/s12665-017-6575-z

Llera, F.J., Sato, M., Nakatsuka, K., Yokoyama, H., 1990. Temperature dependence of the electrical resistivity of water-saturated rocks. GEOPHYSICS 55, 576–585.

LLUR, 2019. Umweltaltlas Schleswig-Holstein. Map obtained from www.umweltdaten.landsh.de/atlas/script/index.php, call date 25.09.2019. State office for agriculture, environment and rural areas of the German State of Schleswig-Holstein.

Lüders, K., Dahmke, A., Fiedler, M., Köber, R., 2020. Temperature influence on mobilisation and (re)fixation of trace elements and heavy metals in column tests with aquifer sediments from 10 to 70 °C. Water Res. 169, 115266. https://doi.org/10.1016/j.watres.2019.115266

Lüders, K., Firmbach, L., Ebert, M., Dahmke, A., Dietrich, P., Köber, R., 2016. Gas-phase formation during thermal energy storage in near-surface aquifers: experimental and modelling results. Environ. Earth Sci. 75. https://doi.org/10.1007/s12665-016-6181-5

Lüders, K., Hornbruch, G., Zarrabi, N., Heldt, S., Dahmke, A., Köber, R., 2021. Predictability of initial hydrogeochemical effects induced by short-term infiltration of ∼75 °C hot water into a shallow glaciogenic aquifer. Water Res. X 13, 100121. https://doi.org/10.1016/j.wroa.2021.100121

Ma, R., McBratney, A., Whelan, B., Minasny, B., Short, M., 2011. Comparing temperature correction models for soil electrical conductivity measurement. Precis. Agric. 12, 55–66.

Maaß, C., Sandrock, M., 2017. Erneuerbare Energien im Fernwärmenetz Hamburg - Teil 2: Transformationsstrategie Fernwärme 1–38.

Maji, S.K., Pal, A., Pal, T., Adak, A., 2007. Adsorption thermodynamics of arsenic on laterite soil. J. Surf. Sci. Technol. 23, 161–176.

Matthes, G., 1990. Die Beschaffenheit des Grundwassers, 2nd edn. ed. Gebrüder Bornträger, Berlin - Stuttgart.

Matthey, A., Bünger, B., 2019. Methodenkonvention 3.0 zur Ermittlung von Umweltkosten - Kostensätze.

Matty, J.M., Tomson, M.B., 1988. Effect of multiple precipitation inhibitors on calcium carbonate nucleation. Appl. Geochemistry 3, 549–556. https://doi.org/10.1016/0883-2927(88)90026-1

McCleskey, R.B., Nordstrom, D.K., Ryan, J.D., 2011. Electrical conductivity method for natural waters. Appl. Geochemistry 26, 227–229.

McIntosh, J.C., Grasby, S.E., Hamilton, S.M., Osborn, S.G., 2014. Origin, distribution and hydrogeochemical controls on methane occurrences in shallow aquifers, southwestern Ontario, Canada. Appl. Geochemistry 50, 37–52. https://doi.org/10.1016/j.apgeochem.2014.08.001

Meier-Ewert, G., 2018. Geotechnische Wärmespeicheroptionen im urbanen Raum: Untersuchungen am Beispiel der Stadt Kiel. Master-Thesis. Kiel University.

Meier zu Beerentrup, K. et al. Influence of a temperature change from 10 to 60 °C on the pore water composition of North German glacial till (in preperation).

Meier zu Beerentrup, K., Hornbruch, G., Köber, R., Wang, B., Dahmke, A., 2021. GEWS-System: Erprobung eines Geologischen Eis-Wärme-Speichers am Testfeld „TestUM". Vor. Futur. Energies Sci. Match, Sess. II Infrastruktur. Wunderino Arena Kiel 01.12.2021.

Mellefont, L.A., Ross, T., 2003. The effect of abrupt shifts in temperature on the lag phase duration of Escherichia coli and Klebsiella oxytoca. Int. J. Food Microbiol. 83, 295–305. https://doi.org/10.1016/S0168-1605(02)00378-1

Men, J., Cheng, F., 2011. Biodegradation and growth characteristics of a toluene- degrading strain. African J. Biotechnol. 10, 13299–13306.

Metzgen, A.D., Dahmke, A., Ebert, M., 2022. Temperature Effects on PCE Degradation on ZVI in Column Experiments with Deionized Water. Environ. Sci. Technol. 56, 10084–10094. https://doi.org/10.1021/acs.est.2c01235

Metzgen, A.D., Dahmke, A., Ebert, M., 2021. Anaerobic corrosion of zero-valent iron at elevated temperatures. Environ. Sci. Technol. 55, 8010–8019. https://doi.org/10.1021/acs.est.1c00748

Molz, F.J., Parr, A.D., Andersen, P.F., 1981. Thermal energy storage in a confined aquifer: Second cycle. Water Resour. Res. 17, 641–645. https://doi.org/10.1029/WR017i003p00641

Mualem, Y., Friedman, S.P., 1991. Theoretical Prediction of Electrical Conductivity in Saturated and Unsaturated Soil. Water Resour. Res. 27, 2771–2777.

Mumford, K.G., Martin, E.J., Kueper, B.H., 2021. Removal of trichloroethene from thin clay lenses by electrical resistance heating: Laboratory experiments and the effects of gas saturation. J. Contam. Hydrol. 243, 103892. https://doi.org/10.1016/j.jconhyd.2021.103892

Něměček, J., Steinová, J., Špánek, R., Pluhař, T., Pokorný, P., Najmanová, P., Knytl, V., Černík, M., 2018. Thermally enhanced in situ bioremediation of groundwater contaminated with chlorinated solvents – A field test. Sci. Total Environ. 622–623, 743–755. https://doi.org/10.1016/j.scitotenv.2017.12.047

Nielsen, J.E., Vangkilde-Pedersen, T., 2019. Underground Thermal Energy Storage (UTES) – general specifications and design. HEATSTORE project report, GEOTHERMICA – ERA NET Cofund Geothermal.

Obringer, R., Nateghi, R., Maia-Silva, D., Mukherjee, S., Vineeth, C.R., McRoberts, D.B., Kumar, R., 2022. Implications of Increasing Household Air Conditioning Use Across the United States Under a Warming Climate. Earth's Futur. 10, 1–18. https://doi.org/10.1029/2021EF002434

Ogwada, R.A., Sparks, D.L., 1986. A Critical Evaluation on the Use of Kinetics for Determining Thermodynamics of Ion Exchange in Soils1. Soil Sci. Soc. Am. J. 50, 300. https://doi.org/10.2136/sssaj1986.03615995005000020009x

Opel, O., Eggerichs, T., Otte, T., Ruck, W.K.L., 2014. Monitoring of microbially mediated corrosion and scaling processes using redox potential measurements. Bioelectrochemistry 97, 137–144. https://doi.org/10.1016/j.bioelechem.2013.11.004

Palmer, C.D., Blowes, D.W., Frind, E.O., Molson, J.W., 1992. Thermal Energy Storage in an Unconfined Aquifer - 1. Field Injection Experiment. Water Resour. Res. 28, 2845–2856.

Palmer, C.D., Cherry, J.A., 1984. Geochemical reactions associated with low-temperature thermal energy storage in aquifers. Can. Geotech. J. 21, 475–488. https://doi.org/10.1139/t84-051

Pannike, S., Kölling, M., Panteleit, B., Reichling, J., Scheps, V., Schulz, H.D., 2006. Auswirkung hydrogeologischer Kenngrößen auf die Kältefahen von Erdwärmesondenanlagen in Lockersedimenten. Grundwasser 11, 6–18. https://doi.org/10.1007/s00767-006-0114-2

Parida, K.M., Das, J., 1997. Studies on ferric oxide hydroxides. J. Colloid Interface Sci. 185, 355–362. https://doi.org/10.1007/BF00356646

Parkhurst, D.L., Appelo, C.A.J., 2013. Description of input and examples for PHREEQC version 3--A computer program for speciation, batch-reaction, one-dimensional transport, and inverse geochemical calculations, in: U.S. Geological Survey Techniques and Methods, Book 6. p. 497.

Pehnt, M., Nast, M., Götz, C., Blömer, S., Barckhausen, A., Schröder, D., Miljes, R., Pottbäcker, C., Breier, H., Nabe, C., Lindnder, S., Dannemann, B., 2017. Wärmenetzsysteme 4.0 Endbericht 49, 202.

Perlinger, J.A., Almendinger, J.E., Urban, N.R., Eisenreich, S.J., 1987. Groundwater geochemistry of aquifer thermal energy storage: Long-term test cycle. Water Resour. Res. 23, 2215–2226. https://doi.org/10.1029/WR023i012p02215

Peter, A., Lamert, H., Beyer, M., Hornbruch, G., Heinrich, B., Schulz, A., Geistlinger, H., Schreiber, B., Dietrich, P., Werban, U., Vogt, C., Richnow, H.H., Großmann, J., Dahmke, A., 2012. Investigation of the geochemical impact of CO2 on shallow groundwater: Design and implementation of a CO2 injection test in Northeast Germany. Environ. Earth Sci. 67, 335–349. https://doi.org/10.1007/s12665-012-1700-5

Pfeiffer, W.T., Bauer, S., 2015. Subsurface Porous Media Hydrogen Storage - Scenario Development and Simulation. Energy Procedia 76, 565–572. https://doi.org/10.1016/j.egypro.2015.07.872

Picone, S., Bloemendal, M., Pellegrini, M., Hoekstra, N., Andreu Gallego, A., Rodriguez Comins, J., Murrel, A., 2019. Novel combinations of aquifer thermal energy storage with solar collectors, soil remediation and other types of geothermal energy systems, in: Proceedings of the European Geothermal Congress 2019: Den Haag, The Netherlands, 11-14 June 2019.

Popp, S., Beyer, C., Dahmke, A., Bauer, S., 2015. Model Development and Numerical Simulation of a Seasonal Heat Storage in a Contaminated Shallow Aquifer. Energy Procedia 76, 361–370. https://doi.org/10.1016/j.egypro.2015.07.842

Possemiers, M., Huysmans, M., Batelaan, O., 2014. Influence of Aquifer Thermal Energy Storage on groundwater quality: A review illustrated by seven case studies from Belgium. J. Hydrol. Reg. Stud. 2, 20–34. https://doi.org/10.1016/j.ejrh.2014.08.001

Puckett, L.J., Cowdery, T.K., 2002. Transport and Fate of Nitrate in a Glacial Outwash Aquifer in Relation to Ground Water Age, Land Use Practices, and Redox Processes. J. Environ. Qual. 31, 782–796.

Ramboll, 2015. Südjütland speichert Wärme der Sonne im weltgrößten Grubenwärmespeicher [WWW Document]. URL https://de.ramboll.com/projects/re/south-jutland-stores-the-suns-heat-in-the-worlds-largest-pit-heat-storage (accessed 9.19.22).

Reddy, M.M., Nancollas, G.H., 1976. The crystallization of calcium carbonate. IV. The effect of magnesium, strontium and sulfate ions. J. Cryst. Growth 35, 33–38. https://doi.org/10.1016/0022-0248(76)90240-2

Reeburgh, W., 2007. Oceanic methane biogeochemistry. Am. Chem. Soc. 107, 486–513. https://doi.org/10.1021/cr050362v

Rhoades, J.D., Chanduvi, F., Lesch, S., 1999. Soil salinity assessment: Methods and interpretation of electrical conductivity measurements, FAO Irrigation and Drainage Paper. Food and Agriculture Organization of the United Nations, Rome.

Richards, L.A., 1954. Diagnoses and Improvement of Saline and Alkaline Soils. U.S. Department of Agriculture, Washington, DC.

Robador, A., Brüchert, V., Steen, A.D., Arnosti, C., 2010. Temperature induced decoupling of enzymatic hydrolysis and carbon remineralization in long-term incubations of Arctic and temperate sediments. Geochim. Cosmochim. Acta 74, 2316–2326. https://doi.org/10.1016/j.gca.2010.01.022

Robinson, D.A., Friedman, S.P., 2003. A method for measuring the solid particle permittivity or electrical conductivity of rocks, sediments, and granular materials. J. Geophys. Res. 108, 2076. https://doi.org/10.1029/2001JB000691

Rodda, D.P., Johnson, B.B., Wells, J.D., 1993. The Effect of Temperature and pH on the Adsorption of Copper(II), Lead(II), and Zinc(II) onto Goethite. J. Colloid Interface Sci. 161, 57–62. https://doi.org/10.1006/jcis.1993.1440

Saito, T., Hamamoto, S., Ueki, T., Ohkubo, S., Moldrup, P., Kawamoto, K., Komatsu, T., 2016. Temperature change affected groundwater quality in a confined marine aquifer during long-term heating and cooling. Water Res. 94, 120–127. https://doi.org/10.1016/j.watres.2016.01.043

Sanchez de Lozada, D., Vandevivere, P., Baveye, P., Zinder, S., 1994. Decrease of the hydraulic conductivity of sand columns by Methanosarcina barkeri. World J. Microbiol. Biotechnol. 10, 325–333. https://doi.org/10.1007/BF00414873

Sanner, B., 2004. Schlussbericht zum FuE-Vorhaben 0329809 B „ Thermische Untergrundspeicherung auf höherem Temperaturniveau : Begleitforschung mit Messprogramm Aquiferspeicher Reichstag “.

Sanner, B., Kalf, R., Land, A., Mutka, K., Papillom, P., Stryi-Hipp, G., Weiss, W., 2011. 2020 – 2030 – 2050 Common Vision for the Renewable Heating & Cooling sector in Europe. https://doi.org/10.2788/20474

Scheckel, K.G., Sparks, D.L., 2001. Temperature Effects on Nickel Sorption Kinetics at the Mineral?Water Interface. Soil Sci. Soc. Am. J. 65, 719. https://doi.org/10.2136/sssaj2001.653719x

Schmidt, T., Benner, M., Heidemann, W., Müller-Steinhagen, H., 2003. Saisonale Wärmespeicher – aktuelle Speichertechnologien und Entwicklungen bei Heißwasser-Wärmespeichern. OTTI, Fachseminar Oberflächennahe Geotherm. 1–12.

Schmidt, T., Müller-Steinhagen, H., 2005. Erdsonden- und Aquifer-Wärmespeicher in Deutschland, in: OTTI, Profiforum Oberflächennahe Geothermie. Regenstauf, pp. 1–12.

Schout, G., Drijver, B., Gutierrez-Neri, M., Schotting, R., 2014. Analysis of recovery efficiency in high-temperature aquifer thermal energy storage: a Rayleigh-based method. Hydrogeol. J. 22, 281–291. https://doi.org/10.1007/s10040-013-1050-8

Schroth, M.H., Istok, J.D., Ahearn, S.J., Selker, J.S., 1996. Characterization of Miller-Similar Silica Sands for Laboratory Hydrologic Studies. Soil Sci. Soc. Am. J. 60, 1331. https://doi.org/10.2136/sssaj1996.03615995006000050007x

Schulz, S., Conrad, R., 1995. Effect of algal deposition on acetate and methane concentrations in the profundal sediment of a deep lake (Lake Constance). FEMS Microbiol. Ecol. 16, 251–260.

Schwardt, A., Dahmke, A., Köber, R., 2021. Henry’s law constants of volatile organic compounds between 0 and 95 °C – Data compilation and complementation in context of urban temperature increases of the subsurface. Chemosphere 272, 129858. https://doi.org/10.1016/j.chemosphere.2021.129858

Schwardt, A., Dahmke, A., Köber, R. Temperature effect on nanoscale zero-valent iron corrosion and PCE degradation rates (in preparation).

Schwarz, F.P., 1977. Determination of Temperature Dependence of Solubilities of Polycyclic Aromatic Hydrocarbons in Aqueous Solutions by a Fluorescence Method. J. Chem. Eng. Data 22, 273–277.

Schwarz, F.P., Miller, J., 1980. Determination of the aqueous solubilities of organic liquids at 10.0, 20.0, and 30.0.degree.C by elution chromatography. Anal. Chem. 52, 2162–2164. https://doi.org/10.1021/ac50063a038

Shaw, D.M., 1952. The geochemistry of thallium. Geochim. Cosmochim. Acta 2, 118–154. https://doi.org/10.1016/0016-7037(52)90003-3

Shipton, Z.K., Evans, J.P., Dockrill, B., Heath, J., Williams, A., Kirchner, D., Kolesar, P.T., 2005. Natural leaking CO2- charged systems as analogs for failed geologic storage reservoirs, in: Thomas, D.C., Benson, S.M. (Eds.), Carbon Dioxyde CO2 Capture for Storage in Deep Geologic Formations. Elsevier, Amsterdam, pp. 699–712.

Slenders, H.L.A., Dols, P., Verburg, R., de Vries, A.J., 2010. Sustainable remediation panel: Sustainable synergies for the subsurface: Combining groundwater energy with remediation. Remediat. J. 20, 143–153. https://doi.org/10.1002/rem.20246

Smedley, P.L., Kinniburgh, D.G., 2002. A review of the source , behaviour and distribution of arsenic in natural waters. Appl. Geochemistry 17, 517–568.

Snijders, A.L., 1990. Research on hydrochemistry and water treatment for geat storage; state of the art, in: Hydrochemistry and Energy Storage in Aquifers. pp. 125–135.

Sommer, W., Drijver, B., Verburg, R., Slenders, H., de Vries, E., Dinkla, I., Leusbrock, I., Grotenhuis, T., 2013. Combining shallow geothermal energy and groundwater remediation, in: Proceedings of the European Geothermal Congress, Pisa, Italy, 3-7 June, 2013.

State of Green, 2020. District Energy - Green heating and cooling for urban areas.

State of Green, 2014. World largest thermal heat storage pit in Vojens [WWW Document]. URL https://stateofgreen.com/en/solutions/world-largest-thermal-pit-storage-in-vojens/ (accessed 9.18.22).

Stookey, L.L., 1970. Ferrozine-A New Spectrophotometric Reagent for Iron. Anal. Chem. 42, 779–781. https://doi.org/10.1021/ac60289a016

Taniguchi, M., Uemura, T., Jago-on, K., 2007. Combined Effects of Urbanization and Global Warming on Subsurface Temperature in Four Asian Cities. Vadose Zo. J. 6, 591. https://doi.org/10.2136/vzj2006.0094

Ten Hulscher, T.E.M., Cornelissen, G., 1996. Effect of temperature on sorption equilibrium and sorption kinetics of organic micropollutants - A review. Chemosphere 32, 609–626. https://doi.org/10.1016/0045-6535(95)00345-2

Tesoriero, A.J., Liebscher, H., Cox, S.E., 2000. Mechanism and rate of denitrification in an agricultural watershed: Electron and mass balance along groundwater flow paths. Water Resour. Res. 36, 1545–1559.

Tewari, P.H., McLean, A.W., 1972. Temperature dependence of point of zero charge of alumina and magnetite. J. Colloid Interface Sci. 40, 267–272. https://doi.org/http://dx.doi.org/10.1016/0021-9797(72)90016-1

Thamling, N., Langreder, N., Rau, D., Wünsch, M., Maaß, C., Sandrock, M., Fuß, G., Möhring, P., Purkus, A., Strodel, N., 2020. Perspektive der Fernwärme - Maßnahmenprogramm 2030: Aus- und Umbau städtischer Fernwärme als Beitrag einer sozial-ökologischen Wärmepolitik.

Thomson, A.M., Calvin, K. V., Smith, S.J., Kyle, G.P., Volke, A., Patel, P., Delgado-Arias, S., Bond-Lamberty, B., Wise, M.A., Clarke, L.E., Edmonds, J.A., 2011. RCP4.5: A pathway for stabilization of radiative forcing by 2100. Clim. Change 109, 77–94. https://doi.org/10.1007/s10584-011-0151-4

Tsang, C.F., 1979. A Review of current Aquifer Thermal Energy Storage Projects, in: Recent Work - Lawrence Berkelay National Laboratory. Presented at the International Assembly on Energy Storage, Dubrovnik, Yugoslavia, May 27-June 1, 1979. pp. 35–43.

UBA, 2022. Bundesweite Übersicht zur Altlastenstatistik. Umweltbundesamt.

Udo, E.J., 1978. Thermodynamics of Potassium-Calcium and Magnesium-Calcium Exchange Reactions on a Kaolinitic Soil Clay1. Soil Sci. Soc. Am. J. 42, 556. https://doi.org/10.2136/sssaj1978.03615995004200040004x

Ueckert, M., Baumann, T., 2019. Hydrochemical aspects of high-temperature aquifer storage in carbonaceous aquifers: evaluation of a field study. Geotherm. Energy 7, 4. https://doi.org/10.1186/s40517-019-0120-0

Vail, L.W., Jenne, E.A., Eary, L.E., 1992. H2OTREAT: A Software Aid for Evaluating Water Treatment Requierements for Aquifer Thermal Energy Storage Systems, in: Aquifer Thermal Energy (Heat and Chill) Storage: Proceedings of the 27th Intersociety Energy Conversion Engineering Conference. pp. 105–110.

van Breukelen, B.M., Bonte, M., 2016. Comment on “Thermally Released Arsenic in Porewater from Sediments in the Cold Lake Area of Alberta, Canada.” Environ. Sci. Technol. 50, 7263–7264. https://doi.org/10.1021/acs.est.6b02106

van Genuchten, M.T., 1980. A Closed-form Equation for Predicting the Hydraulic Conductivity of Unsaturated Soils. Soil Sci. Soc. Am. J. 44, 892–898. https://doi.org/10.2136/sssaj1980.03615995004400050002x

van Loon, L., van der Heide, K., 1992. High-Temperature ATES at the State University of Utrecht, The Netherlands, in: Aquifer Thermal Energy (Heat and Chill) Storage: Proceedings of the 27th Intersociety Energy Conversion Engineering Conference. pp. 47–50.

van Loon, L.J.M., 1991. Relevant characteristics for open (ATES) storage. IEA ECES Annex 7., in: Chant, V.G. (Ed.), Proc. Workshop on Generic Configuration Of Seasonal Cold Storage Applications; Utrecht Sep 18-19, 1991. International Energy Agency, Paris.

van Stempvoort, D., Maathuis, H., Jaworski, E., Mayer, B., Rich, K., 2005. Oxidation of Fugitive Methane in Ground Water Linked to Bacterial Sulfate Reduction. Groundwater 43, 187–199.

VDI, 2010. Guideline 4640: Thermal use of the Underground. The Association of German Engineers.

Visser, A., Broers, H.P., Bierkens, M.F.P., 2007. Dating degassed groundwater with 3H/3He. Water Resour. Res. 43. https://doi.org/10.1029/2006WR005847

Visser, A., Schaap, J.D., Peter, H.P., Bierkens, M.F.P., 2009. Degassing of 3H/3He, CFCs and SF6 by denitrification: Measurements and two-phase transport simulations. J. Contam. Hydrol. 103, 206–218. https://doi.org/10.1016/j.jconhyd.2008.10.013

Visser, A., Singleton, M., Madrid, V., Esser, B., 2014. Summary and Preliminary Interpretation of Tritium and Dissolved Noble Gas Data from Site 300. Lawrence Livermore National Laboratory LLNLTR-649041.

Vogel, J.C., Talma, A.S., Heaton, T.H.E., 1981. Gaseous nitrogen as evidence for denitrification in groundwater. J. Hydrol. 50, 191–200.

Wang, B., Delfs, J.-O., Beyer, C., Bauer, S., 2021. Numerical investigation of induced thermal impacts from high-temperature thermal energy storage in porous aquifers. EGU Gen. Assem. 2021, online 19–30 Apr 2021 EGU21-8302. https://doi.org/10.5194/egusphere-egu21-8302

Wang, Q., Guo, S., Ali, M., Song, X., Tang, Z., Zhang, Z., Zhang, M., Luo, Y., 2022. Thermally enhanced bioremediation: A review of the fundamentals and applications in soil and groundwater remediation. J. Hazard. Mater. 433, 128749. https://doi.org/10.1016/j.jhazmat.2022.128749

Wendland, F., Bach, M., Kunkel, R., 1998. Soil and Water Quality at Different Scales: Proceedings of the Workshop "Soil and Water Quality at Different Scales''' held 7--9 August 1996, Wageningen, The Netherlands," in: Finke, P.A., Bouma, J., Hoosbeek, M.R. (Eds.), . Springer Netherlands, Dordrecht, pp. 167–179. https://doi.org/10.1007/978-94-017-3021-1_17

Wenzel, W.W., Kirchbaumer, N., Prohaska, T., Stingeder, G., Lombi, E., Adriano, D.C., 2001. Arsenic fractionation in soils using an improved sequential extraction procedure. Anal. Chim. Acta 436, 309–323.

WHO, 2017. Guidelines for Drinking-water Quality - Fourth Edition. World Health Organization.

Willemsen, A., 1992. PHREEQM-2D: A Computer Model to Calculate Geochemical Reactions During Transport of Groundwater; Model Description and Application to the Utrecht University ATES, in: Aquifer Thermal Energy (Heat and Chill) Storage: Proceedings of the 27th Intersociety Energy Conversion Engineering Conference. pp. 89–98.

Willemsen, A., 1990. Water treatment and environmental effects, in: Hooghart, J., Posthumus, C. (Eds.), Hydrochemistry and Energy Storage in Aquifers. pp. 105–123.

Willemsen, A., Appelo, C.A.J., 1985. Chemical reactions during heat storage in shallow aquifers in the Netherlands: Laboratory experiments and Geochemical Modelling, in: Downing, R.A., Jones, G.P. (Eds.), Hydrogeology in the Service of Man, Mémoires of the 18th Congress of the International Association of Hydrogcologists. Cambridge, pp. 68–78.

Wilson, G.B., Andrews, J.N., Bath, A.H., 1990. Dissolved gas evidence for denitrification in the Lincolnshire Limestone aquifer, eastern England. J. Hydrol. 113, 51–60.

Xu, N., Saiers, J.E., 2010. Temperature and hydrologic controls on dissolved organic matter mobilization and transport within a forest topsoil. Environ. Sci. Technol. 44, 5423–5429. https://doi.org/10.1021/es1002296

Yang, X., Lassen, R.N., Jensen, K.H., Looms, M.C., 2015. Monitoring CO2 migration in a shallow sand aquifer using 3D crosshole electrical resistivity tomography. Int. J. Greenh. Gas Control 42, 534–544. https://doi.org/10.1016/j.ijggc.2015.09.005

Ye, S., Sleep, B.E., Chien, C., 2009. The impact of methanogenesis on flow and transport in coarse sand. J. Contam. Hydrol. 103, 48–57. https://doi.org/10.1016/j.jconhyd.2008.09.004

Zuurbier, K.G., Hartog, N., Valstar, J., Post, V.E.A., van Breukelen, B.M., 2013. The impact of low-temperature seasonal aquifer thermal energy storage (SATES) systems on chlorinated solvent contaminated groundwater: Modeling of spreading and degradation. J. Contam. Hydrol. 147, 1–13. https://doi.org/10.1016/j.jconhyd.2013.01.002

Datenanhang (nur auf CD)

1. Dissertation
    a. Eingereichte Version dieser Dissertation *(im .pdf Format)*

2. Veröffentlichte Versionen der Publikationen zu den Kapiteln 2-4 *(im .pdf Format)*
    a. Lüders, K., Firmbach, L., Ebert, M., Dahmke, A., Dietrich, P., Köber, R., 2016. Gas-phase formation during thermal energy storage in near-surface aquifers: experimental and modelling results. Environ. Earth Sci. 75.
    b. Lüders, K., Dahmke, A., Fiedler, M., Köber, R., 2020. Temperature influence on mobilisation and (re)fixation of trace elements and heavy metals in column tests with aquifer sediments from 10 to 70 °C. Water Res. 169.
    c. Lüders, K., Hornbruch, G., Zarrabi, N., Heldt, S., Dahmke, A., Köber, R., 2021. Predictability of initial hydrogeochemical effects induced by short-term infiltration of ∼75 °C hot water into a shallow glaciogenic aquifer. Water Res. X 13, 100121.

3. Rohdaten der experimentellen Laborarbeiten und des Feldversuches aus den Kapiteln 2-4 *(im .xlsx oder .xlsm Format)*
    a. Kap. 2: Gas-phase formation during thermal energy storage in near-surface aquifers: experimental and modelling results.
        i. Hydrochemische Daten der Durchflusssäulenversuche mit den Sedimenten OR und BS
        ii. Kombinierte Daten der Druck- und Wagenaufzeichnungen für die Durchflusssäulenversuche mit den Sedimenten OR und BS
        iii. Daten zur Bestimmung des Gasvolumens in den Versuchssäulen
    b. Kap. 3: Temperature influence on mobilisation and (re)fixation of trace elements and heavy metals in column tests with aquifer sediments from 10 to 70 °C.
        i. Hydrochemische Daten zu Spurenkomponenten und Schwermetallen der Durchflusssäulenversuche mit Sediment C
        (Sediment C in Kap. 3 entspricht Sediment BS aus Kap. 2; Daten der Hauptkomponenten sind daher unter Kapitel 2 aufgeführt)
        ii. Hydrochemische Daten der Kreislaufsäulenversuche mit den Sedimenten A, B, C und D
        iii. Geochemische Daten der Säure-Druck-Aufschlüsse von den Sedimenten A, B, C und D
    c. Kap. 4: Predictability of initial hydrogeochemical effects induced by short-term infiltration of ∼75 °C hot water into a shallow glaciogenic aquifer.
        i. Hydrochemische Daten des Feldveruchs-Monitorings vom TestUM-Testfeld in Wittstock
        ii. Temperaturdaten des Feldversuches
        iii. Hydrochemische Daten der Batchversuche mit 28 Sedimentproben von der Testfeldlokation
        iv. Geochemische Daten der Festphasenanalytik

CD

(nur in gedruckter Version)

Erklärung

Hiermit erkläre ich, Klas Lüders,

1. dass diese Arbeit nach Inhalt und Form, abgesehen von der Beratung durch meinen Betreuer, vollständig das Ergebnis meiner eigenen Arbeit ist und alle Quellen entsprechend im Literaturverzeichnis gelistet sind;
2. dass die zugrundeliegenden Publikationen aus den Kapiteln 2 bis 4 dieser Dissertation bereits in den Fachzeitschriften *Environmental Earth Sciences* (Kap. 2), *Water Research* (Kap. 3) und *Water Research X* (Kap. 4) veröffentlicht sind, diese Dissertation als solche bislang aber keiner anderen Stelle in einem Prüfungsverfahren vorgelegen hat;
3. dass die Arbeit unter Einhaltung der Regeln guter wissenschaftlicher Praxis der Deutschen Forschungsgemeinschaft entstanden ist; und
4. dass mir kein akademischer Grad entzogen worden ist.

Kiel, Juli 2023

Klas Lüders